Chapter 11: Near-term Climate Change: Projections and Predictability

Coordinating Lead Authors: Ben Kirtman (USA), Scott Power (Australia)

Lead Authors: Akintayo John Adedoyin (Botswana), George Boer (Canada), Roxana Bojariu (Romania), Ines Camilloni (Argentina), Francisco Doblas-Reyes (Spain), Arlene Fiore (USA), Masahide Kimoto (Japan), Gerald Meehl (USA), Michael Prather (USA), Abdoulaye Sarr (Senegal), Christoph Schaer (Switzerland), Rowan Sutton (UK), Geert Jan van Oldenborgh (Netherlands), Gabriel Vecchi (USA), Hui-Jun Wang (China)

Contributing Authors: Nathan Bindoff, Yoshimitsu Chikamoto, Javier García-Serrano, Paul Ginoux, Lesley Gray, Ed Hawkins, Marika Holland, Christopher Holmes, Masayoshi Ishii, Thomas Knutson, David Lawrence, Jian Lu, Vaishali Naik, Lorenzo Polvani, Alan Robock, Luis Rodrigues, Doug Smith, Steve Vavrus, Apostolos Voulgarakis, Oliver Wild, Tim Woollings

Review Editors: Pascale Delecluse (France), Tim Palmer (UK), Theodore Shepherd (Canada), Francis Zwiers (Canada)

Date of Draft: 16 December 2011

Notes: TSU Compiled Version

Table of Contents

Executive Summary

[A major focus of this chapter will be an assessment of research based on analyses of CMIP5 projections and predictions. Extremely little is currently available. Consequently the plots presented that are based on CMIP5 models are preliminary, and in some cases (e.g., runoff) may be unreliable estimates of Second Order Draft plots that will be based on a much larger number of CMIP5 models. In many cases analyses of CMIP5 output has not been performed to allow key statistics identified below to be calculated.]

How will climate evolve over the next few decades? In order to address this important question this chapter assesses the literature describing projected (when the climate is most influenced by changes in external forcing such as increasing greenhouse gases) *and* predicted (when the climate is most influenced by the time evolution of processes related to the observed initial state) changes in climate during the "near term". "Near term" refers to future decades up to mid-century, the period for which the climate response to different future emissions scenarios are generally similar. Greatest emphasis is given to the period 2016–2035, though some information on projected changes before and after this period (up to mid-century) is assessed. We consider the mechanisms responsible for near-term changes in climate, the degree of "predictability" (as defined below) evident in the climate system, and the processes underpinning predictability. The size of the externally-forced signal relative to internal variability and the degree to which externally-forced near-term changes will emerge from internally generated natural variability are also discussed.

The near-term projections discussed in this chapter complement the mid-century and longer-term projections presented in Chapters 12 and 14. Projected changes in sea level are presented in Chapter 13.

This assessment evaluates new emission scenarios for climate change, the four Representative Concentration Pathways (i.e., RCP2.6, RCP4.5, RCP6.0, and RCP8.5), which were developed for, but independently of, this IPCC assessment. The SRES scenarios, developed as part of the IPCC process and used in the TAR and AR4, were mapped from emissions to greenhouse gas abundances to radiative forcing to climate change based on the IPCC assessments. The RCPs use a single parametric box-model for this mapping. The AR5 climate model simulations (CMIP5, ACCMIP) use the abundances of the long-lived greenhouse gases as modelled by the RCPs. But even for the same scenario, the CMIP5 models project RF trajectories differing by ±X% (tbd) because of their individual treatment of atmospheric chemistry and aerosols. The UNFCCC reporting and mitigation strategies are emissions-based, and application of current best knowledge of atmospheric chemistry and biogeochemistry using globally resolved models including natural emissions and feedbacks (as in CMIP5 and ACCMIP) projects greenhouse gases and radiative forcing for the RCP emissions that are systematically larger/smaller than those used in CMIP5 by Y% to Z% (tbd), although the uncertainties in RF, typically ±W% (tbd) encompass the results. In terms of the short-lived species (e.g., NOx, CO, NMVOC, NH_3, SOx, BC and OC aerosols) that control tropospheric ozone, aerosols and the loss rate of CH_4 and HFCs, the RCP emissions are unusually low and do not fully represent the range of possible futures affecting air quality and CH_4 abundance.

For the near term, the range in anthropogenic RF of the RCPs is similar across the RCPs and close to that of the SRES scenarios, but after 2040 RCP2.6 drops well below the lowest SRES used in AR4. Thus the range of new CMIP5 results are similar to those in AR4 for the near term. Considering that RCP2.6 involves major mitigation of greenhouse gas emissions in attempting to keep global mean surface warming below 2°C, the range of continued near-term warming under this pathway is narrow.

Variations from these paths will be strongly influenced by natural variability. The magnitude of externally-forced near-term changes relative to the magnitude of internally generated natural variability varies from quantity to quantity and from location to location.

The majority of the information below comes from AOGCM integrations that were performed as part of a major international activity called the Coupled Model Intercomparison Project phase 5 CMIP5 (Taylor et al., 2008; 2011). New results on projections corroborate key results in the Fourth Assessment Report (AR4) for the near term. We are already "committed" to further externally forced near-term warming due to past emissions, this warming will be reinforced by emissions over the near term, and the climate we observe in the near term will also be strongly influenced by the internally generated natural variability of the climate system.

Projections of GHGs and aerosols, air quality and air pollution to mid-century are also assessed using a hierarchy of modelling approaches which includes coupled chemistry-climate modelling.

The development of near-term prediction systems in which internally generated natural variability is initialized using observational data for the ocean and other components of the climate system, is a new research area for climate science since the AR4 (Smith et al., 2007; Keenlyside et al., 2008; Meehl et al., 2009). This chapter therefore assesses current capabilities in making predictions, and the degree to which these predictions add value to (initialized) projections. Previous assessments (FAR, SAR, TAR, AR4) only described climate-change projections wherein the externally forced component of future climate was included but no attempt was made to initialize the internally generated climate variability. Predictions, on the other hand, are intended to predict both the externally forced component of future climate change, and the internally generated natural component. Near-term predictions do not provide detailed information of the evolution of weather. Instead they can provide estimated changes in the time evolution of the statistics of near-term climate (FAQ 11.1), which can be used as a scenario-independent basis for adaptation in the near term (see WGII) in which uncertainty associated with internal variability can be reduced.

Predictability

In climate science the "predictability" of a given climatic feature is a quantifiable intrinsic property of the climate system. Predictability can be loosely regarded as an estimate of our ability to predict the future under ideal circumstances. "Predictive skill", on the other hand, describes the extent to which the climate feature can be predicted in practice. There might be, and in general are, technical reasons why we are not able to fully exploit the intrinsic predictability, e.g., a dearth of observational data in particular locations to initialize predictions and deficiencies in climate models. Predictability, prediction, projection and the differences between them are discussed further in FAQ 11.1, Box 11.1 and Sections 11.1, 11.3.1, and 11.4.1.

The predictability of internally generated decadal changes in surface temperature is generally low over land. Predictability over the ocean tends to be higher, especially in middle and high latitudes of the North Atlantic, North Pacific and Southern Oceans. This is largely associated with deep ocean mixed layers in these regions. Some additional predictability arises in association with ocean currents. Predictability in surface temperature arising from external sources of predictability tends to complement predictability arising from internal variability, so that net predictability is more spatially uniform than either of its two contributing components.

The magnitude and structure of the decadal predictability of precipitation is very different to that of decadal predictability of surface temperature. The predictability of rainfall is very low in the first future decade. Predictability remains low on multi-decadal time-scales. By the end of the first decade the low level of predictability in precipitation evident is almost entirely dominated by the forced component.

A number of studies indicate that the Atlantic Meridional Overturning Circulation (AMOC) exhibits decadal predictability though estimates of the lead-time for which predictability exists varies from model to model, ranging from several years to ten years, and the level of predictability might be state-dependent. A smaller number of studies examining predictability in the Pacific suggest that: internally generated changes in ENSO activity drives changes that are, in part, predictable in off-equatorial sea-surface temperature (SST) and sub-surface ocean temperature on multi-year and decadal time-scales respectively; that the dominant spatial patterns of annual mean and upper ocean temperature variability in the North Pacific may be predictable for up to 6–10 years; and that the predictability of ocean temperature is a minimum in the surface waters of the equatorial Pacific Ocean but tends to increase with latitude and depth.

Arctic sea ice area tends to exhibit predictability for about two years in areas where it is thick.

Predictability associated with the initial state of internal variability tends to decay with time, while the relative importance of predictability due to the externally forced component increases with time. The lead-time at which the level of predictability arising from the two contributions are equal, varies depending on the variable and region considered. For globally average heat content in the upper 700 m (tbc) of the ocean, in experiments initiated in the year 2000, the two contributions are of the same size approximately six years after initiation.

Atmospheric Composition and Air Quality

Overall, the evolution of atmospheric composition closely follows the projected anthropogenic emissions, with shorter-lived greenhouse gases like CH_4 and HCF-134a in near steady state with rising or falling emissions, but longer-lived gases N_2O, PFCs and HFC-23 continuing to rise over the century. Emissions of short-lived reactive species such as NOx, CO, NMVOC, and aerosols alter the background chemistry of the atmosphere as does the overall global warming. Climate change is expected to shift the natural emissions of CH_4 and some aerosols, such as mineral dust. These latter changes have greater control over the CH_4 abundance for RCPs 2.6, 4.5 and 6.0 since projected anthropogenic CH_4 changes are modest. For aerosols and tropospheric O_3, regional variations in climate change (e.g., temperature, precipitation, and atmospheric circulation), will contribute to non-uniform trends.

Large projected shifts in air quality for polluted regions that are subject to high surface ozone and particulate matter (PM or aerosols) are driven primarily by changes in local anthropogenic emissions of short-lived, reactive species. There are also important contributions from regional transport of anthropogenic PM and ozone on continental scales, and from ozone on a near-global scale driven by emissions of NOx and CH_4. In addition, there is increasing evidence that, with climate change, meteorological conditions are more conducive to producing extreme pollution events at the regional and even urban scales due to increasing temperature and stagnation episodes. Multiple lines of evidence (from observations, modelling and theoretical studies) indicate that future warming alone will likely increase O_3 in polluted regions. In contrast, the expected increase of water vapour will likely decrease baseline O_3 levels in surface air for RCPs 2.6, 4.5, and 6.0, but not necessarily RCP 8.5 due to offsetting rise in baseline O_3 from CH_4 increases. The sign of the PM response to climate change is uncertain and will likely vary regionally, reflecting major uncertainties in projecting regional precipitation changes, and offsetting influences of a warming climate on different aerosol components (e.g., nitrate versus sulphate). In such cases, confidence in projections is largest in regions where regional climate responses, including changes in surface temperature, humidity, ventilation of the polluted boundary layer, and interactions with the biosphere (which acts both as a source and sink of air pollutants) are most robust.

Near-term Projections of the Climatic Response to External Forcing

Research since the AR4 lends further weight to many of the conclusions relating to near-term projections given in the AR4 and to the inferences that can be drawn from material presented in the AR4.

Temperature Changes

Multi-model global mean warming over the period 2016–2035 relative to the reference period 1986–2005 amongst the RCP scenarios RCP2.6, RCP4.5, RCP6.0, and RCP8.5 lies in a narrow range of 0.65xx°C to 0.7xx°C. The mean values of global average temperature change for these four scenarios are ww, xx, yy, and zz respectively, indicating that differences are very small. Possible future natural forcing (e.g., a large volcanic eruption) could change these values somewhat. The AR4 concluded that, based on climate change commitment (further warming that would occur if concentrations of GHGs were instantly stabilized), the system is already committed to warming that amounts to about xx per decade out to several decades. Therefore, approximately 50xx% of the 2016–2035 warming occurs in response to past emissions.

Near-term projections based on CMIP5 models are broadly consistent with the projections described in the AR4 (tbc): largest near-term warming occurs at high northern latitudes; minimum warming occurs over the Southern Ocean and the northern North Atlantic. Near-term warming also tends to be greater over land than over the oceans. Maximum atmospheric warming occurs in the upper tropical troposphere, while cooling is widespread in the stratosphere.

Hydrological Cycle

Precipitation in the near-term is projected to increase in regions of tropical precipitation maxima and at high latitudes, with general decreases in drier regions of the tropics and sub-tropics. The magnitude of near-term changes in precipitation are expected to be absent or small relative to the magnitude of internal variability in some of the regions lying in between. The magnitude of the projections vary considerably from model to model.

Atmospheric Circulation

The tropospheric temperature changes noted above tend to stabilize the atmosphere in the subtropics and much of the mid-latitudes. These changes are associated with a weakening of the Walker circulation, a poleward expansion of the Hadley Circulation and to a widening and poleward shift of mid-latitude storm tracks. However, future internally generated variability in the Walker circulation in association with e.g., the Pacific Decadal Oscillation (PDO) and the Interdecadal Pacific Oscillation (IPO) more widely, could easily mask the externally forced component during the near-term.

Stratospheric Forcing of the Troposphere

As noted in Chapter 10, modelling and observational studies have identified stratospheric ozone depletion as the main driver of the observed positive trend in Southern Annular Mode (SAM) during the southern hemisphere summer (DJF). As stratospheric ozone is expected fully recover by approximately 2060, this recovery is expected to offset the strengthening of the (SAM) caused by increased greenhouse gases. As SAM changes are also linked to a widening of the southern hemisphere Hadley Circulation, such expansion might also be arrested, with the possibility of a contraction be mid-century, and an associated equatorward shift of the jet stream. The projected fate of SAM, the Hadley Circulation and the associated jet streams after 2060 is discussed in Chapter 12.

The Cryosphere

Sea ice area is projected to decrease by xx% in the Arctic and yy% in the Antarctic in 2016–2035 relative to 1986–2005. The volume loss of Arctic sea ice is projected to be larger where the ice is thickest initially, with an accumulated mass loss of about 0.5xxm by 2020, and 1.0xxm by 2050, and considerable model-to-model differences. Global average annual snow cover is projected to decrease by xx-xx% by 2050 (Section 11.4.5.2). Global warming diminishes both snow cover and the amount of water in the form of snow by reducing the fraction of precipitation that falls as snow and by increasing snowmelt. There are important regional contrasts to these global average changes. For example, over much of the northern high latitudes snowfall is projected to increase, and the net result of this increase and increased melt changes sign within the region. Annual average decreases in permafrost are approximately xx% for 2016–2035 and yy% by 2050.

Extremes

Near-term projections include changes with the same sign as the long-term projected changes in the AR4: a general significant decrease in the frequency of cold nights; an increase in the frequency of warm days and nights; and an increase in the duration of warm spells. While externally forced signals in the global integral of some extremes emerge over the near-term, emergence is far less obvious regionally. The changes are remarkably insensitive to the emission scenario considered.

Near-term results from regional climate modelling efforts are also presented. For example, in the ENSEMBLES projections for Europe, daytime extreme temperatures are projected to warm at a faster rate than mean temperature, while daytime winter temperatures are projected to warm at a slower rate than mean temperature.

For the near term, CMIP5 projections confirm a clear tendency for increases in heavy precipitation events in the global mean seen in the AR4, but there are significant variations across regions. Past observations have also shown that interannual and decadal variations in mean and heavy precipitation are large, and are strongly affected by natural variations e.g., ENSO), volcanic forcing, and anthropogenic aerosol loads.

There is little confidence in basin-scale projections of trends in tropical cyclone frequency and intensity to the mid-21st century. It is very likely that tropical cyclone frequency, intensity and spatial distribution globally and in individual basins will vary from year-to-year and decade-to-decade in association with e.g., natural modes of variability including e.g., ENSO and the IPO.

Differences Between Near-Term Projections of Climate Under Different RCPs

Globally and regionally, the surface temperature response is fairly independent of scenario until after 2040. Some global methane and aerosol mitigation scenarios suggest a possible near-term sensitivity of surface temperature to those forcings.

Multi-year and Decadal Predictions

[PLACEHOLDER FOR SECOND ORDER DRAFT: Discussion of actual forecasts will be provided if justified by hindcast evaluation, or else a comment that no skill exists will be provided. Awaiting analysis of CMIP5 and other prediction intercomparisons.]

While numerous studies have investigated and estimated predictability, very little information on the verification of actual retrospective decadal climate predictions or hindcasts is currently available. The small number of studies conducted so far does not provide convincing evidence of appreciable decadal predictive skill over land. Evidence of predictive skill is stronger in certain parts of the ocean. For example, decadal changes in North Pacific SST and sea-level associated with internal variability can be predicted with a degree of skill. Predictive skill has also been demonstrated for SST over the North Pacific in association with the combined impact of interannual (ENSO) variability and external forcing.

[PLACEHOLDER FOR SECOND ORDER DRAFT: give scores and lead-times.]

Retrospective predictions suggest that additional skill from the initialisation of the ocean, including internally generated variability, seems to occur in both the North Atlantic and North Pacific

[PLACEHOLDER FOR SECOND ORDER DRAFT: give scores and lead-times.]

The ability to verify hindcasts of past AMOC variability is severely hampered by the absence of records of past variability that do not depend on the models incorporated into the prediction systems. So while multi-model, multi-ensemble prediction systems can hindcast proxies of AMOC variability up to 5 years ahead, the proxies are highly model-dependent. The agreement between the proxy and hindcasted variability is therefore best considered as further evidence of multi-year *predictability*, rather than definitive *predictive skill*. This predictability has been attributed to predictability arising from the internal variability rather than to external forcing. Assessments of the skill with which associated impacts over land can be predicted have not been conducted but skill is likely to be very low.

While predictability studies and the assessment of seasonal-to-interannual predictions show that the sub-surface ocean is a major source of predictability, in practice the predictive skill that can be obtained is severely limited by the sparseness of sub-surface ocean data and observational errors. The ability to verify forecasts is also limited by inhomogenieties in the data record arising from e.g., the changes in the density of the observing system, which can give rise to spurious decadal changes in the record used to benchmark the hindcasts.

[PLACEHOLDER FOR SECOND ORDER DRAFT: Future analyses of CMIP5 hindcasts will be used to assess the level of additional skill providing by initialising internal variability as a function of lead-time, temporal averaging, variable (e.g., precipitation, temperature), location, spatial scale and, for ocean variables, depth. We will also assess the level of consistency between predictability studies and skill estimates and the degree of confidence we have in the skill assessments presented.]

Predictability studies indicate that estimates of skill will vary from variable to variable, location to location and be greater early in the forecast and for larger spatial scales.

Climatic surprises in the near-term

In the near term, explosive volcanic eruptions and unexpectedly large variations in solar output, for example, could force the climate system to values not encompassed by the CMIP5 projections. Large internally generated variations are also possible, even if of low probability, and could result in unanticipated extremes of climate.

11.1 Introduction

This chapter describes and assesses current scientific understanding of "near-term" climate over the coming decades to mid-century, including atmospheric composition and air quality. This emphasis on near-term climate arises from (i) a recognition of its importance to decision makers in government and industry; (ii) an increase in the international research effort aimed at improving our understanding of near-term climate; and (iii) a recognition that near-term projections are generally less sensitive to differences between future emissions scenarios than are long-term projections. Near-term decadal climate prediction (Smith et al., 2007; Keenlyside et al., 2008; Meehl et al., 2009) provides information not available from existing seasonal to interannual (months to a year or two) predictions or from long-term (late 21st century and beyond) climate change projections (Chapters 12-14). Prediction efforts on seasonal to interannual timescales require accurate estimates of the initial climate state with less concern extended to changes in external forcing[1], while long-term climate projections rely more heavily on estimations of external forcing with little reliance on the initial state of internal variability. Estimates of near-term climate depends partly on the committed warming (caused by the inertia of the oceans as they respond to historical external forcing) the time evolution of internally-generated climate variability, and the future path of external forcing. Near-term predictions out to about a decade, unlike near-term projections beyond a decade to about mid-century that are affected mostly by the external forcing, depend more heavily on an accurate depiction of the internally generated climate variability (see Box 11.1).

The need for near-term climate information has spawned a new field of climate science, decadal climate prediction (Meehl et al., 2009). Reflecting this new activity, the Coupled Model Intercomparison Project phase 5 (CMIP5) experimental protocol includes, as one of its foci, near-term predictions (10- to 30-years), where there is an emphasis on the initialization of the climate system with observations. The other focus of CMIP5 is long-term climate change experiments often referred to as 'uninitialized' or 'non-initialized' projections or simply as 'projections'. The objectives of this chapter are to assess the state of the science for both near-term predictions and projections. Thus both CMIP5 foci noted above are considered for the near term as well as other published near-term predictions and projections.

The chapter consists of four major assessments:

- (i) the scientific basis for near-term prediction as reflected in estimates of predictability (see Box 11.1), and the dynamical and physical mechanisms underpinning predictability, and the processes that limit predictability (see Section 11.2);
- (ii) the current state of knowledge in near-term projection (see Section 11.4). Here the emphasis is on what the climate in next few decades may look like relative to 1986–2005, based on near-term projections (i.e., the forced climatic response). The focus in on the "core" near-term period (2016–2035), but some information prior to this period and out to mid-century is also discussed. A key issue is when, where and how the signal of externally-forced climate change is expected to emerge from the background of natural climate variability;
- (iii) near-term projected changes in atmospheric composition and air quality, and their interactions with climate change; and
- (iv) the current state of knowledge in near-term prediction (see Section 11.3). Here the emphasis is placed on the results from the decadal (10-year) multi-model prediction experiments in the CMIP5 database.

[START BOX 11.1 HERE]

Box 11.1: Climate Prediction, Projection and Predictability

This Box clarifies the meaning of various terms used extensively in this chapter, as they are defined in the scientific literature on climate.

Internally generated and externally forced climate components

[1] Seasonal-to-interannual predictions typically include the impact of external forcing.

The black line in Figure 11.1 plots the evolution of the global and annual average temperature, *T(t),* as the difference from the 1901–1950 average. A change in temperature or other climate system variable may be represented as $T(t) = T_f(t) + T_i(t)$, the sum of an *externally forced* and an *internally generated* component. Changes in GHG concentrations, natural and anthropogenic aerosol loadings, land use etc. provide the external forcings which determine $T_f(t)$, while $T_i(t)$ arises spontaneously due to the internal workings of the climate system.

Climate projection

A *climate projection* attempts to determine the evolution of the forced component $T_f(t)$ and the envelope of $T_i(t)$ over the next decade(s) but not the particular evolution of $T_i(t)$ that will occur. The yellow lines in the Figure are different realizations of the evolution of the global mean temperature from 1900 to 2000 produced by a group of climate models. This ensemble of realizations indicates the range of possible evolutions of the system for the given forcing and provides statistical information on climate variability.

Climate prediction

A *climate prediction* or *climate forecast* is a statement about the future evolution of some aspect of the climate system encompassing both forced and internally generated components. Climate predictions do not attempt to forecast the actual day-to-day progression of the system but rather the evolution of some climate statistic. The global and annually averaged temperature of Figure 11.1 is an example. Both climate predictions and climate projections are usually made with numerical models which represent the system mathematically using the equations of fluid mechanics, thermodynamics, cloud physics, radiative transfer etc. that account for the energy flow and behaviour of the system. A climate prediction proceeds by integrating the governing equations forward in time from observation-based initial conditions. Climate predictions may also be made using statistical models which relate current to future conditions using statistical relationships derived from observations of past system behaviour.

A climate model is deterministic in the sense that if the governing equations are integrated forward in time from identical initial conditions the evolution of the system is reproducible. Nevertheless, because of the chaotic and non-linear nature of the climate system, minor differences in initial conditions or in some aspect of the model give different evolutions with time. This divergence is represented schematically in Figure 11.2a.

A *deterministic forecast* (such as a weather forecast for the next day or two) attempts to trace out the actual evolution of the climate variable (the black line in Figure 11.1-2). If differences in initial conditions represent observational and analysis errors, with trajectories that are affected by model deficiencies, the divergence of the predicted from the actual evolution represents the growth of forecast error. Under some circumstances, the spread among predictions gives an indication of the likelihood of a particular forecast result and may be represented as a probability distribution.

A *probabilistic* climate prediction takes the form of a probability distribution. This probabilistic view is depicted in Figure 11.3. The initial state has a sharply peaked distribution representing the comparatively small uncertainty in the observation-based initial state. The growth of error with forecast time broadens the probability distribution until, ultimately, it becomes indistinguishable from that of an uninitialized climate projection.

Climate predictability

The rate of separation or divergence of initially close states of the climate system with time (as represented schematically in Figure 11.2), or the rate of broadening of its probability distribution (as in Figure 11.3), is a measure of the system's predictability. If the states separate rapidly, the predictability of the system is low; if they separate slowly, predictability is high. In the same way, initial error grows rapidly if the predictability of the system is low but more slowly if predictability is high. The inherent growth of small errors limits the duration of a useful forecast even for a highly accurate forecast system.

Formally, predictability is a feature of the physical system itself, rather than of our "ability to predict" which depends on the accuracy of our models and initial conditions. Climate predictability may be studied diagnostically, by analyzing past climate system behaviour (observed or modelled), or prognostically by making a sequence of predictions with a model of the system. The rate of separation of initially close states or, in the probabilistic view, the evolution of the probability distribution is studied and quantified. The predictability of different variables in the atmosphere and ocean will be different and will also vary with location. Estimates of the predictability of the climate system provide insight into the possibility of, and the expected limitations to, skilful climate forecasts.

Forecast quality

Forecast quality measures the success of a prediction against observation-based information. The average over a sequence of forecasts made for past cases, termed *retrospective forecasts* or *hindcasts*, gives an indication of the quality that may be expected, on average, for future forecasts for a particular variable at a particular location. Forecast quality measures the "ability to predict" and, since forecast systems are not without error, will generally underestimate the "predictability" of the system.

[INSERT FIGURE 11.1 HERE]

Figure 11.1: The evolution of observed global mean temperature as the difference from the 1901–1950 average (the black line) where $T(t) = T_f(t) + T_i(t)$ is the sum of an externally forced component T_f (red line) and an internally generated component T_i (the difference between the black and red lines). An ensemble of possible "realizations" of temperature evolution is represented by the yellow lines.

[INSERT FIGURE 11.2 HERE]

Figure 11.2: A schematic representation of predictability as the rate of separation of initially close states and the connection with forecast error growth. The actual evolution of the system is represented as the black line, the uncertainty in initial conditions by the yellow oval and the resulting cloud of trajectories by the thin lines. A deterministic climate prediction attempts to follow the black line to predict *T((t)*, or other climate variable, at some time *t* beyond the present. A probabilistic climate prediction takes the form of a probability distribution *p(T,t)* providing information on the probability of realizing a particular result.

[INSERT FIGURE 11.3 HERE]

Figure 11.3: Schematic evolution of predictability and error growth in terms of probability. The probability distribution corresponding to the forced component $p(T_f,t)$ is in red with the deeper shades indicating higher probability. The probabilistic representation of the forecast *p(T,t)* is in blue. The initially sharply peaked distribution broadens with time as information about the initial conditions is lost until the initialized climate prediction becomes indistinguishable from an uninitialized climate projection.

[END BOX 11.1 HERE]

11.2 Uncertainty and Signal-to-Noise in Near-Term Climate Predictions and Projections

Climate projections and predictions necessarily involve uncertainty: exact knowledge of the future is unobtainable. Understanding the sources of uncertainty, and quantifying uncertainties where this is possible, is essential if projections are to be used effectively.

11.2.1 Uncertainty in Near-Term Climate Projections

Climate projections are subject to three sources of uncertainty. The first arises from the natural *internal variability* of the climate system (see Box 11.1) which is superimposed on the externally-forced component. This variability, which is intrinsic to the climate system, includes phenomena such as variability in the mid-latitude storm tracks and the Interdecadal Pacific Oscillation (IPO). With projections, no attempt is made to predict the evolution of the internal variability. Instead the statistics associated with the variability based on observations or simulations of the past are sometimes included as a component of the uncertainty associated with the projection. The existence of internal variability places fundamental limits on the precision with which future climate variables can be projected. The second is uncertainty concerning the past, present and future *forcing* of climate system by natural and anthropogenic influences such as greenhouse gases and aerosols. The third is uncertainty concerning the *response* of the climate system to forcing.

Quantifying the uncertainty that arises from each of the three sources is an important challenge. The magnitude of internal climate variability can be estimated from observations (Chapter 2) or from climate models (Chapter 9). Challenges arise in estimating the variability on decadal and longer time scales, and for rare events such as extremes as observational records are often too short to provide reliable estimates, and greater reliance must be placed on model results.

Uncertainty concerning the past forcing of the climate system arises from a lack of direct or proxy observations, and from observational errors. This uncertainty can influence future projections of some variables (particularly large-scale ocean variables) for years or even decades ahead (e.g., Meehl et al., 2006; Gregory, 2010; Stenchikov et al., 2009). Uncertainty about future forcing arises from the inability to predict future anthropogenic emissions and land use change as well as natural forcings (e.g., volcanoes). The RCP scenarios (Chapter 1) provide a range of plausible trajectories for future anthropogenic emissions and land use change. The consequences of this uncertainty for climate projections are discussed in Section 11.4.6. Carbon cycle and other biogeochemical feedbacks (Chapter 6) can give rise to interactions between forcing uncertainty and response uncertainty. Such interactions are important for long-term climate projections (Chapter 12, Annex II.4.1, but have limited importance for near term climate - for further discussion see Section 11.4.7 and Chapter 6.

R*esponse uncertainty* is arguably the most difficult contribution to quantify. Climate models provide estimates of the response to specified forcing agents such as GHGs and aerosols, but different models typically show similar but not identical responses. The range, or spread, of climate model responses is often used as a measure of response uncertainty (also known as 'model uncertainty'), but such a measure is crude as it takes no account of factors such as model quality (Chapter 9) or model independence (e.g., Pennel and Reichler, 2011; Masson and Knutti, 2011), and not all variables of interest are adequately simulated by global climate models. Some alternative approaches are discussed in Section 11.4.2. To generate projections of extreme events such as tropical cyclones, or regional phenomena such as orographic rainfall, it is sometimes necessary to employ a dynamical or statistical downscaling procedure. Such downscaling introduces a further dimension of response uncertainty.

The relative importance of internal variability, forcing uncertainty and response uncertainty depends on the variable of interest, the space and time scale (Meehl et al, 2007: Section 10.5.4.3), and the lead-time of the projection. Figure 11.4 provides an illustration of these dependencies based on an analysis of climate model projections (Hawkins and Sutton, 2009, 2010). In this example, only the forcing uncertainty related to future greenhouse gas concentrations is considered, and model spread is used as a measure of response uncertainty. Key points are: 1) the uncertainty in *near term* projections is dominated by internal variability and response uncertainty. This finding provides some of the rationale for considering near-term projections separately from long-term projections. Note that aerosol forcings, not shown in the figure, are an exception (discussed in Section 11.4.6); 2) internal variability becomes increasingly important on smaller space and time scales; 3) for projections of precipitation forcing uncertainty is less important and (on regional scales) internal variability is generally more important than for projections of surface air temperature change.

A key quantity for any climate projection is the "signal-to-noise" ratio (Christensen et al, 2007), where the "signal" is a measure of the amplitude of the projected climate change, and the noise is a measure of the uncertainty in the projection. Higher signal-to-noise ratios indicate more robust projections of change and/or changes that are large relative to background levels of variability. Depending on the purpose, it may be useful to identify the noise with the total uncertainty, or with a specific component such as the internal variability). The evolution of the signal-to-noise ratio with lead-time depends on whether the signal grows more rapidly than the noise, or vice versa. Figure 11.4 (top right) shows that, when the noise is identified with the total uncertainty, the signal-to-noise ratio for surface air temperature is typically higher at lower latitudes and has a maximum at a lead time of a few decades (Cox and Stephenson, 2007; Hawkins and Sutton, 2009). The former feature is primarily a consequence of the greater amplitude of internal variability in mid-latitudes. The latter feature arises because over the first few decades, when forcing uncertainty is small, the signal grows most rapidly, but subsequently the contribution from forcing uncertainty grows more rapidly than does the signal, so the signal-to-noise ratio falls.

11.2.2 Uncertainty in Near-Term Climate Predictions

Initialized climate predictions attempt to predict both the externally-forced and internally-generated near-term variation in climate variables. Predictions are subject to all the sources of uncertainty that affect climate projections, but the contribution from internal variability must be considered separately. The purpose of initialization is to exploit the *predictability* of internal variability (Box 11.1 and Section 11.3.1) with the goal of reducing the uncertainty in predictions, relative to that of projections. The extent to which this goal is achievable depends on a range of factors including the available observations (particularly of the ocean state), the quality of the climate model, and the assimilation and initialization procedure. Thus uncertainties arise from imperfect knowledge of the initial state and from model errors and uncertainties. Strategies to quantify these uncertainties have been developed and are the subject of active research (see Sections 11.2 and 11.3.1 for further discussion).

[INSERT FIGURE 11.4 HERE]

Figure 11.4: Sources of uncertainty in climate projections as a function of lead time. a) Projections of global mean decadal mean surface air temperature to 2100 together with a quantification of the uncertainty arising from internal variability (orange), response uncertainty (blue), and forcing uncertainty (green). b) shows the same results as in (a) but expressed as a percentage of the total uncertainty at each lead time. c), e), f) show results for: global mean decadal and annual mean precipitation, British Isles decadal mean surface air temperature, and boreal winter (December-February) decadal mean precipitation. d) shows signal-to-noise ratio for decadal mean surface air temperature for the regions indicated. The signal is defined as the simulated multi-model mean change in surface air temperature relative to the simulated mean surface air temperature in the period 1971–2000, and the noise is defined as the total uncertainty. See text and Hawkins & Sutton (2009,2010) for further details. This version of the figure is based on CMIP3 results and neglects the contribution from carbon cycle (and other biogeochemical) feedbacks to response uncertainty.

11.3 Near-Term Predictions

11.3.1 Decadal Climate Prediction

The scientific impetus for decadal prediction arises from improved understanding of the physical basis of long timescale variations in climate and improvements in climate models (Chapter 9), the availability of information on the state of the atmosphere, ocean and cryosphere (Chapters 2-4) and from predictability studies, early decadal forecasting attempts and from the development of multi-model and other approaches for combining, calibrating and verifying climate predictions. Decadal predictions are of interest for socio-economic reasons as discussed, for instance, in WMO (2009).

11.3.1.1 Predictability Studies

The innate behaviour of the climate system imposes limits on the ability to predict its evolution. Predictability studies indicate where and to what extent skillful climate predictions might be possible. Prognostic predictability studies analyze the time-dependent behaviour of actual or idealized predictions while diagnostic predictability studies are based on analyses (diagnoses) of observations of the climate system or on simulation results from climate models.

11.3.1.1.1 Prognostic predictability studies

The study of Griffies and Bryan (1997) is one of the earliest predictability studies of internally generated decadal variability in a coupled atmosphere/ocean climate model. It concentrates on the North Atlantic and the subsurface ocean temperature while the somewhat similar studies of Boer (2000) and Collins (2002) deal mainly with surface temperature. Long timescale temperature variability in the North Atlantic has received considerable attention (Figure 11.5a-c) together with its possible connection to the variability of the Atlantic Meridional Overturning Circulation (AMOC) in predictability studies by Grotzner et al., (1999), Collins and Sinha (2003), Pohlman (2004), Collins et al., (2006), Latif et al., (2006, 2007), Hawkins and Sutton, (2009), Msadek et al. (2010) and Teng et al. (2011). There is a broad indication of predictability for sea-surface temperature (SST) in the North Atlantic while the predictability of the AMOC varies among models and, to some extent, with initial model states, ranging from several to 10 or more years. The predictability of the North Atlantic SST is typically weaker than that of the AMOC and the connection between the predictability of the AMOC and the SST is inconsistent among models.

Prognostic predictability studies of the Pacific are less plentiful even though Pacific Decadal Variability (PDV) itself has received considerable study. Sun and Wang (2006) suggest that some of the variability linked to the Pacific Decadal Oscillation (PDO) can be predicted approximately 7 years in advance. Teng and Branstator (2011) investigate the predictability of the first two EOFs of annual mean SST and upper ocean temperature, identified with PDV, and find predictability of the order of 6–10 years. Meehl et al.

(2010) focus on the low-frequency decadal component of SST, including both forced and internally generated components, in the broader Pacific region (to 40°S). Power and Colman (2006) found that off-equatorial multi-year variability in the eastern Pacific of their climate model was largely driven by preceding multi-year variability in ENSO. The resulting variability in off-equatorial SST could be predicted more than one year in advance, while sub-surface ocean temperature variability (associated with the excitation of low-frequency equatorially-trapped Rossby waves) could be predicted several years in advance. McGregor et al. (2008; 2009) presented evidence that off-equatorial wind-stress changes in the Pacific can lead to small but predictable changes to equatorial SST and to near-zonal changes in the equatorial thermocline. While evidence for multi-year predictability in the Pacific Ocean away from the equator is strong, Power et al. (2006) were unable to detect any predictability of internally generated in decadal changes to ENSO teleconnections to Australian rainfall.

Hermanson and Sutton (2010) report that predictable signals in different regions and for different variables may arise from differing initial conditions. Ocean variables exhibit predictability for several years or more compared to other variables in two case studies. Branstator and Teng (2010) analyze upper ocean temperatures, and some SSTs, for the North Atlantic, North Pacific and the tropical Atlantic and Pacific in the NCAR model. Predictability associated with the initial state of the system decreases while that due to the forced component increases with time (Figure 11.5d). The "cross-over" time is longer in extratropical (7–11 years) compared to tropical (2 years) regions and in the North Atlantic compared to the North Pacific.

[INSERT FIGURE 11.5 HERE]

Figure 11.5: (a) Control run MOC (black line), prediction results (thin coloured lines) and ensemble mean (red line) in predictability experiments with the GFDL model. (b) predictability measures of the MOC (black) and of North Atlantic subsurface temperature, heat content and sea surface height (from Msadek et al), (c) initial condition (green) and externally forced (blue) components of predictability of the North Atlantic MOC, 500m temperature and SST (from Teng et al.), (d) initial condition (green) and externally forced (blue) predictability for upper ocean temperature predictability in extratropical and tropical ocean basins from the NCAR model, (e) initial condition predictability for different models for N. Atlantic and N. Pacific upper ocean temperatures (from Branstator et al. 2011)

11.3.1.1.2 Diagnostic predictability studies

Because long data records are needed, diagnostic decadal predictability, studies based on observational data are few. Newman (2007) and Alexander et al. (2008) develop multivariate empirical Linear Inverse Models (LIMs) from observation-based SSTs and find predictability for ENSO and PDV type patterns that are generally limited to the order of a year although exceeding this in some areas. Tziperman et al. (2008) and Hawkins and Sutton (2009) apply similar methods to GFDL and Hadley Centre model output and find predictability of from one to several decades respectively for the AMOC and North Atlantic SST.

Branstator et al. (2011) use analog and multivariate linear regression methods to quantify the predictability of the internally generated component of upper ocean temperature in six coupled models. Results differ across models but offer some common areas of nominal predictability. Basin estimates indicate predictability for up to a decade in the North Atlantic and somewhat less in the North Pacific (Figure 11.5e).

The diagnostic "potential predictability" considers the ratio of long timescale variability to the total to indicate where long timescales are important and where their lack limits predictability. The potential predictability of the internally generated component for temperature is studied in Boer (2000), Collins (2002), Pohlman et al. (2004), Power and Colman (2006) and, in a multi-model context, in Boer (2004) and Boer and Lambert (2008). Power and Colman (2006) concluded that potential predictability in the ocean tended to be a minimum in the surface waters of the equatorial Pacific Ocean, but tends to increase with latitude and depth. Multi-model results for both externally forced and internally generated components are studied in Boer (2010) and Figure 11.6 displays the geographic distribution of potential predictability for temperature based on CMIP5 simulations. Long-timescale potential predictability for precipitation is weak and associated with the forced component.

[INSERT FIGURE 11.6 HERE]

Figure 11.6: Contributions to decadal potential predictability from the externally forced component (upper panel), internal generated component (middle panel) and both together (lower panel). Multi-model results from CMIP3.

11.3.1.1.3 Summary

At long timescales, predictability studies are based mainly on coupled models. Results are model dependent although there are commonalities while multi-model approaches give a "consensus" view. There is evidence of predictability on decadal timescales for both the externally forced and internal generated components of temperature with the former dominating. Long timescale predictability for precipitation is weak and due mainly to the forced component. Predictability of temperature associated with the initial state of the system is decreases with time while that due to the forced component increases, with average cross-over times of the order of 4–9 years.

11.3.1.2 Climate Prediction on Seasonal to Decadal Timescales

11.3.1.2.1 Seasonal to decadal prediction

Seasonal model-based predictions for the globe are routinely produced by some twelve WMO "Global Producing Centres (GPCs) for Long Range Forecasts" as well as by other global and regional centres. Such results are from dynamical systems, however, they are typically post-processed by statistical methods (Stephenson et al., 2005; Lang and Wang, 2010; Wang and Fan, 2009. Statistical methods alone are used to produce forecasts (van den Dool, 2007; Sun and Chen 2011). Very similar methodologies are used for decadal predictions.

11.3.1.2.2 Initial conditions

A typical seasonal, interannual or decadal prediction consists of an ensemble of forecasts produced by integrating a climate model forward in time from a set of observation-based initial conditions. As forecast range increases, processes in the ocean become increasingly important and the sparseness, non-uniformity and secular change in sub-surface ocean observations is a challenge (Meehl et al., 2009; Murphy et al., 2010) and can lead to differences among ocean analyses (Stammer 2006). Approaches to ocean initialization range from assimilating only SSTs and relying on ocean transports to initialize the sub-surface ocean indirectly (Keenlyside et al. 2008); forcing an ocean model with atmospheric observations (being tested at NCAR and MPI) and direct assimilation or insertion of ocean reanalyses. Most seasonal and decadal predictions systems determine initial states separately for the atmosphere and ocean although more sophisticated, fully coupled data assimilation schemes (e.g., Sugiura et al., 2009; Zhang et al., 2007) are being investigated.

Dunstone and Smith (2010) investigate the impact of SST and subsurface ocean data in an idealized experiment and find the expected improvement in skill when sub-surface information is used. Assimilation of atmospheric data, however, gives little impact after the first year. Section 1.3.2 discusses this for actual forecasts. The initialization of sea ice, snow cover, frozen soil and soil moisture may all contribute to predictive skill beyond the seasonal timescale although direct initialization of these variables has not yet been attempted.

11.2.1.2.3 Full-field and anomaly initialization

Models may be initialized using *full-field* or *anomaly* approaches. Forecasts are represented as $Y(t_j,\tau)$ where t_j is the start date and τ is the forecast range, i.e., the time after the beginning of the forecast. The corresponding observation-base values are represented as $X(t_j,\tau)$. Full-field initialization constrains the model values to be near the observation-based values with $Y(t_j,0) \approx X(t_j)$ at initial time $\tau = 0$. However, model results "drift" from their initial observation-based state toward the model's climate on timescales of a few years and this drift may be sufficient to confound the evolution of the forecast. An empirical a posteriori drift adjustment is typically applied (Section 11.3.2) to remove the drift.

Model drift may be at least partially offset by using anomaly initialization in which observed anomalies are added to the model climate (Smith et al. 2007; Pohlmann et al., 2009; Mochizuki et al., 2010). In that case $Y(t_j,0) \approx <Y> + (X(t_j) - <X>) = (<Y> - <X>) + X(t_j)$, where $<Y>$ and $<X>$ are the model and observation-based climatologies respectively. As modeled and observed climatologies approach one another so do the two initialization methods. The relative merits of the two approaches have yet to be quantified in terms of the quality of the resulting decadal forecasts.

11.3.1.2.4 Ensemble generation

An ensemble of initial conditions is generated in order to sample the probability distribution of the observation-based initial state of a variable and the ensuing ensemble of forecasts to characterize its evolution (Fig 11.2-3). Ensemble generation is important in seasonal prediction (Stockdale et al., 1998; Stan and Kirtman, 2008) but not yet fully investigated for decadal prediction. Methods being investigated include adding random perturbations to initial conditions, using atmospheric states displaced in time, using parallel assimilation runs, (Doblas-Reyes et al., 2011) and perturbing ocean initial conditions by ensemble assimilation (Mochizuki et al., 2010; Zhang et al., 2007). Perturbations leading to rapidly growing modes, common to weather forecasting, are also being investigated (Kleeman et al., 2003; Vikhliaev et al., 2007; Hawkins and Sutton, 2009). The uncertainty associated with a model's representation of the climate system may be partially represented by the perturbed physics (Stainforth et al., 2005, Murphy et al., 2007) or stochastic physics (Berner et al., 2008) approaches applied to decadal predictions (Doblas-Reyes et al., 2009; Smith et al., 2010).

The multi-model approach combines ensembles of predictions from a collection of models thereby increasing the sampling of both initial conditions and model properties. Multi-model approaches are used across timescales ranging from seasonal- interannual (eg. DEMETER, Palmer et al. 2004), to seasonal-decadal (e.g., ENSEMBLES, van der Linden, and Mitchell, 2009), in climate change simulation (e.g., IPCC2007, Chapter 10, Meehl et al., 2007) and in the ENSEMBLES and CMIP5-based decadal predictions assessed in Section 11.3.2.

11.3.2 Prediction Quality

11.3.2.1 Decadal Prediction Experiments

Decadal prediction for specific variables can be made by exploiting empirical relationships based on past observations as well as expected physical relationships. Predictions of the North Pacific Ocean temperatures have been achieved using prior wind stress observations (Schneider and Miller, 2001). Regional predictions of surface temperature have been made based on projected changes in external forcing and the state of ENSO (Lean and Rind, 2009; Krueger and von Storch, 2011).

Predictions for a range of variables other than temperature can be achieved using dynamical models that simulate the climate system based on the fundamental physical principles. Evidence for skilful interannual to decadal temperature predictions using dynamical models forced only by previous and projected changes in anthropogenic greenhouse gases and aerosols and natural variations in volcanic aerosols and solar irradiance was reported by Lee et al. (2006), Raisanen and Ruokolainen (2006) and Laepple et al. (2008).

Additional skill could be realized by initializing the models with observations to also predict natural internal variability and to correct the model's response to previous changes in radiative forcing (Smith et al., 2007; Hawkins and Sutton, 2009). The recent recognition that decadal climate prediction is important motivated the research community to design coordinated experiments. The ENSEMBLES project (van der Linden and Mitchell, 2009) has conducted a multi-model decadal hindcast study, and the Coupled Model Intercomparison Project phase 5 (CMIP5) proposed a coordinated experiment that focuses on decadal, or near-term, prediction (Meehl et al., 2009; Taylor et al., 2008; 2011). Prior to these initiatives, a few pioneering attempts at initialized decadal prediction have been made (Pierce et al., 2004; Troccoli and Palmer, 2007; Smith et al., 2007; Pohlmann et al., 2009; Keenlyside et al., 2008; Mochizuki et al., 2010). Results from the CMIP5 coordinated experiment are the basis for the assessment reported here.

Both ENSEMBLES and the CMIP5 near-term prediction performed a series of ten-year hindcasts initialized by observations every five years starting near 1960. Initialized runs from three initial conditions, 1960, 1980, and 2005, are further extended to 30 years, to the range more likely to be dominated by anthropogenic external forcing. Since the practice of decadal prediction is in its infancy, details of how to initialize the models were left to the discretion of the modeling groups. In CMIP5 experiments, volcanic aerosol and solar cycle variability are prescribed along the integration using actual values up to 2005, and assuming a climatological 11-year solar cycle and a background volcanic aerosol load in the future. These forcings are shared with the uninitialized CMIP5 historical runs started from pre-industrial control simulations enabling an assessment of impact of initialization. The specification of the volcanic aerosol load and the solar irradiance in the hindcasts gives an optimistic estimate of the forecast quality with respect to an operational prediction system. Table 11.3.2.1 summarizes the initialization methods used in the CMIP5 near-term experiment. The coordinated nature of ENSEMBLES and CMIP5 experiments offer a good opportunity to study *multi-model* ensembles (van Oldenborgh et al., 2011 – under review; García-Serrano and Doblas-Reyes, 2012 – under review), although some modelling groups have adopted perturbed physics approaches in decadal predictions (Smith et al., 2010). The impact of the different approaches on decadal predictions has yet to be assessed.

[INSERT TABLE 11.1]

Table 11.1: Initialization methods used in models that entered CMIP5 near-term experiments.

One of the most serious difficulties in climate prediction consists in dealing with the so-called climate drift in initialized predictions. When initialized with states close to the observations, models drift towards their preferred imperfect climatology, leading to systematic errors in the forecasts. The time scale of the drift is in most cases a few years (e.g., Figure 1 of Doblas-Reyes et al., 2010) and the magnitude is comparable to signals to be predicted. Biases can be removed by an a posteriori empirical correction computed from a collection of past forecasts or hindcasts.

Bias adjustment is a method of statistically post-processing forecasts that linearly corrects for model drift (e.g., Stockdale, 1997). A temperature forecast, for instance, may be represented as $T(\tau) = \overline{T}(\tau) + T'(\tau)$ where the forecast range τ is the time beyond the initial time. The overbar represents the average over the hindcasts and $T'(\tau)$ the difference from the average. The observed temperatures corresponding to the forecasts are similarly expressed as $T_o(\tau) = \overline{T}_o(\tau) + T_o'(\tau)$. The average error or bias in this context is $b(\tau) = \overline{T}(\tau) - \overline{T}_o(\tau)$ that estimates the rate at which the model drifts away from the observed climate and towards the model climate on average as the forecast evolves. This drift is subtracted from the forecast to give a bias-adjusted prediction $\hat{T}(\tau) = T(\tau) - b(\tau) = \overline{T}_o(\tau) + T'(\tau)$. The approach assumes that the model bias is stable over the prediction period (from 1960 onward in the CMIP5 experiment). This might not be the case, for instance, if the predicted temperature trend differs from the observed trend (Fyfe et al., 2012 - accepted).

To reduce these problems, many of the early attempts at decadal prediction (Smith et al., 2007; Keenlyside et al., 2008; Pohlmann et al., 2009; Mochizuki et al., 2010) used an approach called anomaly initialization (Schneider et al., 1999; Pierce et al., 2004; Smith et al., 2007). The anomaly initialization approach attempts to circumvent model drift and the need for a time-varying bias correction. The models are initialized with observed anomalies added with some empirical method to the model climate. The mean model climate state is then subtracted to obtain forecast anomalies. In both approaches, full or anomaly initialization, the forecast information essentially consists of the evolution of the forecast *anomaly,* i.e., $T'(\tau)$. Sampling error in the calculation of the means affects the success of these approaches. Relative merits of anomaly versus "*full*" initialization approaches have yet to be quantified (Anderson et al. 2009). Ideally, model improvements are expected to reduce and ultimately eliminate the need for bias correction or anomaly initialization.

[PLACEHOLDER FOR SECOND ORDER DRAFT: Include assessment on anomaly vs. full initialization when studies become available].

11.3.2.2 Forecast Quality Assessment

A distinction between model validation and forecast quality assessment is typically made (NRCNA, 2010). The quality of a forecast system is assessed by estimating the accuracy, skill and reliability of a set of hindcasts (Jollife and Stephenson, 2003). No single metric can provide a complete picture of prediction quality, even for a single variable. A suite of metrics needs to be considered, particularly when a forecast system is compared with others or with previous versions. The accuracy of a forecast system refers to the precision with which the forecast system tends to match the observed changes that the system is trying to predict. The skill is the accuracy of the system relative to the accuracy of some reference prediction method (e.g., climatology or persistence). The reliability measures how well the predicted probability distribution matches the observed relative frequency of the forecast event.

The assessment of forecast quality depends on what characteristics of the prediction are of greatest interest to those who would use the information. WMO's Standard Verification System (SVS) for Long Range Forecasts (LRF) (2002) outlines specifications for long-range (sub-seasonal to seasonal) forecast quality assessment. For deterministic forecasts, the recommended metrics are the mean square skill score and the relative operating characteristics (ROC) curve and area under the ROC curve (Mason and Weigel, 2009) for the accuracy and the correlation for skill. For probabilistic forecasts, the recommended metrics are the ROC area, the Brier skill score and the reliability diagram. All these measures are described in Jolliffe and Stephenson (2003) and Wilks (2006). Measures of reliability are related to the spread of the system. For dynamical ensemble systems, a useful measure of the characteristics of an ensemble forecast system is its spread. The relative spread can be described in terms of the ratio between the mean spread around the ensemble mean and the ensemble-mean RMSE, or spread-to-RMSE ratio. A ratio of one is considered a desirable feature for a Gaussian-distributed variable of a well-calibrated prediction system (Palmer et al., 2006). It has been recently emphasized the importance of using statistical inference in forecast quality assessments. This is even more important when both the small samples available and the small number of degrees of freedom are taken into account. Confidence intervals for the scores are typically computed using either parametric or bootstrap methods (Lanzante, 2005; Jolliffe, 2007).

11.3.2.3 Pre-CMIP5 Decadal Prediction Experiments

Early decadal prediction studies found little additional predictability from initialization, over that due to changes in radiative forcing, on global (Pierce et al., 2004) and regional scales (Troccoli and Palmer, 2007), but neither study considered more than two start dates. More comprehensive tests, which considered at least nine different start dates indicated generalized temperature skill (Smith et al., 2007, 2010; Keenlyside et al., 2008; Pohlmann et al., 2009; Sugiura et al., 2009; Mochizuki et al., 2010; van Oldenborgh et al., 2011 – under review; Doblas-Reyes et al., 2011; García-Serrano and Doblas-Reyes, 2012 – under review; García-Serrano et al., 2012 - submitted; Guémas et al., 2012 - submitted). That skill was enhanced by the initialization mostly over the ocean in the North Atlantic and subtropical Pacific.

The ENSEMBLES multi-model consists of four forecast systems: CERFACS, ECMWF, IFM-GEOMAR and Met Office with the HadGEM2 model (van Oldenborgh et al., 2011 – under review). Three-member ensemble hindcasts were run for ten years starting on November 1 from 1960 to 2005 every five years. Volcanic aerosol concentrations from eruptions before the analysis date were relaxed to zero with a time scale of one year in the IFM-GEOMAR system (Keenlyside et al., 2008), while the other three models did not include any volcanic aerosol effect. In all cases, the effects of eruptions during the hindcasts were not included to reproduce a realistic forecasting context. This is a major difference from the CMIP5 experiment. Three of the four models (the ECMWF, Met Office and CERFACS systems) used a full initialisation strategy. In contrast, IFM-GEOMAR used observed SST anomaly information to generate the initial conditions. A second ENSEMBLES contribution (DePreSys; Smith et al., 2010) was run by the Met Office using a nine-member ensemble of HadCM3 model variants sampling modelling uncertainties through perturbations to poorly constrained atmospheric and surface parameters. Ten-year long hindcasts were started on the first of November in each year from 1960 to 2005. In order to assess the impact of initialization an additional parallel set of hindcasts (referred to as NoAssim) with the same nine model versions was run. The NoAssim hindcasts are identical to those of DePreSys except that they are not explicitly initialized with the contemporaneous state of the climate system, the initial conditions obtained from the restarts of the corresponding long-term climate change integrations. NoAssim is used to assess the impact of the initial conditions in near-term climate prediction.

11.3.2.4 CMIP5 Decadal Prediction Experiment

Figure 11.7 shows the global-mean temperature correlation for the CMIP5 decadal forecasts. While the correlation of both Assim and NoAssim is significant, the Assim correlation is above the NoAssim one, especially in the early forecast ranges. A similar conclusion holds for the DePreSys Assim and NoAssim experiments. The high correlation is due to the almost monotonic increase in temperature. A comparison with the DePreSys and ENSEMBLES time series explains the higher correlation of the CMIP5 predictions observed in the first half of the forecast period. Both DePreSys and ENSEMBLES do not properly reproduce the impact of volcanoes, in particular for Pinatubo, because the volcanic aerosol load is not specified during the prediction as in the case of the CMIP5 experiments.

[INSERT FIGURE 11.7 HERE]

Figure 11.7: Ensemble-mean correlation with the observations (left column) and time series of 2–5 (middle column) and 6–9 (right column) year average predictions of the global-mean temperature (top row), AMV (middle row) and IPO (bottom row) from the ENSEMBLES (black), CMIP5 Assim (dark green) and NoAssim (light green) and DePreSys Assim (dark purple) and NoAssim (light purple) forecast systems. The AMV index was computed as the SST anomalies averaged over the region Equator-60ºN and 80º–0ºW minus the SST anomalies averaged over 60ºS–60ºN (Trenberth and Shea 2006). The IPO index is the principal component of the leading EOF of each model using SSTs in the region 50ºS–50ºN / 100ºE–290ºE where the mean SST over 60ºS–60ºN have been previously removed. Predictions initialized once every five years over the period 1960–2005 have been used. The CMIP5 multi-model includes experiments from the HadCM3, MIROC5, MIROC4h and MRI-CGCM3 systems. The one-side 95% confidence level is represented in grey, where the number of degrees of freedom has been computed taking into account the autocorrelation of the observational time series. The observational time series, GISS global-mean temperature and ERSST for the AMV and IPO, are represented with red (positive anomalies) and blue (negative anomalies) vertical bars, where a four-year running mean has been applied for consistency with the time averaging of the predictions.

The systems in Figure 11.8 have significant skill over large regions, especially over the tropical oceans and the North Atlantic, but also over large parts of the continents. The CMIP5 multi-model ensemble mean has a similar skill distribution as DePreSys and ENSEMBLES. The impact of the initialization can be estimated in a comparison between Assim and NoAssim. The skill differences, although showing some regions with negative values, are mainly positive for the three forecast periods depicted. However, given that the differences are small and the limited sample used, they are not statistically significant with 95% confidence. The small differences reveal that most of the skill in temperature is due to the changing radiative forcing, although an overall larger skill is found for the Assim experiment, in agreement with improvements due to initialization found over the North Atlantic in DePreSys (Smith et al., 2010).

[INSERT FIGURE 11.8 HERE]

Figure 11.8: Near surface air temperature ensemble-mean correlation of the CMIP5 multi-model for the Assim (left column), NoAssim (middle column) and their difference (right column) for the first year (top row) and the averaged 2–5 (middle row) and 6–9 (bottom row) years forecast period. The CMIP5 multi-model includes experiments from the HadCM3, MIROC5, MIROC4h and MRI-CGCM3 systems. The black dots correspond to the points where the correlation is statistically significant with 95% confidence using a one-sided (two sided for the correlation differences) parametric test. A Fisher Z-transform of the correlations has been applied before applying the inference test to the correlation differences. A combination of GHCN (Fan and van den Dool, 2007), ERSST (Smith and Reynolds 2003) and GISS (Hansen et al., 2010) temperatures is used as a reference. The correlation has been computed with hindcasts started over the period 1960–2005. The left- (right-) hand side colour bar is for the correlations (differences between the correlations).

Figure 11.9 shows the ensemble-mean correlation for the precipitation over land averaged over different forecast periods. The values are much lower than for the temperature, with very few regions showing statistically significant values. It is difficult to single out regions with large positive differences, apart from those in the first forecast year that are typically influenced by ENSO.

[INSERT FIGURE 11.9 HERE]

Figure 11.9: Land precipitation ensemble-mean correlation of the CMIP5 multi-model for the Assim (left column), NoAssim (middle column) and their difference (right column) for the first year (top row) and the averaged 2–5 (middle row) and 6–9 (bottom row) years forecast period. The CMIP5 multi-model includes experiments from the HadCM3, MIROC5, MIROC4h and MRI-CGCM3 systems. The black dots correspond to the points where the correlation is statistically significant with 95% confidence using a one-sided (two sided for the correlation differences) parametric test. A Fisher Z-transform of the correlations has been applied before applying the inference test to the correlation differences. GPCC precipitation is used as a reference. The correlation has been computed with hindcasts started over the period 1960–2005. The left- (right-) hand side colour bar is for the correlations (differences between the correlations).

The initialization has been suggested to improve skill mainly through atmospheric teleconnections from improved surface temperature predictions in the North Atlantic and tropical Pacific (Smith et al., 2010; Dunstone et al., 2011). Skill in predicting north Atlantic SST is thought to be related to skill in predicting the AMOC (Knight et al., 2005), but this cannot be verified directly because of a lack of observations. However, using proxies of the AMOC, a multi-model can skilfully predict it up to five years ahead using an ensemble of initialized model hindcasts, while uninitialized experiments failed to capture the signal. The lack of adequate observations (Zhang et al., 2007), though, might also limit the initialization of the predictions.

The skill in the North Atlantic basin in Figure 11.8 is consistent with previous studies (e.g., Knight et al., 2005) linking Atlantic multi-decadal variability (AMV) with variations of the AMOC. An AMV index, computed as the SST anomalies averaged over the region Equator-60ºN and 80º–0ºW minus the SST anomalies averaged over 60ºS–60ºN (Trenberth and Shea 2006), shows decadal variability and has multi-year predictability (Murphy et al., 2010). Figure 11.7 shows that the CMIP5, ENSEMBLES multi-model and DePreSys ensemble mean have a similar skill as a function of the forecast time, which is statistically significant for all forecast times showed and is generally larger correlation than the single-model forecast systems (García-Serrano and Doblas-Reyes 2012 – under review). CMIP5 Assim has the highest skill of all the systems. However, the differences in skill between the three systems are subtle and not statistically significant as the uncertainty in the correlation is large. The initialization improves the AMV skill over the first few forecast years, although the CMIP5 and DePreSys NoAssim hindcasts are also significantly skilful at longer lead times highlighting the relevance of the external forcing. The AMV has been connected to multi-decadal variability of Atlantic tropical cyclones (Dunstone et al., 2011), and initialization of the sub-polar Atlantic provides skill in an idealized predictability study of Atlantic tropical storm frequency (Dunstone et al., 2011), suggesting that the AMV was behind the skill found in hindcasts of multi-year North Atlantic tropical storm frequency (Smith et al., 2010).

A comparison of the AMV ensemble-mean correlation for DePreSys using one- and five-year intervals between start dates shows that, although a five-year interval sampling allows to estimate the level of skill, local maxima along the forecast time might well be due to poor sampling of the start dates (García-Serrano and Doblas-Reyes, 2012 – under review). Figure 11.10d shows the temperature skill for DePreSys when one start date per year is used. A comparison with the skill of Panel b indicates that the spatial distribution of the skill does not change substantially with the different start date frequency, although the values are slightly reduced in the results with yearly start dates. The low sampling frequency of the start dates is one of the difficulties of the core CMIP5 decadal prediction experiment. Apart from the poor sampling of the start dates, the length of the forecasting period is limited to the period over which reasonably accurate estimates of the ocean initial state can be made, which starts around 1960. This fact also limits the sample size to estimate the forecast quality.

[INSERT FIGURE 11.10 HERE]

Figure 11.10: Near surface air temperature ensemble-mean centred correlation for DePreSys b) with five-year intervals between start dates and d) with one-year intervals between start dates, for the forecast period 2-5 years. A combination of GHCN (Fan and van den Dool, 2007), ERSST (Smith and Reynolds, 2003) and GISS (Hansen et al., 2010) temperatures is used as a reference. The correlation has been computed with hindcasts started over the period 1960–2005.

Pacific decadal variability is also associated with potentially important climate impacts, including rainfall over America, Asia, Africa and Australia (Power et al., 1999; Deser et al., 2004). The combination of Pacific and Atlantic variability and climate change appears to explain much of the multidecadal US drought frequency (McCabe et al., 2004) including key events like the American dustbowl of the 1930s (Schubert et al., 2004). In a prediction context, Sugiura et al. (2009) report skill in hindcasts of the PDO, which is ascribed to the interplay between Rossby waves and a clockwise propagation of ocean heat content anomalies along the Kuroshio-Oyashio extension and subtropical subduction pathway. However, as Figure 11.8 shows, the central North Pacific is one of the regions with the lowest skill worldwide. Guémas et al. (2012) argue that this regional minimum is associated with the failure of the forecast systems to capture the largest warming events in the North Pacific beyond a few months into the forecast. Van Oldenborgh et al. (2011 – under review) reported significant skill of the IPO in the ENSEMBLES multi-model. Figure 11.7 suggests, however, that the ensemble-mean skill is barely significant for all forecast systems and that there is no consistent impact of the initialization.

[PLACEHOLDER FOR SECOND ORDER DRAFT: Include figure with CMIP5 global and North Atlantic ocean heat content results (time series, reliability and skill) and discussion].

[PLACEHOLDER FOR SECOND ORDER DRAFT: Responding to the gain in decadal skill in certain regions due to the initialization, a coordinated quasi-operational initiative has been organized. Different institutions regularly exchange initialized decadal predictions.]

11.3.2.5 Realizing Potential

Although idealized model experiments show considerable promise for predicting internal variability, realizing this potential is a challenging task. There are 3 main hurdles: (1) the limited availability of data to initialize and verify predictions, (2) limited progress in initialization techniques for decadal predictions and (3) dynamical model shortcomings.

It is expected that the availability of temperature and salinity data in the top two km of the ocean through the global deployment of Argo floats will give a step change in our ability to initialize and predict ocean heat and density anomalies (Zhang et al., 2007). Another important recent advancement is the availability of altimetry data. Argo and altimeter data only became available in 2000 and 1992 respectively, so an accurate estimate of their impact on real forecasts has to wait (Dunstone and Smith, 2010).

Improved initialization of other aspects such as sea ice, snow cover, frozen soil and soil moisture, may also have potential to contribute to predictive skill beyond the seasonal timescale. This could be investigated, for example by using measurements of soil moisture from the planned Soil Moisture and Ocean Salinity (SMOS) satellite, or by initializing sea-ice thickness with observations from the planned CryoSat-2 satellite.

Many of the current decadal prediction systems use relatively simple initialization schemes and do not adopt fully coupled initialization/ensemble generation schemes. Sophisticated assimilation schemes, such as 4DVAR (Sugiura et al., 2008) and ensemble Kalman filter (Zhang et al., 2007), offer opportunities for fully coupled initialization including assimilation of variables such as sea ice, snow cover and soil moisture.

Bias correction is used to reduce the effects of model drift, but the non-linearity in the climate system (e.g., Power, 1995) might limit the effectiveness of bias correction and thereby reduce the forecast quality. Understanding and reducing both drift and systematic errors is important, as it is also for seasonal-to-interannual climate prediction and for climate change projections. While improving models is the highest priority, efforts to quantify the degree of interference between model bias and predictive signals should not be overlooked.

11.4 Near Term Projections

11.4.1 Introduction

In the previous section (Section 11.3) a limited number of predictions (i.e., in which internal variability was initialized) for the period 2016–2025 were presented. In this section we assess climate change projections driven by scenarios of anthropogenic forcing in which the internal variability has not been initialized. Most emphasis is given to the period 2016–2035, though some information on projected changes before and after this period (up to mid-century) is assessed. Longer-term projections are assessed in Chapters 12 and 13. The crucial questions assessed in this section are: *what is the externally forced near-term signal, how large is it compared to natural variability, does the signal emerge from natural variability during the near term, and thus can adaptation/impact studies reliably use these projections?* It is important to recognize that, from the point of view of climate impacts, the absolute magnitude of climate change may be less important than the magnitude relative to the local level of natural variability. Because many systems are naturally adapted to the background level of variability, it is changes that move outside of this range that are most likely to trigger impacts that are unprecedented in the recent past (e.g., Lobell and Burke, 2008, for crops). It follows that the future date at which the climate change signal reaches sufficient magnitude to "emerge" clearly from the noise of natural variability is an important issue for climate risk assessments, and for adaptation planning.

An important conclusion of the AR4 (Chapter 10, Section 10.3.1) was that near-term climate projections are not very sensitive to plausible alternative non-mitigation scenarios for greenhouse gas concentrations (specifically the SRES scenarios – see discussion of comparison with RCP scenarios in Chapter 1), i.e., in the near term different scenarios give rise to similar magnitude and patterns of climate change. For this reason, most of the projections presented in this chapter are based on one specific RCP scenario, RCP4.5. RCP4.5 was chosen because of its intermediate greenhouse gas forcing. However, the sensitivity of near term projections across the RCPs and to alternative scenarios, including for anthropogenic methane and aerosols, is discussed explicitly in Section 11.4.6.

In many of the plots presented below in Sections 11.4.2–11.4.5 an ad-hoc indication of uncertainty is provided using the spread of projected changes evident amongst the CMIP5 models – a so-called "ensemble of opportunity".

11.4.2 Atmosphere and Land Surface

11.4.2.1 Surface Temperature

11.4.2.1.1 Global mean surface air temperature

For a given greenhouse gas concentration scenario, different climate models project different rates of global mean surface air temperature change due to different representations of a wide range of processes, including radiative transfer, clouds, and physical climate feedbacks (see Chapters 9, 10 and 12). In addition, the climate forcing by aerosols and ozone cannot be specified as a global mean abundance, and hence climate models use different physical-chemical models to calculate the anthropogenic radiative forcing from emissions of short-lived species. 11.25 (a) shows projections for the CMIP5 models under RCP4.5. The projected rate of warming over the period 2016 to 2035 is 0.16–0.44 K/decade [PLACEHOLDER FOR SECOND ORDER DRAFT: To be updated]. However, this range provides only a very crude measure of the uncertainty in future global mean temperature change. In particular, it takes no account of model quality (Chapter 9), and there is no guarantee that the real world must lie within the range spanned by the CMIP5 models.

Quantifying the true uncertainty in future global mean temperature change is an important challenge. There are two main approaches. One involves applying weights to individual models according to some measure of their quality (See Chapter 9). A second approach, known as ASK (Allen et al, 2000; Stott and Kettleborough, 2002) is based on the use of results from detection and attribution studies (Chapter 10), in which the fit between observations and model simulations of the past is used to scale projections of the future. ASK may be viewed as a variant of the first approach, but it requires specific simulations to be carried out with individual forcings (e.g., anthropogenic greenhouse gas forcing alone). Only some of the centres participating in CMIP5 have carried out the necessary integrations. Biases in ASK derived projections may arise from model errors in simulating the patterns of response to different forcings.

Figure 11.11 (b) shows the projected range of global mean surface air temperature change derived using the ASK approach (Stott and Jones, 2011. [PLACEHOLDER FOR SECOND ORDER DRAFT: These results are from one model only – further models to be included], and compares this with the range derived from the CMIP5 models. In this case decadal means are shown. The 5–95% confidence interval for the projected rate of warming over period 2016 to 2035, based on the ASK method, is 0.14–0.25 K/decade. The lower and upper rates of warming are below the minimum and maximum rates obtained from the raw CMIP5 results, but the ±1 standard deviation range from CMIP5 falls within the 5–95% confidence interval derived from ASK. However, the ASK results do suggest that those CMIP5 models that warm most rapidly may be inconsistent with the observations. (This possibility is also suggested by comparing the models with the observed rate of warming since 1986, but see Chapter 10 for a full discussion of this comparison.) Lastly, Figure 11.11 also shows a statistical prediction for global mean surface air temperature, using the method of Lean and Rind (2009). This prediction is very similar to the CMIP5 multi-model mean.

[PLACEHOLDER FOR SECOND ORDER DRAFT: discussion of sensitivity of CMIP5 range to excluding or weighting models, as informed by Chapter 9; further discussion of statistical predictions, and discussion of possible near-term effects of large amplitude internal variability (e.g., AMO).]

[PLACEHOLDER FOR SECOND ORDER DRAFT: discuss possibility that RCPs may assume overly rapid decay of aerosols, and consequences for projected rate of warming.]

On the basis of the results shown in Figure 11.11, and assuming that radiative forcing does not depart strongly from the assumed scenario (see Sections 11.4.6 and 11.4.7), we conclude that in the absence of major volcanic eruptions, which would cause significant but temporary cooling, it is *likely* that, over the period 2016 to 2035, global mean surface air temperature will rise at an average rate in the range 0.1–0.3 K/decade. This range includes allowances, based on expert judgment, for the potential influence of model biases on the CMIP5 and ASK results. It is consistent with the AR4 SPM statement that "For the next few decades a warming of about 0.2°C per decade is projected for a range of SRES emission scenarios".

The ASK method is only useful for quantifying the uncertainty in large-scale and well observed variables such as global mean surface air temperature. Consequently, for the remaining projections in this chapter the spread amongst the CMIP5 models is used as a simple, but crude, measure of uncertainty. The extent of agreement between the CMIP5 projections provides some rough guidance about the likelihood of a particular outcome. But it must be kept firmly in mind that the real world could fall outside of the range spanned by these particular models. See Sections 11.4.6 and 11.4.7 for further discussion.

[INSERT FIGURE 11.11 HERE]

Figure 11.11: a) Projections of global mean, annual mean surface air temperature 1986–2050 (anomalies relative to 1986–2005) under RCP4.5 from CMIP5 models (grey lines, one ensemble member per model), with five observational estimates (HadCRUT3 – Brohan et al., 2006; ERA-Interim - Simmons et al., 2010; GISTEMP - Hansen et al., 2010; NOAA – Smith et al., 2008; 20th century reanalysis – Compo et al., 2011) for the period 1986–2010 (black lines); b) as a) but showing the range (grey shades, with the multi-model mean in white) of decadal mean CMIP5 projections using (where relevant) the ensemble mean from each model, and decadal mean observational estimates (black lines). An estimate of the projected 5–95% range for decadal mean global mean surface air temperature for the period 2016–2040 derived using the ASK methodology applied to simulations with the HadGEM2ES climate model is also shown (dashed black lines). The red line shows a statistical prediction based on the method of Lean and Rind (2009).

11.4.2.1.2 Regional and seasonal patterns of surface warming

The geographical pattern of near term surface warming simulated by the CMIP5 models (Figure 11.12) is consistent with previous IPCC reports and observational trends in a number of key aspects. First, temperatures over land increase more rapidly than over sea (e.g., Manabe et al., 1991; Sutton et al., 2007). Processes that contribute to this land-sea warming contrast are the ocean heat uptake (Lambert and Chiang, 2007), the partitioning of the surface energy budget over arid regions (e.g., Vidale et al., 2007), the nonlinearity of the moist-adiabatic lapse rate in a warming environment and its disproportionate influence over the ocean (Joshi et al., 2008), as well as radiative and cloud feedbacks associated with a reduction of relative humidity over land (Shimpo and Kanamitsu, 2009; Fasullo, 2010).

Second, the projected warming in wintertime shows a polar amplification that is particularly large over the Arctic. This feature is found in virtually all coupled model projections, but the CMIP3 simulations generally appeared to underestimate this effect in comparison to observations (Stroeve et al., 2007; Screen and Simmonds, 2010). Several studies have isolated mechanisms behind this amplification, which include: reductions in snow cover and retreat of sea ice (e.g., Serreze et al., 2007; Comiso et al., 2008); changes in atmospheric and oceanic circulations (Simmonds and Keay, 2009; Chylek et al., 2009; Chylek et al., 2010); and increases in cloud cover and water vapour (Francis et al., 2007; Schweiger et al., 2008). Most studies argue that changes in sea ice are central to the polar amplification - see Section 11.4.5 for further discussion. Further information about the regional changes in surface air temperature projected by the CMIP5 models is presented in the Atlas (Annex I).

[PLACEHOLDER FOR SECOND ORDER DRAFT: could include a table showing CMIP5 temperature ranges for 2016–2035, together with a measure of natural internal variability, for specific (continental scale) regions. A similar table will be in Chapter 12.]

[INSERT FIGURE 11.12 HERE]

Figure 11.12: CMIP5 multi-model ensemble median of projected changes in surface air temperature for the period 2016–2035 relative to 1986–2005 under RCP4.5 relative to the 2086–2005 period (left panels). The right panels show an estimate of the natural internal variability in the quantity plotted in the left panels (see Annex I Atlas for details of method). Hatching in left panels indicates areas where projected changes are less than one standard deviation of estimated natural variability of these 20-year differences.

As discussed in Sections 11.1, 11.2 and 11.4.1, the signal of climate change is emerging against the background of natural internal variability. The natural internal variability of surface air temperature is greater in some regions than others (see Chapters 9 and 10, and Figure 11.12). For example, it is greater at mid latitudes than in the tropics. This regional variation has implications for the emergence of the climate change signal. Information on the time at which a significant warming signal is expected to emerge in different regions was presented in tabular form in the AR4 (Chapter 11, Table 11.1). Consistent with the AR4, Mahlstein et al. (2011) recently showed using CMIP3 simulations that the earliest emergence of significant warming occurs in the summer season in low latitude countries (~25°S–25°N), and that in many low latitude regions significant local warming, relative to pre-industrial climate, has already occurred. Figure 11.13 quantifies the "Time of Emergence" (ToE) of the warming signal relative to the recent past (1986–2005), based on the CMIP3 [PLACEHOLDER FOR SECOND ORDER DRAFT: to be updated with CMIP5 results] projections. Over many tropical land areas the median time for a significant warming signal to emerge occurs by the 2030s, whereas over higher latitudes the median time is generally after 2040. Over North Africa and Asia emergence occurs sooner for the warm half-year (April-September) than for the cool half-year, consistent with Mahlstein et al (2011). ToE generally occurs sooner for larger space and time scales, because the variance of natural internal variability decreases with averaging (Section 11.2.3 and AR4, Chapter 10, Section 10.5.4.3). This tendency can be seen in Figure 11.13 by comparing the median value of the histograms for area averages with the area average of the median ToE inferred from the maps (e.g., for Region 3). The histograms also illustrate the large range of values for ToE that is implied by different CMIP3 models. This large range, which can be as much as 50 years, is a consequence of differences both in the magnitude of the warming signal simulated by the models (i.e., response uncertainty, see Section 11.2.3) and differences in the amplitude of simulated internal natural variability.

In summary, it is *very likely* that anthropogenic warming of surface air temperature over the next few decades will proceed more rapidly over land areas than over oceans, and that the warming over the Arctic in winter will be greater than the global mean warming. Relative to background levels of natural internal variability it is *likely* that the anthropogenic warming relative to the recent past will become apparent soonest in the summer season in low latitude countries.

[INSERT FIGURE 11.13 HERE]

Figure 11.13: Time of emergence of significant local warming derived from CMIP3 models under the SRES A1B scenario. Warming is quantified as the half-year mean temperature anomaly relative to 1986–2005, and the noise as the standard deviation of half-year mean temperature derived from a control simulation of the relevant model. Central panels show the median time at which the signal-to-noise ratio exceeds a threshold value of 2 for (left) the October-March half year and (right) the April-September half year, using a spatial resolution of 5° x 5°. Histograms show the distribution of emergence times for area averages over the regions indicated obtained from the different CMIP3 models. Full details of the methodology may be found in Hawkins and Sutton (2011).

11.4.2.2 Free Atmospheric Temperature and Humidity

Changes in zonal mean temperature for the near-term period (2016–2035 compared to the base period 1986–2005) for the multi-model CMIP5 ensemble in Figure 11.14 shows a pattern similar to that in the IPCC AR4, with warming in the troposphere and cooling in the stratosphere of a couple of degrees that is significant even in the NT period. There is relatively greater warming in the tropical upper troposphere and northern high latitudes in both DJF and JJA as well as in the annual mean. Stratospheric cooling extends nearly into the upper troposphere in the high southern latitudes in JJA, but that is not evident in DJF or the annual mean.

For surface relative humidity in Figure 11.15, the CMIP5 multi-model ensemble shows changes on the order of several percent, with general decreases over most land areas, and increases over the oceans. Most of these changes are not significant for the near term, though this general pattern grows in amplitude with time and is projected to become more significant later in the 21st century (Chapter 12). Some of the greatest regional decreases occur over south Asia and southern South America in DJF, and over most of Europe, the U.S., northern South America, and southern Africa in JJA.

[INSERT FIGURE 11.14 HERE]

Figure 11.14: Zonal mean temperature differences, 2016–2035 minus 1986–2005, for the CMIP5 multi-model ensemble (°C), for a) DJF, b) JJA, and C) annual mean.

[INSERT FIGURE 11.15 HERE]

Figure 11.15: Surface atmospheric humidity differences, 2016–2035 minus 1986–2005, for the CMIP5 multi-model ensemble (%), for a) DJF, b) JJA, and C) annual mean.

11.4.2.3 The Water Cycle

As discussed in the AR4 (Meehl et al., 2007) and the IPCC Technical Paper on Climate Change and Water (Bates et al., 2008) a general intensification of the global hydrological cycle, and of precipitation extremes, are expected for a future warmer climate (e.g., Huntington, 2006; Williams et al., 2007; Wild et al., 2008; Chou et al., 2009; Déry et al., 2009; Seager et al., 2010; Wu et al., 2010). In this section we discuss projected changes in the time-mean hydrological cycle; changes in extremes, are discussed in Section 11.4.2.5

There are very close links between the global water and energy cycles. A rapid increase in atmospheric water vapour content (~ 7%K^{-1}) is an expected and observed response to warming, as a consequence of the Clausius–Clapeyron equation (Allen and Ingram, 2002; Trenberth et al., 2003). However, global mean precipitation and evaporation are projected to increase more slowly (1–3% K^{-1}), constrained by the atmospheric and surface energy budgets (Held and Soden 2006; Vecchi and Soden 2007; Lambert and Webb, 2007; Pall et al., 2007, O'Gorman and Schneider, 2008; Stephens and Ellis, 2008; Allan 2009; Wild and Leipert, 2010). There is evidence that shortwave forcings with little atmospheric radiative absorption including scattering anthropogenic aerosols, and natural solar variability, can be more effective than thermal greenhouse gas forcings in modifying the intensity of the global hydrological cycle (Lambert et al., 2008; Andrews et al., 2010; Bala et al., 2010; Previdi, 2010; Wild and Leipert, 2010; Frieler et al., 2011; O'Gorman et al., 2011). Further discussion of the global mean hydrological cycle is provided in Chapter 12 (Section 12.4.5.2).

AR4 projections of the spatial patterns of precipitation change in response to greenhouse gas forcing showed consistency between models on the largest scales, but large uncertainty on smaller scales. The consistent pattern was characterized by increases in wet regions (including the maxima in mean precipitation found in the tropics and at high latitudes), and decreases in dry regions (including large parts of the subtropics). Large uncertainties in the sign and magnitude of projected change were seen especially in regions located on the borders between regions of increases and regions of decreases.

Since the AR4 there has been considerable progress in understanding the factors that govern the spatial pattern of change in precipitation (P) and precipitation-evaporation (P-E), and inter-model differences in these patterns. The general pattern of wet-get-wetter (also referred to as "rich-get-richer", e.g., Held and Soden, 2006; Chou et al., 2009; Allan et al., 2010) and dry-get-drier has been confirmed, and it has been demonstrated that this pattern implies an enhanced seasonal precipitation range between wet and dry seasons in the tropics, and enhanced inter-hemispheric precipitation gradients (Chou et al., 2007). The basic structure of this pattern is a direct consequence of the increases in atmospheric water vapour, and enhancement of horizontal moisture transports (Held and Soden, 2006; Chou et al., 2009; Seager et al., 2010). However, this basic thermodynamic response is modified by dynamical changes in atmospheric circulation, some of which are less well understood and less consistent between different models (Chou et al., 2009; Seager et al., 2010; Williams and Ringer, 2010; Allan, 2012). The dynamical changes can increase or decrease P and P-E anomalies (Vecchi and Soden, 2007; Chou et al., 2009; Seager et al., 2010).

Some aspects of tropical circulation changes in response to GHGs, in particular a projected weakening of the tropical divergent circulation (Held and Soden, 2006; Vecchi and Soden, 2007) and an expansion of the Hadley Circulation (see Section 11.4.2.4.3, Lu et al., 2007) have important consequences for regional changes in the water cycle. For example, Lu et al. (2007) argue that poleward expansion of the Hadley Circulation leads to poleward expansion of the subtropical dry zone (defined in terms of zonal mean P-E; see also Seager et al., 2010). However, these circulations can be strongly impacted by radiative forcing agents other than GHGs (see Section 11.4.2.4), and even the GHG-driven changes in tropical circulation can be masked on multi-decadal time-scales by substantial internal climate variability (see Section 11.4.2.4).

It has recently been proposed that analysis of the energy budget, previously applied only to the global mean, may provide further insights into the controls on regional changes in P (Levermann et al., 2009; Muller and O'Gorman, 2011; O'Gorman et al., 2011). Muller and O'Gorman (2011) argue in particular that changes in radiative and surface sensible heat fluxes provide a guide to the local P response over land. Projected and observed patterns of oceanic precipitation change in the tropics tend to follow patterns of SST change because of local changes in atmospheric stability, such that regions warming more than the tropics as a whole tend to exhibit an increase in local precipitation, while regions warming less tend to exhibit reduced precipitation (Xie et al., 2010; Johnson and Xie, 2011).

A further result of the AR4 was that, especially in the near term, and on regional or smaller scales, the magnitude of projected changes in mean precipitation was small compared to the magnitude of natural internal variability - the signal-to-noise ratio is much lower than for projected changes in surface air temperature. Recent work has confirmed this result, and provided more quantification (e.g., Hawkins and Sutton, 2011; Deser et al., 2010; Hoerling et al., 2011; Power et al., 2011; Rowell, 2011). Hawkins and Sutton (2011) presented further analysis of CMIP3 results and found that internal variability contributes 50–90% of the total uncertainty in all regions for projections of decadal and seasonal mean precipitation change for the next decade, and is the most important source of uncertainty for many regions for lead times up to three decades ahead. Thereafter, response uncertainty is generally dominant. Forcing uncertainty (except for that relating to aerosols, see Section 11.4.7) is generally negligible for near term projections. The signal-to-noise ratio for seasonal mean precipitation is highest in the subtropics and at high-latitudes. Power et al (2011) and Tebaldi et al. (2011) demonstrated that some of the apparent differences between the CMIP3 models in their simulation of the sign of the precipitation response to greenhouse gas forcing occur in regions where the models tend to agree that the signal-to-noise ratio is low. These studies highlight that agreement on precipitation changes amongst models is more widespread than might have previously been interpreted from the AR4.

Rowell (2011) investigated relationships between model formulation and response uncertainty. He found that the contribution of response uncertainty to the total uncertainty (response plus internal variability) in local precipitation change is highest in the deep tropics, particularly over South America, Africa, the east and central Pacific, and the Atlantic. He also showed that over tropical land and summer mid-latitude continents the representation of SST changes, atmospheric processes, land surface processes, and the terrestrial carbon cycle all contribute to the uncertainty in projected changes in rainfall.

In addition to the response to greenhouse gas forcing, the forcing that arises from natural and anthropogenic aerosols has the potential to exert significant impacts on regional patterns of precipitation change (as well as on global mean precipitation, see above). Precipitation responses may arise as a consequence of temperature changes caused by aerosol effects on radiation and atmospheric heating, and/or as a direct consequence of aerosol effects on clouds (Chapter 7). Future emissions of aerosols and aerosol precursors are subject to large uncertainty, and further large uncertainties arise in assessing the responses to these emissions. These issues are discussed in Sections 11.4.4 and 11.4.7 (see also Chapter 14).

Figures 11.16 and 11.17 present projections of near term changes in precipitation from CMIP5. The basic pattern of wet regions tending to get wetter and dry regions tending to get dryer is apparent. However, the large response uncertainty is evident in the substantial spread in the magnitude of projected change simulated by different climate models (Figure 11.29). In addition, it is important to recognize - as discussed in previous sections - that models may agree and still be in error (e.g., Power et al., 2011). In particular, there is some evidence from comparing observations with simulations of the recent past that climate models might be underestimating the magnitude of changes in precipitation. This evidence is discussed in detail in Chapter 10 (Section 10.3.2), and could imply that projected future changes in precipitation are underestimated by current models; however, the magnitude of any underestimation has yet to be quantified, and is subject to considerable uncertainty.

Figures 11.16 and 11.17 also highlight the large amplitude of the natural internal variability of mean precipitation. Even for zonal means (Figure 11.29), the projected changes are substantially larger than the estimated standard deviation of internal variability only at high latitudes. On regional scales, the median projected changes are almost everywhere less than the estimated standard deviation of natural internal variability. The only exceptions are at northern high latitudes.

Overall, it is *more likely than not* that over the next few decades there will be increases in mean precipitation in regions and seasons where the mean precipitation is relatively high, and decreases in regions and seasons where mean precipitation is relatively low. However, it is likely that these changes will only be significant, relative to natural internal variability, on the largest spatial scales (e.g., zonal means), and changes in specific smaller regions may show departures from the large-scale pattern. Anthropogenic aerosols could have important complicating or dominant effects in some regions.

[INSERT FIGURE 11.16 HERE]

Figure 11.16: CMIP5 multi-model ensemble median of projected changes in precipitation for the period 2016–2035 relative to 1986–2005 under RCP4.5 in mm/day (upper panels). The lower panels show an estimate of the natural internal variability in the quantity plotted in the upper panels (see Annex I Atlas for details of method). Hatching in upper panels indicates projected changes are everywhere less than 2 times standard deviation of estimated natural variability**.**

[INSERT FIGURE 11.17 HERE]

Figure 11.17: CMIP5 multi-model projections of changes in annual mean zonal mean precipitation (mm/day) for the period 2016–2035 relative to 1986–2005 under RCP4.5. Vertical lines indicate median, inter-quartile and 5–95% ranges of the model responses. Shading indicates 1 standard deviation of the estimated natural internal variability (see Annex I Atlas for details of method).

11.4.2.3.1 Changes in evaporation, run-off, soil moisture, and specific humidity

As discussed in the AR4 (Meehl et al., 2007; Trenberth et al., 2007) and the IPCC Technical Paper on Climate Change and Water (Bates et al., 2008), global mean increases in evaporation are required to balance increases in precipitation in response to greenhouse gas forcing. Based upon bulk formula used in models, global evaporation is constrained by the Clausius Clapeyron equation to increase at around 7%/K. However, a more "muted" response, consistent with increases in global P, is achieved in CMIP3 models through small yet systematic decreases in wind stress and near surface temperature lapse rate and increases in relative humidity (Richter and Xie, 2008). Changes in evapotranspiration over land are influenced not only by the response to radiative forcing due to greenhouse gases, but also by vegetation responses to elevated CO_2 concentrations. Physiological effects of CO2 may involve both the stomatal response, which acts to restrict evapotranspiration (e.g., Field et al., 1995; Hungate et al., 2002; Cao et al., 2009, 2010; Lammertsma et al., 2011), and an increase in plant growth and leaf area, which acts to increase evapotranspiration (e.g., El Nadi, 1974). Simulation of the latter process requires the inclusion of a dynamic vegetation model. Evidence of the physiological response has been found in observed continental river runoff over the twentieth century, with positive trends that are consistent with a reduction of plant transpiration due to CO2-induced stomatal closure (Gedney et al., 2006).

[PLACEHOLDER FOR SECOND ORDER DRAFT: discuss impact of aerosol forcing on evaporation]

Soil moisture plays an important role in climate and the hydrological cycle, and directly influences evapotranspiration. In response to greenhouse gas forcing dry land areas tend show a reduction of evaporation and precipitation, accompanied by drying of the soil and an increase of surface temperature, as a result of the decrease in latent heat flux from the surface (e.g., Seneviratne et al., 2010). AR4 projections (Meehl et al., 2007) of annual mean soil moisture changes for the 21st century showed a tendency for decreases in the subtropics, southern South America and the Mediterranean region, and increases in limited areas of east Africa and central Asia. Changes seen in other regions were mostly not consistent or significant.

Changes in runoff arise from changes in precipitation and evapotranspiration. AR4 projections of 21st century runoff changes (Meehl et al., 2007) showed consistency in sign among models indicating a reduction in southern Europe and increases in Southeast Asia and at high northern latitudes. Projected changes in global mean runoff associated with the physiological effect of doubled carbon dioxide concentrations show increases of 6%–8% relative to pre-industrial levels, an increase that is comparable to or even larger than that simulated in response to radiative forcing changes (11 ± 6%) (Betts et al., 2007; Cao et al., 2010). Gosling et al. (2011) assess the projected impacts of climate change on river runoff from global and basin-scale hydrological models obtaining increase runoff with global warming in the Liard (Canada), Rio Grande (Brazil) and Xiangxi (China) basins and decrease for the Okavango (SW Africa).

The global distribution of the 2016-2035 changes in annual median evaporation, surface run-off, soil moisture and specific humidity from the CMIP5 multi-model ensemble under RCP4.5 are shown in Figure 11.18, together with estimates of the natural internal variability in these quantities. [NB: These are preliminary results based on a small number of models.] Changes in evaporation over land are mostly positive, except in north-western Africa, with largest values at northern high latitudes in agreement with projected temperature increases (Figure 11.18). Over the oceans evaporation is also projected to increase in most regions. Projected changes are larger than the estimated standard deviation of internal variability only at high latitudes and over the tropical oceans. Soil moisture shows decreases in most subtropical regions and in central Europe, and increases in the Maritime continent and other regions of northern mid-to-high latitudes, but in all regions the projected changes are smaller than the estimated natural internal variability.

Changes in near surface specific humidity are mostly positive with largest values at northern high latitudes in agreement with projected increases in temperature and evaporation. These changes are larger than the estimated standard deviation of internal variability almost everywhere: the only exceptions are north-western Africa and northern North Atlantic. Projections of runoff are currently based on only a few models, which show a high level of inconsistency, so this figure should be considered a placeholder at this stage.

Over the next few decades increases in near surface specific humidity are *likely*, and increases in evaporation are *more likely than not* in most regions. There is low confidence in projected changes in soil moisture and surface run off. Natural internal variability will continue to have a major influence on all aspects of the water cycle.

[INSERT FIGURE 11.18 HERE]

Figure 11.18: CMIP5 multi-model mean projected changes in annual mean runoff (%), evaporation (%), soil moisture (%) [and specific humidity (%)] for the period 2016–2035 relative to 1986–2005 under RCP4.5.

11.4.2.4 Atmospheric Circulation

11.4.2.4.1 Northern Hemisphere extra-tropical circulation

In the Northern Hemisphere extra-tropics, some AOGCMs indicate changes to atmospheric circulation from anthropogenic forcing by the mid-21st century resembling the projected response at the end of the 21st century. This includes a poleward shift of the jet streams and associated zonal mean storm tracks (Miller et al., 2006; Pinto et al., 2007; Paeth and Pollinger, 2010) and a strengthening of the Atlantic storm track (Pinto et al., 2007), Figure 11.19. However, there is considerable response uncertainty across AOGCMs for northern hemisphere storm track position (Ulbrich et al., 2008), stationary waves (Brandefelt and Kornich, 2008) and the jet streams (Miller et al., 2006; Ihara and Kushnir, 2009; Woollings and Blackburn, 2011). The response of the Northern Hemisphere jet streams and stationary waves can be sensitive even to small changes in model formulation (Sigmond et al., 2007), and to features that are known to be poorly simulated in many climate models, such as oceanic and stratospheric dynamics and high- and low-latitude physics (Rind, 2008; Woollings, 2010). Several stratosphere-resolving models exhibit an equatorward shift of the storm track and jet stream in response to greenhouse forcing (Huebener et al., 2007; Morgenstern et al., 2010).

Further, the response of NH extra-tropical circulation to even strong greenhouse forcing can be weak compared to recent multi-decadal changes (Miller et al., 2006; Woollings and Blackburn, 2011), with some AOGCMs simulating multi-decadal NAO variability as large as recently observed changes with no external forcing (Selten et al., 2004; Semenov et al., 2008). This suggests that natural variability could dominate the anthropogenically forced response in the near-term. Some studies have predicted a shift to the negative phase of the Atlantic Multidecadal Oscillation (AMO) over coming few decades, with potential impacts on atmospheric circulation around the Atlantic sector (Knight et al., 2005; Sutton and Hodson, 2005; Folland et al., 2009). It has also been suggested that there may be significant changes in solar forcing over the next few decades, which could have an important influence on NAO-related atmospheric circulation (Lockwood et al. 2011), although these predictions are highly uncertain (see Section 11.4.7).

The large response uncertainty and the potentially large influence of internal variability mean there is limited confidence in near-term projections of Northern Hemisphere circulation change.

11.4.2.4.2 Southern Hemisphere extra-tropical circulation

A key issue for in projections of near-term Southern Hemisphere (SH) extra-tropical circulation change is the extent to which changes driven by stratospheric ozone recovery will counteract changes driven by increasing greenhouse gases. Over the late-20th century and early 21st century, the impacts of stratospheric ozone depletion and increasing greenhouse gases have reinforced each other to contribute to a poleward expansion of SH tropospheric circulation (a positive *Southern Annular Mode, or SAM*; Gillet and Thompson, 2003; Shindell and Schmidt, 2004; Roscoe and Haigh, 2007; Fogt et al., 2009; Arblaster and Meehl, 2006). Recovery of the Antarctic ozone hole will impact the SH circulation in the austral summer, but there is expected to be competition between the ozone recovery producing an equatorward shift of the circumpolar trough around Antarctica, and ongoing increases of GHGs maintaining the southward-shifted circumpolar trough (Arblaster et al., 2011; McLandress et al., 2011). Even though a full recovery of the ozone hole is not expected until 2070 (Table 5.4, WMO, Rep. No. 52, 2010; see Chapter 12), it is likely that over the near-term there will be a reduced rate in the summertime poleward shift of the circumpolar trough compared to its movement over the past 30 years as indicated by AOGCMs and stratosphere-resolving models that suggest some near-term poleward shifts in SH extra-tropical storm tracks and winds (Figure 11.19).

11.4.2.4.3 Tropical circulation

As with near-term changes in SH extra-tropical circulation, a key for near-term projections of the structure of the Hadley Circulation (Figure 11.20) is the extent to which future stratospheric ozone recovery will counteract the impact of greenhouse gases. The poleward expansion of the Hadley Circulation, particularly of the SH branch during austral summer, during the later decades of the 20th century has been largely attributed to the combined impact of stratospheric ozone depletion (Thompson and Solomon, 2002; Son et al., 2008, 2009, 2010) and the concurrent increase in GHGs (Ablaster and Meehl, 2006; Arblaster et al., 2011) as discussed in the previous section. The poleward expansion of the Hadley Circulation driven by the response of the atmosphere to increasing GHGs (Chen and Held, 2007; Lorenz and DeWeaver, 2007, Lu et al., 2007; Frierson et al., 2007; Chen et al., 2008; Korty and Schneider, 2008; Lu et al., 2008; Son et al., 2010; Butler et al., 2011; Kang and Polvani, 2011) would be counteracted in both hemispheres by reduced stratospheric ozone depletion (Son et al., 2010) but depends on the rate of ozone recovery (see WMO, 2010). The poleward extent of the Hadley Circulation and associated dry zones can exhibit substantial internal variability (e.g., Lu et al., 2007), which can be as large as its near-term projected changes (Figure 11.20). There is also considerable uncertainty in the amplitude of the poleward shift of the Hadley Circulation in response to GHGs across multiple AOGCMs (Lu et al., 2007, Figure 11.20). Because of the counteracting impacts of future changes in stratospheric ozone and greenhouse gas concentrations and strong internal variability, it is unlikely that it will continue to expand poleward in either the northern and southern hemisphere as rapidly as it did in recent decades.

Global climate models and theoretical considerations suggest that a warming of the tropics should lead to a reduction of atmospheric circulation in general, primarily by weakening the tropical divergent circulation – largely in the zonally-asymmetric or Walker circulation (Knutson and Manabe, 1995; Held and Soden, 2006; Vecchi and Soden, 2007; Gastineau et al., 2009). Aerosol forcing can modify both Hadley and Walker circulations, which – depending on the details of the aerosol forcing - may lead to temporary reversals or enhancements in any GHG-driven weakening of the Walker circulation (Bollasina et al., 2011, Science; Sohn and Park, 2010; Merrifield, 2011; Zhan and Allan, 2011). Meanwhile, the strength and structure of the Walker circulation are impacted by internal climate variations, such as the El Niño/Southern Oscillation (e.g., Battisti and Sarachik, 1995), the PDO (e.g., Zhang et al., 1996) and the IPO (Power et al., 1999, 2006; Meehl and Hu, 2006; Meehl and Arblaster, 2011; Power and Kociuba, 2011a). Even on timescales of thirty to one hundred years, substantial variations in the strength of the Pacific Walker circulation in the absence of changes in radiative forcing are possible (Vecchi et al., 2006; Power et al., 2006). Estimated near-term weakening of the Walker circulation from CMIP3 models under the A1B scenario (Vecchi and Soden, 2007; Power and Kociuba, 2011b) are very likely to be smaller than the impact of internal climate variations over fifty-year timescales (Vecchi et al., 2006). There is also considerable response uncertainty in the amplitude of the weakening of Walker Circulation in response to GHG increase across multiple AOGCMs (Vecchi and Soden, 2007; DiNezio et al., 2009; Power and Kociuba, 2011ab, Figure 11.20). It is *very likely* that there will be decades in which the Walker circulation strengthens and weakens due to internal variability through the mid-century as the externally forced change is small compared to internally generated decadal variability (Figure 11.21).

[INSERT FIGURE 11.19 HERE]

Figure 11.19: [PLACEHOLDER FOR SECOND ORDER DRAFT: to make final; Projected changes in annual-averaged zonal (west-to-east) wind at 850hPa based on the average of 23 AOGCMs from the CMIP3 (Meehl et al.,

2007) multi-model ensemble, under 21st Century Emissions Scenario SRESA1B. Gray shading indicates where the multi-model average AOGCM anomalies are smaller than two standard deviations of the multi-AOGCM estimate of internal variability from the control climate integrations. Values referenced to the 1986–2005 climatology.]

[INSERT FIGURE 11.20 HERE]

Figure 11.20: Projected changes in the annual-averaged poleward edge of the Hadley Circulation (horizontal axis) and sub-tropical dry zones (vertical axis) based on 19 AOGCMs from the CMIP3 (Meehl et al., 2007) multi-model ensemble, under 21st Century Emissions Scenario SRESA1B. Orange symbols show the change in the northern edge of the Hadley Circulation/dry zones, while blue symbols show the change in the southern edge of the Hadley Circulation/dry zones. Open circles indicate the multi-model average, while horizontal and vertical colored lines indicate the ±1-standard deviation range for internal climate variability estimated from each model. Values referenced to the 1986–2005 climatology. Figure based on the methodology of Lu et al., 2007.

[INSERT FIGURE 11.21 HERE]

Figure 11.21: Projected changes in the strength of the Pacific Walker Circulation, as estimated using the east-west sea level pressure gradient across the equatorial Pacific (Vecchi and Soden, 2007), based on 24 AOGCMs from the CMIP3 (Meehl et al., 2007) multi-model ensemble, under 21st Century Emissions Scenario SRESA1B. Thin gray lines indicate the five-year running average for each model, red line indicates the multi-model five-year running average. Blue horizontal lines indicate the 2016–2035 values for each model, with the orange line indicating the multi-model averaged projection for 2016–2035. Values referenced to the 1986–2005 climatology.

11.4.2.5 Atmospheric Extremes

Extreme events in a changing climate and their impacts upon the natural physical environment are the subject of Chapter 3 (Seneviratne et al., 2012) of the IPCC Special Report on Managing the Risks of Extreme Events and Disasters to Advance Climate Change Adaptation (SREX). This comprehensive chapter provides an assessment of more than 1000 studies and forms the basis of much of the AR5 assessment on extremes.

The overwhelming majority of past studies on extremes in a changing climate have addressed long-term projections (i.e., 50 to 100 years into the future), while the focus of the current section is on near-term projections. When addressing near-term changes in extremes, natural variability plays an important role in determining the uncertainties (see Section 11.2.3). In addition, the uncertainty strongly depends upon the type of extremes considered, and is larger for small-scale extremes (such as heavy precipitation events) than for large-scale extremes (such as temperature extremes).

11.4.2.5.1 Temperature extremes

In the AR4 (Meehl et al., 2007b), cold episodes were projected to decrease significantly in a future warmer climate and it was considered *very likely* that heat waves would be more intense, more frequent and last longer towards the end of the 21st century. These conclusions have generally been confirmed in subsequent studies addressing both global scales (e.g., Orlowsky and Seneviratne, 2011) and regional scales (e.g., Gutowski et al., 2008; Meehl et al., 2009c; Alexander and Arblaster, 2009; Marengo et al., 2009a; Fischer and Schär, 2009; Fischer and Schär, 2011). In the SREX assessment it is concluded that increases in the number of warm days and nights and decreases in the number of cold days and nights are *virtually certain* on the global scale.

None of the aforementioned studies specifically addressed the near-term. Detailed analysis of the CMIP5 global projections however suggest that changes in temperature extremes are to be expected already for the near term. The CMIP5 model ensemble exhibits a general significant decrease in the frequency of cold nights, an increase in the frequency of warm days and nights, and an increase in the duration of warm spells (Sillman and Kharin, 2011). These changes particularly evident in global mean projections (see Figure 11.22). The figure shows that – as discussed in the introduction to the current chapter – these changes are remarkably insensitive to the emission scenario considered.

[INSERT FIGURE 11.22 HERE]

Figure 11.22: Global mean projections for the occurrence of warm and wet days from CMIP5 for the RCP2.6, RCP4.5 and RCP8.5 scenarios relative to 1986–2005. Panel (a) shows percentage of warm days (tx90p: Tmax exceeds the 90th percentile), panel (b) shows relative change of very wet days (pr95p: annual total precipitation when daily precipitation exceeds 95th percentile).

Near-term results from the ENSEMBLES projections for Europe are shown in Figure 11.23, displaying near-term changes in mean and extreme temperature (left-hand panels) and precipitation (right-hand panels) relative to the control period 1986–2005. In terms of JJA temperatures (Figure 11.4.2.1b a-b), projections show a warming of 0.6–1.5°C, with highest changes in the Mediterranean. The north-south gradient in the projections is consistent with the AR4. Daytime extreme temperatures (Figure 11.22b) are projected to warm substantially faster than mean temperatures (compare panels (a) and (b)). This difference between changes in mean and extremes can be explained by increases in interannual and/or synoptic variability, or increases in diurnal temperature range (Gregory and Mitchell, 1995; Schär et al., 2004; Fischer and Schär, 2010). In contrast, daytime winter temperatures are projected to warm slower than mean temperatures (compare panels (c) and (d)), which is indicative of reductions in variability. Such variability reductions might be linked to changes in storm track activity and/or changes in snow cover [reference].

[INSERT FIGURE 11.23 HERE]

Figure 11.23: European-scale projections from the ENSEMBLES regional climate modelling project for 2016–2035 relative to 1986–2005, with top and bottom panels applicable to JJA and DJF, respectively. For temperature, projected changes (°C) are displayed in terms of ensemble mean changes of (a,c) mean seasonal surface temperature, and (b,d) the 90th percentile of daily maximum temperatures. For precipitation, projected changes (%) are displayed in terms of ensemble mean changes of (e,g) mean seasonal precipitation and (f,h) the 95th percentile of daily precipitation. The stippling in (e-h) highlights regions where 80% of the models agree in the sign of the change (for temperature all models agree on the sign of the change). The analysis includes the following 10 RCM-GCM simulation chains for the SRES A1B scenario (naming includes RCM group and GCM simulation): HadRM3Q0-HadCM3Q0, ETHZ-HadCM3Q0, HadRM3Q3-HadCM3Q3, SMHI-HadCM3Q3, HadRM3Q16-HadCM3Q16, SMHI-BCM, DMI-ARPEGE, KNMI-ECHAM5, MPI-ECHAM5, DMI-ECHAM5 (Figure courtesy of Jan Rajczak, ETH Zürich).

11.4.2.5.2 Heavy precipitation events

The AR4 concluded that heavy precipitation events were *very likely* to increase over most areas of the globe in the 21st century (IPCC, 2007a). This tendency was found in many regions including some regions in which the total precipitation was projected to decrease. The SREX concluded that changes in heavy precipitation events were most likely in high latitudes and stronger in DJF than JJA, but were subject to considerable uncertainties related to climate model uncertainties, statistical downscaling and natural variability. In SREX, heavy precipitation was projected to also increase in some (but not all) regions with projected decreases of total precipitation (medium confidence). For precipitation extremes, results depend more strongly upon the region under consideration than with temperature extremes.

For the near term, CMIP5 global projections confirm a clear tendency for increases in heavy precipitation events in the global mean (Figure 11.22b), but there are significant variations across regions (Sillman and Kharin, 2011). Past observations have also shown that interannual and decadal variations in mean and heavy precipitation are large, and are in addition strongly affected by natural variations (e.g., El Niño), volcanic forcing, and anthropogenic aerosol loads (see Section 2.3.1.2). In general models have difficulties to represent these variations, particularly in the tropics (see Section 9.4.4.2).

Simulations with regional climate models demonstrate that the response in terms of heavy precipitation events to anthropogenic climate change may become evident in some but not all regions in the near-term. For instance, ENSEMBLES projections for Europe (see Figure 11.23e-h) confirm the previous IPCC results that changes in mean precipitation as well as heavy precipitation events are characterized by a pronounced north-south gradient in the extratropics, with precipitation increases (decreases) in the higher latitudes (subtropics). However, these projected changes are statistically significant only in a fraction of the domain. The results appear to be affected by (i) changes in water vapour content as induced by large-scale warming, and (ii) the large-scale circulation changes. Figure 11.23e-h also shows that projections for changes in extremes and means are qualitatively very similar in the near term. This indicates that changes in variability are less important for precipitation than temperature extremes.

11.4.2.5.3 Tropical cyclones

Two recent reports, the SREX (IPCC, 2012, particularly Seneviratne et al., 2012) assessment and a WMO Expert Team report on tropical cyclones and climate change (Knutson et al., 2010) indicate the response of global tropical cyclone frequency to projected radiative forcing changes is likely to be either no change or a decrease of up to a third by the end of the 21st Century. However, little confidence was placed on projections for individual basins. At the individual basin scale, a recent statistical downscaling exercise of models from CMIP3 indicates little consistency in projections of North Atlantic tropical storm frequency to the mid 21st Century, with the possibility of positive and negative trends (Villarini et al., 2011), a result consistent with dynamical model based projections of North Atlantic tropical storm frequency to the end of the 21st century that include possibilities of increases or decreases (e.g., Oouchi et al., 2005; Bengtsson et al., 2006; Gualdi et al., 2007; Emanuel et al., 2008; Knutson et al., 2008; Zhao et al., 2009; Sugi et al., 2009). The average projected signal in Atlantic tropical storm frequency is smaller than the overall uncertainty estimated from a statistical downscale of the CMIP3 models over the first half of the 21st Century (Villarini et al., 2011), with internal climate variability being a leading source of uncertainty through the mid-21st Century. A recent dynamical modelling study suggested that greenhouse warming could lead to a substantial increase in the frequency of extreme (Category 4–5) hurricanes in the North Atlantic by the end of the 21st Century, but estimated a detection timescale on the order of 60 years for an A1B future emission scenario (Bender et al. 2010). Therefore, we have little confidence in basin-scale projections of trends in tropical cyclone frequency and intensity to the mid-21st century. Villarini et al. (2011) noted that the CMIP3 AOGCMs indicate continued year-to-year and decade-to-decade variations in North Atlantic tropical storm frequency through the mid-21st Century. Modes of climate variability that in the past have led to variations in the intensity, frequency and structure of tropical cyclones across the globe - such as the El Niño Southern Oscillation (Vecchi and Wittenberg 2010, Collins et al. 2010; Callaghan and Power 2011) and the Indian Ocean Dipole Mode (Zheng et al. 2009) are very likely continue to exist through the mid-21st Century. Therefore, it is very likely that tropical cyclone frequency, intensity and spatial distribution globally and in individual basins will vary from year-to-year and decade-to-decade, as they have in the past (Chapters 2 and 10).

11.4.3 Atmospheric Composition and Air Quality

Future atmospheric composition depends on anthropogenic emissions, natural emissions and uptake (Chapter 6), and chemical-physical processes in the atmosphere (Chapters 2, 6, 7, 8). IPCC emission scenarios prescribe only emissions that can be directly ascribed to human activities (anthropogenic) and do not include projections for shifting natural emissions. The latter may occur in response to changes in climate or land-use, changes in the solar flux or volcanic aerosols, all of which alter climate and composition (Chapter 8). This chapter assesses projected atmospheric abundances and uncertainties of CH_4, N_2O, other well-mixed greenhouse gases, plus O_3 and aerosol optical depth for the RCP scenarios (Moss et al., 2010) over the 21st century (Section 11.4.3.1). Also included is an assessment of projected near-term changes in ambient air quality: surface O_3 and particulate matter (PM, a general measure of aerosols) (see Chapter 6 and AII.7.3-4 for nitrogen and acid deposition; air toxics such as mercury (Jacob and Winner, 2009) and biological aerosols such as pollen (Jacobson and Streets, 2009) are not considered here). Projected CO_2 abundances, controlled by emissions and interaction with the terrestrial and oceanic carbon cycle, are discussed in Chapters 6 and 12. The 21st-century scenarios, from emissions to radiative forcing are collected in the tables of Annex II.

The connections between air pollution, global atmospheric chemistry and climate change were recognized in the TAR (Johnson et al., 1999; Prather et al., 2001; Jacob et al., 1993; Penner et al., 1993), and the SRES scenarios were assessed for changes in surface O_3 from emissions (Prather et al., 2003), changes in radiative forcing from emissions of air pollutants (Gauss et al., 2003; Shindell et al., 2007), and changes in global tropospheric O_3 driven by climate (Johnson et al., 2001). In the AR4, these SRES scenarios were contrasted with newer near-term scenarios to 2030, the Current Legislation (CLE) and Maximum Feasible Reductions (MFR) scenarios to illustrate the impacts of explicit air pollution control strategies on air pollution, global atmospheric chemistry, and near-term climate (Stevenson et al., 2006; Dentener et al., 2005; Dentener et al., 2006b). Section 11.4.6 discusses the climate impacts of efforts directed at improved air quality. Technology shifts in the energy or agriculture sectors (e.g., Galloway et al., 2008; Schultz et al., 2003; Jacobson, 2008a), or changes in land-use land-cover (LULC) and associated biospheric emissions (Chen et al. 2009a, Ganzeveld et al., 2010) could result in future pathways outside the range of the air quality projections assessed here.

All of the emission scenarios assessed here are designed for projecting compositional changes with global atmospheric chemistry-climate models, which are not adequate for estimating air quality changes at the local scales of cities or air quality management districts. Rather, these changes require higher spatial resolution emissions and models, as assessed in AR5 WGII (see also Chapters 9 and 14 for evaluation of climate projections at the regional-urban scale). The WGI global chemistry and climate models, with horizontal resolutions of 100 km at best, however, provide two key elements of global change that drive local air quality: an estimate of the changing chemical background of O_3 and aerosols, relevant for estimating impacts on rural agriculture and ecosystems, as well as the baseline pollution levels upon which local pollution builds (Section 11.4.3.2.1); and changing weather patterns, such as heat waves (Cox and Chu, 1996; Stott et al., 2004) and stagnation episodes (Mickley et al., 2004), that drive peak pollution events (Section 11.4.3.2.2).

11.4.3.1 Greenhouse Gases and Aerosols

The IPCC has assessed previous emission-based scenarios for future greenhouse gases and aerosols in the SAR (IS92) and TAR/AR4 (SRES). The new RCP scenarios, developed independently of the IPCC assessment and review process, each have an integrated but simplified single model that goes from human activities to emissions to greenhouse gases to climate change (van Vuuren et al., 2011; Lamarque et al., 2011a; Meinshausen et al., 2011). Emissions of highly reactive, non-greenhouse species (e.g., NOx, CO, NMVOC) control O_3, aerosols, global air quality, and the abundances of CH_4 and HFCs, but their emissions are difficult to quantify or project, and alternative near-term scenarios are also evaluated (Kloster et al., 2008; Dentener et al., 2005; Cofala et al., 2007). Each of the steps from emissions to composition to radiative forcing is critically re-evaluated here using the current scientific basis to correct and apply uncertainties. Where appropriate, results from the SAR (IS92a) and TAR (SRES B1&A2) are shown. The RCP-prescribed emissions, abundances and radiative forcing used in the CMIP5 model ensembles are not based on current best understanding of natural and anthropogenic emissions, atmospheric chemistry and biogeochemistry, and radiative forcing of climate. The uncertainty in projecting RCP emissions to radiative forcing and climate change is not negligible, see below, but still much less than the range of RF between the RCP2.6 and RCP8.5 scenarios.

Anthropogenic emissions of the industrially produced greenhouse gases (e.g., fossil-fuel CO_2 and the synthetic fluorinated F-gases, AII.2.1a, AII.2.4–15) are generally accurate to 10% or better based on bottom-up inventory methods, whereas those from the agriculture, forestry and other land-use sectors (AFOLU, AII.2.1b, AII.2.3–4) have uncertainties typically 25% or larger (NRC, 2010; Prather et al., 2009). Thus, the RCP emissions of CH_4 and N_2O have been rescaled through 2005 to match current atmospheric abundances and trends, with assumed atmospheric lifetimes and pre-industrial (natural) sources. Such harmonization was done previously for the SRES emissions in the TAR (Prather et al., 2001). The current best estimates for the lifetimes and budgets (Chapter 8) give Y2010 anthropogenic emissions of 318 ± 48 (1 SD) Tg-CH_4/yr and 6.5 ± 1.0 Tg-N(N_2O)/yr, with total emissions of 504 ± 43 Tg-CH_4/yr and 15.6 ± 1.0 Tg-N(N_2O)/yr. In our projections we thus scale the RCP (anthropogenic only) CH_4 and N_2O emissions by a constant factor for years 2010–2100 based on the 2010 emissions for each of the RCPs (see AII.2.2–3). In addition to this scaling, we also project the ±1-SD uncertainty ranges these anthropogenic emissions, with each range being matched by shifts in natural emissions to maintain the total emissions.

RCPs use a parametric model to project the lifetimes and thus integrate the greenhouse gas and aerosol abundances (MAGICC6: (Meinshausen M, Wigley TML and SCB 2011). Current atmospheric chemistry and climate models along with observational data are used here to derive best current lifetimes and the changes driven by emissions and climate. In terms of stratospheric chemistry, the current N_2O lifetime, 131 ± 10 yr, is expected to decrease linearly from 2000 to 2100 for SRES A1B by about 10 yr because of changes in stratospheric circulation, but increase by about 7 yr because of changes in chemical composition (Fleming et al. 2011), including the self feedback decrease of about 3 yr as N_2O increases from 320 to 420 ppb (Hsu and Prather 2010)(updated). Recent chemistry-climate model validation (CCMVal) studies project a more vigorous stratospheric overturning by 2100, but did not diagnose the N_2O lifetime (Oman et al. 2010, Strahan et al. 2011). Because the current lifetime, emissions, and abundances are self-consistent, only the uncertainty in the change in N_2O lifetime (e.g., -3 ± 5 yr) projects to uncertainty in future abundances (AII.5.10). All RCPs scenarios project increasing N_2O abundances from 2010 to 2100 ranging from 6% (RCP2.6) to 40% (RCP8.5)

Reactions with the tropospheric hydroxyl radical (OH) are the dominant atmospheric removal of CH_4 and HFCs (Chapter 8). Projections of future OH levels, globally integrated as the effective OH-lifetime of CH_4 (AII.5.9 [PLACEHOLDER FOR SECOND ORDER DRAFT] Table), involve many, often cancelling factors and thus the sign of the change reported in some of the CMIP5 ensemble ranges from –15% to +15% by

2100 within the same RCP scenario. Projected changes in tropospheric OH are based on sensitivities to changing emissions and climate derived from several multi-model evaluations, including uncertainties (HTAP, CMIP5; Stevenson et al., 2006). Projected CH_4 abundances include uncertainty in the current lifetime, but this is linked to correlated uncertainties in anthropogenic vs. natural emissions necessary to match the pre-industrial and present-day abundances for the same reasons as N_2O, but HFC abundances do include this primary uncertainty in OH loss (10%) because the HFC emissions inventories should be independently accurate as noted above. Lifetimes for the PFCs and SF_6 are held constant (Chapter 8). In projecting future abundances, the budget lifetime of the gas should be used, not the residence time of a pulse (8% shorter for N_2O, 40% longer for CH_4). Figure 11.24 shows the published RCP anthropogenic emissions and mean tropospheric abundances of CH_4 for 2010 to 2100, along with this assessment's best estimates (designated RCP&) including ±1 SD uncertainties. For RCP2.6, CH_4 abundances are projected to decline continuously over the century by about 30%; whereas RCP 4.5 and 6.0 peak and then decline below Y2010 abundances. Only RCP8.5 has such large increase in anthropogenic emissions (150%) that abundances increase throughout the century. Projected CH_4 abundances respond within a decade to changing emissions and atmospheric chemistry, with all RCP scenarios diverging before 2050. Additional factors driving CH_4 projections for RCP8.5 include anthropogenic emissions of NOx, natural emissions, and climate change. In most cases the assessed CH_4 abundances (RCP&) based on emissions are similar to the RCP published values, although outside of the uncertainty range; and the uncertainty in future abundances is much smaller than the difference between scenarios.

[INSERT FIGURE 11.24 HERE]

Figure 11.24: Projected CH4 (a) anthropogenic emissions and (b) atmospheric abundances for the four RCP scenarios (2010–2100). The thick solid lines show the published RCP values: black +, RCP8.5; red square, RCP6.0; blue o, RCP4.5; green *, RCP 2.6. Thin lines with markers show values from this assessment. The shaded region shows the ±1 SD from the Monte Carlo calculations that consider uncertainties, including the current magnitude of the anthropogenic emissions.

The tropospheric mean abundances of the Kyoto greenhouse gases projected to 2100 (AII.4.1–15) show both the RCP published values (Meinshausen et al., 2011) and those estimated in this assessment (denoted RCP&), which include where possible uncertainty estimates as ±1 standard deviation. RCP scenarios also project emissions and abundances for the ozone-depleting GHG (CFCs, HCFCs, halons) under control of the Montreal Protocol. In AR5 the abundances of CFCs and HCFCs (AII.4.16) are taken from scenario A1 of the 2010 WMO Ozone Assessment (WMO, 2011, Table 5-A3). All of the CFC abundances decline throughout the century, but some of the HCFC's increase to 2030 before their phase-out and decline. Their combined RF (Table AII.6.5) is calculated using the methodology in Chapter 8 plus a simple estimate of uncertainty in their decay from 2005 to 2100 as described in the table notes. Radiative forcing from the sum of these Montreal gases decreases from 0.33 ± 0.01 W m^{-2} in 2010 to 0.10 ± 0.02 W m^{-2} in 2100.

Projected O_3 changes are broken into tropospheric and stratospheric columns (DU) because each has a different impact on RF (AII.5.1–2). Stratospheric O_3 is being driven by declining chlorine levels, increasing N_2O and CH_4, cooler temperatures from increased CO_2, and a more vigorous overturning circulation driven by more wave propagation under climate change but overall is expected to increase in the coming decades, reversing ozone loss since 1960. Results here are taken from the WMO Assessment (2011) and CCMVal studies. Tropospheric O_3 changes are driven by anthropogenic emissions of CH_4, NOx, CO, NMVOC (AII.2.2,16–18) and are projected to follow the dominant emission trends over the next few decades (e.g., increasing due to CH4 in RCP8.5 in spite of falling NOx emissions). Overall, tropospheric climate change drives a decline in tropospheric O_3, but enhanced stratospheric circulation can counter that (Lamarque et al., 2011b; Kawase et al., 2011). Natural emissions of these species are also important in today's O_3 budget, but reliable estimates of their change with climate cannot be made (Chapter 6, Table AII.3.2). Best estimates for tropospheric O_3 change are based on some CMIP5 models and multi-model studies of tropospheric O_3 response to key factors like individual emissions, climate-driven increases in water vapour and temperature, and increased stratospheric influx (Prather et al., 2001; Stevenson et al., 2006; Wild et al., 2011; Oman et al., 2010). CMIP5 models show a wide range in tropospheric O_3 changes from 2000–2100, and uncertainties are hard to estimate, probably of order 100% of the estimated change.

Aerosol species can be emitted directly (mineral dust, black carbon and some organic carbon) or indirectly through precursor gases (sulphate, ammonium, nitrate, some organics). All of these aerosol sources are projected to change under the RCPs and alternative scenarios. Some CMIP5 models (Lamarque et al., 2011c) have projected changes in aerosol optical depth (AOD) to 2100 (AII.5.3–8). Projections of AOD to 2100 are described in Chapter 8, along with the projected RFs from all greenhouse gases, aerosols and aerosol-cloud indirect effects (AII.6.1–11). Overall, aerosols decrease under RCPs due to emissions reductions in all relevant species except NH_3.

Natural emissions of CO_2, CH_4 and N_2O, plus highly reactive species like NOx, CO, and NMVOC control in part the abundance of most greenhouse gases and some aerosols. Models predict that these emissions will change in a warming climate and with land-use change, and where possible projections for the period 2000–2100 are given along with uncertainty estimates in Tables AII.3.1–10. See discussion in Chapter 6.

Uncertainty estimates in projecting atmospheric composition under a changing climate are based in large part on expert judgment. Our understanding of the atmospheric processes that control the abundance of greenhouse gases and aerosols has been tested and calibrated with intensive in situ observations over the past couple decades, and has been incorporated into modern three-dimensional chemistry-transport or chemistry-climate models (CTMs or CCMs) (Chapter 9). With climate change, we expect that the atmospheric processes calibrated under historical conditions (e.g., harmonization of N_2O observations, budgets, and lifetimes) will shift, and thus uncertainty in projecting changes under a given emissions scenario will be greater than the errors in current models.

11.4.3.2 Projections of Global and Regional Air Quality

Air quality changes in the 21st century are tied to global emissions, local emissions, and the physical climate change itself (e.g., Meleux, Solmon and Giorgi, 2007; Wu et al., 2008b; Steiner et al., 2006; Steiner et al., 2010; Carlton et al., 2010; Tai et al, 2010; Hoyle et al., 2011; Doherty et al., 2009; Tao et al., 2007) and thus we consider air quality changes projected due to changes in both emissions and climate. The emphasis on ozone and aerosols reflects the large focus in the literature to date on the response of these chemical species to climate [Box in Ch7 AR4; (as reviewed byWeaver et al., 2009; Jacob and Winner, 2009) and emission changes [(e.g., TFHTAP, 2007; Dentener et al., 2006b; Wild et al., 2011; HTAP, 2010) with ozone receiving the most attention (Figure 11.25). While air pollution remains a concern over the entire century, most research focuses on the next few decades, for which air quality management strategies and technologies can be more readily projected (e.g., Dentener et al., 2006a)

The air quality projections assessed here include: estimates from off-line chemical transport models (CTMs) or AOGCMs run with stable climate but changing emissions; a parameterization developed from sensitivities diagnosed from a coordinated multi-model set of regional emission perturbation simulations with CTMs; CTMs using meteorological fields projected from separate AOGCMs; a suite of linked climate and atmospheric chemistry models from global to regional scales; and global climate models with interactive chemistry. Empirical relationships between certain meteorological variables and air quality provide crucial information for evaluating models and for improving our understanding of the links between air quality and climate (e.g., Lin, Jacob and Fiore, 2001; Rasmussen et al., 2011; Tai et al., 2010; Bloomer et al., 2009). Their application for statistical downscaling of local air quality (e.g., Mahmud et al., 2008; Holloway et al., 2008), however, may be limited by non-linear sensitivities or the inherent correlations of many individual meteorological variables (e.g., Murazaki and Hess, 2006; Weaver et al., 2009; Steiner et al., 2010; Dawson et al., 2009; Nolte et al., 2008; Forkel and Knoche, 2006; Katragkou et al., 2010). Such results are subject to the same problems with predictability in a changing climate as is the down-scaling of regional climate from the CMIP5 results (Chapters 9 and 14, WGII).

Reliable air quality projections require confidence in the regional climate responses, including precipitation, convection, and the positioning of mid-latitude storm tracks and subtropical high pressure systems (e.g., Liang et al. 2006, Jacob and Winner 2009, Weaver et al. 2009) and are only as good as the regional climate modeling (Chapter 9 & 14). Ecosystem interactions are particularly uncertain since vegetation acts as both a source and a sink for many air pollutants (e.g., Andersson and Engardt, 2010) and incomplete understanding of chemical oxidation pathways limits confidence in the sign of air pollutant responses to changing biogenic emissions (e.g., Pacifico et al., 2009; Ito, Sillman and Penner, 2009; Paulot et al., 2009; Carlton, Wiedinmyer and Kroll, 2009; Hallquist et al., 2009).

11.4.3.2.1 Climate-driven changes from meteorology and natural emissions

Ozone

The observed correlation of high-O_3 events with temperature in polluted regions is well documented and largely reflects the correlation of temperature with stagnation episodes, cloud-free enhanced photochemistry, higher biogenic emissions, wildfires, and possibly other contributing factors (e.g., AR4 Chapter 7 Box) (e.g., Jacob and Winner, 2009; Carvalho et al., 2011; Weaver et al., 2009; Murazaki and Hess, 2006; Wu et al., 2008b; Menon and et al., 2008; Avise et al., 2009; Jacobson and Streets, 2009; Nolte et al., 2008; Jaffe et al., 2008; Mickley et al., 2004; Leibensperger, Mickley and Jacob, 2008; Ordóñez et al., 2005). Warming climate, in the absence of emission changes, is thus likely to increase O_3 in polluted regions, and may also lengthen the O_3 pollution season (Nolte et al., 2008; Racherla and Adams, 2008). Surface O_3 levels in unpolluted regions are very likely to decrease in a warmer climate because higher water vapor abundances enhance O_3 destruction in low-NO_x regions of the atmosphere (Johnson et al., 1999). Climate-driven increases in biogenic emissions from vegetation and soils, lightning NO_x, influx of stratospheric O_3, as well as shifts in intercontinental transport pathways for pollutants, could offset this decrease in some regions (Nolte et al., 2008; Kawase et al., 2011; Zeng et al., 2010; Zeng, Pyle and Young, 2008; Wu et al., 2008a; Wu et al., 2008b; Katragkou et al., 2011); but these processes are poorly understood relative to the water vapor response.

Figure 11.25 summarizes estimates for surface ozone response to climate change (blue lines). A major caveat is that many published simulations for present-day and future climate conditions span only a few years each; while they highlight the response of air quality to meteorological changes, the short simulation length precludes clean attribution to climate change as opposed to climate variability. These models project increases of up to 10 ppb over populated regions within the United States by 2050 and up to 6 ppb within Central Europe in 2030 during the O_3 pollution season. The plotted ranges in Figure 11.25 reflect spatial variability as well as differences across models, scenarios, reported O_3 statistics, and in some cases short simulation lengths. The climate-driven changes bracketing zero in 2030 are annual, spatial, multi-model averages and standard deviations (Dentener et al., 2006b). They are the net sum of the opposing influences exerted by a warming climate in the absence of anthropogenic emission changes: to decrease background levels but increase O_3 in polluted regions and seasons. The inclusion of several studies reporting spatial ranges in summer daytime statistics contributes to the wider range of climate-driven changes plotted for 2050 and are not an assessment of changes in uncertainty.

Aerosols

The conclusion as to whether climate change will worsen or improve aerosol (PM) pollution remains model-dependent, confounded by opposing influences on individual PM components, and large inter-annual variability (e.g., Mahmud et al., 2010). Rising temperatures and water vapor enhance SO_2 oxidation relative to surface loss, thus increasing sulphate aerosol and decreasing nitrate aerosol (e.g., Racherla and Adams, 2006; Hedegaard et al., 2008; Unger et al., 2006a; Pye et al., 2009; Liao, Chen and Seinfeld, 2006; Aw and Kleeman, 2003; Kleeman, 2008). Potential exists for large feedbacks from "natural" aerosol sources, particularly carbonaceous aerosols from wildfires, mineral dust, and biogenic precursors to secondary organic aerosol (Spracklen et al., 2009; Jickells et al., 2005; Carvalho et al., 2011; Jiang et al., 2010; Mahowald and Luo, 2003; Tegen et al., 2004; Woodward et al., 2005; Mahowald et al., 2006; Mahowald, 2007). The biogenic secondary organic aerosol contribution to PM is generally expected to grow as temperatures rise (Tagaris et al., 2007; Heald et al., 2008; Liao et al., 2007).

Most components of PM are expected to correlate negatively with precipitation (Tai et al., 2010), such that aerosol burdens will likely decrease in regions with increased precipitation (Racherla and Adams, 2006; Liao et al., 2007; Avise et al., 2009; Tagaris et al., 2007; Zhang et al., 2008; Pye et al., 2009). Projecting precipitation at the regional or urban scale is much more uncertain than temperature, and additional uncertainties apply to polluted regions where aerosols are likely to interfere with the hydrologic cycle (Chapters 7, 14). Seasonal differences in aerosol burdens versus precipitation preclude simple scaling of aerosol response to precipitation changes (Kloster et al., 2010b; Fang et al., 2011). Other meteorological changes, such as mixing depths and ventilation of the continental boundary layer, also influence the sign of the aerosol changes (e.g., Mahmud et al., 2010; Dawson et al., 2009; Jacob and Winner, 2009; Kleeman, 2008).

The coupling between changes in O_3 and aerosol precursor emissions (both biogenic and anthropogenic) with the physical climate is complex and not well understood. For example, biogenic aerosol formation depends on anthropogenic emissions and atmospheric oxidizing capacity (Carlton et al., 2010; Jiang et al., 2010). In addition to climate-driven feedbacks from the biosphere (Section 11.4.3.2.1), future land-use changes may also influence regional air quality (Heald et al., 2008; Wu et al., 2011; Chen et al., 2009a; Cook et al., 2009).

11.4.3.2.2 Changes driven by non-local anthropogenic pollutant emissions

Overall, the uncertainty associated with the influence of near-term climate change on global and regional O_3 air quality is small relative to the uncertainty in possible emission-driven changes (Figure 11.25; Dentener et al., 2006b). Near-term projections for annual mean surface O_3, spatially averaged over selected world regions, due to the combined impacts of emission and climate change under the RCP trajectories are shown in Figure 11.26 for multi-model ensembles of CMIP5 transient chemistry-climate simulations and of the ACCMIP 10-year time slice simulations for 2030 and 2050. Large inter-annual and regional variations are evident, and even larger variability is expected as one considers smaller regions, specific seasons, or the frequency of high-O_3 pollution events (cf. Extreme Events discussion below). While the regions considered are not identical, comparison between the O_3 changes driven by emissions-only scenarios with fixed climate under the RCPs (Figure 11.25; Wild et al., 2011) are roughly equivalent to the changes estimated with the full chemistry-climate models (Figure 11.26), implying a major role for emissions in determining near-term O_3 air quality. Under RCP8.5 (Annex II; Figures 11.25 and 11.26), the prominent rise in methane raises background O_3 levels (Kawase et al., 2011), including in regions with aggressive controls on other O_3 precursors (Lamarque et al., 2011b; Wild et al., 2011). Numerous earlier studies have demonstrated the potential for rising global anthropogenic emissions of O_3 precursors, including CH_4 and NOx, to enhance the O_3 background in surface air and offset improvements to air quality from local emission reductions (Jacob et al., 1999; Fiore et al., 2009; Wild, 2011; Granier et al., 2006; Wild et al., 2011; Fiore et al., 2002; Hogrefe et al., 2004; Tao et al., 2007; Wu et al., 2008; Avise et al., 2009; Chen et al., 2009b; Szopa et al., 2006; Lin et al., 2008; Prather et al., 2003; Huang et al., 2008; Prather et al., 2001; HTAP, 2010).

While aerosol changes driven by anthropogenic emissions depend somewhat on oxidant levels (e.g., Unger et al. 2006b, Kleeman 2008), generally sulphate follows SO_2 emissions. Nitrates follow ammonia but are also inversely dependent on sulphate (and less sensitive to NO_x) such that allowing ammonia to increase while reducing sulphate will offset some of benefit from SO_2 controls (Pye et al., 2009) (see Chapters 7 and 8, where such mechanisms are discussed.). Continued reductions in SO_2 emissions alongside rising NH_3 emissions, as occurs in the RCP scenarios (Annex II) could lead to nitrate aerosol levels equivalent to or surpassing sulphate aerosol levels in some regions over the next few decades (Bauer et al., 2007; Bellouin et al., 2011). The balance between the relative importance of emission versus climate-driven changes for aerosol is likely to vary regionally, but confidence in both sign and magnitude of overall changes is low.

11.4.3.2.3 Extreme weather and air pollution

Air pollution events are typically associated with stagnation events, often concurrent with heat waves, whose frequency of occurrence can vary greatly from decade to decade (AR4 Chapter 7 Box) (Tai et al., 2010; Leibensperger et al., 2008). The 2003 European heat wave is associated with air-pollution mortalities (Filleul et al., 2006; Stedman, 2004), and all such heat waves are associated with poor air quality (Tressol et al., 2008; Vieno et al., 2010; Vautard et al., 2005; Ordóñez et al., 2005). Anthropogenic climate change, even over the next few decades, has increased the risk of such heat waves (Clark, Murphy and Brown, 2010; Diffenbaugh and Ashfaq, 2010; Stott et al., 2004). One study indicates a warming climate would lead to future summer O_3 more similar to the exceptional 2003 European heat wave (Meleux et al., 2007). Indeed, Section 11.4.2.5 indicates an increase in warm spell duration index which in the absence of emission reductions, is expected to increase the incidence of extreme air pollution events globally, with [xxx] regions particularly susceptible.

Meteorological conditions tied to O_3 and PM pollution events are likely to increase in frequency and duration with climate change, although the severity of pollution events depend on the local emissions scenario (Chen et al., 2009b; Tai et al., 2010; Murazaki and Hess, 2006; Hogrefe et al., 2004; Mickley et al., 2004; Forkel and Knoche, 2006; Nolte et al., 2008; Racherla and Adams, 2008; Wu et al., 2008b; Tagaris et al., 2007; Szopa et al., 2006; Liao et al., 2009; Jiang et al., 2008; Vautard et al., 2005; Mahmud et al., 2008). Positive feedbacks from vegetation (higher emissions and lower stomatal deposition) and urbanization may further worsen air pollution during heat waves (Royal Society, 2008; Jiang et al., 2008; Andersson and Engardt, 2010). Over the United States and Europe, some studies suggest near-term increases in the extreme O_3 values (95%-ile) of O_3, but they do not agree at the regional level (Jacobson, 2008b; Weaver et al., 2009; Jacob and Winner, 2009; Kleeman, 2008; Katragkou et al., 2011). Our understanding of observations and models indicates it is very likely that, statistically, a warming climate will exacerbate extreme O_3 and PM pollution events for some populated regions in the near term, even if the effect is not uniform.

[INSERT FIGURE 11.25 HERE]

Figure 11.25: Changes in surface O_3 solely due to climate (blue) or emissions (colored by emission scenario) reported in the literature in 2030 (top) and 2050 (bottom) for selected world regions. Results from individual studies are labeled by letters underneath the corresponding plot symbols. Vertical bars represent a combination of ranges as reported in the literature: (1) multi-model mean and standard deviations in annual mean, spatial averages from the ACCENT/Photocomp study for 2030 ((Dentener et al., 2006b), A); (2) application of a parameterization developed from the multi-model ensemble of the Task Force on Hemispheric Transport of Air Pollution [TF HTAP, 2010] regional source-receptor relationships to estimate surface O_3 response for several emission scenarios in 2030 and 2050 globally and within the TF HTAP continental regions (Wild et al., 2011, C); (3) spatial averages across a region, denoted by filled squares (Szopa et al., 2006, D; Avise et al., 2009, E; Tagaris et al., 2007, I; Racherla and Adams, 2006, K; Hogrefe et al., 2004, M; Unger et al., JGR, 2006, Q; Fiore et al., JGR, 2008, T; West et al., PNAS, 2006, U; Fiore et al., GRL, 2002, W; Katragkou et al., in press JGR, X)(4) spatial ranges across a region as estimated with one model or combined across several individual modeling studies, denoted by dashed lines ([Need to insert “Royal” before “Society” in endnotes] ((Society 2008b), B; Szopa et al., 2006, D; Forkel and Knoche, 2006, F; Wu et al., 2008a (air quality), G; Wu et al., 2008b (background), H; Nolte et al., JGR, 2008, J; Racherla and Adams 2006, K; Zhang et al., 2008, L; Racherla and Adams, 2008, P; Tagaris et al., 2009, R; Stevenson et al., 2005, S; Dentener et al., ACP 2005, V; Y; Lam et al., 2011, Z) Regional definitions, methods, and reported metrics (e.g., 24-hour versus daily maximum values over a 1-hour or 8-hour averaging period, annual or seasonal averages) vary across studies. Climate change scenarios vary across studies, but are combined into ranges denoted by blue bars for two reasons: (1) there is little detectable cross-scenario difference in the climate response in 2030 (Section 11.4.7), and (2) many of these estimated are based on simulations that are too short to cleanly attribute a climate change signal and thus it is not appropriate to attribute differences to particular forcing scenarios.

[INSERT FIGURE 11.26a HERE]

Figure 11.26a: Changes in near-term annual mean surface ozone (ppb) following the RCP scenarios, spatially averaged over selected world regions (shaded land regions) and from CMIP5 chemistry-climate model ensemble (3 models, colored lines denote ensemble mean and shading denotes full range across models for each RCP). Filled circles with vertical lines indicate the multi-model average and full cross-model range from the 2030 and 2050 ACCMIP decadal time slice simulations, colored by RCP scenario (4 models for RCP2.6 and RCP4.5; 3 models for RCP8.5; 2 models for RCP6.0 in 2030, and 1 model for all RCP scenarios in 2050). Changes are relative to the 1986–2005 reference period for the transient simulations, and relative to the average of the 1980 and 2000 decadal time slices for the ACCMIP ensemble. The average ozone value during the reference period, spatially averaged over each region, is shown in each panel, with the standard deviation reflecting the cross-model range (transient CMIP5 models on the left; ACCMIP models on the right). In cases where multiple ensemble members were available from a single model, they were averaged first before inclusion into the multi-model mean.

[INSERT FIGURE 11.26b HERE]

Figure 11.26b: [PLACEHOLDER FOR SECOND ORDER DRAFT: As in 11.24a, but for PM2 if sufficient number of models are available.]

[INSERT FIGURE 11.27 HERE]

Figure 11.27: [PLACEHOLDER FOR SECOND ORDER DRAFT: Illustrate projected change in extreme metric, following general structure of Figure 11.24 but considering e.g., frequency of days above a threshold value for ozone and/or PM due to climate change only – if sufficient number of models contribute results from ACCMIP RCP8.5 climate-change-only simulations.]

11.4.4 Near-Term Projections of Oceanic Conditions

11.4.4.1 Temperature

Globally-averaged surface and near surface ocean temperatures are projected by AOGCMs to warm over the early 21st Century, in response to both present day atmospheric concentrations of greenhouse gases (“committed warming”; e.g., Meehl et al., 2006), and projected changes (Figure 11.28). Globally-averaged SST shows substantial year-to-year and decade-to-decade variability (e.g., Knutson et al., 2006; Meehl et al., 2011), whereas the variability of depth-averaged ocean temperatures is much less (e.g., Meehl et al., 2011; Palmer et al., 2011). The rate at which globally-averaged temperatures rise in response to a given scenario for radiative forcing shows a considerable spread between models (an example of response uncertainty, see Section 11.2.3), due to differences in climate sensitivity and ocean heat uptake (e.g., Gregory and Forester, 2008). In the CMIP3 models under SRESA1B [PLACEHOLDER FOR SECOND ORDER DRAFT] globally averaged SSTs increase by 0.3°C–0.6°C over the near-term relative to 1986–2005 (Figure 11.28).

A key uncertainty in the future evolution of globally averaged oceanic temperature are possible future large volcanic eruptions, which could impact the radiative balance of the planet for 2–3 years after their eruption and act to reduce oceanic temperature for decades into the future (Delworth et al., 2005; Stechnikov et al., 2010; Gregory, 2010). An estimate using the GFDL-CM2.1 coupled AOGCM (Stechnikov et al., 2010) suggests that a single Tambora (1851)-like volcano could erase the projected global ocean depth-averaged temperature increase for many years to a decade. A Pinatubo (1991)-like volcano could erase the projected increase for 2–10 years. See Section 11.4.7 for further discussion.

In the absence of multiple major volcanic eruptions, it is *extremely likely* that globally-averaged surface and upper ocean (top 700m) temperatures averaged 2016–2035 will be warmer than those averaged over 1986–2005.

Projected ocean temperature changes tend to be largest near the surface, and decrease with depth (Figures 11.28, 11.29 and 11.30). This results in an increase in the near surface stratification of temperature, particularly in the tropical Pacific and Indian Oceans. In the Atlantic and Southern Oceans models suggest that warming penetrates more rapidly to greater depths (Figure 11.31). Projections for the Arctic Ocean suggest a subsurface maximum in warming, at a depth of a few hundred meters.

There are regional variations in the projected amplitude of ocean temperature change (Figure 11.30), which are influenced by ocean circulation as well as surface warming. (Vecchi and Soden, 2007; Yin et al., 2009; 2010; DiNezio et al., 2009; Timmermann et al., 2010; Xie et al., 2010). Inter-decadal variability of upper ocean temperatures is larger in mid-latitudes, particularly in the Northern Hemisphere, than in the tropics (Figure 11.31). A consequence of this contrast is that it will take longer in the mid-latitudes than in the tropics for the anthropogenic warming signal to emerge from the noise of internal variability (Figure 11.30, Wang et al., 2010).

The Southern Ocean shows significant local spread in its temperature projections, particularly in the Weddell Gyre and north of the Ross-Sea gyre. These differences between models tend to be displaced from regions of high internal variability and are likely to be caused the same model biases of the surface mixed layer depths and water mass formation found in century scale simulations (Sloyan and Kamenkovich, 2007) (Figure 11.30 lower panels). The relative role of stratospheric ozone and anthropogenic forcing on the Southern Ocean temperature and salinity remains for recent past and near term is an important issue (Sections 9.3.2 and 10.3), but the role of these forcings on the near term projections on ocean circulation have not been assessed in the literature. [PLACEHOLDER FOR SECOND ORDER DRAFT: if literature emerges]

Projected changes to thermal structure of the tropical Indo-Pacific are strongly dependent on future behaviour of the Walker circulation (Vecchi and Soden, 2007; Timmermann et al., 2010; DiNezio et al., 2009). Since the projected weakening of the Walker circulation through the mid-21st century is smaller than the expected variability on timescales of decades to years (Section 11.4.2.4.3), it is *likely* that internal climate variability will be a dominant contributor to changes in the depth and tilt of the equatorial thermocline, and the strength of the east-west gradient of SST across the Pacific through the mid-21st Century, thus it is *likely* there will be multi-year periods with increases or decreases, but no clear longer term trend

[INSERT FIGURE 11.28 HERE]

Figure 11.28: Projected changes in annual-averaged, globally-averaged, depth-averaged ocean temperature based on twelve AOGCMs from the CMIP3 (Meehl et al., 2007) multi-model ensemble, under 21st Century Emissions Scenario SRESA1B. Top panel shows changes of sea surface temperature, middle panel ocean temperature changes averaged over the upper 700 meters of the ocean, bottom panel shows changes averaged over the full ocean depth. Thin black lines show the evolution for each of the twelve AOGCMs, red line shows the average of all twelve projections, the blue line indicates an estimate of the average magnitude of internal variability of all twelve AOGCMs (2sigma).Gray horizontal lines indicate the 2016–2035 average anomaly for each of the twelve AOGCMs, while the orange horizontal

line indicates the multi-model average 2016–2035 anomaly. The fifty-year running average from each model's control climate integration was removed from each line. Values referenced to the 1986–2005 climatology of each AOGCM.

[INSERT FIGURE 11.29 HERE]
Figure 11.29: Projected changes, as a function of depth, in annual-averaged, globally-averaged ocean temperature based on the average of twelve AOGCMs from the CMIP3 (Meehl et al., 2007) multi-model ensemble, under 21st Century Emissions Scenario SRESA1B. Gray shading indicates where the multi-model average AOGCM anomalies are smaller than two standard deviations of the multi-AOGCM estimate of internal variability from the control climate integrations. The fifty-year running average from each model's control climate integration was removed from each line. Values referenced to the 1986-2005 climatology of each AOGCM.

[INSERT FIGURE 11.30 HERE]
Figure 11.30: Upper panels show the projected changes averaged 2016–2035 relative to 1986–2005 in sea surface temperature (left panels) and temperature averaged over the upper 700 meters of the ocean (right panels), as a function of latitude and longitude. Lower panels show the standard deviation of twenty-year averages of sea surface temperature (left panels) and temperature averaged over the upper 700 meters of the ocean (right panels) arising from internal climate variability in these models. Figures based on the average of twelve AOGCMs from the CMIP3 (Meehl et al., 2007) multi-model ensemble, under 21st Century Emissions Scenario SRESA1B. Gray shading indicates where the multi-model average AOGCM anomalies are smaller than two standard deviations of the multi-AOGCM estimate of internal variability from the control climate integrations, black stippling indicates where at least four (1/3) of the models disagree on the sign of the change. The fifty-year running average from each model's control climate integration was removed from each line.

[INSERT FIGURE 11.31 HERE]
Figure 11.31: [PLACEHOLDER FOR SECOND ORDER DRAFT: Currently shaded at 1 sigma. Same as Figure 11.XX, but for regional averages]

11.4.4.2 Salinity

Changes in sea surface salinity are expected in response to changes in precipitation, evaporation and run-off (see Section 11.4.2.4); in general (but not in every region), salty regions are expected to become saltier and fresh regions fresher (e.g., Durack and Wijffels, 2009). As discussed in Chapter 10, observation-based and attribution studies have found some evidence of an emerging anthropogenic signal in salinity change, in particular increases in surface salinity in the subtropical North Atlantic, and decreases in the west Pacific warm pool region (Stott et al., 2008; Durack and Wijffels, 2009; Terray et al., 2011). However, the extent to which the observed changes are clearly outside the range of natural internal variability, and the extent to which current models are providing an adequate simulation of salinity change, has yet to be firmly established (Durack and Wijffels, 2009; Terray et al., 2011). This said, models generally predict increases in salinity in the tropical and (especially) subtropical Atlantic, and decreases in the western tropical Pacific over the next few decades (Figure 7b of Terray et al., 2011).

Projected near-term increases in fresh water flux into the Arctic Ocean produce a fresher surface layer and increased transport of fresh water into the North Atlantic (Holland et al., 2006, 2007; Vavrus et al., 2011). Such contributions to decreased density of the ocean surface layer in the North Atlantic could help stabilize deep ocean convection there and contribute to a near-term reduction of strength of Atlantic Meridional Ocean Circulation. There is also a projected increase in the temperature of intermediate depth water penetrating the Arctic from the North Atlantic with greater warming than the surface layer (Vavrus et al., 2011).

11.4.4.3 Circulation

As discussed in previous assessment reports, the AMOC is generally projected to weaken over the next century in response the increase in anthropogenic greenhouse gases. However, the rate and magnitude of weakening is very uncertain. Response uncertainty is likely to be a dominant contribution in the near term, but the influence of anthropogenic aerosols and natural radiative forcings (solar, volcanic) cannot be neglected, and could be as important as the influence of greenhouse gases (e.g., Delworth and Dixon, 2006; Stenchikov et al., 2009). In addition, the natural variability of the AMOC on decadal timescales is poorly known and poorly understood, and could dominate any anthropogenic response in the near term (Drijfhout and Hazeleger, 2007). The AMOC is known to play an important role in the decadal variability of the North

Atlantic Ocean (Figure 11.30), but climate models show large differences in their simulation of both the amplitude and spectrum of AMOC variability (e.g., Bryan et al., 2006; Msadek et al., 2011). In some AOGCMs changes in southern hemisphere surface winds influence the evolution of the AMOC on timescales of many decades (Delworth and Zeng, 2008), so the delayed response to southern hemisphere wind changes, driven by the historical reduction in stratospheric ozone along with its projected recovery, could be an additional confounding issue (Section 11.4.2.3). Overall, it is *likely* that there will be some decline in the AMOC by 2050, but decades during which the AMOC increases are also to be expected. There is *low confidence* in projections of when an anthropogenic influence on the AMOC might be detected.

The high uncertainty in projections for the AMOC should not be interpreted as ruling out the possibility of a sudden major reduction or "shutdown" – see Section 11.4.7 and Chapter 12.

Projected changes to oceanic circulation in the Indo-Pacific are strongly dependent on future response of the Walker circulation (Vecchi and Soden, 2007; DiNezio et al., 2009). The projected radiatively-forced weakening of the Walker circulation through the mid-21st century is smaller than the expected variability on timescales of decades to years (Section 11.4.2.3), therefore it is more likely than not that internal climate variability will be a dominant contributor to changes in the strength of equatorial circulation, the shallow subtropical overturning in the Pacific, and the Indonesian Throughflow over the coming decades. The dominant contribution of internal climate variability precludes a confident assessment of their likely changes through the mid-21st Century; however, it is very likely that there will be substantial variations in their strength on timescales of years to decades.

11.4.5 Cryosphere

This section assesses projected near-term changes of elements of the cryosphere. These consist of sea ice, snow cover and permafrost, changes to the Arctic Ocean, and possible abrupt changes involving the cryosphere. The IPCC AR4 showed time series of Arctic and Antarctic sea ice extent following the SRES scenarios in the 21st century, and geographical plots of sea ice extent for those regions only for the end of the 21st century. A comparable time series plot of projected sea ice extent for the duration of the 21st century is shown for the CMIP5 multi-model ensemble in Chapter 12. There was no assessment of near-term changes of snow cover or permafrost in the AR4. Here we assess near term changes in the geographical coverage of sea ice, snow cover and permafrost. As with all projected quantities for the near-term, there is considerable interannual and decadal variability that confounds the emergence of a forced signal above the noise.

11.4.5.1 Sea Ice

Some models project an ice-free summer period in the Arctic Ocean by 2040 (Holland et al., 2006), and even as early as the late 2030s using a criterion of 80% sea ice area loss (e.g., Zhang, 2010). By scaling six CMIP3 models to recent observed September sea ice changes, a nearly ice free Arctic in September is projected to occur by 2037, reaching the first quartile of the distribution for timing of September sea ice loss by 2028 (Wang and Overland, 2009). However, a number of models that have fairly thick Arctic sea ice produce a slower near-term decrease in sea ice extent compared to observations (Stroeve et al., 2007). The credibility of near term predictions for an ice-free Arctic before mid-century depend on at least a reasonable simulation of extent and spatial distribution of present-day ice thickness, accurate representation of the surface energy budget and its influence on the sea ice mass budget, atmospheric energy transports, local feedbacks associated with the stable boundary layer and polar clouds, and the relationship of reduction in ice area per ice thickness change (Bitz, 2008; Holland et al., 2008). Additionally an increase in ocean heat flux convergence to the Arctic could contribute to more rapid ice melt (Bitz et al., 2006; Winton, 2006; Holland et al., 2006; Holland et al., 2008). An analysis of CMIP3 model simulations indicates that for near term predictions the dominant factor for decreasing sea ice is increased ice melt, and reductions in ice growth play a secondary role (Holland et al., 2008). Arctic sea ice has larger volume loss when there is thicker ice initially across the CMIP3 models, with a projected accumulated mass loss of about 0.5 m by 2020, and roughly 1.0 m by 2050 with considerable model spread (Holland et al., 2008).

In early 21st century simulations, Antarctic sea ice cover is projected to decrease more slowly than in the Arctic in the CMIP5 models (Chapter 12, [Figure 12.xx]). The decreases of sea ice area for the time period

2016–2035 for the multi-model ensemble average are [xx%] for September (Figure 11.32), and [xx%] for February for the Arctic (Figure 11.33). Changes for the Antarctic are [xx%] for September (Figure 11.34), and [xx%] for February (Figure 11.35).

11.4.5.2 Snow Cover

Snow cover decreases are highly correlated with a shortening of seasonal snow cover duration (Brown and Mote, 2009). The snow accumulation season by mid-century in one model is projected to begin later in autumn with the melt season initiated earlier in the spring (Lawrence and Slater, 2010). Some climate models have simulated reductions in annual snow cover of –4 to –7% by 2011–2030, and –5 to –13% by 2041–2060 with largest decreases in northern spring (March-April-May) (IASC, 2010). Projected increases in snowfall across much of the northern high latitudes act to increase snow amounts, but warming reduces the fraction of precipitation that falls as snow. Whether the average snow cover decreases or increases by mid-century depends on the balance between these competing factors. The dividing line where models transition from simulating increasing or decreasing maximum snow water equivalent roughly coincides with the –20°C isotherm in the mid-20th century November to March mean surface air temperature (Räisänen, 2008).

Multi-model averages from the CMIP5 AOGCM experiments show decreases of Northern Hemisphere snow cover of about [xx%] for the 2016–2035 time period for a March-April average using a 15% extent threshold for RCP4.5 (Figure 11.36).

11.4.5.3 Permafrost

Virtually all near-term projections indicate a substantial amount of permafrost degradation, and thaw depth deepening over much of the permafrost area (Sushama et al., 2006; Euskirchen et al., 2006; Saito et al., 2007; Zhang et al., 2007; Lawrence et al., 2008a; IASC, 2010). These projections have increased credibility compared to the previous generation of models assessed in the AR4 because current climate models represent permafrost more accurately (Nicolsky et al., 2007; Alexeev et al., 2007; Lawrence et al., 2008a). Changes in annual mean permafrost for the 2016–2035 time period are shown in Figure 11.37 for the CMIP5 multi-model ensemble. Annual average decreases in permafrost for that period are about [xx%].

11.4.5.4 Possible Abrupt Climate Change Involving the Cryosphere

The rapid loss of sea ice such as that which occurred in the late 2000s (see Chapter 4) has been noted to occur in a climate model, raising the possibility of abrupt sea ice loss events sometime in the next 50 years (Holland et al., 2006). In summer, the oceanic heat anomaly is enhanced by ice–albedo feedback, but in winter the excess oceanic heat is lost to the atmosphere due to a lack of insulating sea-ice cover. This raises the possibility of sudden irreversible loss of Arctic summer sea ice during warming conditions (Winton, 2006). Increases in mostly low clouds in autumn, or decreases in summer, can promote rapid sea ice loss events (Vavrus et al., 2010). However, the interactions of clouds and sea ice introduce another element of uncertainty to short term predictions of abrupt changes in sea ice coverage (DeWeaver et al., 2008; Vavrus et al., 2009; Gorodetskaya et al., 2008).

Though permafrost thaw and active layer deepening could initiate abrupt changes in Arctic hydrological, biogeochemical, and ecosystem processes (McGuire et al., 2006), the impact of these potential climate feedbacks is not well quantified for short term climate change (Euskirchen et al., 2006; O'Connor et al., 2010).

It is very likely that there will be continued loss of sea ice extent in the Arctic, decreases of snow cover, and reductions of permafrost at high latitudes of the Northern Hemisphere. Though there is the possibility of sudden abrupt changes in the cryosphere, there is low confidence that these changes could be predicted with any certainty.

[INSERT FIGURE 11.32 HERE]

Figure 11.32: [PLACEHOLDER FOR SECOND ORDER DRAFT: Arctic September sea ice coverage (%) for 2016–2035 from a CMIP5 multi-model average for the RCP4.5 scenario that is representative of all the RCP scenarios for this time period.]

[INSERT FIGURE 11.33 HERE]
Figure 11.33: [PLACEHOLDER FOR SECOND ORDER DRAFT: Same as Figure 11.32 but for February.]

[INSERT FIGURE 11.34 HERE]
Figure 11.34: [PLACEHOLDER FOR SECOND ORDER DRAFT: Same as Figure 11.32 but for the Antarctic.]

[INSERT FIGURE 11.35 HERE]
Figure 11.35: [PLACEHOLDER FOR SECOND ORDER DRAFT: Same as Figure 11.33 but for the Antarctic.]

[INSERT FIGURE 11.36 HERE]
Figure 11.36: [PLACEHOLDER FOR SECOND ORDER DRAFT: Change in snow cover fraction for a March-April average using a 15% extent threshold from the CMIP5 multi-model average for RCP4.5 which is representative of all the RCP scenarios for this time period.]

[INSERT FIGURE 11.37 HERE]
Figure 11.37: [PLACEHOLDER FOR SECOND ORDER DRAFT: Annual mean change in permafrost for 2016–2035 average minus 1986–2005 base period for RCP4.5 from the CMIP5 multi-model average for RCP4.5 which is representative of al l the RCP scenarios for this time period.]

11.4.6 Sensitivity of Near-Term Climate to Anthropogenic Emissions and Land-Use

As discussed in Section 11.41, projections of global mean surface air temperature are mostly independent of greenhouse gas emission scenarios up to 2050 (Meehl et al., 2007; Stott and Kettleborough, 2002; Hawkins and Sutton, 2009; AR4 Chapter 10, Section 10.5.4.5; see also Section 11.2.2.1). This finding, however, does not mean that near-term climate has no sensitivity to alternative scenarios for anthropogenic emissions (and land use). The purpose of this section is to assess this sensitivity.

In contrast to the SRES scenarios used in CMIP3, the RCPs represent mitigation pathways to achieve specified radiative forcing targets (Moss et al., 2010; van Vuuren et al., 2011) (AII.2.18–22, 6.8–9). While RCP 8.5, 6.0 and 4.5 have RF projections similar to the range of the SRES scenarios, RCP2.6 requires net negative CO_2 emissions by 2100, and is much lower than any SRES (see Chapter 1, [Figure 1.x]). Nevertheless, the range in RF across all RCPs is still modest in the near term (e.g., 2.6 to 3.6 W m^{-2} by 2040, see AII.6.12). Crucially, the RCP scenarios differ from one another in projecting different abundances for CO_2 and other anthropogenic greenhouse gases, as well as different emissions of aerosols and their precursors (see Chapter 1 [and 8?]), and thus differences in the climate responses across the RCP scenarios provide information as to the sensitivity of future climate to various emission trajectories.

The sensitivity of climate to CO_2 concentrations is not determined solely by its radiative effects. There are additional effects on plant growth and stomatal conductance that can have important influences on evapotranspiration (e.g., Bates et al., 2008; Section 2.3.4), and hence climate, particularly on regional scales. In many CMIP5 models, these effects are not represented (or only partially so), a limitation which should be noted.

As short-lived, major, anthropogenic greenhouse gases, both CH_4 and O_3 can respond rapidly to changes in emissions. Near-term CH_4 abundances in the SRES and RCP scenarios have similar increasing trajectories, except for RCP2.6, which has a rapid decline over the whole century (AII.4.2, 6.3) (Lamarque et al., 2011c; Meinshausen et al., 2011). Aerosols are also short-lived in the atmosphere, and thus mitigation strategies addressing emission of aerosols and their precursor gases have the potential to produce rapid changes in climate. Models and measurements robustly indicate that aerosols composed of sulphate, nitrate and/or ammonium produce a negative RF for both direct and indirect effects (Chapters 7 and 8). Global precipitation may be much more sensitive to warming driven by aerosol changes than warming induced by greenhouse gases, with projected decreases in scattering (mainly sulphate) aerosols projected to enhance precipitation globally (Kloster et al., 2010a; Dentener et al., 2010; Yoshimori and Broccoli, 2008). Future decreases in absorbing aerosol (black carbon) may also enhance global precipitation (Ming et al., 2010). Large aerosol reductions as projected in the RCPs will impact global precipitation as well as temperature (Kloster et al., 2010a; Ming et al., 2010). Most CMIP5 models include some representation of aerosol indirect effects, but these processes are highly uncertain, resulting in low confidence in the simulated climate responses (Chapters 7-10). The SRES aerosol emissions and RF were poorly defined (see TAR Appendix II) whereas the RCPs explicitly project aerosol emissions, and include rapidly declining sulfur dioxide (SO_2) emissions due to air pollution controls in the next few decades (van Vuuren et al., 2011). Differences between SRES and RCPs in terms of CH_4 and aerosol scenarios (and modeling advances in the case of aerosols) complicate interpretation of differing temperature responses between SRES/CMIP3 and RCP/CMIP5.

The CMIP5 model ensemble, forced by the new RCP scenarios, fall within the warming range for 2020–2030 projected under the older SRES scenarios (Figure 11.38a). The most rapidly warming scenario (RCP8.5) emerges from the interquartile range of the other RCP scenarios by 2040–2050. The enhanced warming in the RCP8.5 and UNEP Ref scenarios in Figure 11.38a (and the SRES A1-A2-B2; AII4.2, TAR Appendix II) by 2040 and 2050 may partially reflect the rapid growth of methane as compared with the RCP2.6-4.5-6.0 scenarios (and SRES B1). For example, current control technology for CH_4 emissions, if implemented worldwide by 2030 (a 24% decrease in anthropogenic CH_4 emissions relative to 2010 levels) is estimated to lessen warming by 0.2–0.4K (estimated central range) between 2030 and 2050 (UNEP and WMO2011; Figure 11.38a). The larger warming at 2020–2030 in RCP2.6 compared to the other RCP scenarios (Figure 11.38a), may reflect the much more rapid decline of SO_2 emissions under RCP2.6 than the other RCPs. The RCP scenarios probably underestimate uncertainties in near-term forcing from aerosols and CH_4 if major climate-specific (vs. local pollution-driven) emissions reductions are implemented (See AII.6.12). For example, the temperature range in both mean values and uncertainty across three alternative scenarios in 2030 and 2040 that implement control technologies on methane and black carbon sources (United Nations and World Meteorological Organization 2011) is wider than the ranges across RCP scenarios from the CMIP5 model ensemble (Figure 11.38a).

By 2040, differences of 0.5–1 degree between RCP2.6 and RCP8.5 emerge over substantial portions of the globe in both summer and winter hemispheres, with less cooling over the Arctic (>1.5°C) during boreal winter; these patterns are further amplified by 2050, with over 1°C temperature differences over large continental regions and >2.5°C during Arctic winter (Figure 11.38b). At the regional scale, however, internal variability and model response uncertainty may still dominate in the near-term (Hawkins and Sutton, 2009; Hawkins and Sutton, 2010). The published literature debates whether the spatial pattern of the future surface temperature response to aerosol forcing mirrors that from greenhouse-gas forcing or rather follows the local aerosol forcing patterns (Levy et al., 2008; Shindell et al., 2008b; Boer and Yu, 2003) (Shindell and Faluvegi, 2009; Mickley et al., 2011; Leibensperger et al., 2011). A multi-model analysis begins to reconcile these previous findings, indicating a strong sensitivity of the surface temperature response to the latitudinal forcing distribution but limited sensitivity to longitude (Shindell at al., 2010). Applying pattern scaling across future scenarios with large decreases in aerosols as for the RCPs may thus not be valid.

Many earlier studies have identified mitigation approaches to simultaneously improve air quality and reduce radiative forcing, with emphasis on reductions in CH_4, tropospheric O_3, and black carbon aerosols (e.g., Bond and Sun, 2005; Fiore et al., 2008; Hansen et al., 2000; United Nations and World Meteorological Organization, 2011; Fiore et al., 2002; Dentener et al., 2005; West et al., 2006; Royal Society, 2008; Jacobson, 2002; Jacobson, 2010). Some have focused on specific sectors such as transportation (e.g., Uherek et al., 2010; Myhre et al., 2011) or domestic fuel burning (e.g., Shindell et al., 2008a; Unger et al., 2008). In the UNEP/WMO assessment, implementing current control technologies on emissions of black carbon (a 78% decrease from 2010 levels) and co-emitted species worldwide by 2030 in the coming decades is estimated to lessen warming by 0.0–0.2 K (central estimate) (UNEP and WMO, 2011; estimated as difference between UNEP CH_4 and UNEP CH_4+BC in Figure 11.38a). Not all mitigation efforts are synergistic; for example emission controls on maritime shipping are predicted to improve air quality but increase near-term climate forcing (Collins, Sanderson and Johnson, 2009; Eyring et al., 2010). Multiple modeling approaches indicate that corollary reductions in sulphate-nitrate aerosols occurring for possible aggressive CO_2 stabilization or air pollutant mitigation scenarios will produce a rapid rise in surface temperatures (e.g., Wigley et al., 2009; Jacobson and Streets, 2009) possibly at rates unsafe for ecosystems (Raes and Seinfeld, 2009). For example, Kloster et al. (2010a) show that following a maximum feasible aerosol-abatement scenario for 2030 results in a near doubling of the warming greenhouse gases alone (from +1 to +2 K). Reducing absorbing aerosols, particularly black carbon from fossil fuels and bio-fuels, may offset some of the warming caused by sulphate-nitrate reductions, and some models predict relatively greater responses over the Arctic (Jacobson, 2010; Ramana et al., 2010; Flanner et al., 2007). There remains considerable uncertainty in the net impact on surface temperatures of black carbon mitigation strategies, primarily because of uncertainty in cloud feedbacks (Koch et al., 2011; Spracklen et al., 2011; Chen et al., 2010; Yoshimori and Broccoli, 2008).

The factor-of-two changes in anthropogenic aerosol sources projected for the RCPs over the next 40 years, which could be even larger if aggressive mitigation strategies are implemented, are expected to induce regional climate responses. Positive feedbacks with soil moisture and low cloud cover imply a larger sensitivity of extremes (heat waves and associated air pollution events) over the United States to the aerosol emission scenario (Leibensperger et al., 2011; Mickley et al., 2011). Similar amplifying feedbacks have been implicated for European warming, including through fog reduction (van Oldenborgh et al., 2009; Ceppi et al., 2010; van Oldenborgh, Yiou and Vautard, 2010). Changes in aerosols have been shown to contribute to circulation changes, ranging from shifts in the width of the tropics, Arctic-Oscillation phasing, monsoons, jet locations, and associated precipitation (Allen and Sherwood, 2010 and references therein; Bollasina, Ming and Ramaswamy, 2011; Leibensperger et al., 2011; Ming and Ramaswamy, 2011; Ming et al., 2011; Ramanation and Carmicheal, 2008; Kawase et al., 2011; Meehl et al., 2008) with absorbing aerosols possibly more potent at altering circulation patterns than CO_2 and scattering aerosols (Ming et al., 2010; Ott et al., 2010; Randles and Ramaswamy, 2010; Wang et al., 2009). Regionally observed drying trends over Africa, South Asia and northern China over the past decades have been attributed at least partially to anthropogenic aerosol forcing (Ramanathan and Carmichael, 2008; Bollasina et al., 2011 and references therein), suggesting that aerosol decreases in these regions over the next century should reverse these trends (cf. also Chapters 10 and 14). Near-term (2030 and 2050) precipitation responses to changes in aerosol optical depth, anthropogenic aerosols, and specific fuel emissions sectors have been documented in several modeling studies (e.g., Jacobson and Streets, 2009; Menon and et al., 2008; Roeckner et al., 2006). The lack of uniformity across studies, which addressed different regions and relative balances of reflecting vs. absorbing aerosols, complicates generalization of these findings.

While many aspects of projected changes in near-term climate are insensitive to alternative scenarios for anthropogenic emissions, plausible changes in anthropogenic methane and aerosols could exert substantial effects (relative to natural internal variability) on global and regional climates.

[PLACEHOLDER FOR SECOND ORDER DRAFT: Land-use changes also have the potential to influence near-term climate by changing albedo and evapotranspiration, which may have large impacts, particularly on the regional scale.]

[INSERT FIGURE 11.38a HERE]

Figure 11.38a: Emergence of near-term differences in global mean surface air temperatures across scenarios. Increases in 10-year mean (2016–2025, 2026–2035, 2036–2045 and 2046–2055) globally averaged surface air temperatures (°C) in the CMIP5 model ensemble following each scenario (11, 15, 8, and 16 models for RCP2.6 (red), RCP4.5 (blue), RCP6.0 (magenta), and RCP8.5 (cyan), respectively and in the CMIP3 model ensemble (22 models; black bars) following the SRES A1b scenario. The multi-model mean (X), median (square), interquartile range (open boxes), 5–95% distribution (whiskers) across all models are shown for each decade and scenario. Also shown are estimates for scenarios that implement technological controls by 2030 on sources of methane (UNEP CH_4) and on sources of methane and black carbon as well as co-emitted species such as carbon monoxide, organic carbon and nitrogen oxides (UNEP CH_4 + BC) relative to the reference scenario (UNEP Ref); symbols denote the average of the two participating models and vertical bars denote uncertainty estimates based on (1) uncertainty in radiative forcing from each atmospheric component (i.e., CH_4, O_3, individual aerosol species) in response to the emission control measures and (2) uncertainty in the temperature response associated with the range of climate sensitivity recommended in AR-4 (United Nations and World Meteorological Organization, 2011). To compare the UNEP and RCP values to a common baseline, the difference between 2009 UNEP reference year temperature and the 1986–2005 average temperature in the historical/RCP4.5 model ensemble was added to the UNEP values.

[INSERT FIGURE 11.38b HERE]

Figure 11.38b: Emergence of near-term differences in regional surface air temperature across the RCP scenarios. Difference between the high (RCP8.5) and low (RCP2.6) scenarios for the CMIP5 model ensemble (12 models) surface air temperatures averaged over 2026–2035 (left), 2036–2045 (middle) and 2046–2055 (right) in boreal winter (DJF; top row) and summer (JJA; bottom row).

11.4.7 The Potential for Surprises in Near-Term Climate

As discussed in Section 11.4.1, most of the projections presented in Sections 11.4.2–11.4.5 rely on the spread amongst the CMIP5 ensemble of opportunity as an ad-hoc measure of uncertainty. It is possible that the real world might follow a path outside (above or below) the range projected by the CMIP5 models. Such an eventuality could arise if there are processes operating in the real world that are missing from, or inadequately represented in, the models. Two main possibilities must be considered: 1) Future radiative and other forcings may fall outside the range of RCP scenarios; 2) The response of the real climate system to radiative and other forcing may differ from that projected by the CMIP5 models. A third possibility arises if internal fluctuations in the real climate system are inadequately simulated in the models. The fidelity of the CMIP5 models in simulating internal climate variability is discussed in Chapter 9.

Future changes in radiative forcing will be caused by anthropogenic and natural processes. The consequences for near-term climate of uncertainties in anthropogenic emissions and land use were discussed in Section 11.4.6. The uncertainties in natural radiative forcing that are most important for near term climate are those associated with future volcanic eruptions and variations in the radiation received from the sun (solar output), and are discussed below. In addition, carbon cycle and other biogeochemical feedbacks in a warming climate could potentially lead to abundances of CO_2 and CH_4 (and hence radiative forcing) outside the range of the RCP scenarios. This can be seen in the AR5 projected abundances of CO_2 for RCP 8.5 (AII.4.1). Large departures from these scenarios would require non-linear responses that are not expected to play a major role in near term climate. However, the possibility of non-linear responses, and their potential impacts on climate, are discussed in Chapters 6 and 12 respectively.

The response of the climate system to radiative and other forcing is influenced by a very wide range of processes, not all of which are adequately simulated in the CMIP5 models (Chapter 9). Of particular concern for projections are mechanisms that could lead to an abrupt or rapid change that affects global-to-continental scale climate. Several such mechanisms are discussed in this assessment report; these include: rapid changes in the Arctic (Section 11.4.5 and Chapter 12); rapid changes in the ocean's overturning circulation (Chapter 12); rapid change of ice sheets (Chapter 13); and rapid changes in regional monsoon systems and hydrological climate (Chapter 14). Additional mechanisms may also exist. A synthetic discussion of the known mechanisms is included in Chapter 12, but it is important to recognise that these mechanisms have the potential to influence climate in the near term as well as in the long term (albeit that the likelihood of substantial impacts is generally lower for the near term). The reader should refer to Chapter 12, and the other chapters indicated, for a detailed assessment of each mechanism.

11.4.7.1 The Effects of Future Volcanic Eruptions

As discussed in Chapter 8, explosive volcanic eruptions are the major cause of natural variations in radiative forcing on interannual to decadal time scales. Most important are large tropical and subtropical eruptions (such as the 1991 eruption of Mount Pinatubo) that inject substantial amounts of sulfur dioxide (SO_2) into the stratosphere. The subsequent formation of sulphate aerosols leads to a negative radiative forcing of several W/m2, with a typical lifetime of a year (Robock, 2000). As discussed in Chapter 10, this negative forcing causes a general cooling of Earth's surface (although some regions warm), of a few tenths of a degree Kelvin. In addition, there are effects on the hydrological cycle (e.g., Trenberth and Dai, 2007), atmosphere and ocean circulation (e.g., Stenchikov et al., 2006). The surface climate response typically persists for a few years, but the subsurface ocean response can persist for decades or centuries, with consequences for sea level rise (Delworth et al., 2005; Stenchikov et al., 2009; Gregory, 2010).
Whilst it is possible to detect when various existing volcanoes become more active, or are more likely to erupt, the precise timing of an eruption, the amount of sulfur dioxide emitted and its distribution in the stratosphere are not predictable years ahead. Eruptions comparable to Mount Pinatubo will cause a short term cooling of the climate with related effects on surface climate that persist for a few years before a return to warming trajectories discussed in Section 11.4.2. Larger eruptions, or several eruptions occurring close together in time, would lead to larger and/or more persistent effects (e.g., Shine and Highwood, 2001).

11.4.7.2 The Effects of Future Changes in Solar Forcing

RCP scenarios assume an 11-year variation in total solar irradiance (TSI) but no underlying trend beyond 2005. As discussed in Chapter 8 (Section 8.3.1), on the multi-decadal timescale, the Sun is in a 'grand solar maximum' of magnetic activity. However, the most recent solar minimum was the lowest and longest since 1920. Some studies (e.g., Lockwood, 2010) suggest there may be a continued decline towards a much quieter period in the coming decades, but there is no consensus on this point (see Section 8.3.1.3). Jones et al. (2011) use historical analogues of the current solar state to construct a range of possible TSI projections. Their projected mean TSI value in the period 2030–2050 range is approximately 0.6 W m^{-2} lower than the average for the period 1986–2005, and the lower end of the range includes the possibility that TSI may fall by 2060 to levels last seen during the Maunder Minimum (MM; late 17th century). However, a smaller decline is more likely: Lockwood (2010) suggests only an 8% chance that the Sun will have returned to MM conditions by 2060. The mean of the projected TSI changes corresponds to a mean change in solar Radiative Forcing (RF) of approximately –0.1 W m^{-2} by 2050. Assuming a climate sensitivity of ~0.5 K (W m^{-2})$^{-1}$ this translates to a global mean temperature change of ~ –0.05 K, and this anomaly is very unlikely to exceed –0.1 K. Using a simplified coupled climate model, Feulner and Rahmstorf (2010) showed that a grand solar minimum, similar to that of the Maunder Minimum in the 17th century, would produce a decrease in global temperatures much smaller than the warming expected from increases in anthropogenic greenhouse gases.

[START FAQ 11.1 HERE]

FAQ 11.1: If You cannot Predict the Weather Next Month, How can You Predict Climate for the Next Decades?

Climate can sometimes be predicted far further into the future than weather can be predicted accurately. Why? The answer has some parallels with the ability of a doctor to provide advice on what might happen to a person in the future if he continues to smoke cigarettes. The doctor will not be able to tell the smoker when or even if he will die from a smoking-related illness if he does not already have the illness. However, the doctor can tell the smoker that his risk of dying from such a disease in the future will be increased if he continues to smoke. An important statistic associated with the smoker's future health – the likelihood of dying from a smoking-related disease - is predicted to change even though the day-to-day evolution of his future health in decades ahead is unpredictable.

With climate predictions we predict changes to the long-term statistics arising from weather variability over coming decades rather than the details of the weather itself. There are natural and anthropogenic sources of decadal climate predictability, and atmospheric, oceanic and other data is available to initialise experimental prediction systems. In practice, however, our ability to predict near-term climate is very limited. Predictive skill varies from place to place and from variable to variable. In fact reliable decadal predictions cannot be provided for all variables or all locations. While prediction systems are expected to improve over coming decades, unavoidable limits to predictive skill arising from the chaotic nature of the climate system will always restrict our ability to predict near-term climate.

Weather and Weather Forecasts

The term "weather" is defined as *the state of the atmosphere at a given time and place*. Weather can change from hour to hour and even minute to minute. "Weather forecasts" or "weather predictions" typically provide detailed information on future air temperature, precipitation, clouds, and/or winds. Weather forecasts help to address questions like: *Will it rain tomorrow? How much rain will fall?* Sometimes weather predictions are provided in terms of probabilities. For example the weather forecast might state that "*the likelihood of rainfall in Apia tomorrow is 75%*".

Modern-day weather forecasters need to have an accurate representation of the current state of the atmosphere in order to make accurate weather predictions. However, because the atmosphere is partially chaotic even the tiniest of errors in the depiction of the current state of the atmosphere will eventually lead to very large errors in forecasts - the so-called "butterfly effect". In practice forecasts of weather for periods beyond one week into the future have very little if any skill. Climate predictions, on the other hand, can have some skill for periods far beyond one week into the future. To understand how we first need to clarify what we mean by "climate" and "climate prediction" and how these terms differ in meaning from "weather" and "weather prediction".

Climate and Climate Predictions

"Climate" is different to "weather". The term "climate" refers to *the statistics of weather conditions over a long period of time* i.e., decades, centuries, millennia or even longer. This includes long-term averages of e.g., air temperature and rainfall, as well as the statistics of the variability about their long-term averages e.g., the standard deviation of year-to-year rainfall variability from the long-term average, or the frequency of days below 5°C.

Averages of climate variables over long periods of time are called climatological averages. We can have climatological averages for individual months (e.g., January), for seasons (e.g., spring) or for the year as a whole (an annual average). A "climate prediction" or "climate forecast" will address questions like: *How likely will it be that the coming summer temperature will be higher than the long-term average of past summers? How likely will it be that the next decade will be warmer than past decades?* Or more specifically: *what is the probability that temperature (in Australia say) averaged over the next ten years will exceed the temperature in Australia averaged over the past 30 years?* Climate predictions do not provide forecasts of the detailed day-to-day evolution of future weather. Instead climate predictions provide probabilities of long-term changes to the statistics of future climatic variables.

Predictability

Predictability in the atmosphere on seasonal, interannual and decadal time-scales can arise from certain forms of internally generated natural climate variability – often connected to oceanic variability - and certain types of external forcing (Sections 11.2.1, 11.2.2). External forcing that can underpin decadal predictability includes the radiative forcing arising from long-lived increases in atmospheric greenhouse gas concentrations. Internal variability that results in e.g., extensive, long-lived, upper ocean temperature anomalies have the potential to provide seasonal, interannual, even decadal predictability in the overlying atmosphere both locally and remotely through atmospheric "teleconnections". This is very well-established for climate predictions for the next few seasons. In Chapter 11 we assess whether or not skill extends to forecasts for the next decade and beyond [PLACEHOLDER FOR SECOND ORDER DRAFT: this sentence to be revised in light of subsequent CMIP5 analysis and assessment to provide a very brief overview of extent to which decadal predictability and prediction is possible].

The magnitude of the changes in the atmosphere associated with any decadal predictability at a specific location is extremely small compared with the size of the day-to-day variability linked to changes in weather at that same location. So while a predictable decadal "signal' can underpin predictability in changes to decadal averages of certain climate variables in particular locations, the same decadal signal provides little if any enhancement in our ability to forecast weather.

The level of predictability and apparent predictive skill arising from both internal and external forcing (Section 11.3.5) can vary markedly from place-to-place and from variable-to-variable. Some of the reasons for this are discussed in Sections 11.2.1 and 11.2.2. In fact recent research [check when CMIP5 data is available] assessed in Sections11.2.4 and 11.3.6 indicates that predictability is absent or very limited in some variables in most locations over the surface of the earth. So in some locations we can not predict all aspects of climate over the next decades with accuracy even if we could perfectly resolve all the technical issues confronted when developing and conducting predictions (Sections 11.2 and 11.3.2.5). The partially chaotic nature of the climate system precludes the possibility of reliable decadal predictions of some climate variables in some locations.

[END FAQ 11.1 HERE]

[START FAQ 11.2 HERE]

FAQ 11.2: How do Volcanic Eruptions Affect Climate and Our Ability to Predict Climate?

[PLACEHOLDER FOR SECOND ORDER DRAFT: The following FAQ is from Robock (2003); text to be revised.] Large volcanic eruptions inject both mineral particles (called ash or tephra) and sulphate aerosol precursors into the atmosphere, but it is the sulphate aerosols, because of their small size and long lifetimes, that are responsible for radiative forcing important for climate. The radiative and chemical effects of this aerosol cloud produce responses in the climate system. The emissions of CO_2 from volcanic eruptions are at least 100 times smaller than anthropogenic emissions, and inconsequential for climate on century time scales. Volcanic eruptions produce global cooling, and are an important natural cause of interdecadal and interannual climate change. Regional responses include winter warming of Northern Hemisphere continents following major tropical eruptions and weakening of summer Asian and African monsoons following tropical and Northern Hemisphere high latitude eruptions. The volcanic cloud also produces stratospheric ozone depletion and enhances the diffuse radiation reaching the surface, with an impact on vegetation and increased uptake of CO_2. Very large, but rare, eruptions, such as that of Toba 74,000 years ago, may have caused very large climate changes, but the size of those changes is not well constrained by existing evidence.

Explosive volcanic eruptions affect climate by injecting gases and aerosol particles into the stratosphere. An eruption cloud rich in SO_2 will produce a long-lived aerosol cloud. Explosive eruptions that only produce large ash particles, such as the 1980 Mount St. Helens eruption, can produce a large local weather perturbation but do not have long-lasting climatic effects. Some volcanoes, such as Kilauea and Etna, produce continuous large tropospheric emissions of sulphate aerosols, but only if there is a dramatic change in these emissions will climate be changed. Stratospheric aerosol clouds last for 1–3 years, reflecting sunlight and cooling the surface. Volcanic aerosols serve as surfaces for chemical reactions that destroy stratospheric ozone, which lowers ultraviolet absorption and allows more ultraviolet radiation to reach the surface. As this chemical effect depends on the presence of anthropogenic chlorine, it has only become important in recent decades. Aerosol clouds also absorb both solar (near infrared) and terrestrial radiation, heating the lower stratosphere. While the decrease in lower tropospheric O3 reduces the radiative heating in the lower stratosphere, the net effect is still heating. Tropical eruptions produce asymmetric stratospheric heating, producing a stronger polar vortex and associated positive mode of the Arctic Oscillation in tropospheric circulation. This pattern is one of enhanced warm advection over Northern Hemisphere continents in winter, producing winter warming after large tropical eruptions. Various analyses of past data and computer simulations suggest a weak effect of volcanic eruptions on sea surface temperature (SST) in the tropical Pacific, but the results conflict with each other, with some suggesting more frequent El Niño events and others suggesting more frequent La Niña events. In any case, ENSO variations must be considered when searching the climatic record for volcanic signals, as they have similar amplitudes and time scales.

There have been several large volcanic eruptions in the past 250 years, and each has drawn attention to the atmospheric and potential climatic effects. The 1783 Laki eruption in Iceland produced large effects in Europe causing Benjamin Franklin, the United States ambassador to France to publish the first paper on the subject in more than 1800 years. The eruption produced famines in Egypt, India, China, and Japan, because it weakened the summer monsoon precipitation over Africa and Asia. The 1815 Tambora eruption, combined with the effects of the unknown 1809 eruption, produced the "Year Without a Summer" in 1816 and inspired *Frankenstein*, written by Mary Shelley on the shores of Lake Geneva, Switzerland, that summer. Agricultural failures in both Europe and the United States that year had profound societal impacts. The 1883 Krakatau eruption was the largest explosion ever observed, and the sound wave was tracked on microbarographs for 4 complete circuits of the Earth, taking almost 2 days for one circuit. The Royal Society report on this eruption published 5 years later remains the most extensive report on the atmospheric effects of a volcanic eruption. The 1963 Agung eruption produced the largest stratospheric dust veil in more than 50 years in the Northern Hemisphere, and inspired many modern scientific studies. The subsequent 1982 El Chichón and 1991 Pinatubo eruptions produced very large stratospheric aerosol clouds and large climatic effects.

The 1982 El Chichón eruption injected about 7 Mt of SO_2 into the atmosphere. There has not been a large stratospheric injection since 1991, when Mt. Pinatubo in the Philippines put about 20 Mt of SO_2 into the lower stratosphere. In 2008 Kasatochi (in the Aleutian Islands of Alaska) and in 2009 Mt. Sarychev (in the Russian Kamchatka Peninsula) each put about 1.5 Mt SO_2 into the lower stratosphere, but that was not enough to have any detectable climatic influence. The Eyjafjallajökull eruption in Iceland in 2010, while very disruptive of air traffic for weeks, had so little SO_2, and with a short lifetime of a week or so in the troposphere, that it no impact on climate. FAQ 11.2, Figure 1 shows the record of temperature change for the past 1000 years in the Northern Hemisphere along with the major volcanic eruptions of the period.

[INSERT FAQ 11.2, FIGURE 1 HERE]

FAQ 11.2, Figure 1: Northern Hemisphere temperature anomaly, 1000–2000 C.E. and the major volcanic eruptions.

Because volcanic aerosols normally remain in the stratosphere no more than two or three years, the radiative effect of volcanoes is interannual rather than interdecadal in scale. A series of volcanic eruptions could, however, give rise to a decadal-scale cooling, such as happened with small eruptions in the decade 2001–2010. If a period of active volcanism ends for a significant period, the climate system will slowly warm, such as happened from 1912 to 1963. Furthermore, it is possible that feedbacks involving ice and ocean, which act on longer time scales, could transform the short-term volcanic forcing into a longer-term effect. As a result, the possible role of volcanoes in decadal-scale climate change remains unclear.

Recent suggestions that we consider using geo-engineering to control global climate through the creation of a permanent stratospheric aerosol cloud have used volcanic eruptions as an analogue (See Chapters 7 and Section 8.3.2). While volcanic eruptions indeed cool the surface, they also produce ozone depletion and drought, and impact the growth of vegetation, thus raising cautions about the wisdom of such ideas.

While volcanologists are able to detect when various volcanoes become more active, they are not able to predict whether a volcano will erupt, and if it does, how much sulphur it would inject into the stratosphere. Nevertheless, it is important to recognize the three distinct ways that volcanoes affect our ability to predict climate (see Box 11.1 for discussion of general prediction and predictability issues). First, if a violent eruption is detected and that eruption leads to a significant injection of sulphur dioxide in the stratosphere, then, we should be able to include this climatic forcing in our near-term (in this case 1–2 years) climate predictions. There are substantial challenges to including this climatic forcing, such as collecting good observational estimates of the sulphate aerosol concentrations, and modelling the life cycle of the aerosols (i.e., their spatial and temporal distribution) and the associated radiative and chemical interactions. And based on our observations and successful modelling of recent eruptions, we can safely predict that following the next large tropical eruption, there will be global cooling for about 2 years, and winter warming of the Northern Hemisphere continents for one or two years. There will also be reduced summer monsoon precipitation over Asia and Africa. A large Northern Hemisphere high latitude eruption, if it occurs in spring or summer, will also produce a weak summer monsoon.

The second effect of volcanoes on our ability to predict climate is to recognize that they are a potential source of uncertainty in our predictions. We cannot predict volcanic eruptions in advance, but they will occur and lead to short-term climatic impacts both on a local and a global scale. We can, in principle, also account for this potential source of uncertainty by including random eruptions or eruptions based on some scenario in our near-term ensemble climate predictions (see Box 11.1 for further discussion on the use of ensembles to quantify prediction uncertainty). This is an area of research that needs further exploration.

Third, we can use the historical climate record along with estimates of observed sulphate aerosols as a test-bed for evaluating the fidelity of our climate simulations (see also Chapter 9). While the climatic response to explosive volcanic eruptions is a useful analogue for some other climatic forcings, there are also limitations. For example, successful climate model simulations of the impact of one eruption can help validate models used for seasonal and interannual predictions. But they cannot test all the mechanisms involved in global warming over the next century, as long-term oceanic feedbacks are involved, which have a longer time scale than the response to individual volcanic eruptions.

[END FAQ 11.2 HERE]

References

Allen, M.R., Stott, P.A., Mitchell, J.F.B., Schnur, R., Delworth, T. Quantifying theuncertainty in forecasts of anthropogenic climate change. Nature, 407:617–620. (2000)

Allen, R., and S. Sherwood, 2010: The impact of natural versus anthropogenic aerosols on atmospheric circulation in the Community Atmosphere Model. *Climate Dynamics*, 1-20.

Allen, M.R. and & W. Ingram. 2002. Constraints on future changes in climate and the hydrologic cycle Nature 419, 224-232ndoi:10.1038/nature01092.

Allan RP (2009) Examination of relationships between clear-sky longwave radiation and aspects of the atmospheric hydrological cycle in climate models, reanalyses, and observations. J Climate 22:3127–4145

Allan, R.P., (2012) Regime dependent changes in global precipitation, Climate Dynamics, accepted (published online 2011)

Allan RP, Soden BJ, John VO, Ingram I William, Good P (2010) Current changes in tropical precipitation. Environ Res Lett 5, DOI 10.1088/1748-9326/5/2/025205

Alexander, M., L. Matrosova, C. Penland, J.D. Scott, and P. Chang, 2008: Forecasting Pacific SSTs: Linear inverse model predictions of the PDO. *J. Climate*, 21, 385-402.

Alexander, L.V., and J.M. Arblaster, 2009: Assessing trends in observed and modelled climate extremes over Australia in relation to future projections. *International Journal of Climatology,* **29(3)**, 417-435

Alexeev, V. A., D. J. Nicolsky, V. E. Romanovsky, and D. M. Lawrence (2007), An evaluation of deep soil configurations in the CLM3 for improved representation of permafrost, *Geophys. Res. Lett.*, *34*, L09502, doi:10.1029/2007GL029536

Anderson, D. L. T., F. J. Doblas-Reyes, M. A. Balmaseda, and A. Weisheimer, 2009: Decadal variability: processes, predictability and prediction. ECMWF technical memoranda, 591, 47 pp.

Andersson, C. & M. Engardt (2010) European ozone in a future climate: Importance of changes in dry deposition and isoprene emissions. *J. Geophys. Res.,* 115**,** D02303

Andrews, T., P. M. Forster, O. Boucher, N. Bellouin, and A. Jones. 2010. Precipitation, radiative forcing and global temperature change, Geophys. Res. Lett., 37, L14701, doi:10.1029/ 2010GL043991.

Arblaster, J. M. and G. A. Meehl: Contribution of external forcings to southern annular mode trends. J. Clim., 19, 2896-2905 (2006)

Arblaster J.M., G.A. Meehl and D.J. Karoly, 2011: Future climate change in the Southern Hemisphere: Competing effects of ozone and greenhouse gases, *Geophys. Res. Lett.,* **38**, L02701, doi:10.1029/2010GL045384.

Avise, J., J. Chen, B. Lamb, C. Wiedinmyer, A. Guenther, E. Salath & C. Mass (2009) Attribution of projected changes in summertime US ozone and PM2.5 concentrations to global changes. *Atmos. Chem. Phys.,* 9**,** 1111-1124.

Aw, J. & M. J. Kleeman (2003) Evaluating the first-order effect of intraannual temperature variability on urban air pollution. *J. Geophys. Res.,* 108**,** 4365

Bala, G., K. Caldeira, and R. Nemani, 2010. Fast versus slow response in climate change: implications for the global hydrological cycle. Climate Dynamics, **35,** 423-434.

Bollasina M., Y. Ming, V. Ramaswamy (2011) Anthropogenic Aerosols and the Weakening of the South Asian Summer Monsoon, Science, 334, 502-505

Barnes, E. A., and D. L. Hartmann, 2010: Influence of eddy-driven jet latitude on North Atlantic jet persistence and blocking frequency in CMIP3 integrations. *Geophys. Res. Lett.*, **37,** L23802.

Bates, B.C., Z.W. Kundzewicz, S. Wu and J.P. Palutikof, Eds., 2008: Climate Change and Water. Technical Paper of the Intergovernmental Panel on Climate Change, IPCC Secretariat, Geneva, 210 pp

Battisti, D.S., and E.S. Sarachik, 1995: Understanding and predicting ENSO. Rev. Geophys., 33(Suppl.), 1367-1376.

Bauer, S. E., D. Koch, N. Unger, S. M. Metzger, D. T. Shindell & D. G. Streets (2007) Nitrate aerosols today and in 2030: a global simulation including aerosols and tropospheric ozone. *Atmos. Chem. Phys.,* 7**,** 5043-5059

Bellouin, N., J. Rae, A. Jones, C. Johnson, J. Haywood, and O. Boucher, 2011: Aerosol forcing in the Climate Model Intercomparison Project (CMIP5) simulations by HadGEM2-ES and the role of ammonium nitrate. *J. Geophys. Res.*, **116,** D20206.

Bengtsson, L., K.I. Hodges, and E. Roeckner, 2006: Storm tracks and climate change. Journal of Climate, 19(15), 3518-3543

Bender, M.A., T.R. Knutson, R.E. Tuleya, J.J. Sirutis, G.A. Vecchi, S.T. Garner, and I.M. Held, 2010: Modeled impact of anthropogenic warming on the frequency of intense Atlantic hurricanes. Science, 327(5964), 454-458.

Berner, J., F. J. Doblas-Reyes, T. N. Palmer, G. Shutts, and A. Weisheimer, 2008: Impact of a quasi-stochastic cellular automaton backscatter scheme on the systematic error and seasonal prediction skill of a global climate model. *Philosophical Transactions of the Royal Society a-Mathematical Physical and Engineering Sciences*, **366,** 2561-2579.

Betts, R.A., O. Boucher, M. Collins, P.M. Cox, P.D. Falloon, N. Gedney, D.L. Hemming, C.Huntingford, C.D. Jones, D.M.H. Sexton and M. J. Webb. 2007. Projected increase in continental runoff due to plant responses to increasing carbon dioxide. Nature 448, 1037-1042.

Bitz, C.M., P.r. Gent, R.A. Woodgate, M.M. Holland, and R. Lindsay, 2006: The influence of sea ice on ocean heat uptke in response to increasing CO2. J. Climate, 19, 2437-2450.

Bitz, C.M., 2008: Some aspects of uncertainty in predicting sea ice thinning. Arctic Sea Ice Decline: Observations, Projections, Mechanisms, and Implications. Geophysical Monographs, 180, American Geophysical Union, 63-76.

Bloomer, B. J., J. W. Stehr, C. A. Piety, R. J. Salawitch & R. R. Dickerson (2009) Observed relationships of ozone air pollution with temperature and emissions. *Geophys. Res. Lett.,* 36**,** L09803.

Boer, G.J. 2000: A study of atmosphere-ocean predictability on long time scales. *Climate Dyn*., 16, 469-477.

Boer, G.J., 2004: Long timescale potential predictability in an ensemble of coupled climate models. *Climate Dyn*., 23, 29-44.

Boer, G. J., and S. J. Lambert, 2008: Multi-model decadal potential predictability of precipitation and temperature, *Geophys. Res. Lett*., 35, L05706, doi:10.1029/2008GL033234.

Boer, G.J. 2010: Decadal potential predictability of 21st century climate. *Climate Dyn*., doi: 10.1007/s00382-010-0747-9

Boer, and Yu, 2003: Climate sensitivity and response. *Climate Dynamics*, **20,** 415-429.

Boer, G. J., 2009: Climate trends in a seasonal forecasting system. *Atmosphere-Ocean*, **47,** 123-138.

Bollasina, M. A., Y. Ming, and V. Ramaswamy, 2011: Anthropogenic Aerosols and the Weakening of the South Asian Summer Monsoon. *Science*.

Bond, T. C., and H. Sun, 2005: Can Reducing Black Carbon Emissions Counteract Global Warming? *Environmental Science & Technology*, **39,** 5921-5926.

Brandefelt, J., and H. Kornich, 2008: Northern Hemisphere Stationary Waves in Future Climate Projections. *Journal of Climate***,** 6341-6353.

Branstator, G. and H. Teng. 2010: Two limits of initial-value decadal predictability in a CGCM. *J. Climate*, 23, 6292-6311.

Branstator, G., H. Teng, G. Meehl, M. Kimoto, J. Knight, M. Latif, A. Rosati, 2011: Systematic estimates of initial value decadal predictability for six AOGCMS. *J. Climate*, doi:10.1175/JCLI-D-11-00227.1.

Burke EJ, Brown SJ, Christidis N (2006) Modeling the recent evolution of global drought and projections for the twenty-first century with the Hadley Centre climate model. J Hydrometeorol 7:1113–1125

Butchart, N., and Coauthors, 2010a: Chemistry–Climate Model Simulations of Twenty-First Carvalho, A., A. Monteiro, M. Flannigan, S. Solman, A. I. Miranda, and C. Borrego, 2011: Forest fires in a changing climate and their impacts on air quality. *Atmospheric Environment*, **45,** 5545-5553.

Bryan, Frank O., Gokhan Danabasoglu, Norikazu Nakashiki, Yoshikatsu Yoshida, Dong-Hoon Kim, Junichi Tsutsui, Scott C. Doney, 2006: Response of the North Atlantic Thermohaline Circulation and Ventilation to Increasing Carbon Dioxide in CCSM3. *J. Climate*, **19**, 2382–2397. doi: 10.1175/JCLI3757.1

Brown, R and P.W. Mote. The response of Northern Hemisphere snow cover to a changing climate, 2009. *J Clim* 22: 2124–2145.

Callaghan, J. and S. B. Power, 2011: Variability and decline in the number of severe land-falling tropical cyclones making land-fall over eastern Australia since the late 19th century. *Climate Dynamics*, **37**, 647-662, DOI 10.1007/s00382-010-0883-2.

Cao, L., G. Bala, K. Caldeira, R. Nemani, and G. Ban-Weiss. 2009. Climate response to physiological forcing of carbon dioxide simulated by the coupled Community Atmosphere Model (CAM3.1) and Community Land Model (CLM3.0), Geophys. Res. Lett., 36, L10402, doi:10.1029/2009GL037724.

Cao, L., G. Bala, K. Caldeira, R. Nemani, and G. Ban-Weiss. 2010. Importance of carbon dioxide physiological forcing to future climate change, Proceedings of the National Academy of Sciences, DOI 10.1073/pnas.0913000107

Carvalho, A., A. Monteiro, M. Flannigan, S. Solman, A. I. Miranda & C. Borrego (2011) Forest fires in a changing climate and their impacts on air quality. *Atmospheric Environment,* 45**,** 5545-5553.

Carlton, A. G., R. W. Pinder, P. V. Bhave & G. A. Pouliot (2010) To What Extent Can Biogenic SOA be Controlled? *Environmental Science & Technology,* 44**,** 3376-3380.

Carlton, A. G., C. Wiedinmyer & J. H. Kroll (2009) A review of Secondary Organic Aerosol (SOA) formation from isoprene. *Atmos. Chem. Phys.,* 9**,** 4987-5005.

Ceppi, P., S. C. Scherrer, A. M. Fischer & C. Appenzeller (2010) Revisiting Swiss temperature trends 1959–2008. *International Journal of Climatology***,** n/a-n/a.

Chen, W., Y. Lee, P. Adams, A. Nenes, and J. Seinfeld, 2010a: Will black carbon mitigation dampen aerosol indirect forcing? *Geophysical Research Letters*, **37,** -.

Chen, W., A. Nenes, H. Liao, P. Adams, J. Li, and J. Seinfeld, 2010b: Global climate response to anthropogenic aerosol indirect effects: Present day and year 2100. *Journal of Geophysical Research-Atmospheres*, **115,** -.

Chen, J., J. Avise, A. Guenther, C. Wiedinmyer, E. Salathe, R. B. Jackson & B. Lamb (2009a) Future land use and land cover influences on regional biogenic emissions and air quality in the United States. *Atmospheric Environment,* 43**,** 5771-5780.

Chen, J., J. Avise, B. Lamb, E. Salath, C. Mass, A. Guenther, C. Wiedinmyer, J. F. Lamarque, S. O'Neill, D. McKenzie & N. Larkin (2009b) The effects of global changes upon regional ozone pollution in the United States. *Atmos. Chem. Phys.,* 9**,** 1125-1141.

Chen, G, and Isaac Held, 2007: Phase speed spectra and the recent poleward shift of Southern Hemisphere surface westerlies. Geophysical Research Letters, 34, L21805, DOI:10.1029/2007GL031200.

Chen, G., J. Lu, and D. Frierson, 2008: The shift in surface westerlies during climate change. J. of Climate 21, 5942-5959.
Chou, C., J. D. Neelin, C. Chen, and j. Tu. 2009. Evaluating the 'Rich-Get-Richer' Mechanism in Tropical Precipitation Change under Global Warming. J. Climate, 22, 1982–2005.
Chou, C., J.-Y. Tu, and P.-H. Tan, 2007: Asymmetry of tropical precipitation change under global warming, *Geophys. Res. Lett*., **34**, L17708, doi:10.1029/ 2007GL030327.
Christensen et al, 2007, Chapter 11 Regional Climate Projections, in IPCC WG1 AR4.
Christensen, J. H. and O. B. Christensen, 2007: A summary of the PRUDENCE model projections of changes in European climate by the end of this century. Climatic Change, 81, 7–30
Chylek P., Folland C.K., Lesins G., Dubey M.K., 2010: Twentieth century bipolar seesaw of the Arctic and Antarctic surface air temperatures. Geophys. Res. Lett., 37, Art. No. L08703
Chylek, P., Folland C.K., Lesins G., Dubey, M.K. and Wang, M.Y., 2009: Arctic air temperature change amplification and the Atlantic multidecadal oscillation. Geophys. Res. Lett. 36, Art. No. L14801
Clark, R. T., J. M. Murphy, and S. J. Brown, 2010: Do global warming targets limit heatwave risk? *Geophys. Res. Lett.*, **37,** L17703.
Cofala, J., M. Amann, Z. Klimont, K. Kupiainen, and L. Hoglund-Isaksson, 2007: Scenarios of global anthropogenic emissions of air pollutants and methane until 2030. *Atmospheric Environment*, **41,** 8486-8499.
Collins, B., M. G. Sanderson, and C. E. Johnson, 2009: Impact of increasing ship emissions on air quality and deposition over Europe by 2030. *Meteorologische Zeitschrift*, **18,** 25-39.
Collins, M. 2002: Climate predictability on interannual to decadal time scales: The initial value problem. *Climate Dyn*., 19, 671-692.
Collins, M., Botzet, M., Carril, A., Drange, H., Jouzeau, A., Latif, M., Otteraa, O.H., Pohlmann, H., Sorteberg, A., Sutton, R., and Terray, L., 2006. Interannual to decadal climate predictability: A multimodel-ensemble study. - Journal of Climate, 19, 1195-1203.
Collins, M., S.I. An, W.J. Cai, A. Ganachaud, E. Guilyardi, F.F. Jin, M. Jochum, M. Lengaigne, S. Power, A. Timmermann, G. Vecchi, and A. Wittenberg, 2010: The impact of global warming on the tropical Pacific ocean and El Nino. Nature Geoscience, 3(6), 391-397
Comiso, J. C., Parkinson, C. L., Gersten, R. & Stock, L. Accelerated decline in the Arctic sea ice cover. Geophys. Res. Lett. 35, doi:10.1029/2007GL031972 (2008).
Cook, B. I., R. L. Miller, and R. Seager, 2009: Amplification of the North American "Dust Bowl" drought through human-induced land degradation. *Proceedings of the National Academy of Sciences*, **106,** 4997-5001.
Cox, W., and S. Chu, 1996: Assessment of interannual ozone variation in urban areas from a climatological perspective. *Atmospheric Environment*, **30,** 2615-2625.
Cox, P., and D. Stephenson, 2007: A changing climate for prediction. *Science,* **317,** 207–208, doi:10.1126/science.1145956.
Delworth, T., and K. Dixon, 2006: Have anthropogenic aerosols delayed a greenhouse gas-induced weakening of the North Atlantic thermohaline circulation? *Geophysical Research Letters***,** -.
Delworth, Thomas L., V Ramaswamy, and G Stenchikov, 2005: The impact of aerosols on simulated ocean temperature and heat content in the 20th century. *Geophysical Research Letters*, **32**, L24709, DOI:10.1029/2005GL024457.
Delworth, T., and F. Zeng, 2008: Simulated impact of altered Southern Hemisphere winds on the Atlantic Meridional Overturning Circulation. *Geophysical Research Letters***,** -.
Dentener, F., D. Stevenson, J. Cofala, R. Mechler, M. Amann, P. Bergamaschi, F. Raes & R. Derwent (2005) The impact of air pollutant and methane emission controls on tropospheric ozone and radiative forcing: CTM calculations for the period 1990-2030. *Atmos. Chem. Phys.,* 5**,** 1731-1755.
Dentener, F., D. Stevenson, K. Ellingsen, T. van Noije, M. Schultz, M. Amann, C. Atherton, N. Bell, D. Bergmann, I. Bey, L. Bouwman, T. Butler, J. Cofala, B. Collins, J. Drevet, R. Doherty, B. Eickhout, H. Eskes, A. Fiore, M. Gauss, D. Hauglustaine, L. Horowitz, I. S. A. Isaksen, B. Josse, M. Lawrence, M. Krol, J. F. Lamarque, V. Montanaro, J. F. Muller, V. H. Peuch, G. Pitari, J. Pyle, S. Rast, J. Rodriguez, M. Sanderson, N. H. Savage, D. Shindell, S. Strahan, S. Szopa, K. Sudo, R. Van Dingenen, O. Wild & G. Zeng (2006a) The global atmospheric environment for the next generation. *Environmental Science & Technology,* 40**,** 3586-3594.
Dentener, F., D. Stevenson, K. Ellingsen, T. van Noije, M. Schultz, M. Amann, C. Atherton, N. Bell, D. Bergmann, I. Bey, L. Bouwman, T. Butler, J. Cofala, B. Collins, J. Drevet, R. Doherty, B. Eickhout, H. Eskes, A. Fiore, M. Gauss, D. Hauglustaine, L. Horowitz, I. S. A. Isaksen, B. Josse, M. Lawrence, M. Krol, J. F. Lamarque, V. Montanaro, J. F. Müller, V. H. Peuch, G. Pitari, J. Pyle, S. Rast, J. Rodriguez, M. Sanderson, N. H. Savage, D. Shindell, S. Strahan, S. Szopa, K. Sudo, R. Van Dingenen, O. Wild & G. Zeng (2006b) The Global Atmospheric Environment for the Next Generation. *Environmental Science & Technology,* 40**,** 3586-3594.
Deser, C., A. S. Phillips, and J. W. Hurrell, 2004: Pacific interdecadal climate variability: Linkages between the tropics and the North Pacific during boreal winter since 1900. *Journal of Climate*, **17,** 3109–3124.
Deser, C, Phillips, A. Bourdette,V. and Teng, H. 2010: Uncertainty in climate change projections: The role of internal variability. *Clim. Dyn*. doi 10.1007/s00382-010-0977-x.
DeWeaver, E.T., E.C. Hunke, M.M. Holland, 2008: Comment on "On the reliability of simulated Arctic sea ice in global climate models" by I. Eisenman, N. Untersteiner, nad J.S. Wettlaufer. Geophys. Res. Lett., 35:L04501. Doi:10.1029/gl031325.

Diffenbaugh, N. S., and M. Ashfaq, 2010: Intensification of hot extremes in the United States. *Geophys. Res. Lett.*, **37,** L15701.
DiNezio, P., A. Clement, G. Vecchi, B. Soden, and B. Kirtman, 2009: Climate Response of the Equatorial Pacific to Global Warming. *Journal of Climate***,** 4873-4892.
Doblas-Reyes, F.J., M.A. Balmaseda, A. Weisheimer and T.N. Palmer (2011). Decadal climate prediction with the ECMWF coupled forecast system: Impact of ocean observations. Journal Geophysical Research, 116, D19111, doi: doi:10.1029/2010JD015394
Doblas-Reyes, F. J., M. A. Balmaseda, A. Weisheimer, and T. N. Palmer, 2010a: Decadal climate prediction with the ECMWF coupled forecast system: Impact of ocean observations. Tech. Memo., 633, ECMWF, www.ecmwf.int/publications/
Doherty, R., M. Heal, P. Wilkinson, S. Pattenden, M. Vieno, B. Armstrong, R. Atkinson, Z. Chalabi, S. Kovats, A. Milojevic & D. Stevenson (2009) Current and future climate- and air pollution-mediated impacts on human health. *Environmental Health,* 8, -.
Drijfhout, S.S. and W. Hazeleger, *Detecting Atlantic MOC changes in an ensemble of climate change simulations* J. Climate, 2007, 20, 8, 1571-1582, doi:10.1175/JCLI4104.1.
Dunstone, N. J., and D. M. Smith, 2010: Impact of atmosphere and sub-surface ocean data on decadal climate prediction. *Geophysical Research Letters*, **37,** L02709.
Dunstone, N. J., D. M. Smith, and R. Eade, 2011: Multi-year predictability of the tropical Atlantic atmosphere driven by the high latitude North Atlantic Ocean. *Geophysical Research Letters*, **38,** L14701.
Durack, Paul J., Susan E. Wijffels, 2010: Fifty-Year Trends in Global Ocean Salinities and Their Relationship to Broad-Scale Warming. *J. Climate*, **23**, 4342–4362. doi: 10.1175/2010JCLI3377.1
Euskirchen, E. S., et al. (2006), Importance of recent shifts in soil thermal dynamics on growing season length, productivity, and carbon sequestration in terrestrial high-latitude ecosystems, *Glob. Change Biol.*, *12*, 731-750.
El Nadi, A.H.1974. The Significance of Leaf Area in Evapotranspiration. Ann. Bot. 38 (3): 607-611.
Emanuel, K., R. Sundararajan, and J. Williams, 2008: Hurricanes and Global Warming: Results from Downscaling IPCC AR4 Simulations. Bulletin of the American Meteorological Society, 89(3), 347-367
Eyring, V., and Coauthors, 2010: Transport impacts on atmosphere and climate: Shipping. *Atmospheric Environment*, **44,** 4735-4771.
Fang, Y., and Coauthors, 2011: The impacts of changing transport and precipitation on pollutant distributions in a future climate. *J. Geophys. Res.*, **116,** D18303.
Fan, Y., and H. van den Dool, 2008: A global monthly land surface air temperature analysis for 1948-present. *Journal of Geophysical Research A*, **113**.
Feulner, G., and S. Rahmstorf, 2010: On the effect of a new grand minimum of solar activity on the future climate on Earth. Geophys. Res. Lett., 37, DOI: 10.1029/2010GL042710
Field, C., Jackson, R. & Mooney, H. 1995. Stomatal responses to increased CO2: implications from the plant to the global scale. Plant Cell Environ. 18, 1214–1255.
Filleul, L., and Coauthors, 2006: The relation between temperature, ozone, and mortality in nine french cities during the heat wave of 2003. *Environmental Health Perspectives*, **114,** 1344-1347.
Fiore, A. M., J. J. West, L. W. Horowitz, V. Naik, and M. D. Schwarzkopf, 2008: Characterizing the tropospheric ozone response to methane emission controls and the benefits to climate and air quality. *J. Geophys. Res.*, **113,** D08307.
Fiore, A. M., D. J. Jacob, B. D. Field, D. G. Streets, S. D. Fernandes, and C. Jang, 2002: Linking ozone pollution and climate change: The case for controlling methane. *Geophys. Res. Lett.*, **29,** 1919.
Fiore, A. M., and Coauthors, 2009: Multimodel estimates of intercontinental source-receptor relationships for ozone pollution. *J. Geophys. Res.*, **114,** D04301.
Fischer, E.M., and C. Schär, 2009: Future changes in daily summer temperature variability: driving processes and role for temperature extremes. Climate Dynamics, 33(7-8), 917-935.
Fischer, E.M., and C. Schär, 2010: Consistent geographical patterns of changes in high-impact European heatwaves. Nature Geoscience, 3(6), 398 – 403
Flanner, M. G., C. S. Zender, J. T. Randerson, and P. J. Rasch, 2007: Present-day climate forcing and response from black carbon in snow. *J. Geophys. Res.*, **112,** D11202.
Fleming, E., C. Jackman, R. Stolarski, and A. Douglass, 2011: A model study of the impact of source gas changes on the stratosphere for 1850-2100. *Atmospheric Chemistry and Physics*, **11,** 8515-8541.
Fogt, R., J. Perlwitz, A. Monaghan, D. Bromwich, J. Jones, and G. Marshall, 2009: Historical SAM Variability. Part II: Twentieth-Century Variability and Trends from Reconstructions, Observations, and the IPCC AR4 Models. *Journal of Climate***,** 5346-5365.
Folland, C., J. Knight, H. Linderholm, D. Fereday, S. Ineson, and J. Hurrell, 2009: The Summer North Atlantic Oscillation: Past, Present, and Future. *Journal of Climate***,** 1082-1103.
Forkel, R., and R. Knoche, 2006: Regional climate change and its impact on photooxidant concentrations in southern Germany: Simulations with a coupled regional climate-chemistry model. *J. Geophys. Res.*, **111,** D12302.
Fowler, H.J., and M. Ekstrom, 2009: Multi-model ensemble estimates of climate change impacts on UK seasonal precipitation extremes. International Journal of Climatology, 29(3), 385-416

Frieler, K., M. Meinshausen, T. Schneider von Deimling, T. Andrews, and P. Forster (2011), Changes in global-mean precipitation in response to warming, greenhouse gas forcing and black carbon, Geophys. Res. Lett., 38,L04702, doi:10.1029/2010GL045953

Frierson, D. M. W., J. Lu, and G. Chen, 2007: Width of the Hadley cell in simple and comprehensive general circulation models. Geophys. Res.Lett., 34, Art. No. L18804

Fyfe, J. C., W. J. Merryfield, V. Kharin, G. J. Boer, W.-S. Lee, and K. von Salzen, 2012: Skillful predictions of decadal trends in global mean surface temperature. *Geophysical Research Letters*, **accepted**.

Galloway, J. N., and Coauthors, 2008: Transformation of the Nitrogen Cycle: Recent Trends, Questions, and Potential Solutions. *Science*, **320,** 889-892.

Ganzeveld, L., L. Bouwman, E. Stehfest, D. P. van Vuuren, B. Eickhout & J. Lelieveld (2010) Impact of future land use and land cover changes on atmospheric chemistry-climate interactions. *J. Geophys. Res.,* 115**,** D23301.

García-Serrano, J., and F. J. Doblas-Reyes, 2012: On the assessment of near-surface global temperature and North Atlantic multi-decadal variability in the ENSEMBLES decadal hindcast. *Climate Dynamics*, **under review**.

Gastineau, G., Li, L. & Le Treut, H. The Hadley and Walker circulation changes in global warming conditions described by idealised atmospheric simulations. J. Climate 22, 3993–4013 (2009).

Gauss, M., and Coauthors, 2003: Radiative forcing in the 21st century due to ozone changes in the troposphere and the lower stratosphere. *Journal of Geophysical Research-Atmospheres*, **108,**

Gedney, N. P. M. Cox, R. A. Betts, O. Boucher, C. Huntingford and P. A. Stott. 2006. Detection of a direct carbon dioxide effect in continental river runoff records. Nature 439, 835–838.

Gillett, N. and D. W. J. Thompson: Simulation of recent Southern Hemisphere climate change. Science, 302, 273-275 (2003)

Gorodetskaya, I.V., L.B. Tremblay, B. Liepert, M.A. Cane, and R.I. Cullather, 2008: The influence of cloud and surface properties on the Arctic Ocean shortwave radiation budget in coupled models. J. Climate, 21, doi:10.1175/2007JCLI1614.1.

Gosling, S. N., Taylor, R. G., Arnell, N. W. and M.C. Todd. 2011. A comparative analysis of projected impacts of climate change on river runoff from global and catchment-scale hydrological models, *Hydrol. Earth Syst. Sci.* 15, 279-294.

Granier, C., and Coauthors, 2006: Ozone pollution from future ship traffic in the Arctic northern passages. *Geophys. Res. Lett.*, **33,** L13807.

Gray, L.J., J. Beer, M. Geller, J. D. Haigh, M. Lockwood, K. Matthes, U. Cubasch, D. Fleitmann, G. Harrison, L. Hood, J. Luterbacher, G. A. Meehl, D. Shindell, B. van Geel and W. White, 2010. Solar influences on climate. Rev. Geophys., 48 (RG4001), doi:10.1029/2009RG000282.

Gregory, J.M., Mitchell, J.F.B., 1995: Simulation of daily variability of surface-temperature and precipitation over Europe in the current and 2xCO2 climates using the UKMO climate model. Quart. J. Roy. Meteorol. Soc., 121 (526), 1451-1476

Gregory, J., 2010: Long-term effect of volcanic forcing on ocean heat content. *Geophysical Research Letters***, 37**, L22701, [doi:10.1029/2010GL045507] 2010

Gregory, J., and Forster, P. M., 2008: Transient climate response estimated from radiative forcing and observed temperature change. /Journal Of Geophysical Research/, 113, D23105, [doi:10.1029/2008jd010405 2008

Gualdi, S., E. Scoccimarro, and A. Navarra, 2008: Changes in Tropical Cyclone Activity due to Global Warming: Results from a High-Resolution Coupled General Circulation Model. Journal of Climate, 21(20), 5204-5228

Gutowski, W.J., G.C. Hegerl, G.J. Holland, T.R. Knutson, L.O. Mearns, R.J. Stouffer, P.J. Webster, M.F. Wehner, and F.W. Zwiers, 2008: Causes of observed changes in extremes and projections of future changes. In: Weather and Climate Extremes in a Changing Climate. Regions of Focus: North America, Hawaii, Caribbean, and U.S. Pacific Islands. [T.R. Karl, G.A. Meehl, D.M. Christopher, S.J. Hassol, A.M. Waple, and W.L. Murray (eds.)]. A Report by the U.S. Climate Change Science Program and the Subcommittee on Global Change Research, Washington, DC

Guémas, V., F. J. Doblas-Reyes, F. Lienert, H. Du, and Y. Soufflet, 2012: Identifying the causes for the low decadal climate forecast skill over the North Pacific. *Nature Geosciences*, **submitted**.

Haigh, J. D., A. R. Winning, R. Toumi and J. W. Harder, 2010. An influence of solar spectral variations on radiative forcing of 415 climate, Nature, 467, 696-699, doi:10.1038/nature09426.

Hallquist, M., and Coauthors, 2009: The formation, properties and impact of secondary organic aerosol: current and emerging issues. *Atmos. Chem. Phys.*, **9,** 5155-5236.

Hansen, J., M. Sato, R. Ruedy, A. Lacis, and V. Oinas, 2000: Global warming in the twenty-first century: An alternative scenario. *Proceedings of the National Academy of Sciences*, **97,** 9875-9880.

Hansen, J., R. Ruedy, M. Sa, and K. Lo, 2010: Global surface temperature change. *Reviews in Geophysics*, **48,** RG4004.

Harder, J. W., J. M. Fontenla, P. Pilewskie, E. C. Richard, and T. N. Woods, 2009. Trends in solar spectral irradiance variability in the visible and infrared, Geophys. Res. Lett., 36, L07801, doi:10.1029/2008GL036797.

Hawkins, E., and R. Sutton, 2009: THE POTENTIAL TO NARROW UNCERTAINTY IN REGIONAL CLIMATE PREDICTIONS. *Bulletin of the American Meteorological Society***,** 1095-+.

——, 2010: The potential to narrow uncertainty in projections of regional precipitation change. *Climate Dynamics***,** 1-12.

Hawkins and Sutton, 2011, Time of Emergence of Climate Signals, **submitted** to GRL

Hawkins, E., J. Robson, R. T. Sutton, D. M. Smith, and N. Keenlyside, 2011: Evaluating the potential for statistical decadal predictions of sea surface temperatures with a perfect model approach. *Climate Dynamics,* DOI: 10.1007/s00382-011-1023-3.

Heald, C. L., and Coauthors, 2008: Predicted change in global secondary organic aerosol concentrations in response to future climate, emissions, and land use change. *J. Geophys. Res.*, **113,** D05211.

Hedegaard, G. B., J. Brandt, J. H. Christensen, L. M. Frohn, C. Geels, K. M. Hansen, and M. Stendel, 2008: Impacts of climate change on air pollution levels in the Northern Hemisphere with special focus on Europe and the Arctic. *Atmos. Chem. Phys.*, **8,** 3337-3367.

Hegglin, M., and T. Shepherd, 2009: Large climate-induced changes in ultraviolet index and stratosphere-to-troposphere ozone flux. *Nature Geoscience***,** 687-691.

Held, I., and B. Soden, 2006: Robust responses of the hydrological cycle to global warming. *Journal of Climate***,** 5686-5699.

Henderson, B. H., and Coauthors, 2011: Evaluation of simulated photochemical partitioning of oxidized nitrogen in the upper troposphere. *Atmos. Chem. Phys.*, **11,** 275-291.

Hermanson, L., and R. T. Sutton, 2009: Climate predictability in the second year. *Philosophical Transactions of the Royal Society a-Mathematical Physical and Engineering Sciences*, **367,** 913-916.

Hoerling et al, 2011, On North American Decadal Climate for 2011-20, to appear in *J. Climate*

Hogrefe, C., and Coauthors, 2004: Simulating changes in regional air pollution over the eastern United States due to changes in global and regional climate and emissions. *J. Geophys. Res.*, **109,** D22301.

Holland, M. M., J. Finnis, and M. C. Serreze, 2006: Simulated Arctic Ocean freshwater budgets in the twentieth and twenty-first centuries. *Journal of Climate*, **19,** 6221-6242.

Holland, M.M., J. Finnis, A.P. Barrett, and M.C. Serreze, 2007: Projected changes in Arctic Ocean freshwater budgets. *J. Geophys. Res*., **112**, G04S55, doi:10.1029/2006JG000354.

Holland, M.M., M.C. Serreze, and J. Stroeve, 2008: The sea ice mass budget of the Arctic and its future change as simulated by coupled climate models. *Climate Dynamics*, doi:10.1007/s00382-008-0493-4.

Holloway, T., and Coauthors, 2008: Change in ozone air pollution over Chicago associated with global climate change. *J. Geophys. Res.*, **113,** D22306.

Holmes, C., Q. Tang, and M. Prather, 2011: Uncertainties in climate assessment for the case of aviation NO. *Proceedings of the National Academy of Sciences of the United States of America*, **108,** 10997-11002.

Hoyle, C. R., and Coauthors, 2011: A review of the anthropogenic influence on biogenic secondary organic aerosol. *Atmos. Chem. Phys.*, **11,** 321-343.

Hsu, J., and M. Prather, 2010: Global long-lived chemical modes excited in a 3-D chemistry transport model: Stratospheric N2O, NOy, O-3 and CH4 chemistry. *Geophysical Research Letters*, **37,** -.

HTAP, 2010: *HEMISPHERIC TRANSPORT OF AIR POLLUTION 2010, PART A: OZONE AND PARTICULATE MATTER.* Vol. 17, United Nations, 278 pp.

Huang, H.-C., and Coauthors, 2008: Impacts of long-range transport of global pollutants and precursor gases on U.S. air quality under future climatic conditions. *J. Geophys. Res.*, **113,** D19307.

Huebener, H., U. Cubasch, U. Langematz, T. Spangehl, F. Niehorster, I. Fast, and M. Kunze, 2007: Ensemble climate simulations using a fully coupled ocean-troposphere-stratosphere general circulation model. *Philosophical Transactions of the Royal Society a-Mathematical Physical and Engineering Sciences***,** 2089-2101.

Hungate, B. A., et al. 2002, Evapotranspiration and soil water content in a scrub-oak woodland under carbon dioxide enrichment, Global Change Biol., 8, 289 – 298, doi:10.1046/j.1365-2486. 2002.00468.x

Hyde, William T., Thomas J. Crowley, 2000: Probability of Future Climatically Significant Volcanic Eruptions. *J. Climate*, **13**, 1445–1450. doi: 10.1175/1520-0442(2000)013<1445:LOFCSV>2.0.CO;2

International Arctic Science Committee (IASC), 2010: Peter Saundry (Topic Editor) "Arctic Climate Impact Assessment (full report)". In: Encyclopedia of Earth. Eds. Cutler J. Cleveland (Washington, D.C.: Environmental Information Coalition, National Council for Science and the Environment).

Ihara, C., and Y. Kushnir, 2009: Change of mean midlatitude westerlies in 21st century climate simulations. *Geophysical Research Letters***,** -.

Ito, A., S. Sillman, and J. E. Penner, 2009: Global chemical transport model study of ozone response to changes in chemical kinetics and biogenic volatile organic compounds emissions due to increasing temperatures: Sensitivities to isoprene nitrate chemistry and grid resolution. *J. Geophys. Res.*, **114,** D09301.

Ineson, S., A.A. Scaife, J.R. Knight, J.C. Manners, NJ. Dunstone, L.J. Gray and J.D. Haigh, 2011. Solar forcing of winter climate variability in the Northern Hemisphere. Nature Geosciences, 4, 753-757.

Jacob, D. J., and coauthors, 1993: Factors regulating ozone over the United State and its export to the global atmosphere. J. Geophys. Res., 98, D8, 14817-14826.

Jacob, D. J., and D. A. Winner, 2009: Effect of climate change on air quality. *Atmospheric Environment*, **43,** 51-63.

Jacob, D. J., J. A. Logan, and P. P. Murti, 1999: Effect of rising Asian emissions on surface ozone in the United States. *Geophys. Res. Lett.*, **26,** 2175-2178.

Jacobson, M., 2006: Effects of externally-through-internally-mixed soot inclusions within clouds and precipitation on global climate. *Journal of Physical Chemistry a***,** 6860-6873.

——, 2008a: Effects of wind-powered hydrogen fuel cell vehicles on stratospheric ozone and global climate. *Geophysical Research Letters***,** -.

——, 2008b: Short-term effects of agriculture on air pollution and climate in California. *Journal of Geophysical Research-Atmospheres*, -.
——, 2010: Short-term effects of controlling fossil-fuel soot, biofuel soot and gases, and methane on climate, Arctic ice, and air pollution health. *Journal of Geophysical Research-Atmospheres*, -.
Jacobson, M., and D. Streets, 2009: Influence of future anthropogenic emissions on climate, natural emissions, and air quality. *Journal of Geophysical Research-Atmospheres*, -.
Jacobson, M., Y. Kaufman, and Y. Rudich, 2007: Examining feedbacks of aerosols to urban climate with a model that treats 3-D clouds with aerosol inclusions. *Journal of Geophysical Research-Atmospheres*, -.
Jacobson, M. Z., 2002: Control of fossil-fuel particulate black carbon and organic matter, possibly the most effective method of slowing global warming. *J. Geophys. Res.*, **107,** 4410.
Jaffe, D., D. Chand, W. Hafner, A. Westerling, and D. Spracklen, 2008: Influence of Fires on O3 Concentrations in the Western U.S. *Environmental Science & Technology*, **42,** 5885-5891.
Jiang, X., Z.-L. Yang, H. Liao, and C. Wiedinmyer, 2010: Sensitivity of biogenic secondary organic aerosols to future climate change at regional scales: An online coupled simulation. *Atmospheric Environment*, **44,** 4891-4907.
Jiang, X., C. Wiedinmyer, F. Chen, Z.-L. Yang, and J. C.-F. Lo, 2008: Predicted impacts of climate and land use change on surface ozone in the Houston, Texas, area. *J. Geophys. Res.*, **113,** D20312.
Jickells, T. D., and Coauthors, 2005: Global Iron Connections Between Desert Dust, Ocean Biogeochemistry, and Climate. *Science*, **308,** 67-71.
Johansson, A., 2007: Prediction skill of the NAO and PNA from daily to seasonal time scales. *Journal of Climate*, **20,** 1957-1975.
Johnson, N.C., and S.-P. Xie, 2010: Changes in the sea surface temperature threshold for tropical convection. *Nature Geosci*., 3, 842-845; advance online publication, 7 November 2010 (doi:10.1038/ngeo1008)
Johnson, C. E., W. J. Collins, D. S. Stevenson, and R. G. Derwent, 1999: Relative roles of climate and emissions changes on future tropospheric oxidant concentrations. *J. Geophys. Res.*, **104,** 18631-18645.
Johnson, C. E., D. S. Stevenson, W. J. Collins, and R. G. Derwent, 2001: Role of climate feedback on methane and ozone studied with a Coupled Ocean‐Atmosphere‐Chemistry Model. *Geophys. Res. Lett.*, **28,** 1723-1726.
Jolliffe, I. T., and D. B. Stephenson, 2003: *Forecast Verification: A Practitioner's Guide in Atmospheric Science.* Wiley and Sons, 240 pp. pp.
Jones G.S., M. Lockwood and P.A. Stott, 2011. What infuence will future solar activity changes overthe 21st century have on projected global near surface temperature changes? **Submitted** to J. Geophys. Res.
Lockwood, M., 2010. Solar change and climate: an update in the light of the current exceptional solar minimum. Proc. Roy. Soc. A., vol 466, no. 2114, 303-329.
Jung, I-W. and Chang, H. 2011. Assessment of future runoff trends under multiple climate change scenarios in the Willamette River Basin, Oregon, USA, Hydrological Processes 25(2): 258-277.
Kang, S.M. and L.M. Polvani: The interannual relationship between the eddy-driven jet and the edge of the Hadley cell, J. Clim., 24, 563-568, doi: 10.1175/2010JCLI4077.1 **(2011)**
Katragkou, E., P. Zanis, I. Kioutsioukis, I. Tegoulias, D. Melas, B. C. Kruger, and E. Coppola, 2011: Future climate change impacts on summer surface ozone from regional climate-air quality simulations over Europe. *J. Geophys. Res.*, **in press**.
——, **in press**: Future climate change impacts on summer surface ozone from regional climate-air quality simulations over Europe. *J. Geophys. Res.*
Katragkou, E., and Coauthors, 2010: Decadal regional air quality simulations over Europe in present climate: near surface ozone sensitivity to external meteorological forcing. *Atmos. Chem. Phys.*, **10,** 11805-11821.
Kawase, H., T. Takemura, and T. Nozawa, 2011a: Impact of carbonaceous aerosols on precipitation in tropical Africa during the austral summer in the twentieth century. *J. Geophys. Res.*, **116,** D18116.
Kawase, H., T. Nagashima, K. Sudo, and T. Nozawa, 2011b: Future changes in tropospheric ozone under Representative Concentration Pathways (RCPs). *Geophys. Res. Lett.*, **38,** L05801.
Keenleyside, N. S., Latif, M., Jungclaus, J., Kornblueh, L., and E. Roeckner, 2008: Advancing decadal-scale climate prediction in the North Atlantic sector, Nature, 453, 84-88, doi:10.1038/nature06921.
Kim, S., E. Nakakita, Y. Tachikawa, and K. Takara, 2010: Precipitation changes in Japan under the A1B climate change scenario. Annual Journal of Hydraulic Engineering, JSCE, 54, 127-132
Korty, R. L., and T. Schneider (2008), Extent of Hadley circulations in dry atmospheres, *Geophys. Res. Lett.*, 35, L23803, doi:10.1029/2008GL035847.
Kleeman, M. J., 2008: A preliminary assessment of the sensitivity of air quality in California to global change. *Climatic Change*, **87 (Suppl 1),** S273-S292.
Kleeman, R., Y. Tang and A.M. Moore, 2003: The calculation of climatically relevant singular vectors in the presence of weather noise as applied to the ENSO problem. J. Atmos. Sci., 60, 2856-2868.
Kloster, S., F. Dentener, J. Feichter, F. Raes, U. Lohmann, E. Roeckner & I. Fischer-Bruns (2010a) A GCM study of future climate response to aerosol pollution reductions. *Climate Dynamics,* 34, 1177-1194.
Kloster et al. (2010b) A GCM study of future climate response to aerosol pollution reductions. *Climate Dynamics,* 34**,** 1177-1194.

Kloster, S., and Coauthors, 2008: Influence of future air pollution mitigation strategies on total aerosol radiative forcing. *Atmospheric Chemistry and Physics*, **8,** 6405-6437.
Knight, J., R. Allan, C. Folland, M. Vellinga, and M. Mann, 2005: A signature of persistent natural thermohaline circulation cycles in observed climate. *Geophysical Research Letters*, -.
KNUTSON, T., and S. MANABE, 1995: TIME-MEAN RESPONSE OVER THE TROPICAL PACIFIC TO INCREASED CO2 IN A COUPLED OCEAN-ATMOSPHERE MODEL. *Journal of Climate*, 2181-2199.
Knutson, Thomas R., Thomas L Delworth, Keith W Dixon, Isaac Held, Jian Lu, V Ramaswamy, M Daniel Schwarzkopf, G Stenchikov, and Ronald J Stouffer, 2006: Assessment of Twentieth-Century regional surface temperature trends using the GFDL CM2 coupled models. Journal of Climate, 19(9), DOI:10.1175/JCLI3709.1.
Knutson, T.R., J.J. Sirutis, S.T. Garner, G.A. Vecchi, and I.M. Held, 2008: Simulated reduction in Atlantic hurricane frequency under twenty-first- century warming conditions. *Nature Geoscience,* **1(6)**, 359-364
Knutson, T.R., J.L. McBride, J. Chan, K. Emanual, G. Holland, C. Landsea, I. Held, J.P. Kossin, A.K. Srivastava, and M. Sugi, 2010: Tropical cyclones and climate change. Nature Geoscience, 3, 157-163
Koch, D., and Coauthors, 2011: Coupled Aerosol-Chemistry,ÄìClimate Twentieth-Century Transient Model Investigation: Trends in Short-Lived Species and Climate Responses. *Journal of Climate*, **24,** 2693-2714.
Krueger, Oliver, Jin-Song Von Storch, 2011: A Simple Empirical Model for Decadal Climate Prediction. J. Climate, 24, 1276–1283. doi: http://dx.doi.org/10.1175/2010JCLI3726.1
Laepple, T., S. Jewson, and K. Coughlin, 2008: Interannual temperature predictions using the CMIP3 multi-model ensemble mean. *Geophysical Research Letters*, **35,** L10701.
Lam, Y. F., J. S. Fu, S. Wu, and L. J. Mickley, 2011: Impacts of future climate change and effects of biogenic emissions on surface ozone and particulate matter concentrations in the United States. *Atmos. Chem. Phys.*, **11,** 4789-4806.
Lambert, H. F., and M. J. Webb, 2008: Dependency of global mean precipitation on surface temperature. Geophys. Res. Lett., 35, L16706, doi:10.1029/2008GL034838.
Lamarque, J.-F., and Coauthors, 2011a: Global and regional evolution of short-lived radiatively-active gases and aerosols in the Representative Concentration Pathways. *Climatic Change*, 1-22.
Lamarque, J.-F. o., and Coauthors, 2011b: Global and regional evolution of short-lived radiatively-active gases and aerosols in the Representative Concentration Pathways. *Climatic Change*, 1-22.
Lamarque, J. F., and Coauthors, 2011c: Global and regional evolution of short-lived radiatively-active gases and aerosols in the Representative Concentration Pathways. *Climatic Change*.
Lammertsma, E.I., de Boer, H.J., Dekker, S.C., Dilcher, D.L., Lotter, A.F. and Wagner-Cremer, F. 2011. Global CO_2 rise leads to reduced maximum stomatal conductance in Florida vegetation. *Proceedings of the National Academy of Sciences USA* **108**: 4035-4040
Lang, X., and H. Wang, 2010: Improving Extraseasonal Summer Rainfall Prediction by Merging Information from GCMs and Observations. *Weather and Forecasting*, **25,** 1263-1274.
Lanzante, J. R., 2005: A cautionary note on the use of error bars. *Journal of Climate*, **18,** 3699-3703.
Latif, M., M. Collins, H. Pohlmann, and N. Keenlyside, 2006: A review of predictability studies of Atlantic sector climate on decadal time scales. *Journal of Climate*, **19,** 5971-5987.
Latif, M., Böning, C. W., Willebrand, J., Biastoch, A., Alvarez-Garcia, A., Keenlyside, N., and Pohlmann, H., 2007: Decadal to Multidecadal Variability of the Atlantic MOC: Mechanisms and Predictability. - In: "Ocean Circulation: Mechanisms and Impacts - Past and Future Changes of Meridional Overturning", Schmittner, A., Chiang, J. C. H., and Hemming, S. R. (Eds.), *AGU Monograph 173* , 149-166.
Lawrence, D.M., A.G. Slater, V.E. Romanovsky, and D.J. Nicolsky, 2008a: The sensitivity of a model projection of near-surface permafrost degradation to soil column depth and inclusion of soil organic matter. *J. Geophys. Res.*, **113**, F02011, doi:10.1029/2007JF000883.
Lawrence, D.M., A.G. Slater, R.A. Tomas, M.M. Holland, and C. Deser, 2008b: Accelerated Arctic land warminng and permafrost degradation during rapid sea ice loss. *Geophys. Res. Lett.*, **35**, L11506, doi:10.1029/2008GL033985.
Lawrence, D.M., and A.G. Slater, 2010: The contribution of snow condition trends to future ground climate. *Clim. Dyn.*, **34**, 969-981, 10.1007/s00382-009-0537-4.Lean, J. L., and D. H. Rind, 2009: How will Earth’s surface temperature change in future decades? *Geophysical Research Letters*, **36,** L15708.
Lee, T. C. K., F. W. Zwiers, X. B. Zhang, and M. Tsao, 2006: Evidence of decadal climate prediction skill resulting from changes in anthropogenic forcing. *Journal of Climate*, **19,** 5305-5318.
Leibensperger, E. M., L. J. Mickley, and D. J. Jacob, 2008: Sensitivity of US air quality to mid-latitude cyclone frequency and implications of 1980–2006 climate change. *Atmos. Chem. Phys.*, **8,** 7075-7086.
Leibensperger, E. M., and Coauthors, 2011a: Climatic effects of 1950,Äì2050 changes in US anthropogenic aerosols ,Äì Part 1: Aerosol trends and radiative forcing. *Atmos. Chem. Phys. Discuss.*, **11,** 24085-24125.
——, 2011b: Climatic effects of 1950,Äì2050 changes in US anthropogenic aerosols ,Äì Part 2: Climate response. *Atmos. Chem. Phys. Discuss.*, **11,** 24127-24164.
Levermann A, Schewe J, Petoukhov V, Held H (2009) Basic mechanism for abrupt monsoon transitions. Proc Nat Acad Sci 106:20,572–20,577
Levy, H., II, M. D. Schwarzkopf, L. Horowitz, V. Ramaswamy, and K. L. Findell, 2008: Strong sensitivity of late 21st century climate to projected changes in short-lived air pollutants. *J. Geophys. Res.*, **113,** D06102.

Liang, X.-Z., J. Pan, J. Zhu, K. E. Kunkel, J. X. L. Wang, and A. Dai, 2006: Regional climate model downscaling of the U.S. summer climate and future change. *J. Geophys. Res.*, **111,** D10108.

Liao, H., W.-T. Chen, and J. H. Seinfeld, 2006: Role of climate change in global predictions of future tropospheric ozone and aerosols. *J. Geophys. Res.*, **111,** D12304.

Liao, H., Y. Zhang, W.-T. Chen, F. Raes, and J. H. Seinfeld, 2009: Effect of chemistry-aerosol-climate coupling on predictions of future climate and future levels of tropospheric ozone and aerosols. *J. Geophys. Res.*, **114,** D10306.

Liao, K.-J., and Coauthors, 2007: Sensitivities of Ozone and Fine Particulate Matter Formation to Emissions under the Impact of Potential Future Climate Change. *Environmental Science & Technology*, **41,** 8355-8361.

Lin, C. Y. C., D. J. Jacob, and A. M. Fiore, 2001: Trends in exceedances of the ozone air quality standard in the continental United States, 1980-1998. *Atmospheric Environment*, **35,** 3217-3228.

Lin, J.-T., D. J. Wuebbles, and X.-Z. Liang, 2008: Effects of intercontinental transport on surface ozone over the United States: Present and future assessment with a global model. *Geophys. Res. Lett.*, **35,** L02805.

Lockwood, M., Harrison, R. G., Owens, M., Barnard, L., Woollings, T., and Stein- hilber, F. (2011). The solar influence on the probability of cold UK winters in the future. Environ. Res. Lett., 6 034004 doi:10.1088/1748-9326/6/3/034004.

Lockwood, M., *2010*, Solar change and climate: an update in the light of the current exceptional solar minimum. *Proceedings of the Royal Society A: Mathematical, Physical and Engineering Sciences, 466 (2114). pp. 303-329. ISSN 1364*-5021

Lorenz, D., and E. DeWeaver, 2007: Tropopause height and zonal wind response to global warming in the IPCC scenario integrations. *Journal of Geophysical Research-Atmospheres*, -.

Lu, J., G. Vecchi, and T. Reichler, 2007: Expansion of the Hadley cell under global warming. *Geophysical Research Letters*, -.

Lu, J., and G. Chen, and D. Frierson, 2008: Response of the zonal mean atmospheric circulation to El Nino versus global warming. *J. of Climate* 21, 5835-5851.

Mahlstein, I., and R. Knutti, 2010: Regional climate change patterns identified by cluster analysis. *Climate Dynamics*, **35,** 587-600.

Mahlstein, I., R. Knutti, S. Solomon and R. W. Portmann, 2011, Early onset of significant local warming in low latitude countries, *Environmental Research Letters*, *6,* 034009, doi:10.1088/1748-9326/6/3/034009

Mahmud, A., M. Tyree, D. Cayan, N. Motallebi, and M. J. Kleeman, 2008: Statistical downscaling of climate change impacts on ozone concentrations in California. *J. Geophys. Res.*, **113,** D21103.

Mahmud, A., M. Hixson, J. Hu, Z. Zhao, S. H. Chen, and M. J. Kleeman, 2010: Climate impact on airborne particulate matter concentrations in California using seven year analysis periods. *Atmos. Chem. Phys.*, **10,** 11097-11114.

Mahowald, N. M., 2007: Anthropocene changes in desert area: Sensitivity to climate model predictions. *Geophys. Res. Lett.*, **34,** L18817.

Mahowald, N. M., and C. Luo, 2003: A less dusty future? *Geophys. Res. Lett.*, **30,** 1903.

Mahowald, N. M., D. R. Muhs, S. Levis, P. J. Rasch, M. Yoshioka, C. S. Zender, and C. Luo, 2006: Change in atmospheric mineral aerosols in response to climate: Last glacial period, preindustrial, modern, and doubled carbon dioxide climates. *J. Geophys. Res.*, **111,** D10202.

Mann, M. E., Z. Zhang, S. Rutherford, R. S. Bradley, M. K. Hughes, D. Shindell, C. Ammann, G. Faluvegi, and F. Ni, 2009. Global signatures of the Little Ice Age and Medieval climate anomaly and plausible dynamical origins, Science, 326, 1256-1260, doi:10.1126/science.1177303.

Marengo, J.A., R. Jones, L.M. Alves, and M.C. Valverde, 2009a: Future change of temperature and precipitation extremes in South America as derived from the PRECIS regional climate modeling system. International Journal of Climatology, 29(15), 2241-2255

Merrifield, M. A., 2011: A shift in western tropical pacific sea level trends during the 1990s. J. Climate, 24, 4126–4138. doi: 10.1175/2011JCLI3932.1

Mason, S. J., and A. P. Weigel, 2009: A Generic Forecast Verification Framework for Administrative Purposes. *Monthly Weather Review*, **137,** 331-349.

McCabe, G. J., M. A. Palecki, and J. L. Betancourt, 2004: Pacific and Atlantic Ocean influences on multidecadal drought frequency in the United States. *PNAS*, **101,** 4136 – 4141.

McGregor, S., N.J. Holbrook, and S. Power, 2008: Interdecadal SST variability in the equatorial Pacific Ocean. Part II: the role of equatorial/off-equatorial wind stresses in a hybrid coupled model. *J. Climate*, **21**, 4242-4256.

McGregor, S., N.J. Holbrook, and S. Power, 2009: The response of a stochastically forced ENSO model to observed off-equatorial wind-stress forcing. *J. Climate*, **22**, 2512-2525.

McGuire, A. D., F. S. Chapin, J. E. Walsh, and C. Wirth, 2006: Integrated Regional Changes in Arctic Climate Feedbacks: Implications for the Global Climate System, *Annual Review of Environment and Resources*, **31,** 61-91.

McLandress, Charles, Theodore G. Shepherd, John F. Scinocca, David A. Plummer, Michael Sigmond, Andreas I. Jonsson, M. Catherine Reader, 2011: Separating the Dynamical Effects of Climate Change and Ozone Depletion. Part II: Southern Hemisphere Troposphere. J. Climate, 24, 1850–1868. doi: http://dx.doi.org/10.1175/2010JCLI3958.1

Mearns, L. O., W. J. Gutowski, R. Jones, L.-Y. Leung, S. McGinnis, A. M. B. Nunes, and Y. Qian, 2009: A regional climate change assessment program for North America. EOS, 90 (36), 311-312 (see also http://www.narccap.ucar.edu)

Meehl, G., and Coauthors, 2006: Climate change projections for the twenty-first century and climate change commitment in the CCSM3. *Journal of Climate*, 2597-2616.

Meehl, G. A., and A. Hu, 2006: Megadroughts in the Indian monsoon region and southwest North America and a mechanism for associated multi-decadal Pacific sea surface temperature anomalies. *Journal of Climate,* **19**, 1605–1623.

Meehl, G. A., J. M. Arblaster, and W. D. Collins, 2008: Effects of Black Carbon Aerosols on the Indian Monsoon. *Journal of Climate*, **21,** 2869-2882.

Meehl, G. A., A. X. Hu, and C. Tebaldi, 2010: Decadal Prediction in the Pacific Region. *Journal of Climate*, **23,** 2959-2973.

Meehl, G. A., C. Covey, T. Delworth,M. Latif, B.McAvaney, J. F. B. Mitchell, R. J. Stouffer, and K. E. Taylor, 2007a: The WCRP CMIP3 multimodel dataset: A new era in climate change research. Bull. Amer. Meteor. Soc., 88, 1383–1394.

Meehl, G.A., T.F. Stocker, W.D. Collins, P. Friedlingstein, A.T. Gaye, J.M. Gregory, A. Kitoh, R. Knutti, J.M. Murphy, A. Noda, S.C.B. Raper, I.G. Watterson, A.J. Weaver and Z.-C. Zhao, 2007: Global Climate Projections. In: Climate Change 2007: The Physical Science Basis. Contribution of Working Group I to the Fourth Assessment Report of the Intergovernmental Panel on Climate Change [Solomon, S.,D. Qin, M. Manning, Z. Chen, M. Marquis, K.B. Averyt, M. Tignor and H.L. Miller (eds.)]. Cambridge University Press, Cambridge, United Kingdom and New York, NY, USA.

——, 2009: Decadal Prediction. *Bulletin of the American Meteorological Society*, **90,** 1467-1485.

Meehl, G.A., C. Tebaldi, G. Walton, D. Easterling, and L. McDaniel, 2009: The relative increase of record high maximum temperatures compared to record low minimum temperatures in the U.S. Geophysical Research Letters, 36(L23701)

Meehl, G. A., and J. M. Arblaster, 2011: Decadal variability of Asian-Australian monsoon-ENSO-TBO relationships. *J. Climate*, **24**, 4925-4940.

Meehl, G.A., J.M. Arblaster, J. Fasullo, A. Hu, and K.E. Trenberth, 2011: Model-based evidence of deep ocean heat uptake during surface temperature hiatus periods. Nature Climate Change, 1, 360—364, doi:10.1038/NCLIMATE1229.

Meinshausen, M., S. Smith, K. Calvin, and J. Daniel, 2011: The RCP greenhouse gas concentrations and their extensions from 1765 to 2300. *Climatic Change*.

Meinshausen M, Wigley TML, and R. SCB, 2011: Emulating atmosphere-ocean and carbon cycle models with a simpler model, MAGICC6—Part 2: applications. *Atmos Chem Phys*, **11,** 1457–1471.

Meinshausen, M., S. Smith, K. Calvin & J. Daniel (2011) The RCP greenhouse gas concentrations and their extensions from 1765 to 2300. *Climatic Change*.

Meleux, F., F. Solmon, and F. Giorgi, 2007: Increase in summer European ozone amounts due to climate change. *Atmospheric Environment*, **41,** 7577-7587.

Menon, S., and et al., 2008: Aerosol climate effects and air quality impacts from 1980 to 2030. *Environmental Research Letters*, **3,** 024004.

Merrifield, M. A., 2011: A Shift in Western Tropical Pacific Sea Level Trends during the 1990s. *Journal of Climate*, **24,** 4126-4138.

Mickley, L. J., D. J. Jacob, B. D. Field, and D. Rind, 2004: Effects of future climate change on regional air pollution episodes in the United States. *Geophys. Res. Lett.*, **31,** L24103.

Mickley, L. J., E. M. Leibensperger, D. J. Jacob, and D. Rind, 2011: Regional warming from aerosol removal over the United States: Results from a transient 2010-2050 climate simulation. *Atmospheric Environment*, **In Press, Accepted Manuscript**.

Miller, R., G. Schmidt, and D. Shindell, 2006: Forced annular variations in the 20th century intergovernmental panel on climate change fourth assessment report models. *Journal of Geophysical Research-Atmospheres***,** -.

Min, S.-K, X. Zhang, F. W. *Zwiers* and G. C. Hegerl.*2011*. Human contribution to more intense *precipitation* extremes. Nature 470, 376-379.

Ming, Y., V. Ramaswamy & G. Persad (2010) Two opposing effects of absorbing aerosols on global-mean precipitation. *Geophys. Res. Lett.,* 37**,** L13701.

Ming, Y., V. Ramaswamy, and G. Chen, 2011: A Model Investigation of Aerosol-induced Changes in Boreal Winter Extratropical Circulation. *Journal of Climate*.

Ming, Y. & V. Ramaswamy (2011) A Model Investigation of Aerosol-induced Changes in Tropical Circulation. *Journal of Climate*.

Mochizuki, T., and Coauthors, 2010: Pacific decadal oscillation hindcasts relevant to near-term climate prediction. *Proceedings of the National Academy of Sciences of the United States of America*, **107,** 1833-1837.

Morgenstern, O., and Coauthors, 2010: Anthropogenic forcing of the Northern Annular Mode in CCMVal-2 models. *Journal of Geophysical Research-Atmospheres***,** -.

Moss, R. H., and Coauthors, 2010: The next generation of scenarios for climate change research and assessment. *Nature*, **463,** 747-756.

Msadek, R., K. Dixon, T. Delworth, and W. Hurlin, 2010: Assessing the predictability of the Atlantic meridional overturning circulation and associated fingerprints. *Geophysical Research Letters*, -.
Muller, C. J. and O'Gorman, P. A. 2011. An energetic perspective on the regional response of precipitation to climate change. Nature Climate Change 1, 266-271.
Murazaki, K., and P. Hess, 2006: How does climate change contribute to surface ozone change over the United States? *J. Geophys. Res.*, **111,** D05301.
Murphy, J., and Coauthors, 2010: **Towards** prediction of decadal climate variability and change. *Procedia Environmental Science*, **1,** *287-304*.
Murphy, J. M., B. B. B. Booth, M. Collins, G. R. Harris, D. M. H. Sexton, and M. J. Webb, 2007: A methodology for probabilistic predictions of regional climate change from perturbed physics ensembles. Philos. Trans. Roy. Soc. London, A365, 1993–2028.
Myhre, G., and Coauthors, 2011: Radiative forcing due to changes in ozone and methane caused by the transport sector. *Atmospheric Environment*, **45,** 387-394.
Newman, M., 2007: Interannual to decadal predictability of tropical and North Pacific sea surface temperatures. *Journal of Climate*, **20,** 2333-2356.
Nicolsky, D. J., V. E. Romanovsky, V. A. Alexeev, and D. M. Lawrence (2007), Improved modeling of permafrost dynamics in a GCM land-surface scheme, *Geophys. Res. Lett.*, *34*, L08501, doi:10.1029/2007GL029525.
Nolte, C. G., A. B. Gilliland, C. Hogrefe, and L. J. Mickley, 2008: Linking global to regional models to assess future climate impacts on surface ozone levels in the United States. *J. Geophys. Res.*, **113,** D14307.
Nordhaus, W. D., 2010: Economic aspects of global warming in a post-Copenhagen environment. *Proceedings of the National Academy of Sciences of the United States of America*, **107,** 11721-11726.
NRC, 2010: *Greenhouse Gas Emissions: Methods to Support International Climate Agreements.* National Research Council.
O'Connor, F. M., and co-authors, 2010: Possible role of wetlands, permafrost, and methane hydrates in the methane cycle under future climate change: A review. *Rev. Geophys*., **48**, RG4005, doi:10.1029/2010RG000326.
O'Gorman, P. A., Allan, R. P., Byrne, M. P. & Previdi, M. 2011. Energetic constraints on precipitation under climate change Surveys in Geophysics (**Submitted**)
Oman, L., and Coauthors, 2010: Multimodel assessment of the factors driving stratospheric ozone evolution over the 21st century. *Journal of Geophysical Research-Atmospheres*, **115,** -.
Orlowsky, B., and S.I. Seneviratne, 2011: Global changes in extremes events: Regional and seasonal dimension. Climatic Change, DOI 10.1007/s10584-011-0122-9, (published online)
Ott, L., and Coauthors, 2010: Influence of the 2006 Indonesian biomass burning aerosols on tropical dynamics studied with the GEOS-5 AGCM. *J. Geophys. Res.*, **115,** D14121.
Pacifico, F., S. P. Harrison, C. D. Jones, and S. Sitch, 2009: Isoprene emissions and climate. *Atmospheric Environment*, **43,** 6121-6135.
Paeth, H. and Pollinger, F. (2010). Enhanced evidence in climate models for changes in extratropical atmospheric circulation. Tellus Series A, 62, 647–660.
Palmer, M.D., D.J. McNeall, and N.J. Dunstone, 2011: Importance of the deep ocean for estimating decadal changes in Earth's radiation balance, *Geophysical Research Letters*, vol. 38, 2011.
Palmer, T.N., Doblas-Reyes, F.J., Hagedorn, R., Alessandri, A., Gualdi, S., Andersen, U., Feddersen, H., Cantelaube, P., Terres, J.-M., Davey, M., Graham, R., Délécluse, P., Lazar, A., Déqué, M., Guérémy, J.-F., Díez, E., Orfila, B., Hoshen, M., Morse, A.P., Keenlyside, N., Latif, M., Maisonnave, E., Rogel, P., Marletto, V. and Thomson, M.C., 2004. Development of a European multimodel ensemble system for seasonal-to-interannual prediction (DEMETER). Bulletin of the American Meteorological Society, 85(6): 853-872.
Palmer, T. N., R. Buzza, R. Hegedorn, A. Lawrence, M. Leutbecher, and L. Smith, 2006: Ensemble prediction: A pedagogical perspective. ECMWF Newsletter. Vol. 106, 10-17.
Paulot, F., J. D. Crounse, H. G. Kjaergaard, J. H. Kroll, J. H. Seinfeld, and P. O. Wennberg, 2009: Isoprene photooxidation: new insights into the production of acids and organic nitrates. *Atmos. Chem. Phys.*, **9,** 1479-1501.
PENNER, J., H. EDDLEMAN, and T. NOVAKOV, 1993: TOWARDS THE DEVELOPMENT OF A GLOBAL INVENTORY FOR BLACK CARBON EMISSIONS. *Atmospheric Environment Part a-General Topics*, **27,** 1277-1295.
Pierce, D. W., T. P. Barnett, R. Tokmakian, A. Semtner, M. Maltrud, J. A. Lysne, and A. Craig, 2004: The ACPI Project, Element 1: Initializing a coupled climate model from observed conditions. *Climate Change*, **62,** 13-28.
Pinto, J., U. Ulbrich, G. Leckebusch, T. Spangehl, M. Reyers, and S. Zacharias, 2007: Changes in storm track and cyclone activity in three SRES ensemble experiments with the ECHAM5/MPI-OM1 GCM. *Climate Dynamics*, 195-210.
Pohlmann, H., J. H. Jungclaus, A. Köhl, D. Stammer, and J. Marotzke, 2009: Initializing decadal climate predictions with the GECCO oceanic synthesis: Effects on the North Atlantic. *Journal of Climate*, **22,** 3926-3938.
Power, S., and I. Smith, 2007: Weakening of the Walker Circulation and apparent dominance of El Nino both reach record levels, but has ENSO really changed? *Geophysical Research Letters*, **34**, L18702, doi: 10.1029/2007GL030854.

Power, S. and R. Colman, 2006: Multi-year predictability in a coupled general circulation model. *Climate Dyn*, 26, 2147-272.
Power, S., T. Casey, C. Folland, A. Colman and V. Mehta, 1999: Interdecadal modulation of the impact of ENSO on Australia, *Climate Dyn*., 15, 319–324.
Power, S.B., 1995: Climate drift in a global OGCM. *J. Phys. Oceanogr.*, **25**, 1025-1036.
Power, S.B., F. Delage, R. Colman and A. Moise, 2011: Consensus on 21st century rainfall projections in climate models more widespread than previously thought. *J. Climate* (accepted).
Power, S.B., M. Haylock, R. Colman, X. Wang, 2006: The predictability of interdecadal changes in ENSO and ENSO teleconnections. *J. Climate*, **19**, 4755-4771.
Power, S.B., and G. Kociuba, 2011a: What caused the observed twentieth century weakening of the Walker Circulation? *J. Climate*, (in press).
Power, S.B., and G. Kociuba, 2011b: The impact of global warming on the Southern Oscillation Index. *Climate Dynamics*, **37**, 1745-1754.
Prather, M., Ehhalt, D., F. Dentener, R. G. Derwent, E. Dlugokencky, E. Holland, I. S. A. Isaksen, J. Katima, V. Kirchhoff, P. Matson, P. M. Midgley, and M. Wang. 2001. Atmospheric Chemistry and Greenhouse Gases. In *Climate Change 2001: The Scientific Basis,* ed. J. T. H. e. al., 239-287. Cambridge, UK: Cambridge University Press.
Prather, M., 2007: Lifetimes and time scales in atmospheric chemistry. *Philosophical Transactions of the Royal Society a-Mathematical Physical and Engineering Sciences*, **365,** 1705-1726.
Prather, M., and J. Hsu, 2010: Coupling of Nitrous Oxide and Methane by Global Atmospheric Chemistry. *Science*, **330,** 952-954.
——, 2009: Tracking uncertainties in the causal chain from human activities to climate. *Geophysical Research Letters*, **36,** -.
——, 2003: Fresh air in the 21st century? *Geophys. Res. Lett.*, **30,** 1100.
Prather, M., Ehhalt, D., F. Dentener, R. G. Derwent, E. Dlugokencky, E. Holland, I. S. A. Isaksen, J. Katima, V. Kirchhoff, P. Matson, P. M. Midgley, and M. Wang, 2001: Atmospheric Chemistry and Greenhouse Gases. *Climate Change 2001: The Scientific Basis*, J. T. H. e. al., Ed., Cambridge University Press, 239-287.
Previdi M.2010. Radiative feedbacks on global precipitation. Environ Res Lett 5, 025211
Pye, H. O. T., H. Liao, S. Wu, L. J. Mickley, D. J. Jacob, D. K. Henze, and J. H. Seinfeld, 2009: Effect of changes in climate and emissions on future sulfate-nitrate-ammonium aerosol levels in the United States. *J. Geophys. Res.*, **114,** D01205.
Racherla, P. N., and P. J. Adams, 2006: Sensitivity of global tropospheric ozone and fine particulate matter concentrations to climate change. *J. Geophys. Res.*, **111,** D24103.
——, 2008: The response of surface ozone to climate change over the Eastern United States. *Atmos. Chem. Phys.*, **8,** 871-885.
Raes, F., and J. H. Seinfeld, 2009: New Directions: Climate change and air pollution abatement: A bumpy road. *Atmospheric Environment*, **43,** 5132-5133.
Ramana, M. V., V. Ramanathan, Y. Feng, S. C. Yoon, S. W. Kim, G. R. Carmichael, and J. J. Schauer, 2010: Warming influenced by the ratio of black carbon to sulphate and the black-carbon source. *Nature Geosci*, **3,** 542-545.
Ramanathan, V., and G. Carmichael, 2008: Global and regional climate changes due to black carbon. *Nature Geosci*, **1,** 221-227.
Randles, C. A., and V. Ramaswamy, 2010: Direct and semi-direct impacts of absorbing biomass burning aerosol on the climate of southern Africa: a Geophysical Fluid Dynamics Laboratory GCM sensitivity study. *Atmos. Chem. Phys.*, **10,** 9819-9831.
Rasmussen, D. J., A. M. Fiore, V. Naik, L. W. Horowitz, S. J. McGinnis, and M. G. Schultz, 2011: Surface ozone-temperature relationships in the eastern US: A monthly climatology for evaluating chemistry-climate models. *Atmospheric Environment*, **submitted**.
Richter I, Xie SP (2008) The muted precipitation increase in global warming simulations: A surface evaporation perspective. J Geophys Res 113:D24118, DOI :10.1029/2008JD010561
Rind, D., 2008: The consequences of not knowing low-and high-latitude climate sensitivity. *Bulletin of the American Meteorological Society***,** 855-864.
Robock, A., 2003: Volcanoes: Role in climate. In: *Encyclopedia of Atmospheric Sciences* [Holton, J., J.A. Curry, and J. Pyle, (eds.). Academic Press, London, UK, 10.1006/rwas.2002.0169, 2494-2500.
Robock, A., 2000: Volcanic eruptions and climate. Rev. Geophys., 38, 191-219, doi:10.1029/1998RG000054.
Roeckner, E., P. Stier, J. Feichter, S. Kloster, M. Esch, and I. Fischer-Bruns, 2006: Impact of carbonaceous aerosol emissions on regional climate change. *Climate Dynamics*, **27,** 553-571.
Roscoe, H., and J. Haigh, 2007: Influences of ozone depletion, the solar cycle and the QBO on the Southern Annular Mode. *Quarterly Journal of the Royal Meteorological Society***,** 1855-1864.
Rowell, 2011: Sources of uncertainty in future changes in local precipitation, *Clim Dyn*, DOI 10.1007/s00382-011-120-2
Räisänen, J., 2008: Warmer climate: less or more snow? *Clim Dyn*, **30**, DOI 10.1007/s00382-007-0289-y.
Raisanen, J. and L. Ruokolainen, 2006: Probabilistic forecasts of near-term climate change based on a resampling ensemble technique. *Tellus*, 58A, 461-472.

Saito, K., M. Kimoto, T. Zhang, K. Takata, and S. Emori,2007: Evaluating a high-resolution climate model: Simulated hydrothermal regimes in frozen ground regions and their change under the global warming scenario, *J. Geophys. Res.*, *112*, F02S11, doi:10.1029/2006JF000577.

Schär, C., P.L. Vidale, D. Lüthi, C. Frei, C. Häberli, M.A. Liniger, and C. Appenzeller, 2004: The role of increasing temperature variability in European summer heatwaves. Nature, 427(322), 332-336

Schneider, E. K., B. Huang, Z. Zhu, D. G. DeWitt, J. L. Kinter, K. B.P., and J. Shukla, 1999: Ocean data assimilation, initialization and predictions of ENSO with a coupled GCM. *Monthly Weather Review*, **127,** 1187-1207.

Schneider, N., and A. J. Miller, 2001: Predicting western North Pacific Ocean climate. *Journal of Climate*, **14,** 3997–4002.

Schubert, S., M. J. Suarez, P. J. Pegion, R. D. Koster, and J. T. Bacmeister, 2004: On the cause of the 1930s Dust Bowl. *Science*, **303,** 1855-1859.

Schultz, M. G., T. Diehl, G. P. Brasseur, and W. Zittel, 2003: Air Pollution and Climate-Forcing Impacts of a Global Hydrogen Economy. *Science*, **302,** 624-627.

Seager, R.; Naik, N.; Vecchi, G. A.,:2010 Thermodynamic and Dynamic Mechanisms for Large-Scale Changes in the Hydrological Cycle in Response to Global Warming*. J. Climate, 23,4651-4668.

Seager, R. and G.A. Vecchi 2010. Greenhouse warming and the 21st Century hydroclimate of southwestern North America. *Proc. Nat. Acad. Sciences*, doi: 10.1073/pnas.0910856107.

Selten, F. M., Branstator, G. W., Dijkstra, H. A., and Kliphuis, M. (2004). Tropical origins for recent and future Northern Hemisphere climate change. Geophys. Res. Lett., 31, L21205.

Semenov, V. A., Latif, M., Jungclaus, J. H., and Park, W. (2008). Is the observed NAO variability during the instrumental record unusual? Geophys. Res. Lett., 35, 11701.

Seneviratne S.I., N. Nicholls N., D. Easterling, C. Goodess, S. Kanae, J. Kossin, Y. Luo, J. Marengo, K. McInnes, M. Rahimi, M. Reichstein, A. Sorteberg, C. Vera, X. Zhang, 2012: Changes in climate extremes and their impacts on the natural physical environment. Chapter 3 in IPCC Special Report on Extreme Events and Disasters (SREX), **In press.**

Sigmond, M., Kushner, P. J., and Scinocca, J. F. (2007). Discriminating robust and non-robust atmospheric circulation responses to global warming. J. Geophys. Res., 112, D20121.

Sohn, B.-J. and S.C. Park (2010), Strengthened tropical circulations in past three decades inferred from water vapor transport, J. Geophys. Res., 115, D15112, doi:10.1029/2009JD013713.

Shindell, D.T., and G.A. Schmidt, 2004: Southern Hemisphere climate response to ozone changes and greenhouse gas increases. *Geophys. Res. Lett.*, **31**, L18209, doi:10.1029/2004GL020724.

Shindell, D., and G. Faluvegi, 2009: Climate response to regional radiative forcing during the twentieth century. *Nature Geosci*, **2,** 294-300.

Shindell, D., M. Schulz, Y. Ming, T. Takemura, G. Faluvegi, and V. Ramaswamy, 2010: Spatial scales of climate response to inhomogeneous radiative forcing. *J. Geophys. Res.*, **115,** D19110.

Shindell, D., and Coauthors, 2007: Climate response to projected changes in short-lived species under an A1B scenario from 2000-2050 in the GISS climate model. *Journal of Geophysical Research-Atmospheres*, **112,** -.

Shindell, D. T., H. Levy, II, M. D. Schwarzkopf, L. W. Horowitz, J.-F. Lamarque, and G. Faluvegi, 2008a: Multimodel projections of climate change from short-lived emissions due to human activities. *J. Geophys. Res.*, **113,** D11109.

——, 2008b: Climate forcing and air quality change due to regional emissions reductions by economic sector. *Atmos. Chem. Phys.*, **8,** 7101-7113.

Shine, K.P. and E.J. Highwood (2002) Problems in quantifying natural and anthropogenic perturbations to the Earth's energy balance. In "Meteorology at the Millennium", International Geophysics Series Volume 83, Edited by R.P. Pearce.

Sloyan, B.M., and I.V. Kamenkovich, 2007: "Simulation of Subantarctic Mode and Antarctic Intermediate Waters in climate models", *J. Climate.,* **20**, 5061-5080.

Smith, D. M., S. Cusack, A. W. Colman, C. K. Folland, G. R. Harris, and J. M. Murphy, 2007: Improved surface temperature prediction for the coming decade from a global climate model. *Science*, **317,** 796-799.

Smith, D.M., Eade, R., Dunstone, N.J., Fereday, D., Murphy, J.M., Pohlmann, H. and Scaife, A.A., 2010. Skilful multi-year predictions of Atlantic hurricane frequency. Nature Geoscience, 3(12): 846-849.

Society, R., 2008: Ground-level ozone in the 21st century: future trends, impacts and policy implicationsISBN: 978-0-85403-713-1.

Smith, T. M., and R. W. Reynolds, 2003: Extended reconstruction of global sea surface temperature based on COADS data (1854-1997). *Journal of Climate*, **16,** 1495-1510.

Sohn, B. J., and S.-C. Park, 2010: Strengthened tropical circulations in past three decades inferred from water vapor transport. *J. Geophys. Res.*, **115,** D15112.

Son, S., N. Tandon, L. Polvani, and D. Waugh, 2009a: Ozone hole and Southern Hemisphere climate change. *Geophysical Research Letters*, -.

Son, S., and Coauthors, 2009b: The Impact of Stratospheric Ozone Recovery on Tropopause Height Trends. *Journal of Climate*, 429-445.

Son, S. W., and Coauthors, 2008: The impact of stratospheric ozone recovery on the Southern Hemisphere westerly jet. *Science*, **320,** 1486-1489.
Spracklen, D. V., K. S. Carslaw, U. P√∂schl, A. Rap, and P. M. Forster, 2011: Global cloud condensation nuclei influenced by carbonaceous combustion aerosol. *Atmos. Chem. Phys.*, **11,** 9067-9087.
Spracklen, D. V., L. J. Mickley, J. A. Logan, R. C. Hudman, R. Yevich, M. D. Flannigan, and A. L. Westerling, 2009: Impacts of climate change from 2000 to 2050 on wildfire activity and carbonaceous aerosol concentrations in the western United States. *J. Geophys. Res.*, **114,** D20301.
Stammer, D., 2006: Report of the First CLIVAR Workshop on Ocean Reanalysis, WCRP Informal Publication No. 9/2006, ICPO Publication Series No. 93.
Stainforth, D.A., T. Aina, C. Christensen, M. Collins, D.J. Frame, J.A. Kettleborough, S. Knight, A. Martin, J. Murphy, C. Piani, D. Sexton, L.A. Smith, R.A. Spicer, A.J. Thorpe and M.R. Allen, 2005: Uncertainty in predictions of the climate response to rising levels of greenhouse gases. Nature, 433, 403-406, doi:10.1038/nature03301
Stan, C. and B.P. Kirtman, 2008: The influence of atmospheric noise and uncertainty in ocean initial conditions on the limit of predictability in a coupled GCM. J. Climate, 21, 3487-3503.
Stedman, J., 2004: The predicted number of air pollution related deaths in the UK during the August 2003 heatwave. *Atmospheric Environment*, **38,** 1087-1090.
Steiner, A. L., S. Tonse, R. C. Cohen, A. H. Goldstein, and R. A. Harley, 2006: Influence of future climate and emissions on regional air quality in California. *J. Geophys. Res.*, **111,** D18303.
Steiner, A. L., A. J. Davis, S. Sillman, R. C. Owen, A. M. Michalak, and A. M. Fiore, 2010: Observed suppression of ozone formation at extremely high temperatures due to chemical and biophysical feedbacks. *Proceedings of the National Academy of Sciences*.
Stenchikov, Georgiy, Kevin Hamilton, Ronald J. Stouffer, Alan Robock, V. Ramaswamy, Ben Santer, and Hans-F. Graf, 2006: Arctic Oscillation response to volcanic eruptions in the IPCC AR4 climate models. *J. Geophys. Res.*, **111**, D07107, doi:10.1029/2005JD006286.
Stenchikov, G, Thomas L Delworth, V Ramaswamy, Ronald J Stouffer, Andrew T Wittenberg, and Fanrong Zeng, August 2009: Volcanic signals in oceans. *Journal of Geophysical Research*, 114, D16104, DOI:10.1029/2008JD011673.
Stephens, G. L. & Ellis, T. D. 2008. Controls of global-mean precipitation increases in global warming GCM experiments. J. Climate, 21, 6141-6155.
Stephenson, D. B., C. A. S. Coelho, F. J. Doblas-Reyes, and M. Balmaseda, 2005: Forecast assimilation: a unified framework for the combination of multi-model weather and climate predictions. *Tellus Series a-Dynamic Meteorology and Oceanography*, **57,** 253-264.
Stevenson, D. S., and Coauthors, 2006: Multimodel ensemble simulations of present-day and near-future tropospheric ozone. *J. Geophys. Res.*, **111,** D08301.
Stockdale, T. N., 1997: Coupled ocean–atmosphere forecasts in the presence of climate drift. *Monthly Weather Review*, **125,** 809-818.
Stockdale, T.N., D.L.T. Anderson, J.O.S. Alves and M.A. Balmaseda, 1998: Global seasonal rainfall forecasts using a coupled ocean–atmosphere model. Nature, 392, 370-373, doi:10.1038/32861 .
Stott, P., D. Stone, and M. Allen, 2004: Human contribution to the European heatwave of 2003. *Nature*, **432,** 610-614.
Stott, P., R. Sutton, and D. Smith, 2008: Detection and attribution of Atlantic salinity changes. *Geophysical Research Letters*, -.
Stott, P. A., and J. A. Kettleborough, 2002: Origins and estimates of uncertainty in predictions of twenty-first century temperature rise. *Nature*, **416,** 723-726.
Stott, P.A. and G. Jones, 2011, Observed 21st century temperatures further constrain decadal predictions of future warming, **submitted** to *Atmospheric Science Letters*.
Strahan, S., and Coauthors, 2011: Using transport diagnostics to understand chemistry climate model ozone simulations. *Journal of Geophysical Research-Atmospheres*, **116,** -.
Stroeve, J., M.M. Holland, W. Meier, T. Scambos, and M. Serreze, 2007: Arctic sea ice decline: Faster than forecast. Geophys. Res. Lett., 34, L09501, doi:10.1029/2007gl029703.
Sugi, M., H. Murakami, and J. Yoshimura, 2009: A reduction in global tropical cyclone frequency due to global warming. SOLA, 5, 164-167
Sugiura, N., and Coauthors, 2008: Development of a four-dimensional variational coupled data assimilation system for enhanced analysis and prediction of seasonal to interannual climate variations. *Journal Geophysical Research C*, **113,** C10017.
——, 2009: Potential for decadal predictability in the North Pacific region. *Geophysical Research Letters*, **36,** L20701.
Sun, J., and H. Chen, 2012: A statistical downscaling scheme to improve global precipitation forecasting. **Submitted**.
Sun., J., H. Wang, 2006: Relationship between Arctic Oscillation and Pacific Decadal Oscillation on decadal timescales. *Chinese Science Bulletin* 2006 Vol. 51 No. 1 75—79, DOI: 10.1007/s11434-004-0221-3
Sushama, L., R. Laprise, and M. Allard,2006: Modeled current and future soil thermal regime for northeast Canada, *J. Geophys. Res.*, *D18*, D18111, doi:10.1029/2005JD007027.
Sutton, R., and D. Hodson, 2005: Atlantic Ocean forcing of North American and European summer climate. *Science*, 115-118.

——, 2007: Climate response to basin-scale warming and cooling of the North Atlantic Ocean. *Journal of Climate*, 891-907.
Szopa, S., D. A. Hauglustaine, R. Vautard, and L. Menut, 2006: Future global tropospheric ozone changes and impact on European air quality. *Geophys. Res. Lett.*, **33,** L14805.
Tagaris, E., and Coauthors, 2007: Impacts of global climate change and emissions on regional ozone and fine particulate matter concentrations over the United States. *J. Geophys. Res.*, **112,** D14312.
Tai, A. P. K., L. J. Mickley, and D. J. Jacob, 2010: Correlations between fine particulate matter (PM2.5) and meteorological variables in the United States: Implications for the sensitivity of PM2.5 to climate change. *Atmospheric Environment*, **44,** 3976-3984.
Tao, Z., A. Williams, H.-C. Huang, M. Caughey, and X.-Z. Liang, 2007: Sensitivity of U.S. surface ozone to future emissions and climate changes. *Geophys. Res. Lett.*, **34,** L08811.
Taylor, K.E, R.J. Stouffer and G.A. Meehl, 2008: A summary of the CMIP5 Experimental Design. http://wwwpcmdi.llnl.gov/.
Taylor, K. E., R. J. Stouffer, G. A. Meehl, 2011: An overview of CMIP and the experimental design. Bulletin of the American Meteorological Society, doi: 10.1175/BAMS-D-11-00094.1
Tegen, I., M. Werner, S. P. Harrison, and K. E. Kohfeld, 2004: Relative importance of climate and land use in determining present and future global soil dust emission. *Geophys. Res. Lett.*, **31,** L05105.
Terray, L., L. Corre, S. Cravatte, T. Delcroix, G. Reverdin, R. Auerlien, 2011: Near-surface salinity as Nature's rain gauge to detect human influence on the tropical water cycle. J. Climate, DOI: 10.1175/JCLI-D-10-05025.1
Thompson, D.W.J., and S. Solomon, 2002: Interpretation of recent Southern Hemisphere climate change.*Science*, **296**, 895-899.
Timmermann, A., S. McGregor, and F. Jin, 2010: Wind Effects on Past and Future Regional Sea Level Trends in the Southern Indo-Pacific. *Journal of Climate*, 4429-4437.
Trenberth, K. E., and D. J. Shea, 2006: Atlantic hurricanes and natural variability in 2005. *Geophysical Research Letters*, **33**.
Trenberth, K.E. and Aiguo Dai, Effects of Mount Pinatubo volcanic eruption on the hydrological cycle as an analog of geoengineering, GEOPHYSICAL RESEARCH LETTERS, VOL. 34, L15702, doi:10.1029/2007GL030524, 2007
Trenberth K E, Dai A, Rasmussen R M and Parsons D B. 2003. The changing character of precipitation Bull. Am. Meteorol. Soc. 84 1205–17.
Trenberth, K.E., P.D. Jones, P. Ambenje, R. Bojariu, D. Easterling, A. Klein Tank, D. Parker, F. Rahimzadeh, J.A. Renwick, M. Rusticucci, B. Soden and P. Zhai, 2007: Observations: Surface and Atmospheric Climate Change. In: Climate Change 2007: The Physical Science Basis. Contribution of Working Group I to the Fourth Assessment Report of the Intergovernmental Panel on Climate Change [Solomon, S., D. Qin, M. Manning, Z. Chen, M. Marquis, K.B. Averyt, M. Tignor and H.L. Miller (eds.)]. Cambridge University Press, Cambridge, United Kingdom and New York, NY, USA
Tressol, M., and Coauthors, 2008: Air pollution during the 2003 European heat wave as seen by MOZAIC airliners. *Atmos. Chem. Phys.*, **8,** 2133-2150.
Troccoli, A., and T. N. Palmer, 2007: Ensemble decadal predictions from analysed initial conditions. *Philosophical Transaction A Math Phys Eng Sci.*, **365,** 2179-2191.
Uherek, E., and Coauthors, 2010: Transport impacts on atmosphere and climate: Land transport. *Atmospheric Environment*, **44,** 4772-4816.
Ulbrich, U., J. Pinto, H. Kupfer, G. Leckebusch, T. Spangehl, and M. Reyers, 2008: Changing northern hemisphere storm tracks in an ensemble of IPCC climate change simulations. *Journal of Climate*, 1669-1679.
Unger, N., D. T. Shindell, D. M. Koch, and D. G. Streets, 2006a: Cross influences of ozone and sulfate precursor emissions changes on air quality and climate. *Proceedings of the National Academy of Sciences of the United States of America*, **103,** 4377-4380.
Unger, N., D. T. Shindell, D. M. Koch, M. Amann, J. Cofala, and D. G. Streets, 2006b: Influences of man-made emissions and climate changes on tropospheric ozone, methane, and sulfate at 2030 from a broad range of possible futures. *J. Geophys. Res.*, **111,** D12313.
Unger, N., D. T. Shindell, D. M. Koch, and D. G. Streets, 2008: Air pollution radiative forcing from specific emissions sectors at 2030. *J. Geophys. Res.*, **113,** D02306.
van den Dool, H.M., 2007. Empirical methods in short-term climate prediction. Oxford University Press.
van der Linden P., and J.F.B. Mitchell (eds.) 2009: ENSEMBLES: Climate Change and its Impacts: Summary of research and results from the ENSEMBLES project. Met Office Hadley Centre, FitzRoy Road, Exeter EX1 3PB, UK. 160pp (available from the internet at http://ensembles-eu.metoffice.com/docs/Ensembles_final_report_Nov09.pdf)
van Oldenborgh, G., and Coauthors, 2009: Western Europe is warming much faster than expected. *Climate of the Past*, **5,** 1-12.
van Oldenborgh, G. J., P. Yiou, and R. Vautard, 2010: On the roles of circulation and aerosols in the decline of mist and dense fog in Europe over the last 30 years. *Atmos. Chem. Phys.*, **10,** 4597-4609.
van Oldenborgh, G. J., F. J. Doblas-Reyes, B. Wouters, and W. Hazeleger, 2011: Decadal prediction skill in a multi-model ensemble. *Climate Dynamics*, **submitted**.

van Vuuren, D., and Coauthors, 2011: The representative concentration pathways: an overview. *Climatic Change***,** 1-27.

van Vuuren, D. P., and Coauthors, 2008: Temperature increase of 21st century mitigation scenarios. *Proceedings of the National Academy of Sciences of the United States of America*, **105,** 15258-15262.
Vautard, R., P. Yiou, and G. J. van Oldenborgh, 2009: Decline of fog, mist and haze in Europe over the past 30[thinsp]years. *Nature Geosci*, **2,** 115-119.
Vautard, R., C. Honoré, M. Beekmann, and L. Rouil, 2005: Simulation of ozone during the August 2003 heat wave and emission control scenarios. *Atmospheric Environment*, **39,** 2957-2967.
Vavrus, S., D. Waliser, A. Schweiger, and J. Francis, 2009: Simulations of 20th and 21st century Arctic cloud amount in the global climate models assessed in the IPCC AR4. *Climate Dynamics*, **33,** 1099-1115.
Vavrus, S., M.M. Holland, and D.A. Bailey, 2010: Changes in Arctic clouds during intervals of rapid sea ice loss, Clim Dynamics, DOI 10.1007/s00382-010-0816-0.
Vavrus, S.J., M.M. Holland, A. Jahn, D.A. Bailey, and B.A. Blazey, 2011: 21st century Arctic climate change in CCSM4. J. Climate, doi: http://dx.doi.org/10.1175/JCLI-D-11-00220.1
Vecchi, G., and B. Soden, 2007: Global warming and the weakening of the tropical circulation. *Journal of Climate***,** 4316-4340.
Vecchi, G., B. Soden, A. Wittenberg, I. Held, A. Leetmaa, and M. Harrison, 2006: Weakening of tropical Pacific atmospheric circulation due to anthropogenic forcing. *Nature***,** 73-76.
Vecchi, G.A., and A.T. Wittenberg, 2010: El Niño and our future climate: where do we stand? Climate Change, 1(2), 260–270
Villarini, G, GA Vecchi, T.R. Knutson, M. Zhao, J.A. Smith, 2011: North Atlantic Tropical Storm Frequency Response to Anthropogenic Forcing: Projections and Sources of Uncertainty. J. Climate, 24 (13), 3224-3238
Vieno, M., and Coauthors, 2010: Modelling surface ozone during the 2003 heat-wave in the UK. *Atmos. Chem. Phys.*, **10,** 7963-7978.
Vikhliaev, Y., B. P. Kirtman, P. Schopf, 2007: North Pacific bred vectors in a coupled GCM. *J. Climate*, **23**, 5744-5764.
Wang GL (2005) Agricultural drought in a future climate: results from 15 global climate models participating in the IPCC 4th assessment. Clim Dyn 25:739–75.
Wang, C., D. Kim, A. M. L. Ekman, M. C. Barth, and P. J. Rasch, 2009: Impact of anthropogenic aerosols on Indian summer monsoon. *Geophys. Res. Lett.*, **36,** L21704.
Wang M., and J.E. Overland, 2009: A sea ice-free summer Arctic within 30 years? Geophys Res Lett, 36, L07502. doi:10.1029/2009 GL037820
Wang, H. and K. Fan, 2009: A new scheme for improving the seasonal prediction of summer precipitation anomalies. Weather Forecasting, DOI: 10.1175/2008WAF2222171.1.
Weaver, C. P., and Coauthors, 2009: A Preliminary Synthesis of Modeled Climate Change Impacts on U.S. Regional Ozone Concentrations. *Bulletin of the American Meteorological Society*, **90,** 1843-1863.
West, J. J., A. M. Fiore, L. W. Horowitz, and D. L. Mauzerall, 2006: Global health benefits of mitigating ozone pollution with methane emission controls. *Proceedings of the National Academy of Sciences of the United States of America*, **103,** 3988-3993.
Wigley, T., and Coauthors, 2009: Uncertainties in climate stabilization. *Climatic Change*, **97,** 85-121.
Wild, M., J. Grieser, and C. Scha¨r (2008), Combined surface solar brightening and increasing greenhouse effect support recent intensification of the global land-based hydrological cycle, Geophys. Res. Lett., 35, L17706, doi:10.1029/2008GL034842.
Wild and Leipert: 2010, The Earth radiation balance as driver of the global hydrological cycle, Env Res Lett, 5, DOI:10.1088/1748-9326/5/2/025003
Wild, O., and Coauthors, 2011: Future changes in surface ozone: A parameterized approach. *Atmos. Chem. Phys. Discuss.*
Wilks, D. S., 2006: *Statistical Methods in the Atmospheric Sciences.* Vol. 91, Academic Press, Elsevier, xvii, 627 p. pp.
Williams and Ringer, 2010: Precipitation changes within dynamical regimes in a perturbed climate, Env Res Lett, 5, DOI:10.1088/1748-9326/5/3/035202
Winton, M., 2006: does the Arctic sea ice have a tipping point? Geophys. Res. Lett., 33, doi:10.1029/2006gl028017.
WMO 2002: Standard Verification System (SVS) for Long-Rang Forecasts (LRF), WMO, Volume 1.
Woodward, S., D. L. Roberts, and R. A. Betts, 2005: A simulation of the effect of climate change–induced desertification on mineral dust aerosol. *Geophys. Res. Lett.*, **32,** L18810.
Woollings, T., 2008: Vertical structure of anthropogenic zonal-mean atmospheric circulation change. *Geophysical Research Letters***,** -.
——, 2010: Dynamical influences on European climate: an uncertain future. *Philosophical Transactions of the Royal Society a-Mathematical Physical and Engineering Sciences***,** 3733-3756.
Woollings, T. and Blackburn, M. (2011). The North Atlantic jet stream underclimate change, as described by the NAO and EA patterns. J. Climate. Submitted
Wu, S., L. J. Mickley, J. O. Kaplan, and D. J. Jacob, 2011: Impacts of changes in land use and land cover on atmospheric chemistry and air quality over the 21st century. *Atmos. Chem. Phys. Discuss.*, **11,** 15469-15495.

Wu, S., L. J. Mickley, D. J. Jacob, D. Rind, and D. G. Streets, 2008a: Effects of 2000–2050 changes in climate and emissions on global tropospheric ozone and the policy-relevant background surface ozone in the United States. *J. Geophys. Res.*, **113,** D18312.
Wu, S., L. J. Mickley, E. M. Leibensperger, D. J. Jacob, D. Rind, and D. G. Streets, 2008b: Effects of 2000–2050 global change on ozone air quality in the United States. *J. Geophys. Res.*, **113,** D06302.
Wu, P., R. Wood, J. Ridley, and J. Lowe. 2010. Temporary acceleration of the hydrological cycle in response to a CO2 rampdown, Geophys. Res. Lett.,37, L12705, doi:10.1029/2010GL043730.
Xie, S., C. Deser, G. Vecchi, J. Ma, H. Teng, and A. Wittenberg, 2010: Global Warming Pattern Formation: Sea Surface Temperature and Rainfall. *Journal of Climate*, 966-986.
Xoplaki, E., P. Maheras, and J. Luterbacher, 2001. Variability of climate in meridional Balkans during the periods 1675-1715 and 1780-1830 and its impact on human life, Clim. Change, 48, 581-615, doi:10.1023/A:1005616424463.
Yin, J, M Schlesinger, and Ronald J Stouffer, April 2009: Model projections of rapid sea-level rise on the northeast coast of the United States. *Nature Geoscience*, 2(4), DOI:10.1038/NGEO462.
Yin, J., S. Griffies, and R. Stouffer, 2010: Spatial Variability of Sea Level Rise in Twenty-First Century Projections. *Journal of Climate*, 4585-4607.
Yoshimori, M. & A. J. Broccoli (2008) Equilibrium Response of an Atmosphere‚ÄìMixed Layer Ocean Model to Different Radiative Forcing Agents: Global and Zonal Mean Response. *Journal of Climate,* 21**,** 4399-4423.
Zahn, M., and R. P. Allan (2011), Changes in water vapor transports of the ascending branch of the tropical circulation, J. Geophys. Res., 116, D18111, doi:10.1029/2011JD016206.
Zeng, G., J. A. Pyle, and P. J. Young, 2008: Impact of climate change on tropospheric ozone and its global budgets. *Atmos. Chem. Phys.*, **8,** 369-387.
Zeng, G., O. Morgenstern, P. Braesicke, and J. A. Pyle, 2010: Impact of stratospheric ozone recovery on tropospheric ozone and its budget. *Geophys. Res. Lett.*, **37,** L09805.
Zhao, M., I.M. Held, S.-J. Lin, and G.A. Vecchi (2009). Simulations of global hurricane climatology, interannual variability, and response to global warming using a 50km resolution GCM. J. Climate, 22(24), 6653-6678, doi:10.1175/2009JCLI3049.1
Zheng, X-T, S-P Xie, G.A. Vecchi, Q. Liu, and J. Hafner (2010). Indian Ocean dipole response to global warming: Analysis of ocean-atmospheric feedbacks in a coupled model. J. Climate. 23(5), 1240-1253. doi: 10.1175/2009JCLI3326.1
Zhang X, 2010: Sensitivity of arctic summer sea ice coverage to global warming forcing: Towards reducing uncertainty in arctic climate change projections. Tellus A, 62, 220–227. DOI: 10.1111/j.1600-0870.2010.00441.x
Zhang, S., M. J. Harrison, A. Rosati, and A. A. Wittenberg, 2007: System design and evaluation of coupled ensemble data assimilation for global oceanic climate studies. *Monthly Weather Review*, **135,** 3541-3564.
Zhang, X., Zwiers, F.W., Hegerl,G.C., Lambert, F.H., Gillett,N.P.; Solomon, S.; Stott, P.A. and Toru Nozawa. 2007. Detection of human influence on twentieth-century precipitation trends. Nature 448, 461-466.
Zhang, Y., J. Wallace, and D. Battisti, 1997: ENSO-like interdecadal variability: 1900-93. *Journal of Climate*, 1004-1020.
Zhang, Y., X.-M. Hu, L. R. Leung, and W. I. Gustafson, Jr., 2008: Impacts of regional climate change on biogenic emissions and air quality. *J. Geophys. Res.*, **113,** D18310.

Tables

Table 11.1: Initialization methods used in models that entered CMIP5 near-term experiments

CMIP5 Near-Term Players	CMIP5 official model_id	AGCM	OGCM	Initialization				Perturbation	
Name of modeling center (or group)				Atmosphere/ Land	Ocean	Sea Ice	Anomaly Assimilation?	Atmos	Ocean
Beijing Climate Center, China Meteorological Administration (BCC) China	BCC-CSM1.1	2.8ºL26	1ºL40	no	SST, T&S (SODA)	no	no	perturbed atmos/ocean	
Canadian Centre for Climate Modelling and Analysis (CCCMA) Canada	CanCM4	2.8ºL35	0.9ºL40	ERA40/Interim	Ocean assimilation (Tang et al. 2004) /forced OGCM	yes	no	ensemble assimilation	
Community Climate System Model (CCSM) USA	CCSM4	0.5ºL30	0.5ºL60	no	forced OGCM / ocean assimilation (DART)				
Centro Euro-Mediterraneo per I Cambiamenti Climatici (CMCC-CM) Italy	CMCC-CM	0.8ºL31	1.2ºL31	no	SST, T&S (INGV ocean analysis)	concentration from ocean analysis	no	ensemble assimilation	
EC-EARTH Consortium (EC-EARTH) Europe	EC-EARTH	1.1ºL62	1ºL42	ERA40/interim	Ocean assimilation (NEMOVAR S3)		no (KNMI & IC3) & yes (SMHI)	start dates and singular vectors	ensemble ocean assimilation (NEMOVAR)
Max Planck Institute for Meteorology (MPI-M) Germany	MPI-ESM	0.9ºL95	0.5ºL40	no	T&S from forced OGCM	no	yes	yes 1-day lagged	
Geophysical Fluid Dynamics Laboratory (GFDL) USA	GFDL-CM2.1	2ºL24	0.9ºL50	NCEP reanalysis	coupled EnKF	no	no	coupled EnKF	
Met Office Hadley Centre (MOHC) UK	HadCM3	2.5ºL19	1.3ºL20	ERA40/ECMWF operational	SST, T&S (Smith and Murphy, 2007)	HADISST	yes	no	SST perturbation
Institut Pierre-Simon Laplace (IPSL) France	IPSL-CM5A-LR	1.9ºL39	2ºL31	reanalysis	SST		yes	no	white nose on SST
AORI/NIES/JAMSTEC (MIROC) Japan	MIROC4h MIROC5	0.6ºL56 1.4ºL40	0.2ºL48 0.8ºL50	no	SST, T&S (Ishii-Kimoto (2009)	no	yes	start dates and ensemble assimilation	

Chapter 11: Near-term Climate Change: Projections and Predictability

Coordinating Lead Authors: Ben Kirtman (USA), Scott Power (Australia)

Lead Authors: Akintayo John Adedoyin (Botswana), George Boer (Canada), Roxana Bojariu (Romania), Ines Camilloni (Argentina), Francisco Doblas-Reyes (Spain), Arlene Fiore (USA), Masahide Kimoto (Japan), Gerald Meehl (USA), Michael Prather (USA), Abdoulaye Sarr (Senegal), Christoph Schaer (Switzerland), Rowan Sutton (UK), Geert Jan van Oldenborgh (Netherlands), Gabriel Vecchi (USA), Hui-Jun Wang (China)

Contributing Authors: Nathan Bindoff, Yoshimitsu Chikamoto, Javier García-Serrano, Paul Ginoux, Lesley Gray, Ed Hawkins, Marika Holland, Christopher Holmes, Masayoshi Ishii, Thomas Knutson, David Lawrence, Jian Lu, Vaishali Naik, Lorenzo Polvani, Alan Robock, Luis Rodrigues, Doug Smith, Steve Vavrus, Apostolos Voulgarakis, Oliver Wild, Tim Woollings

Review Editors: Pascale Delecluse (France), Tim Palmer (UK), Theodore Shepherd (Canada), Francis Zwiers (Canada)

Date of Draft: 16 December 2011

Notes: TSU Compiled Version

Figures

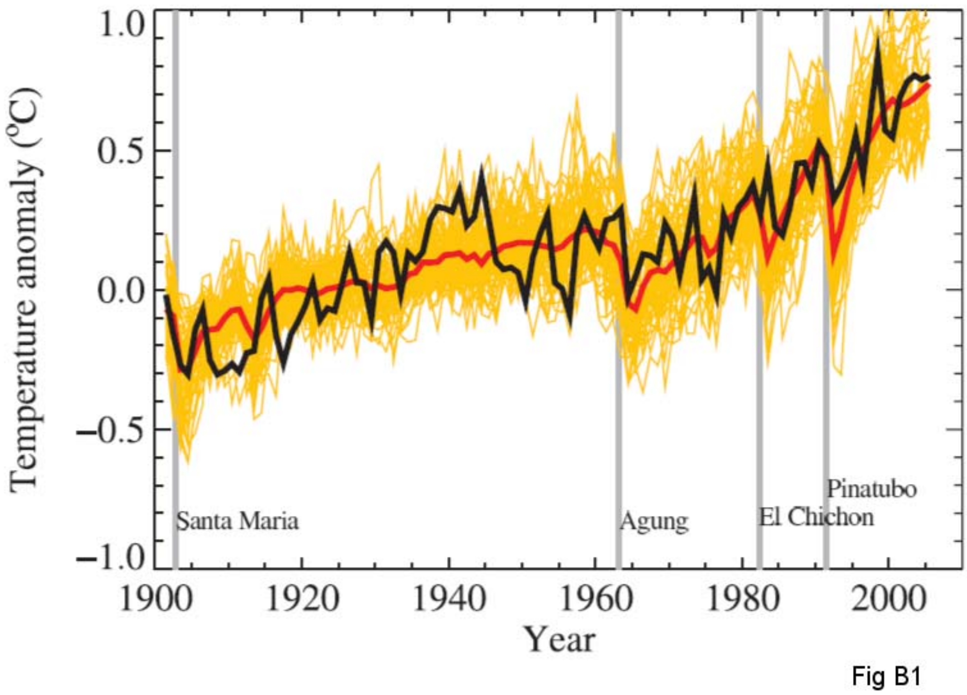

Figure 11.1: The evolution of observed global mean temperature as the difference from the 1901–1950 average (the black line) where $T(t) = T_f(t) + T_i(t)$ is the sum of an externally forced component T_f (red line) and an internally generated component T_i (the difference between the black and red lines). An ensemble of possible "realizations" of temperature evolution is represented by the yellow lines.

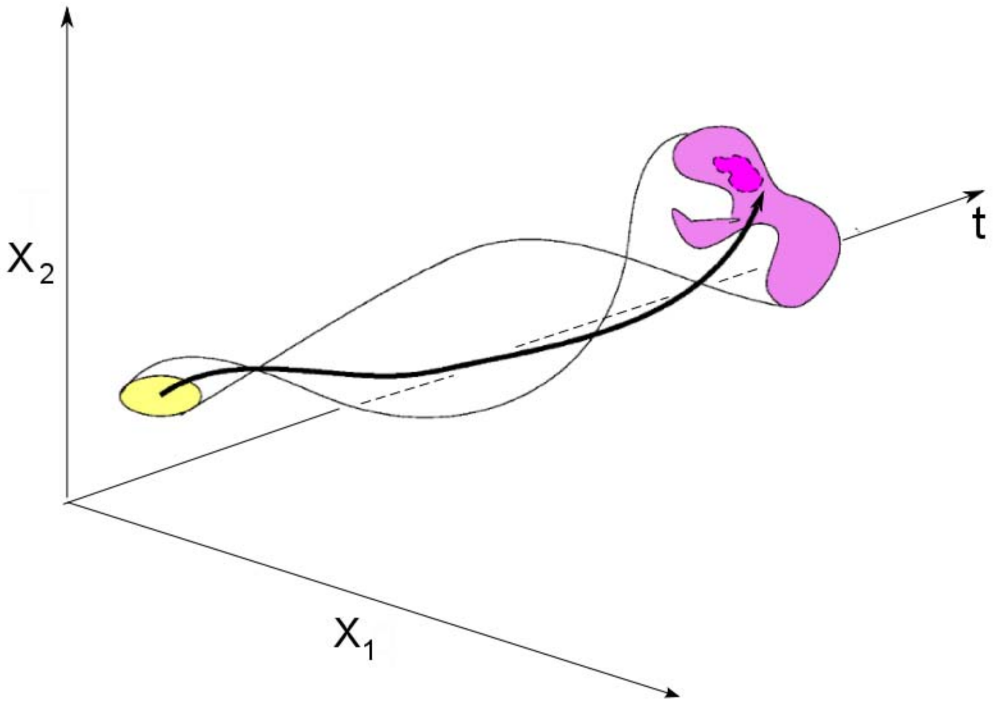

Figure 11.2: A schematic representation of predictability as the rate of separation of initially close states and the connection with forecast error growth. The actual evolution of the system is represented as the black line, the uncertainty in initial conditions by the yellow oval and the resulting cloud of trajectories by the thin lines. A deterministic climate prediction attempts to follow the black line to predict *T*□*(t)*, or other climate variable, at some time *t* beyond the present. A probabilistic climate prediction takes the form of a probability distribution *p(T,t)* providing information on the probability of realizing a particular result.

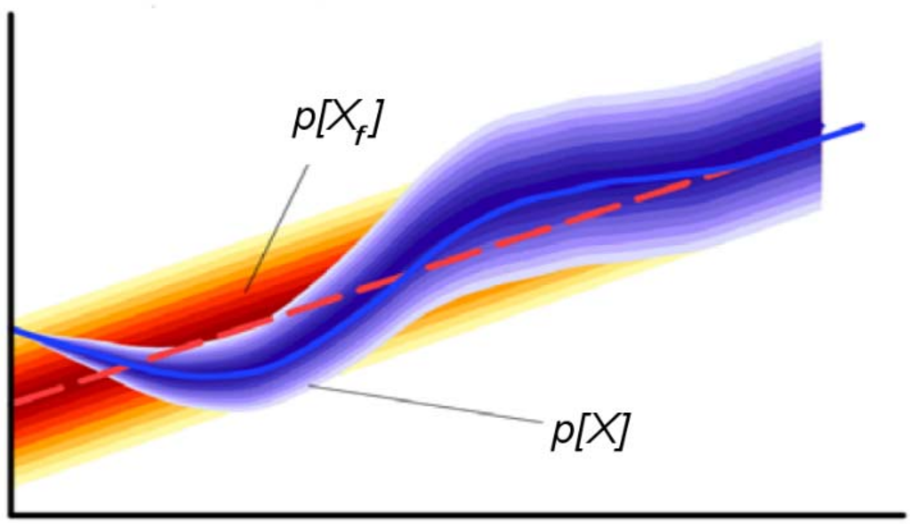

Figure 11.3: Schematic evolution of predictability and error growth in terms of probability. The probability distribution corresponding to the forced component *p(T_f,t)* is in red with the deeper shades indicating higher probability. The probabilistic representation of the forecast *p(T,t)* is in blue. The initially sharply peaked distribution broadens with time as information about the initial conditions is lost until the initialized climate prediction becomes indistinguishable from an uninitialized climate projection.

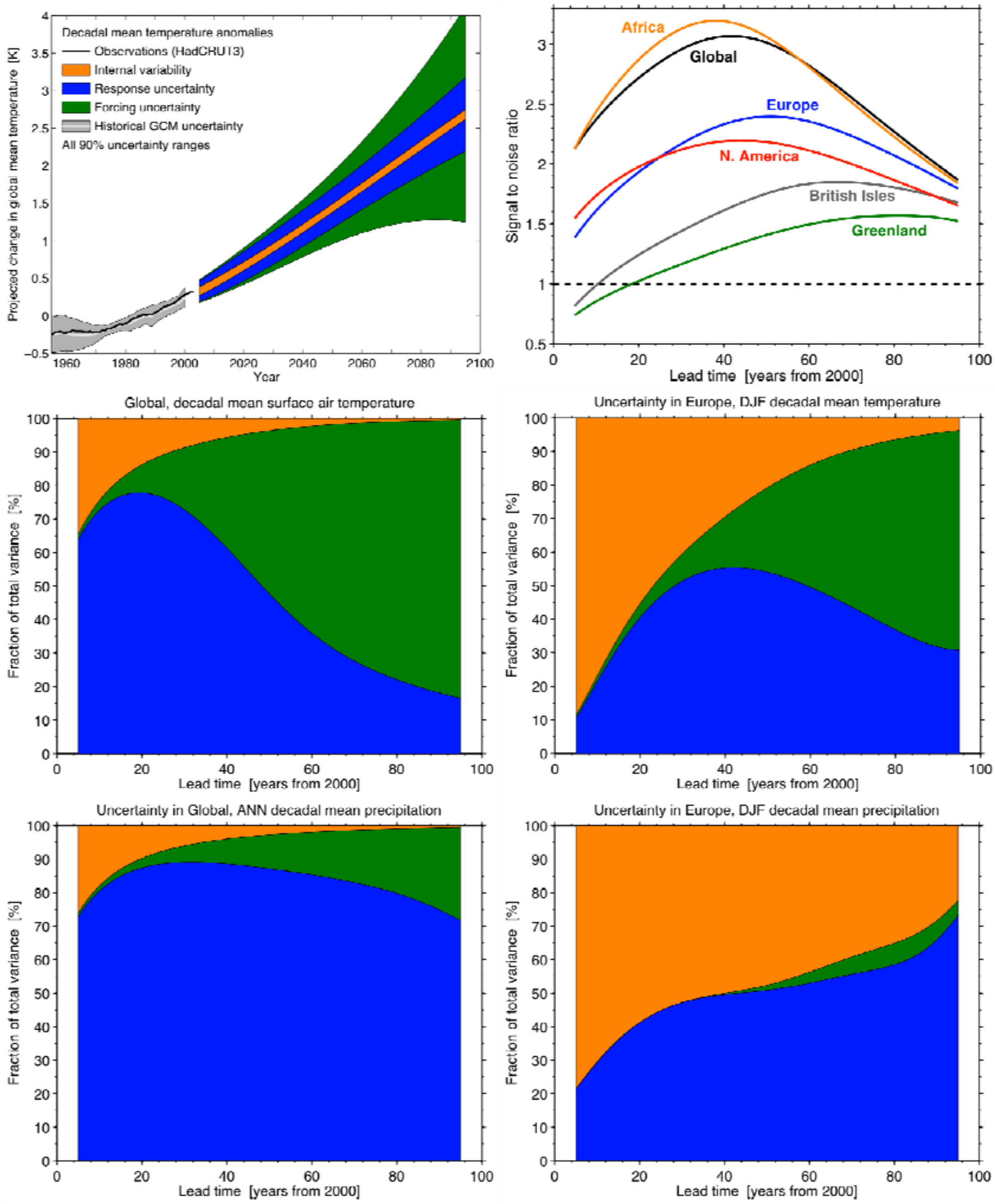

Figure 11.4: Sources of uncertainty in climate projections as a function of lead time. a) Projections of global mean decadal mean surface air temperature to 2100 together with a quantification of the uncertainty arising from internal variability (orange), response uncertainty (blue), and forcing uncertainty (green). b) shows the same results as in (a) but expressed as a percentage of the total uncertainty at each lead time. c), e), f) show results for: global mean decadal and annual mean precipitation, British Isles decadal mean surface air temperature, and boreal winter (December-February) decadal mean precipitation. d) shows signal-to-noise ratio for decadal mean surface air temperature for the regions indicated. The signal is defined as the simulated multi-model mean change in surface air temperature relative to the simulated mean surface air temperature in the period 1971–2000, and the noise is defined as the total uncertainty. See text and Hawkins & Sutton (2009,2010) for further details. This version of the figure is based on CMIP3 results and neglects the contribution from carbon cycle (and other biogeochemical) feedbacks to response uncertainty.

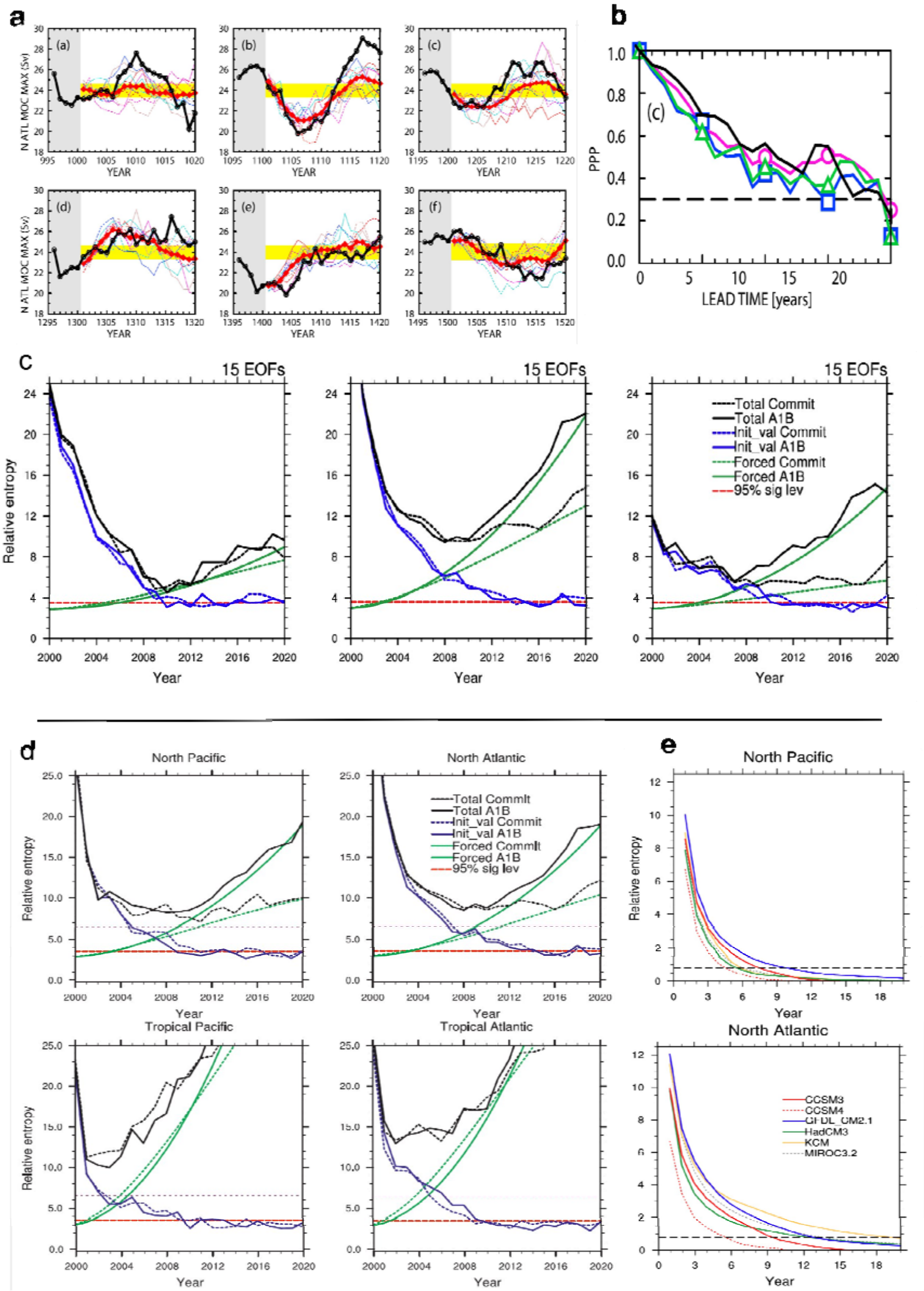

Figure 11.5: (a) Control run MOC (black line), prediction results (thin coloured lines) and ensemble mean (red line) in predictability experiments with the GFDL model. (b) predictability measures of the MOC (black) and of North Atlantic subsurface temperature, heat content and sea surface height (from Msadek et al), (c) initial condition (green) and externally forced (blue) components of predictability of the North Atlantic MOC, 500m temperature and SST (from Teng et al.), (d) initial condition (green) and externally forced (blue) predictability for upper ocean temperature predictability in extratropical and tropical ocean basins from the NCAR model, (e) initial condition predictability for different models for N. Atlantic and N. Pacific upper ocean temperatures (from Branstator et al. 2011) basins from the NCAR model, (e) initial condition predictability for different models for N. Atlantic and N. Pacific upper ocean temperatures (from Branstator et al. 2011).

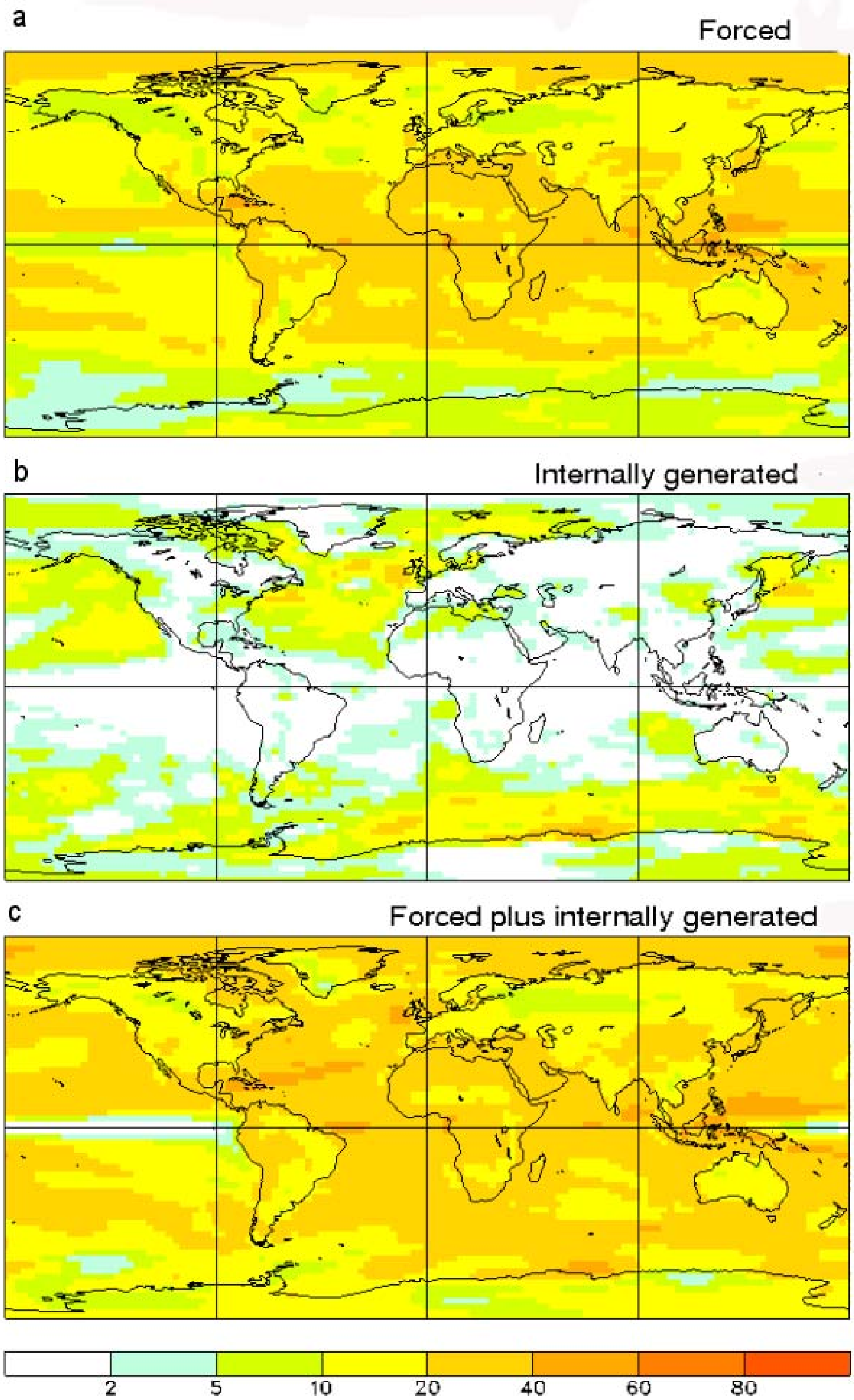

Figure 11.6: Contributions to decadal potential predictability from the externally forced component (upper panel), internal generated component (middle panel) and both together (lower panel). Multi-model results from CMIP3.

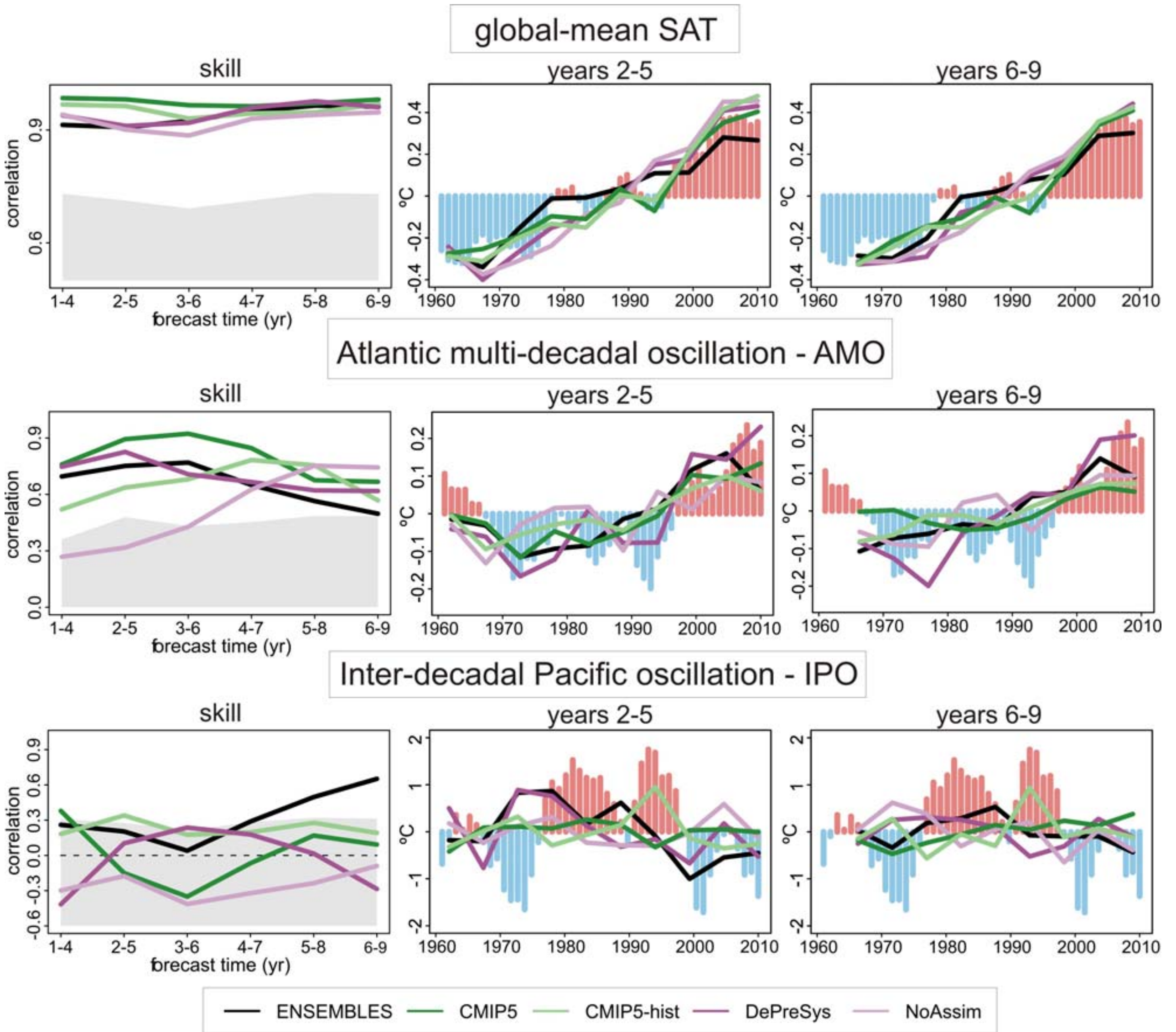

Figure 11.7: Ensemble-mean correlation with the observations (left column) and time series of 2–5 (middle column) and 6–9 (right column) year average predictions of the global-mean temperature (top row), AMV (middle row) and IPO (bottom row) from the ENSEMBLES (black), CMIP5 Assim (dark green) and NoAssim (light green) and DePreSys Assim (dark purple) and NoAssim (light purple) forecast systems. The AMV index was computed as the SST anomalies averaged over the region Equator-60ºN and 80º–0ºW minus the SST anomalies averaged over 60ºS–60ºN (Trenberth and Shea 2006). The IPO index is the principal component of the leading EOF of each model using SSTs in the region 50ºS–50ºN / 100ºE–290ºE where the mean SST over 60ºS–60ºN have been previously removed. Predictions initialized once every five years over the period 1960–2005 have been used. The CMIP5 multi-model includes experiments from the HadCM3, MIROC5, MIROC4h and MRI-CGCM3 systems. The one-side 95% confidence level is represented in grey, where the number of degrees of freedom has been computed taking into account the autocorrelation of the observational time series. The observational time series, GISS global-mean temperature and ERSST for the AMV and IPO, are represented with red (positive anomalies) and blue (negative anomalies) vertical bars, where a four-year running mean has been applied for consistency with the time averaging of the predictions.

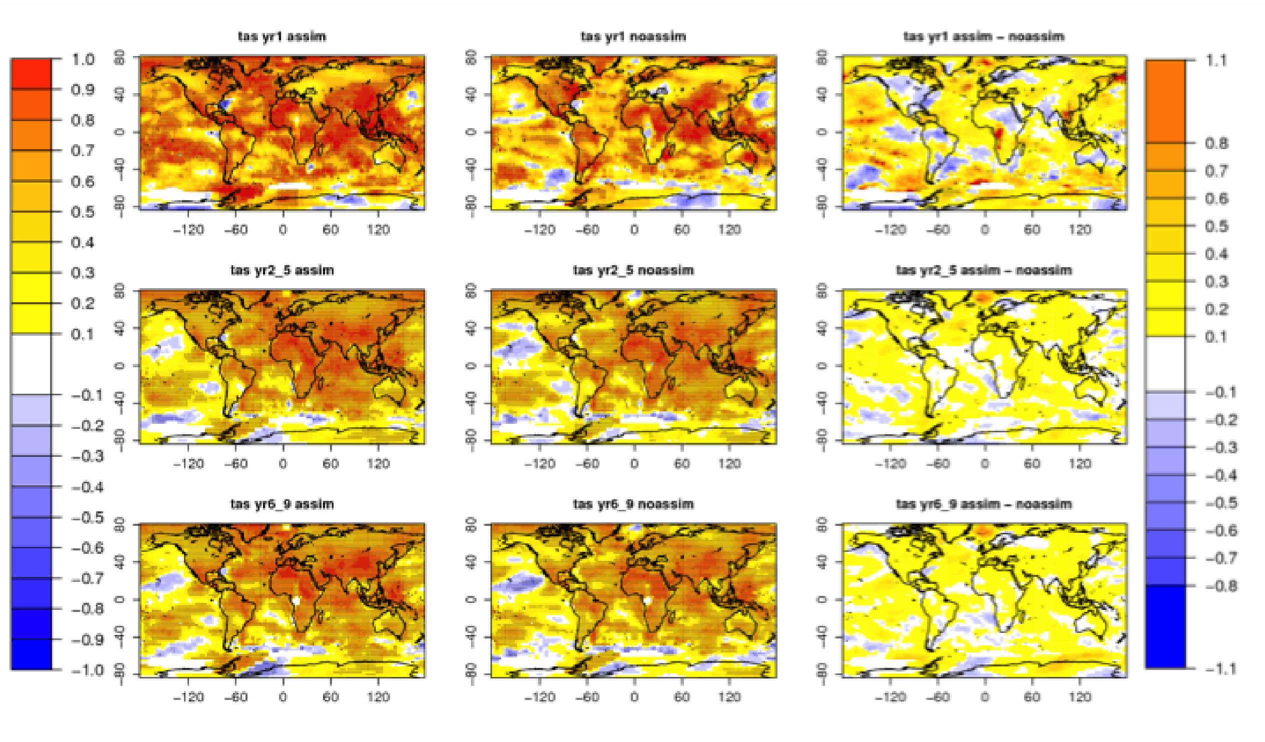

Figure 11.8: Near surface air temperature ensemble-mean correlation of the CMIP5 multi-model for the Assim (left column), NoAssim (middle column) and their difference (right column) for the first year (top row) and the averaged 2–5 (middle row) and 6–9 (bottom row) years forecast period. The CMIP5 multi-model includes experiments from the HadCM3, MIROC5, MIROC4h and MRI-CGCM3 systems. The black dots correspond to the points where the correlation is statistically significant with 95% confidence using a one-sided (two sided for the correlation differences) parametric test. A Fisher Z-transform of the correlations has been applied before applying the inference test to the correlation differences. A combination of GHCN (Fan and van den Dool, 2007), ERSST (Smith and Reynolds 2003) and GISS (Hansen et al., 2010) temperatures is used as a reference. The correlation has been computed with hindcasts started over the period 1960–2005. The left- (right-) hand side colour bar is for the correlations (differences between the correlations).

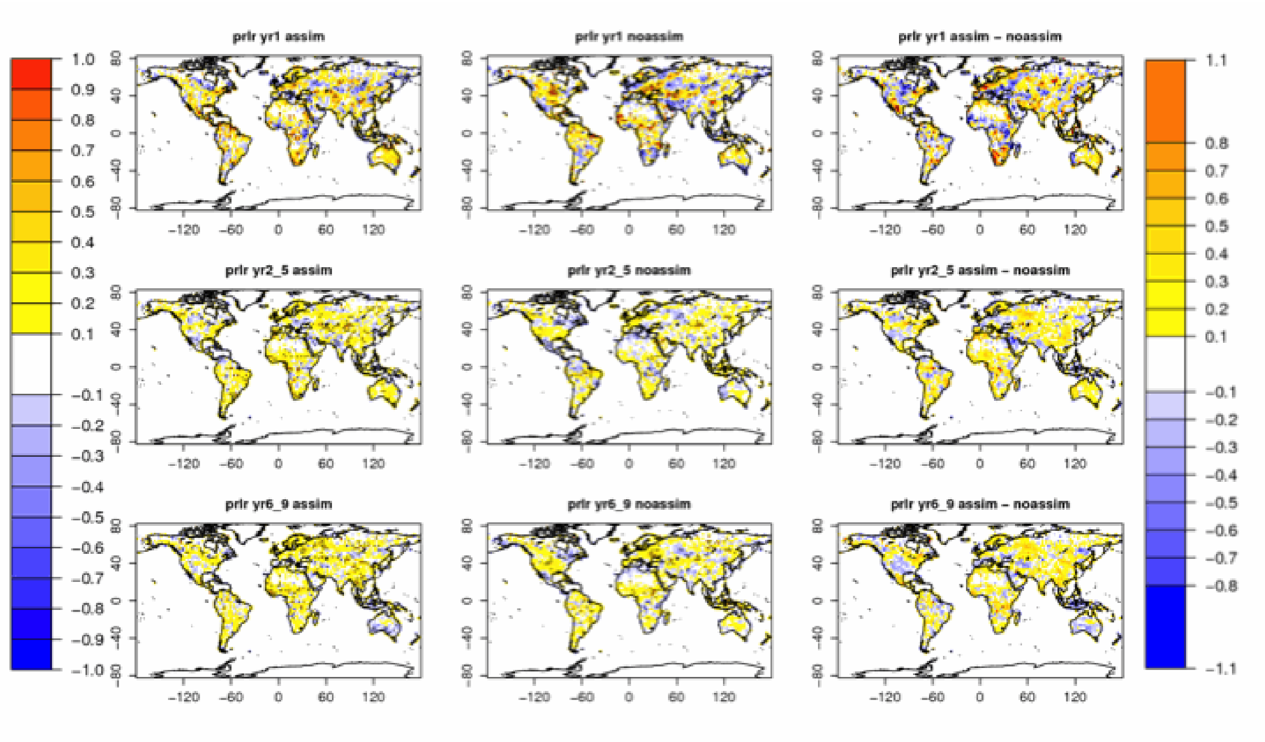

Figure 11.9: Land precipitation ensemble-mean correlation of the CMIP5 multi-model for the Assim (left column), NoAssim (middle column) and their difference (right column) for the first year (top row) and the averaged 2–5 (middle row) and 6–9 (bottom row) years forecast period. The CMIP5 multi-model includes experiments from the HadCM3, MIROC5, MIROC4h and MRI-CGCM3 systems. The black dots correspond to the points where the correlation is statistically significant with 95% confidence using a one-sided (two sided for the correlation differences) parametric test. A Fisher Z-transform of the correlations has been applied before applying the inference test to the correlation differences. GPCC precipitation is used as a reference. The correlation has been computed with hindcasts started over the period 1960–2005. The left- (right-) hand side colour bar is for the correlations (differences between the correlations).

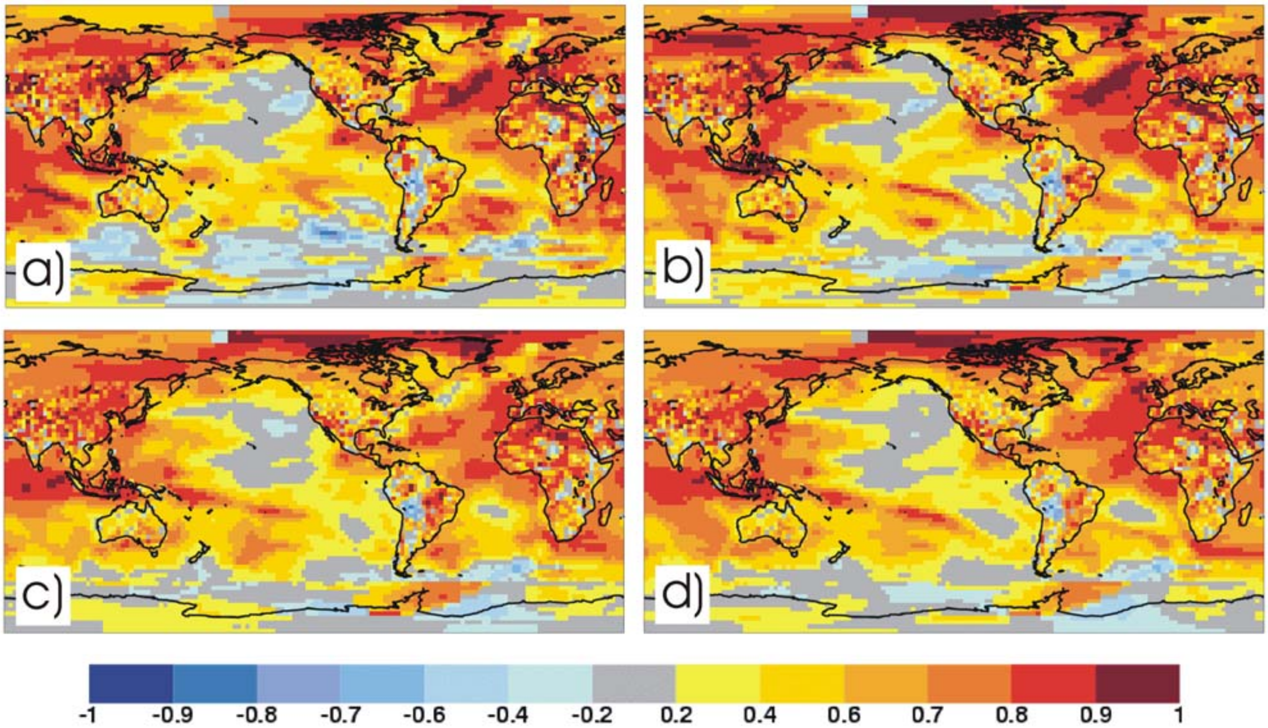

Figure 11.10: Near surface air temperature ensemble-mean centred correlation for DePreSys b) with five-year intervals between start dates and d) with one-year intervals between start dates, for the forecast period 2-5 years. A combination of GHCN (Fan and van den Dool, 2007), ERSST (Smith and Reynolds, 2003) and GISS (Hansen et al., 2010) temperatures is used as a reference. The correlation has been computed with hindcasts started over the period 1960–2005.

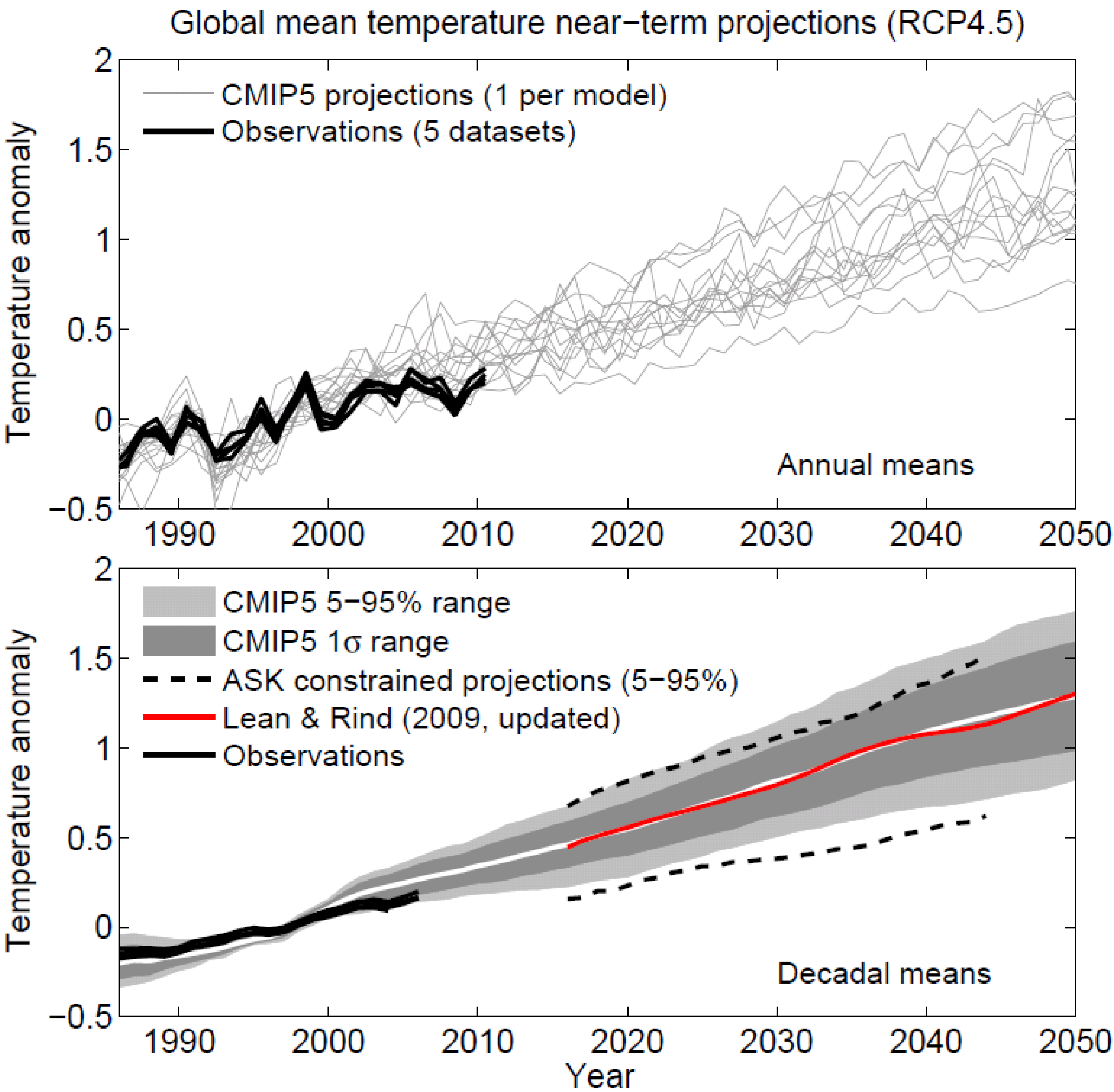

Figure 11.11: a) Projections of global mean, annual mean surface air temperature 1986–2050 (anomalies relative to 1986–2005) under RCP4.5 from CMIP5 models (grey lines, one ensemble member per model), with five observational estimates (HadCRUT3 – Brohan et al., 2006; ERA-Interim - Simmons et al., 2010; GISTEMP - Hansen et al., 2010; NOAA – Smith et al., 2008; 20th century reanalysis – Compo et al., 2011) for the period 1986–2010 (black lines); b) as a) but showing the range (grey shades, with the multi-model mean in white) of decadal mean CMIP5 projections using (where relevant) the ensemble mean from each model, and decadal mean observational estimates (black lines). An estimate of the projected 5–95% range for decadal mean global mean surface air temperature for the period 2016–2040 derived using the ASK methodology applied to simulations with the HadGEM2ES climate model is also shown (dashed black lines). The red line shows a statistical prediction based on the method of Lean and Rind (2009).

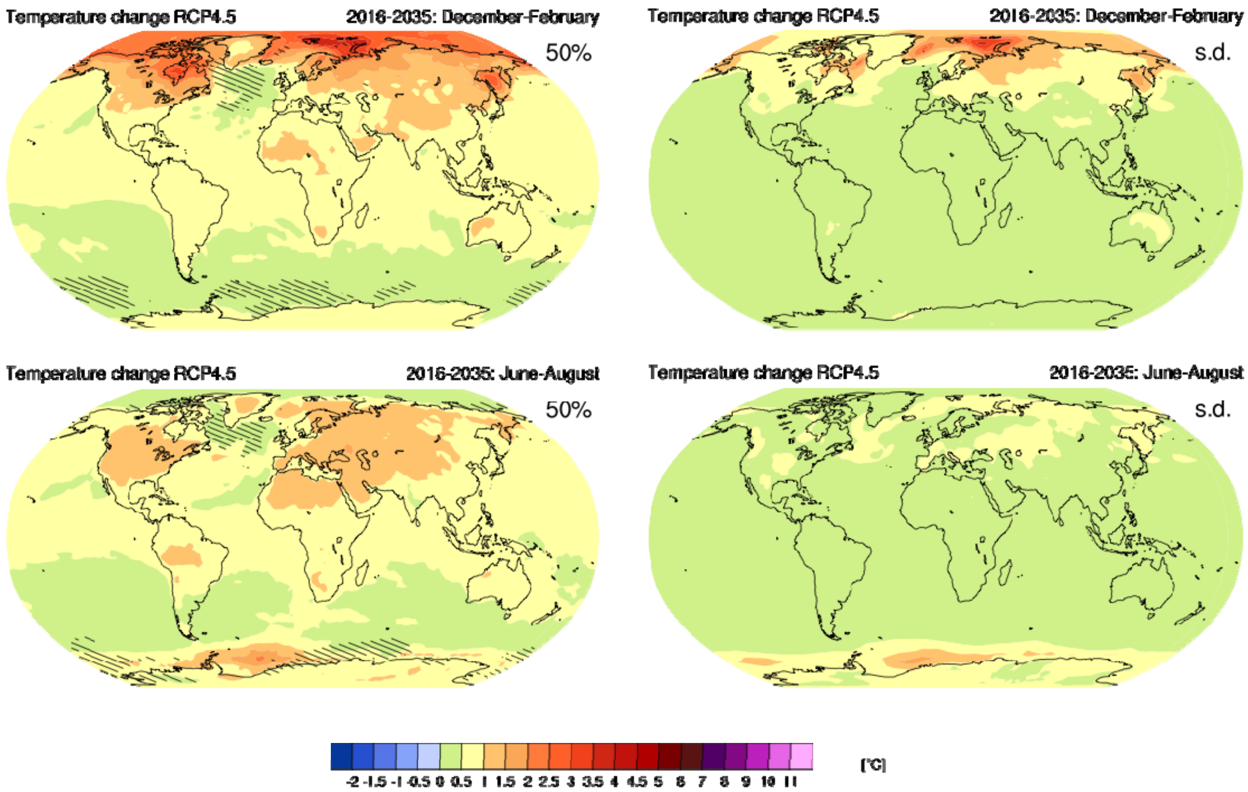

Figure 11.12: CMIP5 multi-model ensemble median of projected changes in surface air temperature for the period 2016–2035 relative to 1986–2005 under RCP4.5 relative to the 2086–2005 period (left panels). The right panels show an estimate of the natural internal variability in the quantity plotted in the left panels (see Annex I Atlas for details of method). Hatching in left panels indicates areas where projected changes are less than one standard deviation of estimated natural variability of these 20-year differences.

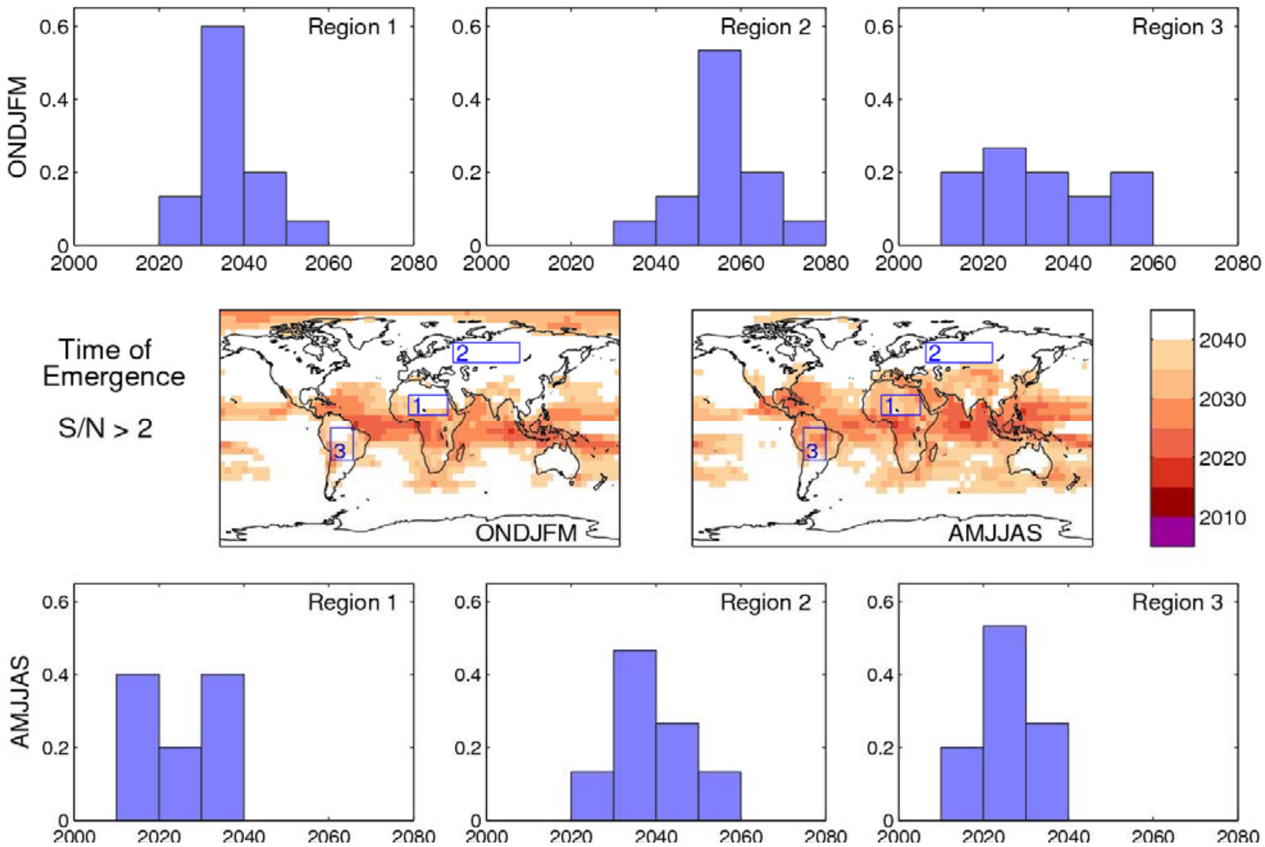

Figure 11.13: Time of emergence of significant local warming derived from CMIP3 models under the SRES A1B scenario. Warming is quantified as the half-year mean temperature anomaly relative to 1986–2005, and the noise as the standard deviation of half-year mean temperature derived from a control simulation of the relevant model. Central panels show the median time at which the signal-to-noise ratio exceeds a threshold value of 2 for (left) the October-March half year and (right) the April-September half year, using a spatial resolution of 5° x 5°. Histograms show the distribution of emergence times for area averages over the regions indicated obtained from the different CMIP3 models. Full details of the methodology may be found in Hawkins and Sutton (2011).

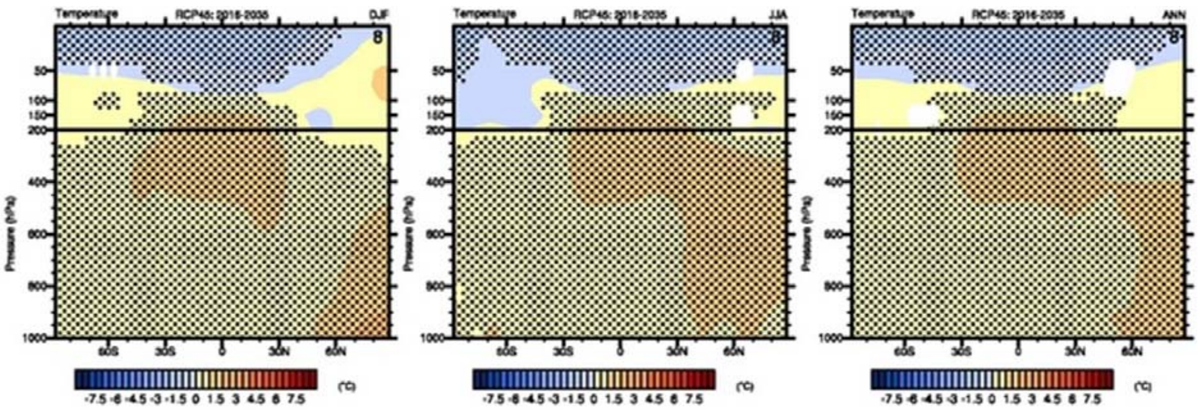

Figure 11.14: Zonal mean temperature differences, 2016–2035 minus 1986–2005, for the CMIP5 multi-model ensemble (°C), for a) DJF, b) JJA, and C) annual mean.

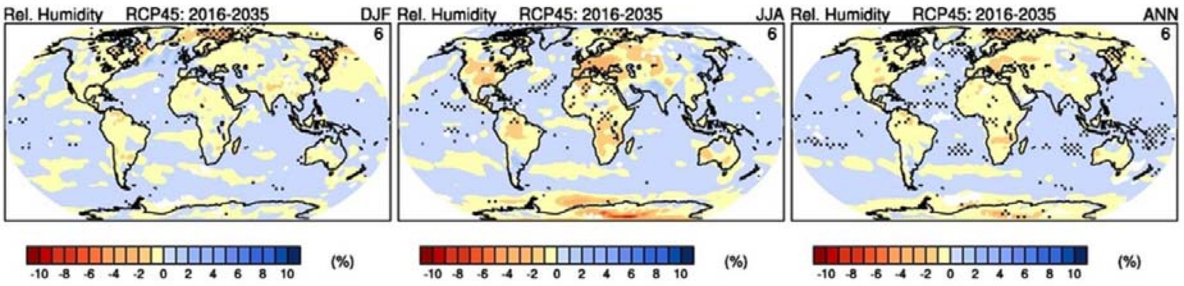

Figure 11.15: Surface atmospheric humidity differences, 2016–2035 minus 1986–2005, for the CMIP5 multi-model ensemble (%), for a) DJF, b) JJA, and C) annual mean.

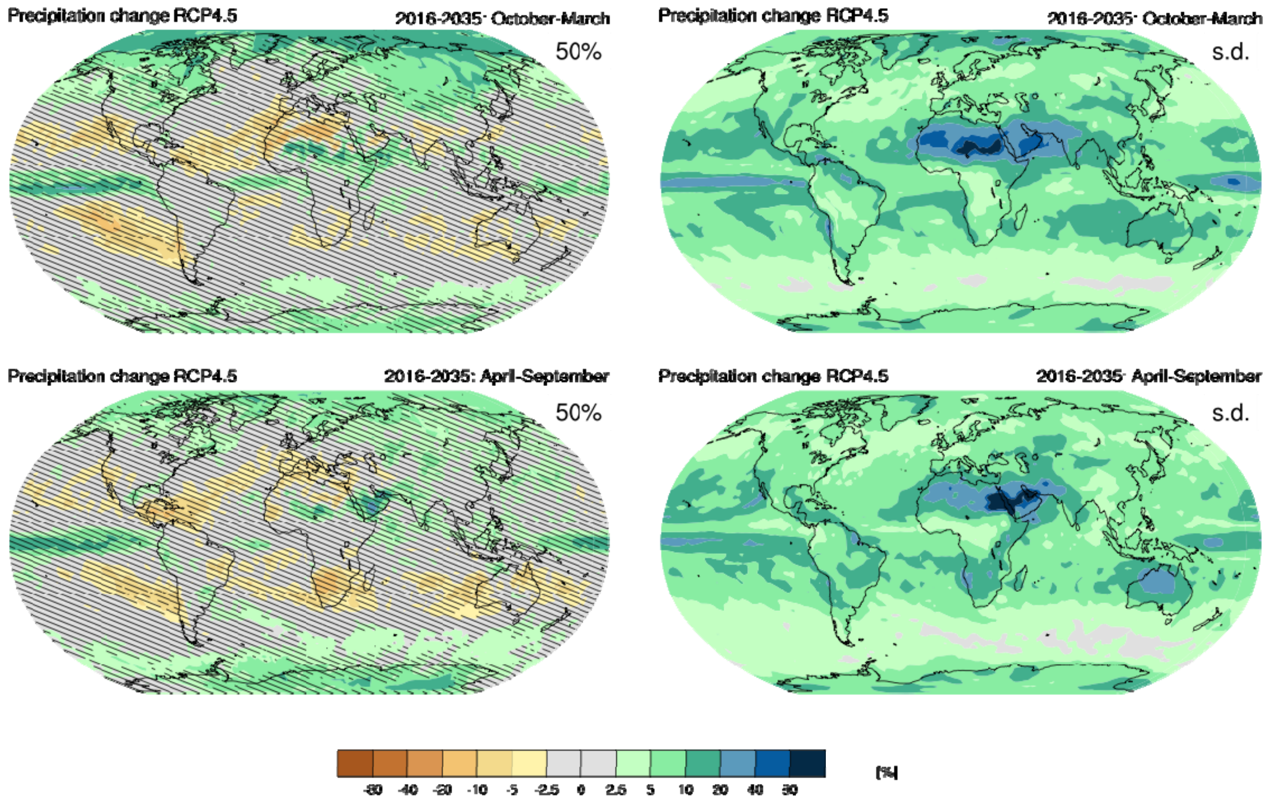

Figure 11.16: CMIP5 multi-model ensemble median of projected changes in precipitation for the period 2016–2035 relative to 1986–2005 under RCP4.5 in mm/day (upper panels). The lower panels show an estimate of the natural internal variability in the quantity plotted in the upper panels (see Annex I Atlas for details of method). Hatching in upper panels indicates projected changes are everywhere less than 2 times standard deviation of estimated natural variability**.**

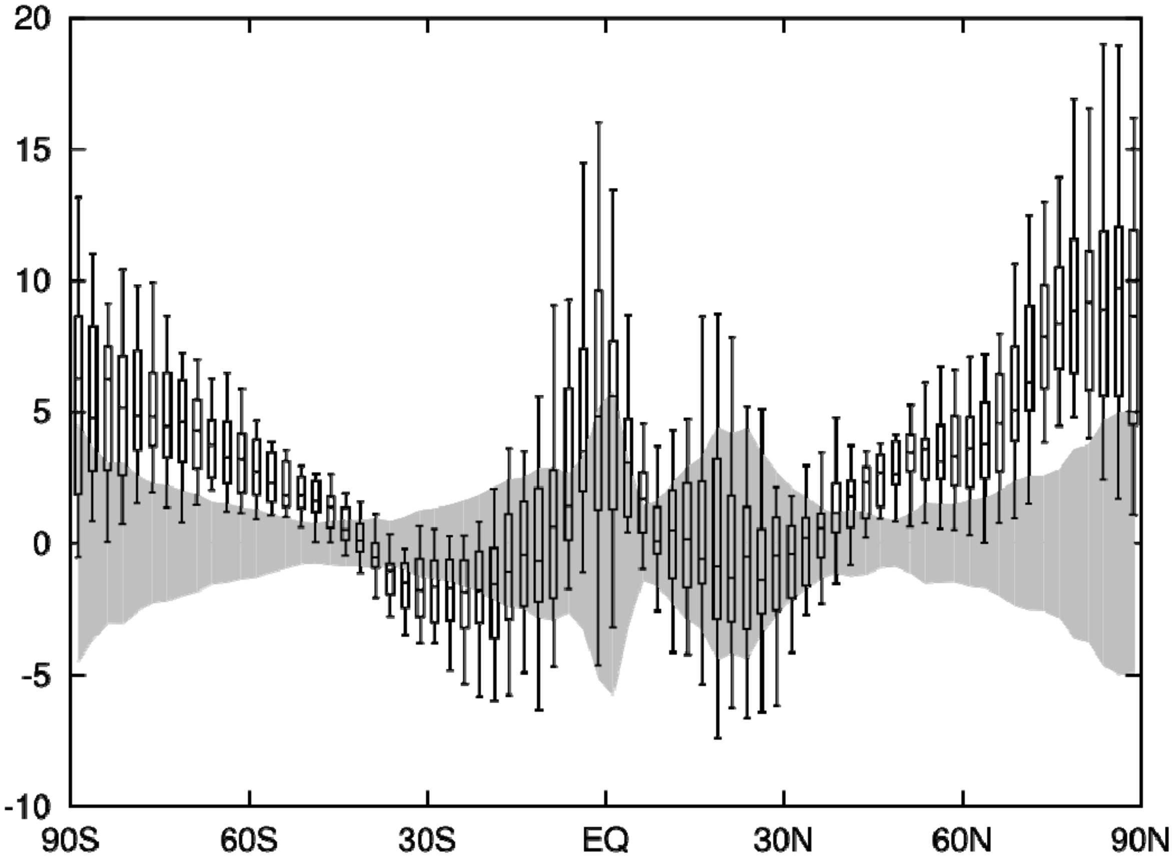

Figure 11.17: CMIP5 multi-model projections of changes in annual mean zonal mean precipitation (mm/day) for the period 2016–2035 relative to 1986–2005 under RCP4.5. Vertical lines indicate median, inter-quartile and 5–95% ranges of the model responses. Shading indicates 1 standard deviation of the estimated natural internal variability (see Annex I Atlas for details of method).

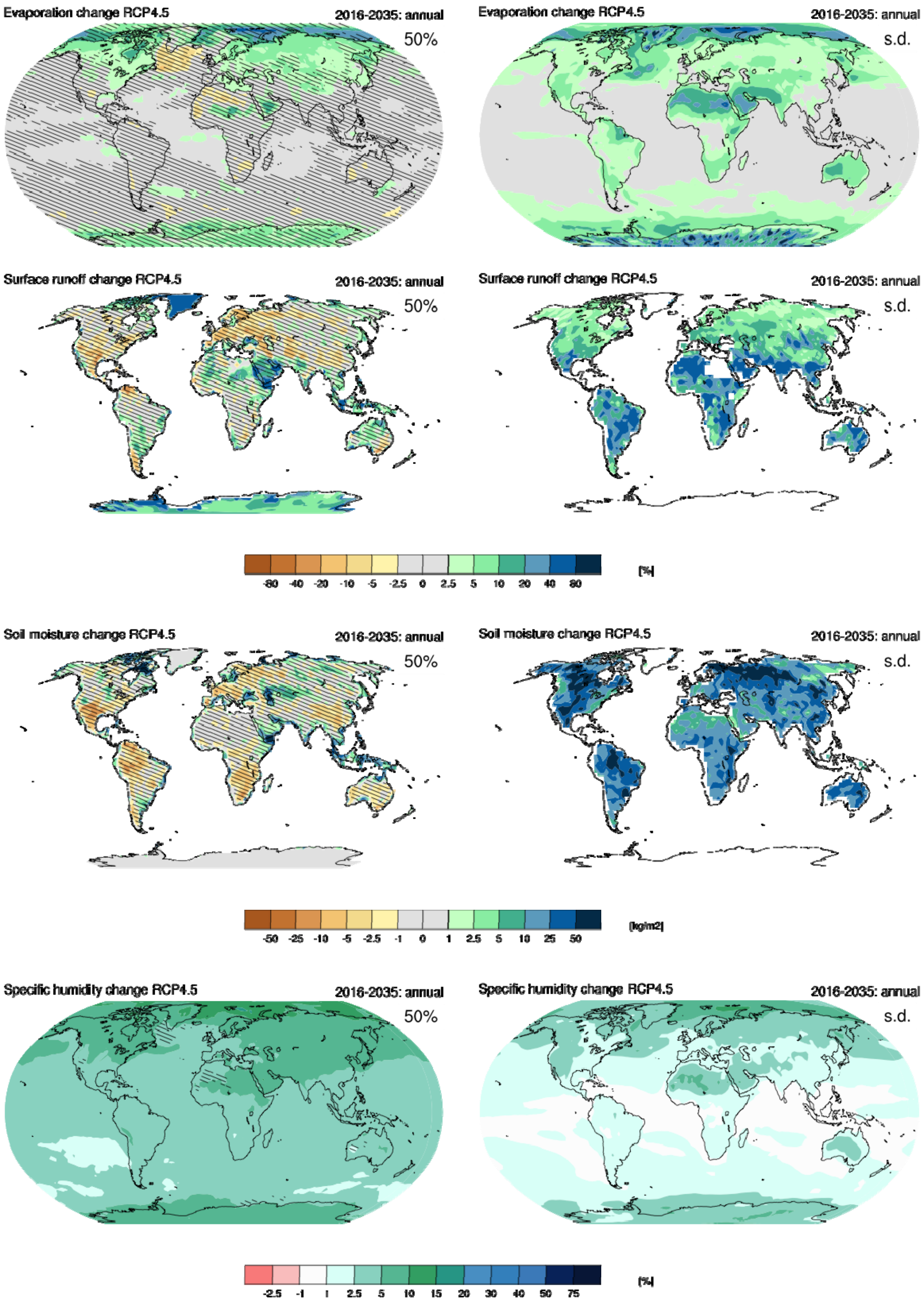

Figure 11.18: CMIP5 multi-model mean projected changes in annual mean runoff (%), evaporation (%), soil moisture (%) [and specific humidity (%)] for the period 2016–2035 relative to 1986–2005 under RCP4.5.

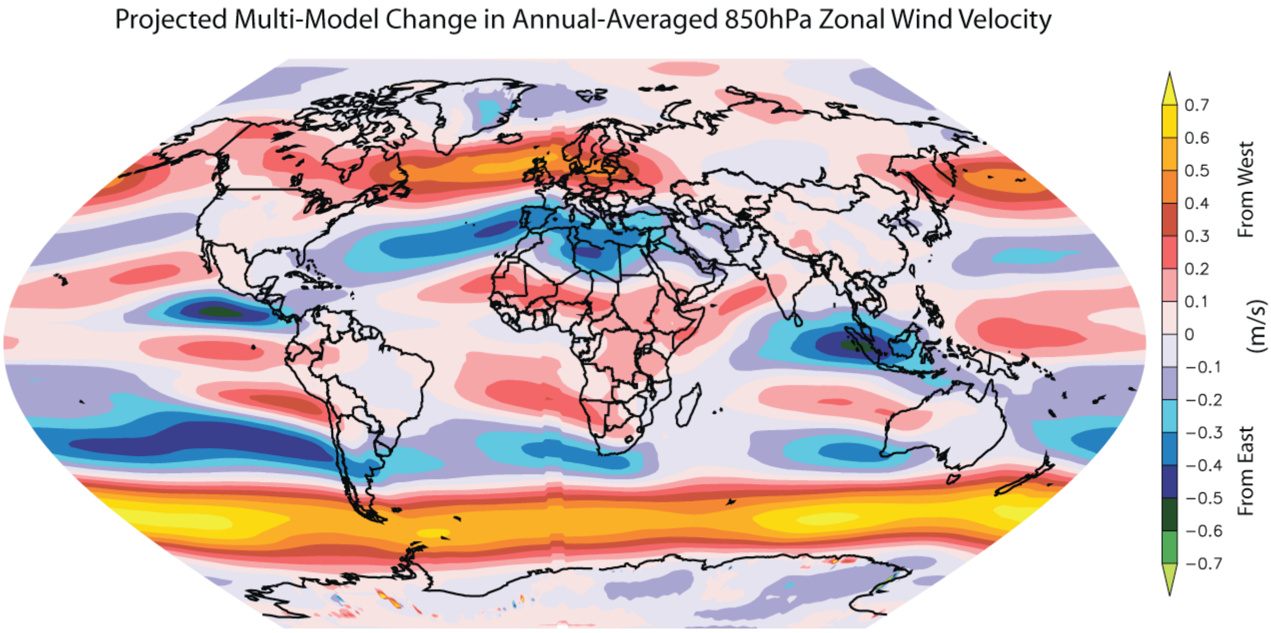

Figure 11.19: [PLACEHOLDER FOR SECOND ORDER DRAFT: to make final; Projected changes in annual-averaged zonal (west-to-east) wind at 850hPa based on the average of 23 AOGCMs from the CMIP3 (Meehl et al., 2007) multi-model ensemble, under 21st Century Emissions Scenario SRESA1B. Gray shading indicates where the multi-model average AOGCM anomalies are smaller than two standard deviations of the multi-AOGCM estimate of internal variability from the control climate integrations. Values referenced to the 1986–2005 climatology.]

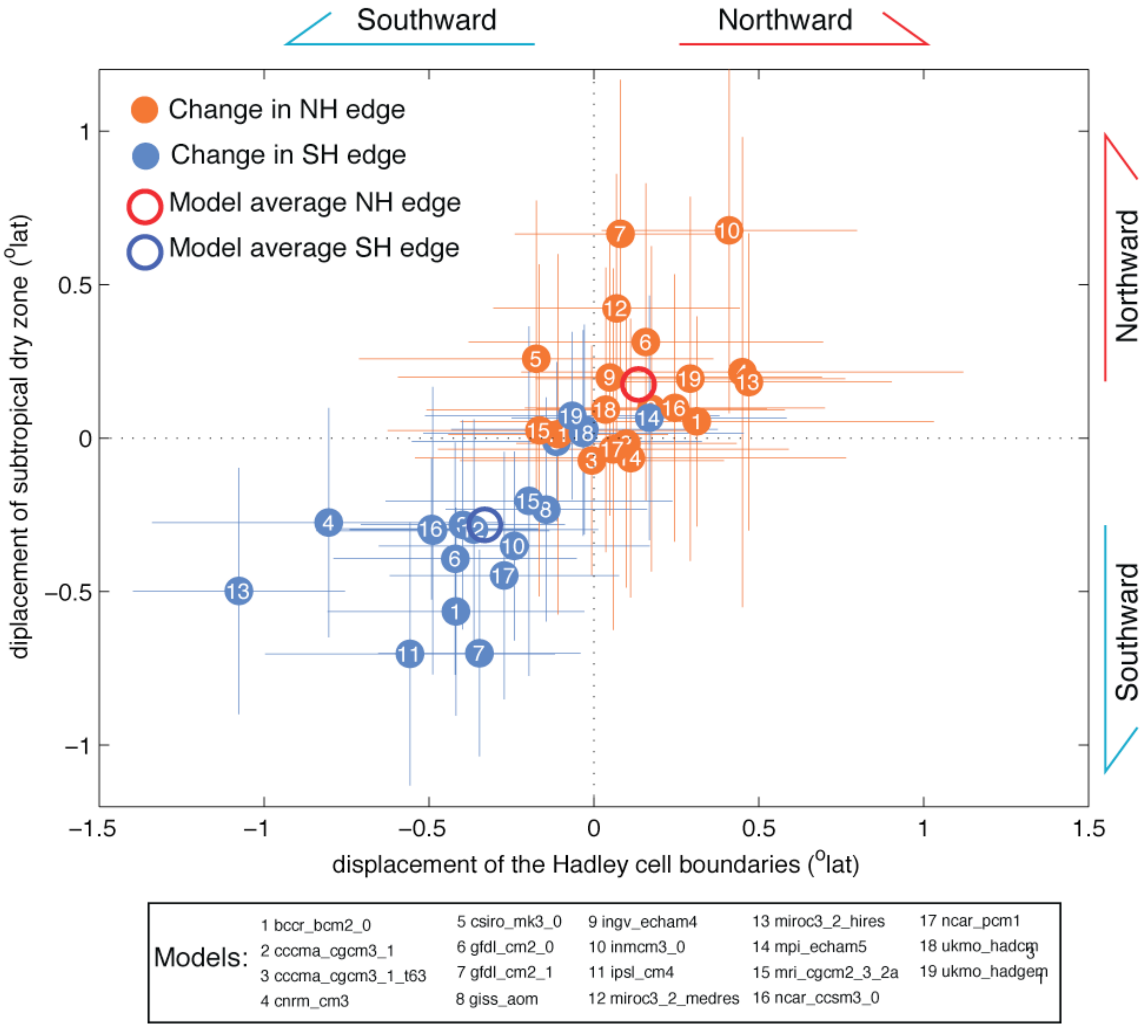

Figure 11.20: Projected changes in the annual-averaged poleward edge of the Hadley Circulation (horizontal axis) and sub-tropical dry zones (vertical axis) based on 19 AOGCMs from the CMIP3 (Meehl et al., 2007) multi-model ensemble, under 21st Century Emissions Scenario SRESA1B. Orange symbols show the change in the northern edge of the Hadley Circulation/dry zones, while blue symbols show the change in the southern edge of the Hadley Circulation/dry zones. Open circles indicate the multi-model average, while horizontal and vertical colored lines indicate the ±1-standard deviation range for internal climate variability estimated from each model. Values referenced to the 1986–2005 climatology. Figure based on the methodology of Lu et al., 2007.

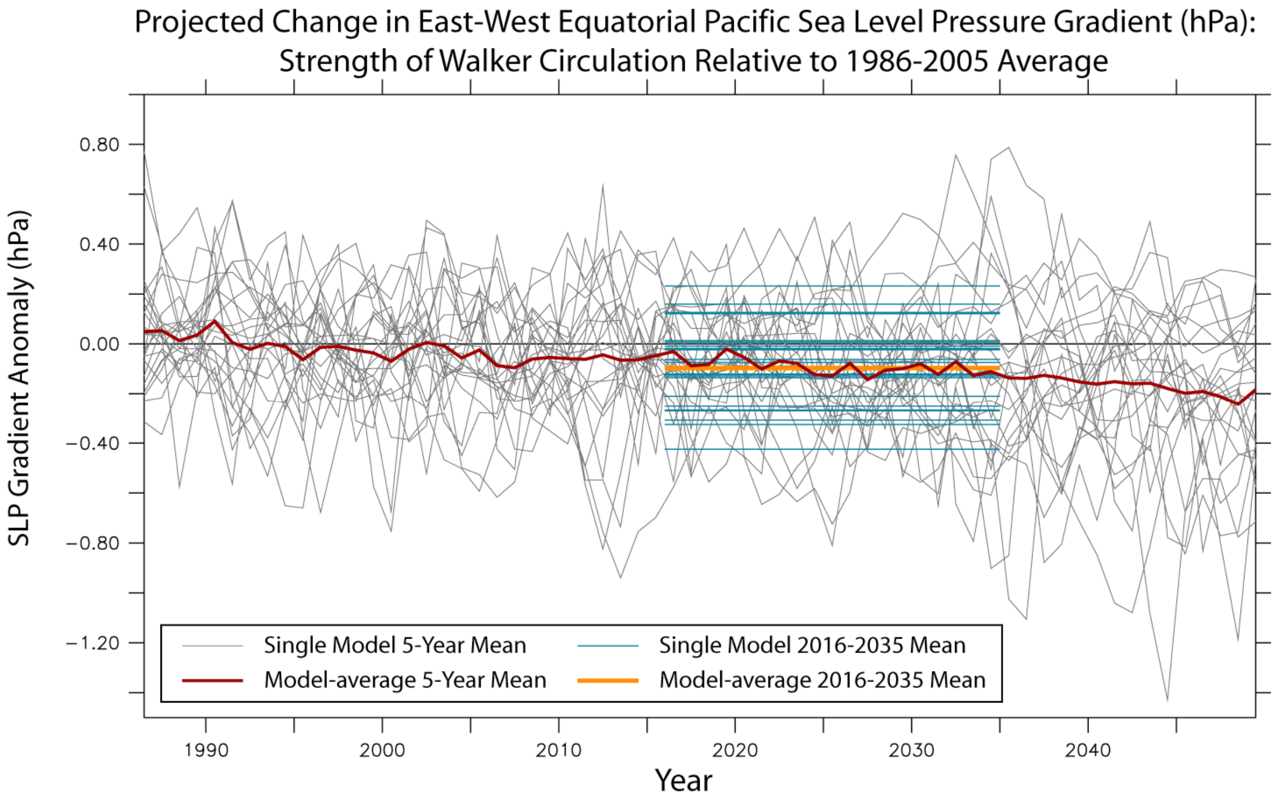

Figure 11.21: Projected changes in the strength of the Pacific Walker Circulation, as estimated using the east-west sea level pressure gradient across the equatorial Pacific (Vecchi and Soden, 2007), based on 24 AOGCMs from the CMIP3 (Meehl et al., 2007) multi-model ensemble, under 21st Century Emissions Scenario SRESA1B. Thin gray lines indicate the five-year running average for each model, red line indicates the multi-model five-year running average. Blue horizontal lines indicate the 2016–2035 values for each model, with the orange line indicating the multi-model averaged projection for 2016–2035. Values referenced to the 1986–2005 climatology.

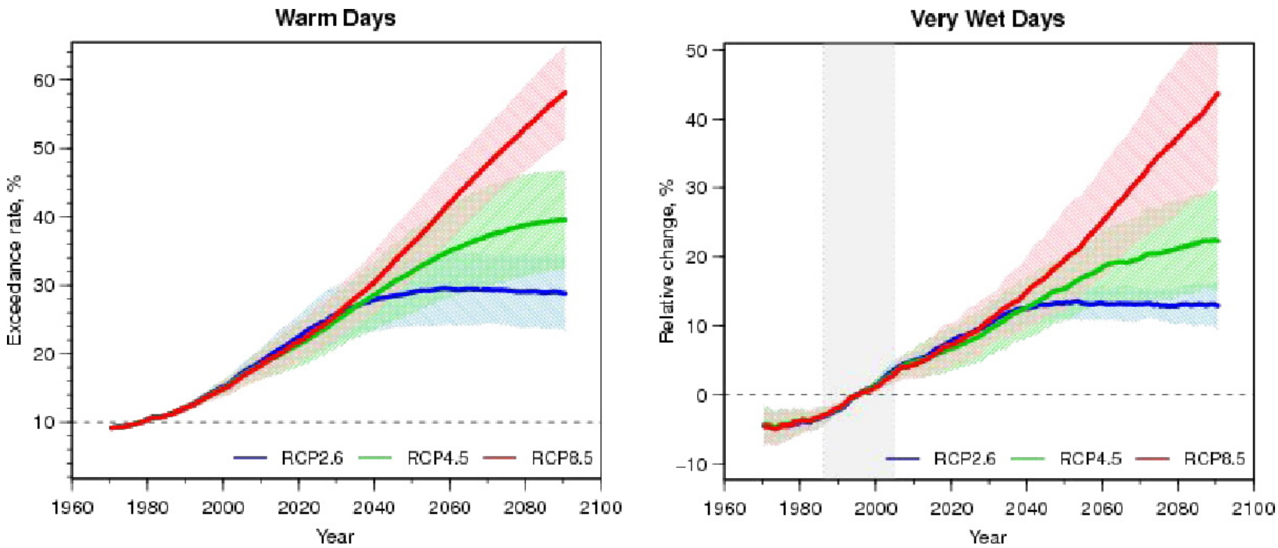

Figure 11.22: Global mean projections for the occurrence of warm and wet days from CMIP5 for the RCP2.6, RCP4.5 and RCP8.5 scenarios relative to 1986–2005. Panel (a) shows percentage of warm days (tx90p: Tmax exceeds the 90th percentile), panel (b) shows relative change of very wet days (pr95p: annual total precipitation when daily precipitation exceeds 95th percentile).

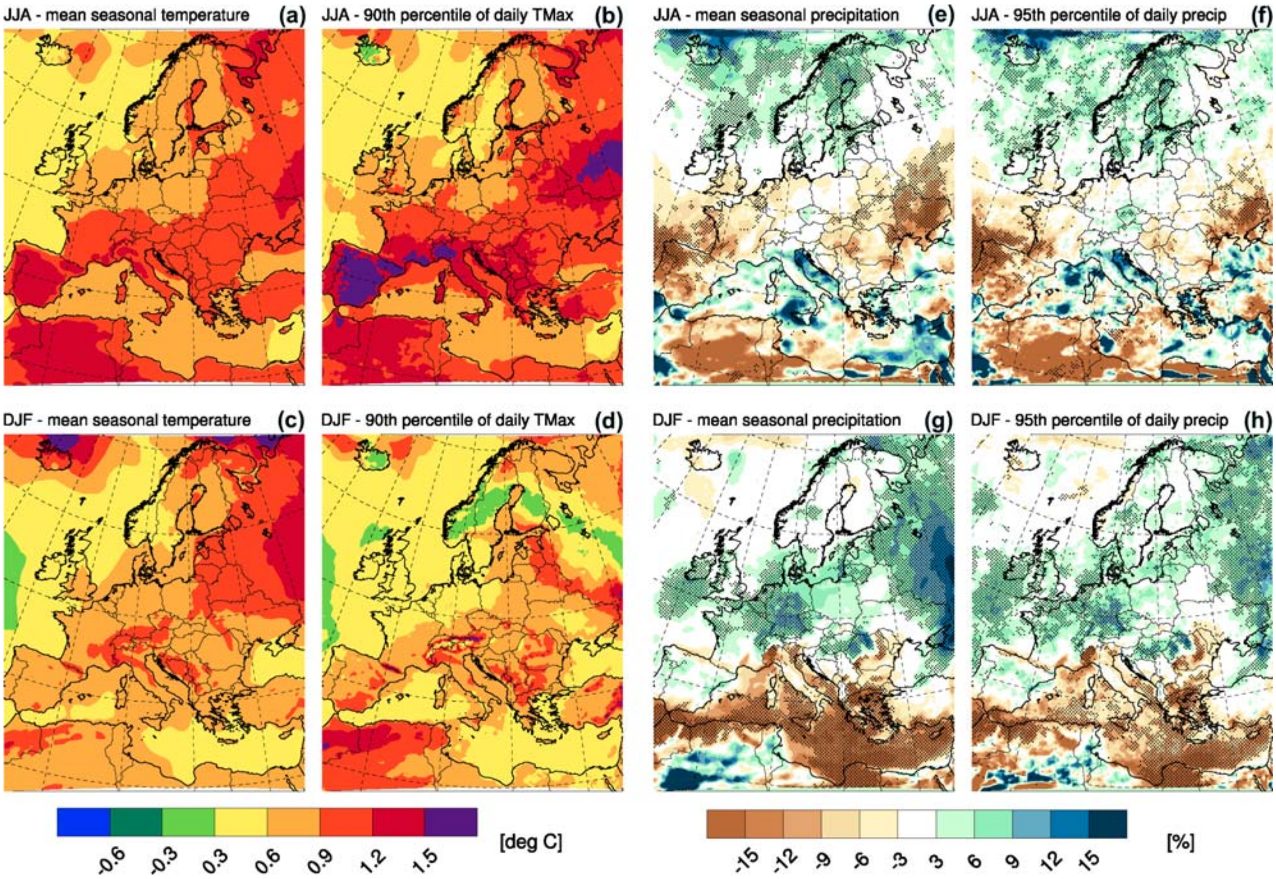

Figure 11.23: European-scale projections from the ENSEMBLES regional climate modelling project for 2016–2035 relative to 1986–2005, with top and bottom panels applicable to JJA and DJF, respectively. For temperature, projected changes (°C) are displayed in terms of ensemble mean changes of (a,c) mean seasonal surface temperature, and (b,d) the 90th percentile of daily maximum temperatures. For precipitation, projected changes (%) are displayed in terms of ensemble mean changes of (e,g) mean seasonal precipitation and (f,h) the 95th percentile of daily precipitation. The stippling in (e-h) highlights regions where 80% of the models agree in the sign of the change (for temperature all models agree on the sign of the change). The analysis includes the following 10 RCM-GCM simulation chains for the SRES A1B scenario (naming includes RCM group and GCM simulation): HadRM3Q0-HadCM3Q0, ETHZ-HadCM3Q0, HadRM3Q3-HadCM3Q3, SMHI-HadCM3Q3, HadRM3Q16-HadCM3Q16, SMHI-BCM, DMI-ARPEGE, KNMI-ECHAM5, MPI-ECHAM5, DMI-ECHAM5 (Figure courtesy of Jan Rajczak, ETH Zürich).

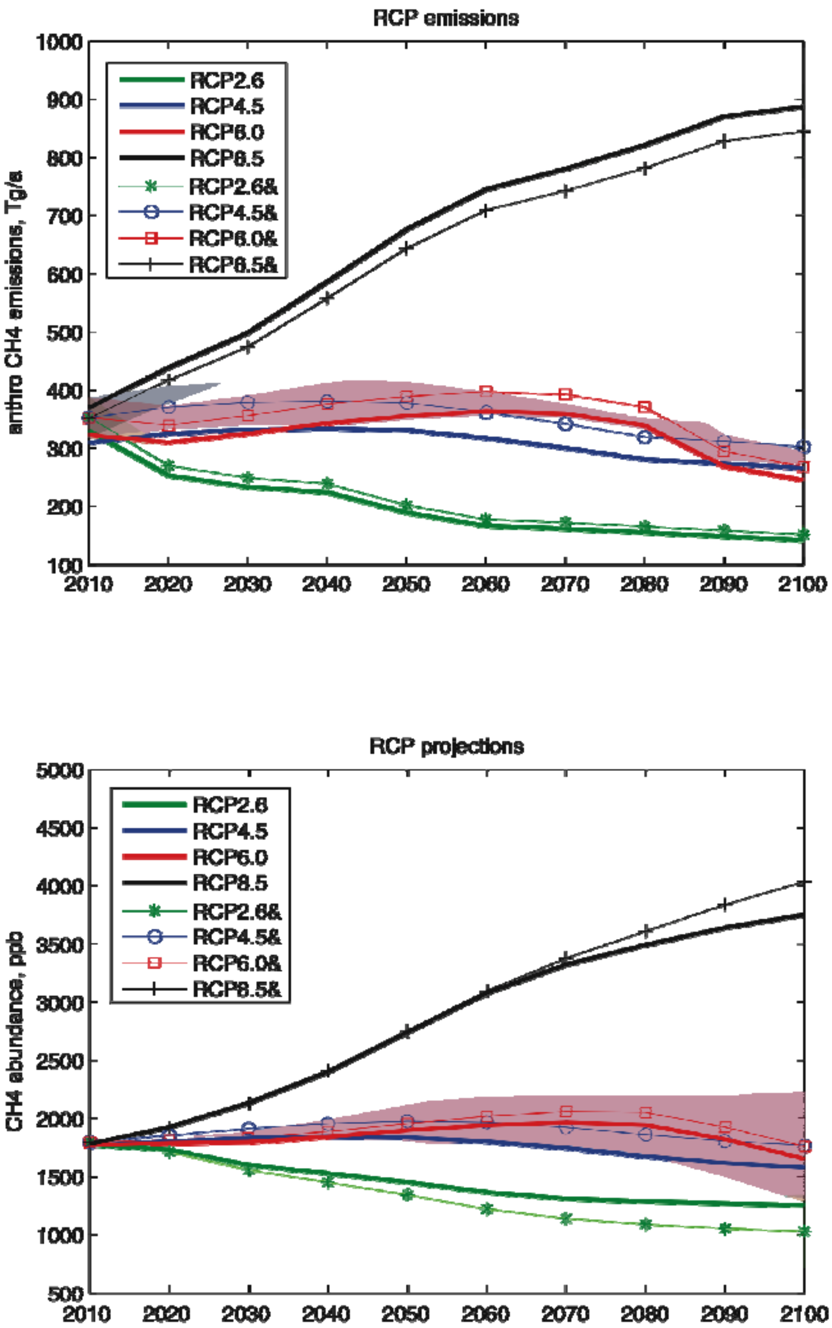

Figure 11.24: Projected CH4 (a) anthropogenic emissions and (b) atmospheric abundances for the four RCP scenarios (2010–2100). The thick solid lines show the published RCP values: black +, RCP8.5; red square, RCP6.0; blue o, RCP4.5; green *, RCP 2.6. Thin lines with markers show values from this assessment. The shaded region shows the ±1 SD from the Monte Carlo calculations that consider uncertainties, including the current magnitude of the anthropogenic emissions.

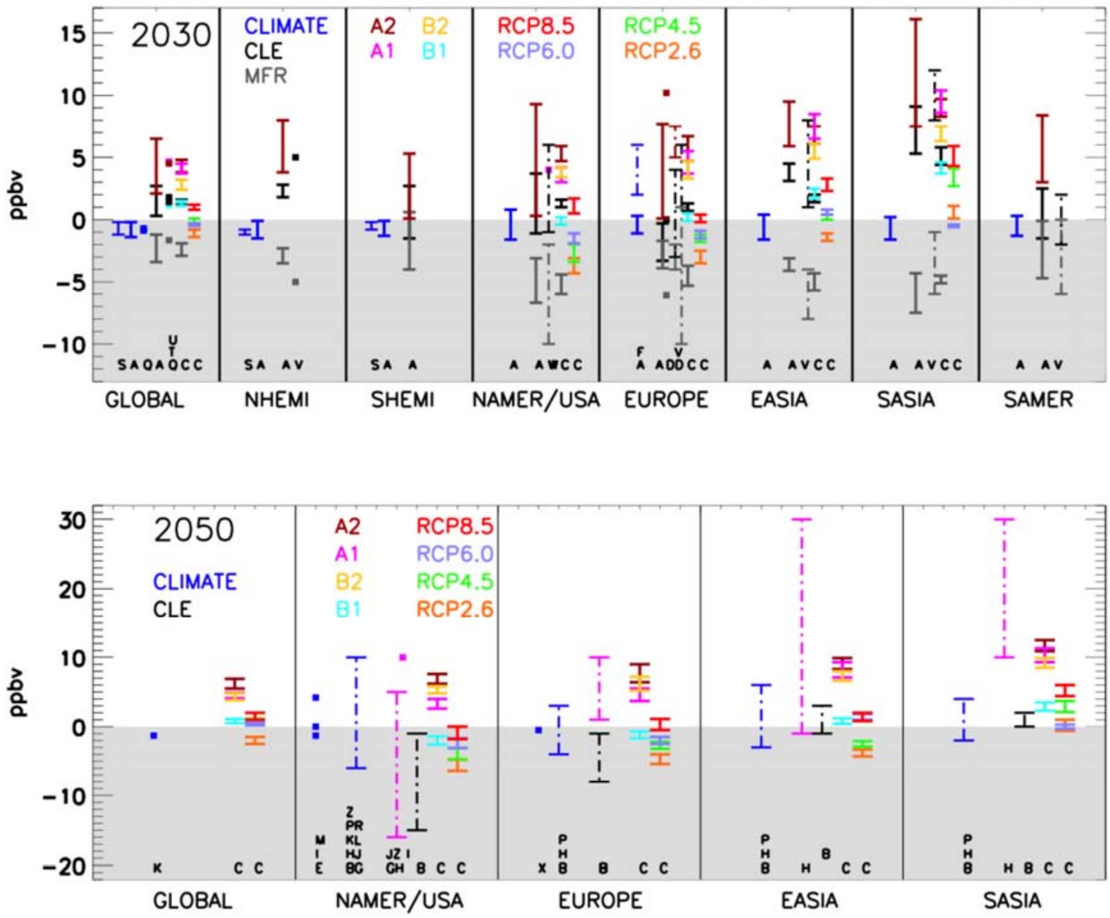

Figure 11.25: Changes in surface O_3 solely due to climate (blue) or emissions (colored by emission scenario) reported in the literature in 2030 (top) and 2050 (bottom) for selected world regions. Results from individual studies are labeled by letters underneath the corresponding plot symbols. Vertical bars represent a combination of ranges as reported in the literature: (1) multi-model mean and standard deviations in annual mean, spatial averages from the ACCENT/Photocomp study for 2030 ((Dentener et al., 2006b), A); (2) application of a parameterization developed from the multi-model ensemble of the Task Force on Hemispheric Transport of Air Pollution [TF HTAP, 2010] regional source-receptor relationships to estimate surface O_3 response for several emission scenarios in 2030 and 2050 globally and within the TF HTAP continental regions (Wild et al., 2011, C); (3) spatial averages across a region, denoted by filled squares (Szopa et al., 2006, D; Avise et al., 2009, E; Tagaris et al., 2007, I; Racherla and Adams, 2006, K; Hogrefe et al., 2004, M; Unger et al., JGR, 2006, Q; Fiore et al., JGR, 2008, T; West et al., PNAS, 2006, U; Fiore et al., GRL, 2002, W; Katragkou et al., in press JGR, X)(4) spatial ranges across a region as estimated with one model or combined across several individual modeling studies, denoted by dashed lines ([Need to insert "Royal" before "Society" in endnotes] ((Society 2008b), B; Szopa et al., 2006, D; Forkel and Knoche, 2006, F; Wu et al., 2008a (air quality), G; Wu et al., 2008b (background), H; Nolte et al., JGR, 2008, J; Racherla and Adams 2006, K; Zhang et al., 2008, L; Racherla and Adams, 2008, P; Tagaris et al., 2009, R; Stevenson et al., 2005, S; Dentener et al., ACP 2005, V; Y; Lam et al., 2011, Z) Regional definitions, methods, and reported metrics (e.g., 24-hour versus daily maximum values over a 1-hour or 8-hour averaging period, annual or seasonal averages) vary across studies. Climate change scenarios vary across studies, but are combined into ranges denoted by blue bars for two reasons: (1) there is little detectable cross-scenario difference in the climate response in 2030 (Section 11.4.7), and (2) many of these estimated are based on simulations that are too short to cleanly attribute a climate change signal and thus it is not appropriate to attribute differences to particular forcing scenarios.

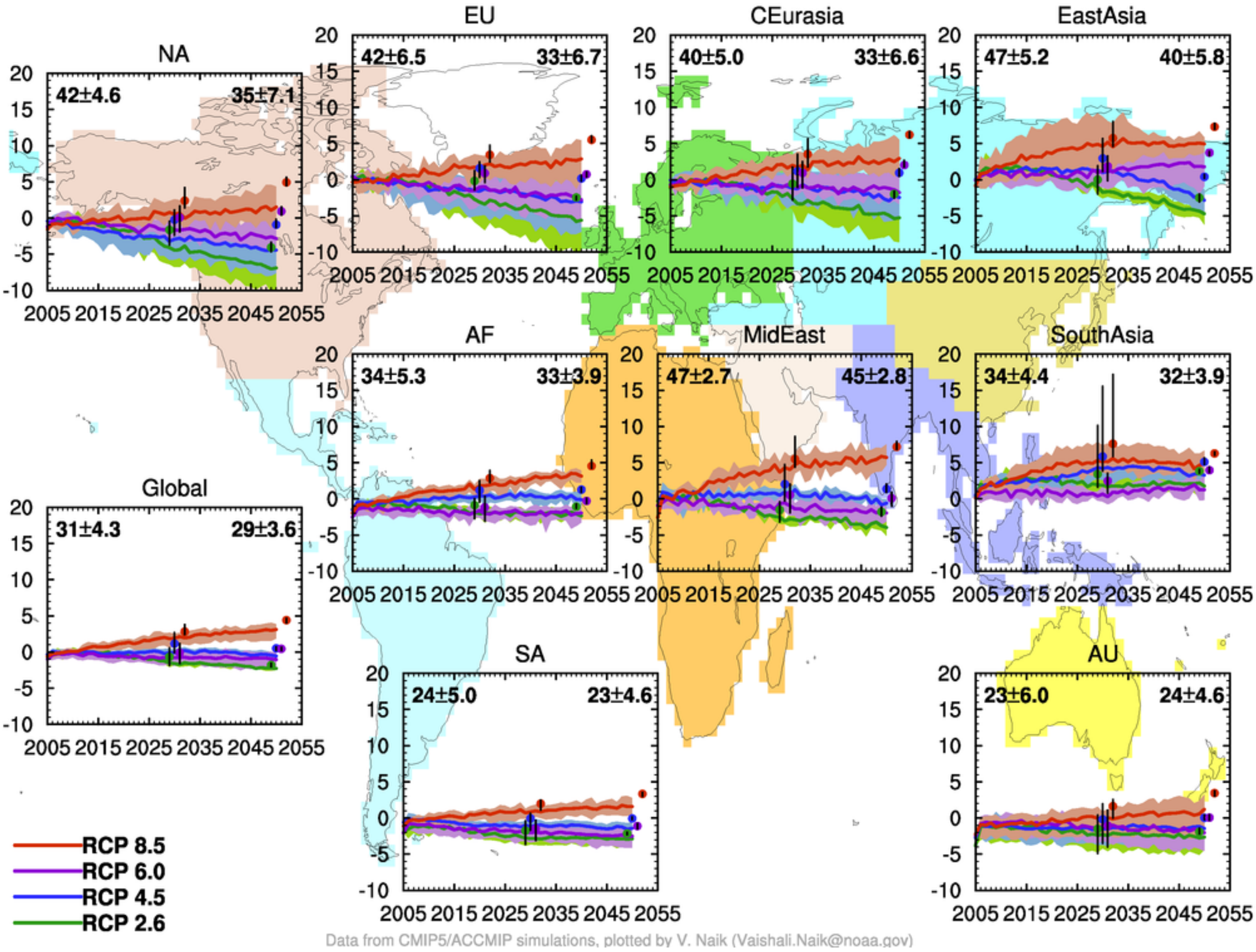

Figure 11.26a: Changes in near-term annual mean surface ozone (ppb) following the RCP scenarios, spatially averaged over selected world regions (shaded land regions) and from CMIP5 chemistry-climate model ensemble (3 models, colored lines denote ensemble mean and shading denotes full range across models for each RCP). Filled circles with vertical lines indicate the multi-model average and full cross-model range from the 2030 and 2050 ACCMIP decadal time slice simulations, colored by RCP scenario (4 models for RCP2.6 and RCP4.5; 3 models for RCP8.5; 2 models for RCP6.0 in 2030, and 1 model for all RCP scenarios in 2050). Changes are relative to the 1986–2005 reference period for the transient simulations, and relative to the average of the 1980 and 2000 decadal time slices for the ACCMIP ensemble. The average ozone value during the reference period, spatially averaged over each region, is shown in each panel, with the standard deviation reflecting the cross-model range (transient CMIP5 models on the left; ACCMIP models on the right). In cases where multiple ensemble members were available from a single model, they were averaged first before inclusion into the multi-model mean.

Figure 11.26b: [PLACEHOLDER FOR SECOND ORDER DRAFT: As in 11.24a, but for PM2 if sufficient number of models are available.]

Figure 11.27: [PLACEHOLDER FOR SECOND ORDER DRAFT: Illustrate projected change in extreme metric, following general structure of Figure 11.24 but considering e.g., frequency of days above a threshold value for ozone and/or PM due to climate change only – if sufficient number of models contribute results from ACCMIP RCP8.5 climate-change-only simulations.]

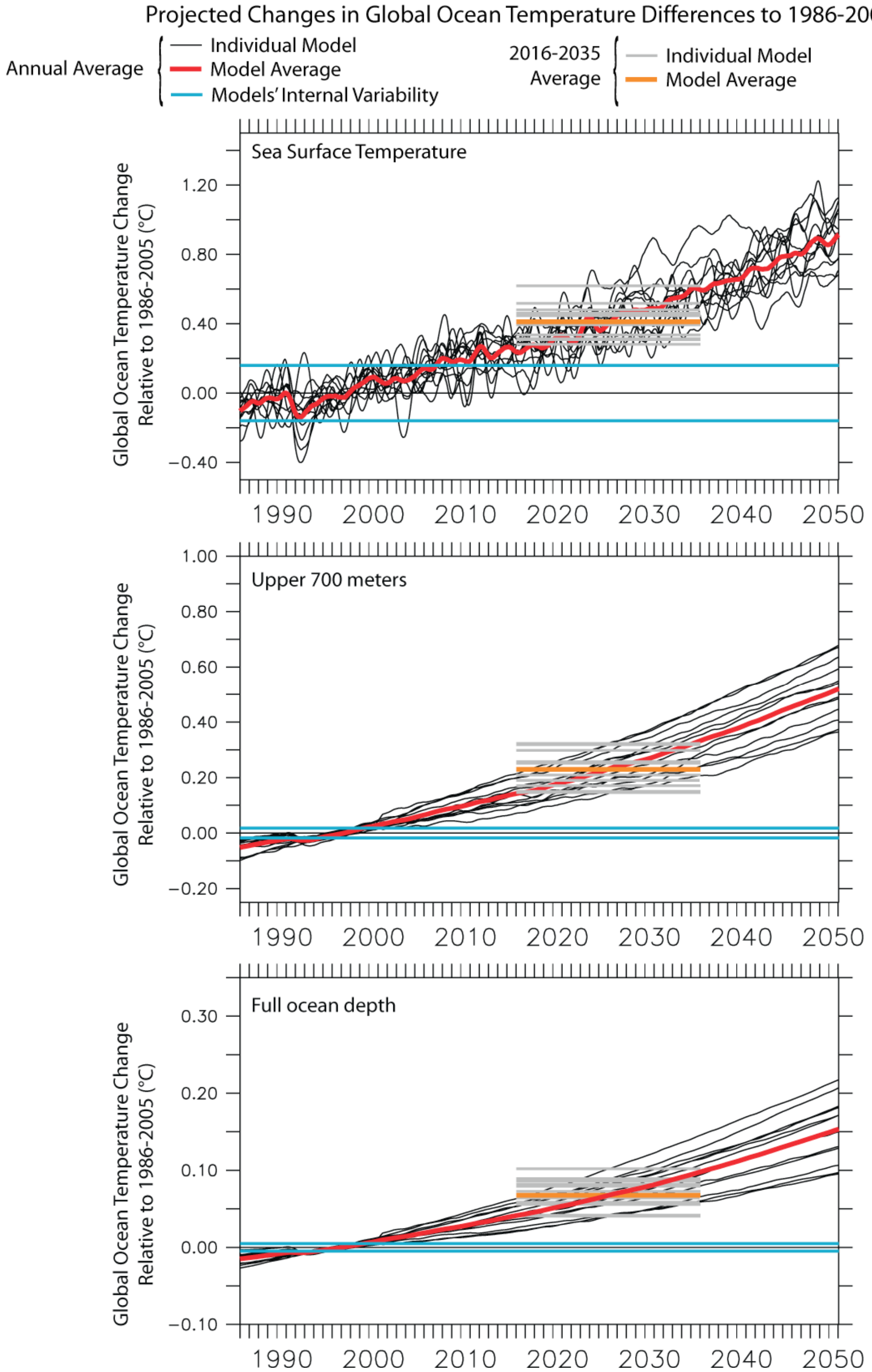

Figure 11.28: Projected changes in annual-averaged, globally-averaged, depth-averaged ocean temperature based on twelve AOGCMs from the CMIP3 (Meehl et al., 2007) multi-model ensemble, under 21st Century Emissions Scenario SRESA1B. Top panel shows changes of sea surface temperature, middle panel ocean temperature changes averaged over the upper 700 meters of the ocean, bottom panel shows changes averaged over the full ocean depth. Thin black lines show the evolution for each of the twelve AOGCMs, red line shows the average of all twelve projections, the blue line indicates an estimate of the average magnitude of internal variability of all twelve AOGCMs (2sigma).Gray horizontal lines indicate the 2016–2035 average anomaly for each of the twelve AOGCMs, while the orange horizontal line indicates the multi-model average 2016–2035 anomaly. The fifty-year running average from each model's control climate integration was removed from each line. Values referenced to the 1986–2005 climatology of each AOGCM.

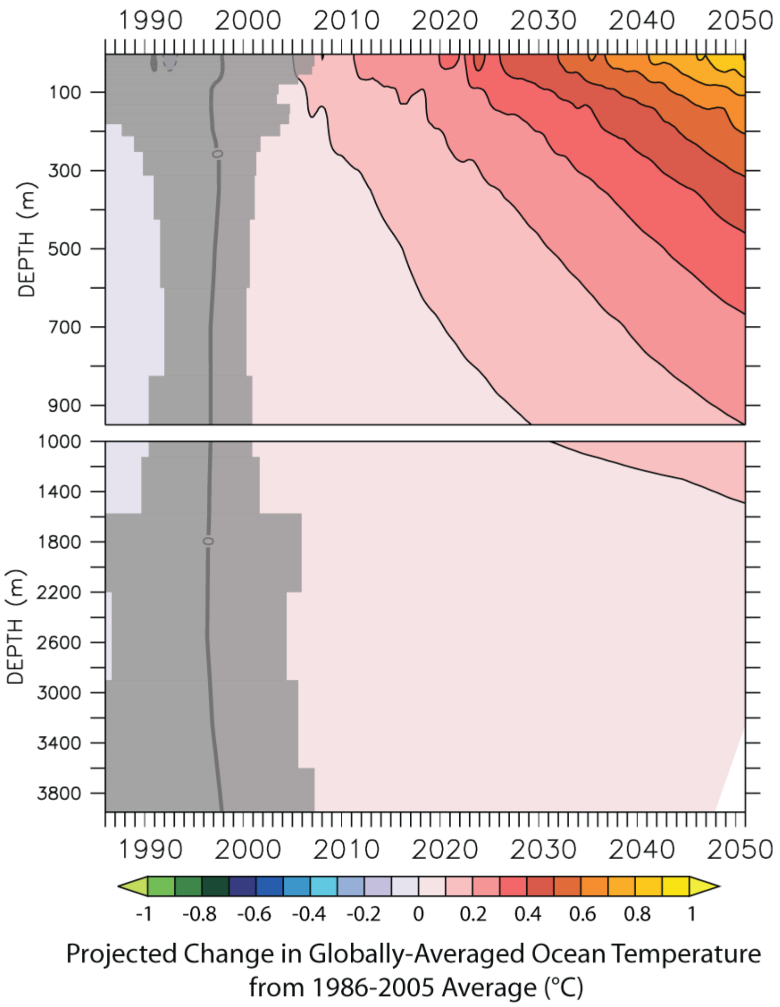

Figure 11.29: Projected changes, as a function of depth, in annual-averaged, globally-averaged ocean temperature based on the average of twelve AOGCMs from the CMIP3 (Meehl et al., 2007) multi-model ensemble, under 21st Century Emissions Scenario SRESA1B. Gray shading indicates where the multi-model average AOGCM anomalies are smaller than two standard deviations of the multi-AOGCM estimate of internal variability from the control climate integrations. The fifty-year running average from each model's control climate integration was removed from each line. Values referenced to the 1986-2005 climatology of each AOGCM.

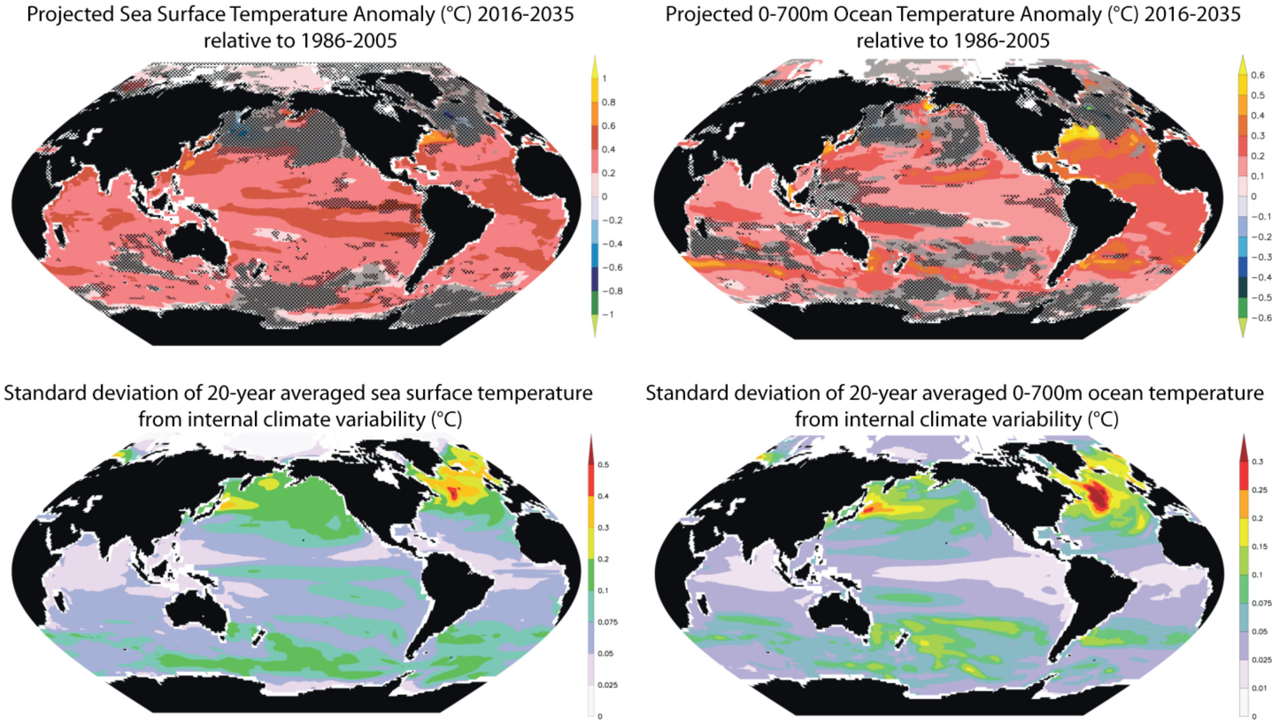

Figure 11.30: Upper panels show the projected changes averaged 2016–2035 relative to 1986–2005 in sea surface temperature (left panels) and temperature averaged over the upper 700 meters of the ocean (right panels), as a function of latitude and longitude. Lower panels show the standard deviation of twenty-year averages of sea surface temperature (left panels) and temperature averaged over the upper 700 meters of the ocean (right panels) arising from internal climate variability in these models. Figures based on the average of twelve AOGCMs from the CMIP3 (Meehl et al., 2007) multi-model ensemble, under 21st Century Emissions Scenario SRESA1B. Gray shading indicates where the multi-model average AOGCM anomalies are smaller than two standard deviations of the multi-AOGCM estimate of internal variability from the control climate integrations, black stippling indicates where at least four (1/3) of the models disagree on the sign of the change. The fifty-year running average from each model's control climate integration was removed from each line.

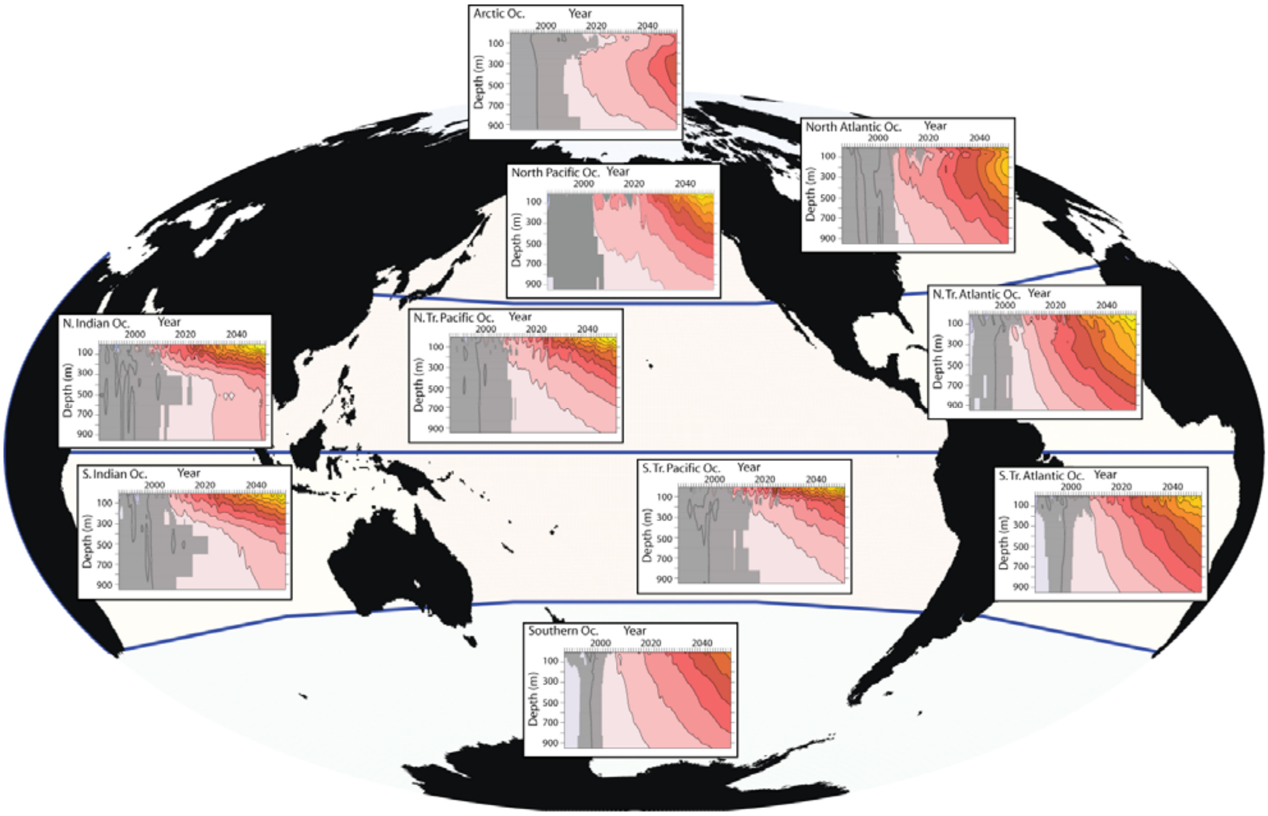

Figure 11.31: [PLACEHOLDER FOR SECOND ORDER DRAFT: Currently shaded at 1 sigma. Same as Figure 11.XX, but for regional averages]

Figure 11.32: [PLACEHOLDER FOR SECOND ORDER DRAFT: Arctic September sea ice coverage (%) for 2016–2035 from a CMIP5 multi-model average for the RCP4.5 scenario that is representative of all the RCP scenarios for this time period.]

Figure 11.33: [PLACEHOLDER FOR SECOND ORDER DRAFT: Same as Figure 11.32 but for February.]

Figure 11.34: [PLACEHOLDER FOR SECOND ORDER DRAFT: Same as Figure 11.32 but for the Antarctic.]

Figure 11.35: [PLACEHOLDER FOR SECOND ORDER DRAFT: Same as Figure 11.33 but for the Antarctic.]

Figure 11.36: [PLACEHOLDER FOR SECOND ORDER DRAFT: Change in snow cover fraction for a March-April average using a 15% extent threshold from the CMIP5 multi-model average for RCP4.5 which is representative of all the RCP scenarios for this time period.]

Figure 11.37: [PLACEHOLDER FOR SECOND ORDER DRAFT: Annual mean change in permafrost for 2016–2035 average minus 1986–2005 base period for RCP4.5 from the CMIP5 multi-model average for RCP4.5 which is representative of al l the RCP scenarios for this time period.]

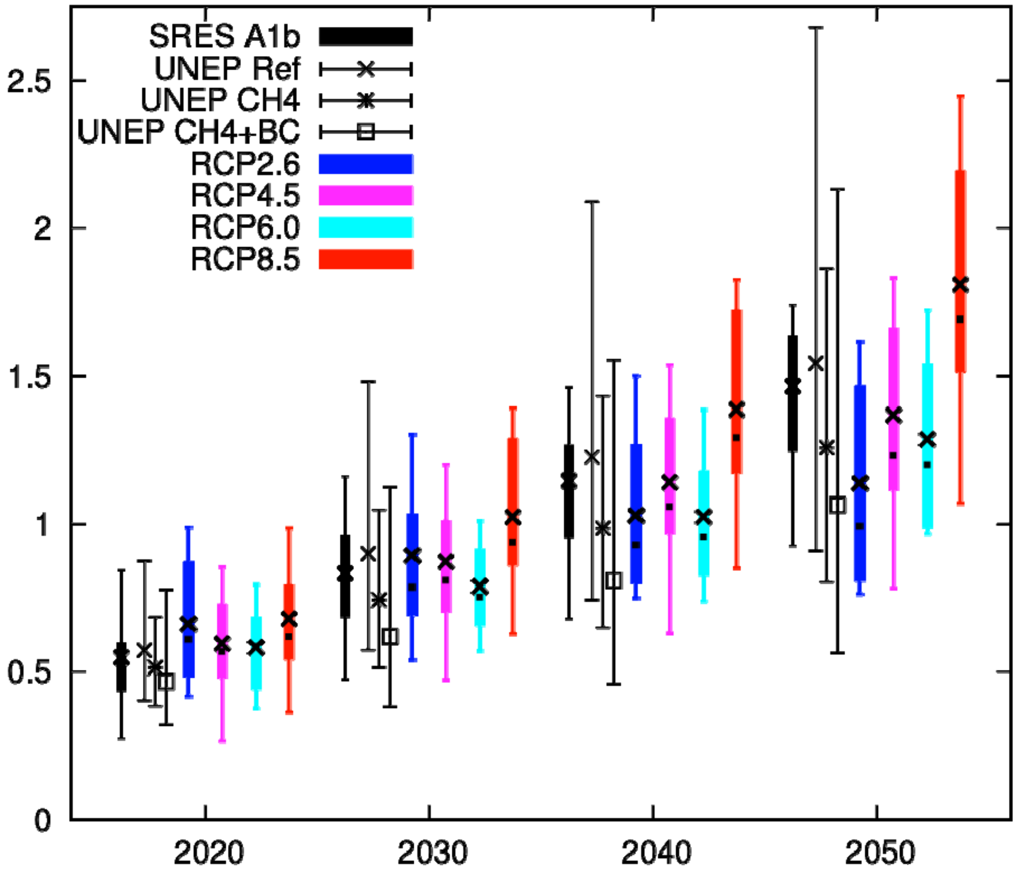

Figure 11.38a: Emergence of near-term differences in global mean surface air temperatures across scenarios. Increases in 10-year mean (2016–2025, 2026–2035, 2036–2045 and 2046–2055) globally averaged surface air temperatures (°C) in the CMIP5 model ensemble following each scenario (11, 15, 8, and 16 models for RCP2.6 (red), RCP4.5 (blue), RCP6.0 (magenta), and RCP8.5 (cyan), respectively and in the CMIP3 model ensemble (22 models; black bars) following the SRES A1b scenario. The multi-model mean (X), median (square), interquartile range (open boxes), 5–95% distribution (whiskers) across all models are shown for each decade and scenario. Also shown are estimates for scenarios that implement technological controls by 2030 on sources of methane (UNEP CH_4) and on sources of methane and black carbon as well as co-emitted species such as carbon monoxide, organic carbon and nitrogen oxides (UNEP CH_4 + BC) relative to the reference scenario (UNEP Ref); symbols denote the average of the two participating models and vertical bars denote uncertainty estimates based on (1) uncertainty in radiative forcing from each atmospheric component (i.e., CH_4, O_3, individual aerosol species) in response to the emission control measures and (2) uncertainty in the temperature response associated with the range of climate sensitivity recommended in AR-4 (United Nations and World Meteorological Organization, 2011). To compare the UNEP and RCP values to a common baseline, the difference between 2009 UNEP reference year temperature and the 1986–2005 average temperature in the historical/RCP4.5 model ensemble was added to the UNEP values.

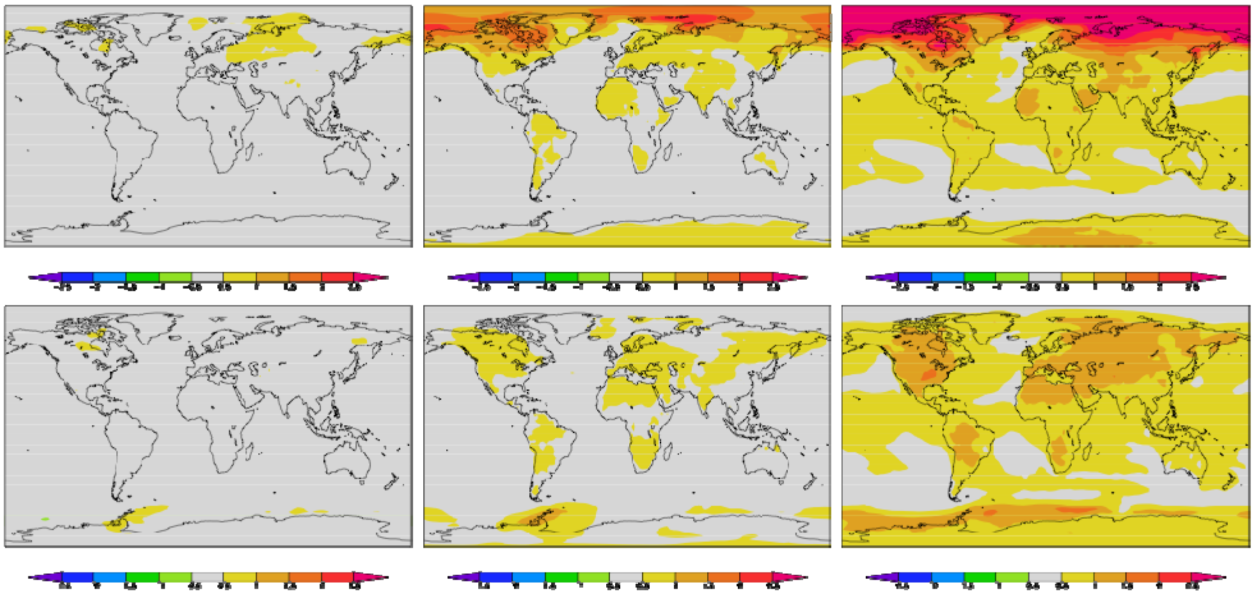

Figure 11.38b: Emergence of near-term differences in regional surface air temperature across the RCP scenarios. Difference between the high (RCP8.5) and low (RCP2.6) scenarios for the CMIP5 model ensemble (12 models) surface air temperatures averaged over 2026–2035 (left), 2036–2045 (middle) and 2046–2055 (right) in boreal winter (DJF; top row) and summer (JJA; bottom row).

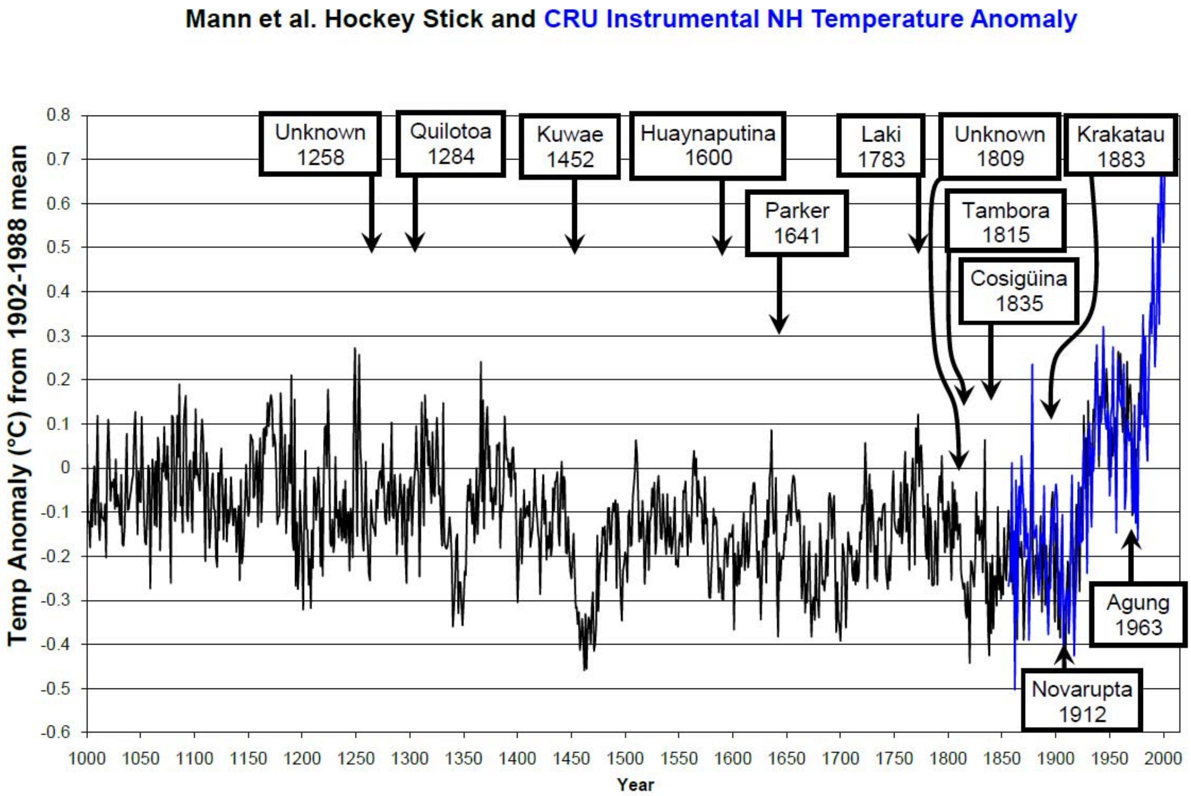

FAQ 11.2, Figure 1: Northern Hemisphere temperature anomaly, 1000–2000 C.E. and the major volcanic eruptions.